THE
PHYSICAL REVIEW

A journal of experimental and theoretical physics established by E. L. Nichols in 1893

SECOND SERIES, VOL. 69, NOS. 11 AND 12 JUNE 1 AND 15, 1946

Characteristic X-Rays Excited by Beta-Particles

J. E. EDWARDS* AND M. L. POOL
Mendenhall Laboratory, Ohio State University, Columbus, Ohio
(Received February 4, 1946)

Characteristic x-rays have been shown to be associated with a β-particle source. The x-rays excited in atoms outside the β-emitting atom were detected by absorption measurements and photographically, with a curved crystal spectrograph. Characteristic Cu x-rays associated with the decay of 12.8-hour Cu^{64} are attributed to the strong beta-activity of the source. Photographs of characteristic x-rays excited by P^{32} β-particles in Cu, Zr, Rh, and Ag were obtained. The characteristic x-rays and general x-radiation excited by P^{32} β-particles in Al, Cu, Ag, Sn, and Pb were studied by absorption of the radiation in Al, Cu, and Pb.

I. INTRODUCTION

WHEN characteristic x-rays are associated with nuclear disintegration it generally indicates a decay process involving electron capture or internal conversion of gamma-radiation. Characteristic x-rays may appear together with a strong β-activity in the same chemical fraction or even in the same isotope. In identifying the source of the x-radiation in this case one must consider the possibility that the β-particles are capable of exciting the characteristic x-rays in the sample.

Continuous x-rays excited by β-particles in atoms outside the β-emitting atom itself have been studied extensively.[1–3] The energy distribution of the harder part of the continuous x-rays excited in various metals by P^{32} β-particles was found to be practically independent of the atomic number.[3] However, the intensity of the harder component of the continuous x-rays was found to be proportional to the square of the atomic number of the target[3] in agreement with theory.[4] The harder continuous x-rays may be studied by absorbing the β-particles completely in a target material. Absorption curves of the radiation emerging from the opposite side of the target material are then obtained. This method is not so suitable for study of the soft charac-

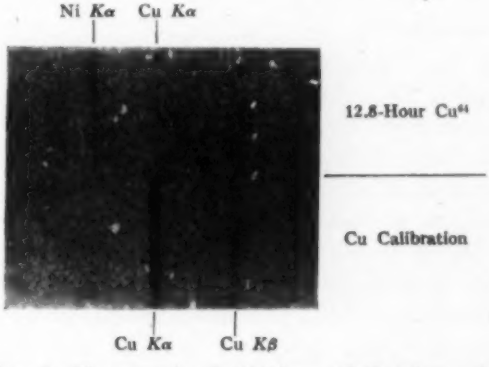

FIG. 1. Photograph of 12.8-hour Cu^{64} taken with a quartz curved crystal spectrograph showing Ni and CuK x-ray lines.

* Now at Ohio University, Athens, Ohio.
[1] Edwin McMillan, Phys. Rev. **47**, 801 (1935).
[2] G. J. Sizoo, C. Eijkman, and P. Green, Physica **6**, 1057 (1939).
[3] C. S. Wu, Phys. Rev. **59**, 481 (1941).
[4] H. Bethe and W. Heitler, Proc. Roy. Soc. **146**, 83 (1934).

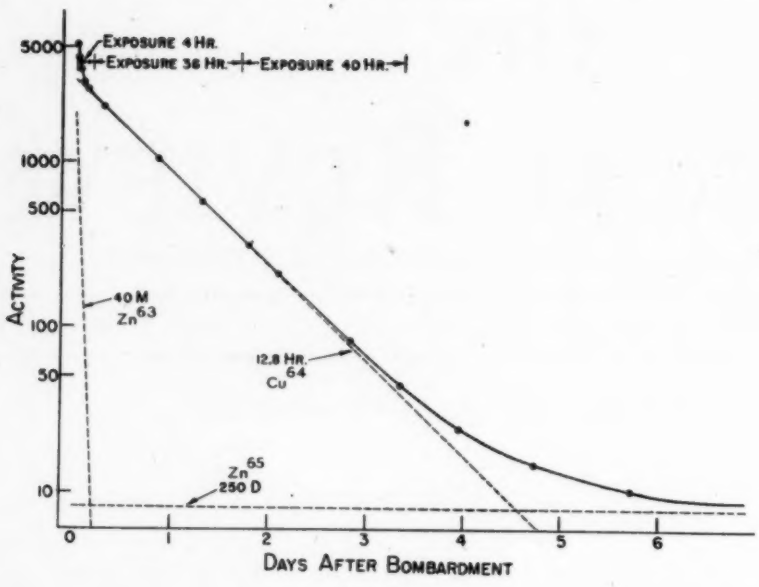

FIG. 2. Decay curve of Cu+d sample showing photographic procedure. Photograph in Fig. 1 was obtained during the 36-hour exposure.

teristic radiation because of the large percentage of the radiation absorbed in the target material.

The present investigation was undertaken to devise methods for studying the nature of characteristic x-rays excited by β-particles. The radiation was studied by absorption and photographically with curved crystal spectrographs.

II. CHARACTERISTIC X-RAYS EXCITED BY 12.8-HOUR Cu^{64} BETA-PARTICLES

Beta-rays, positrons, and x-rays are associated with a 12.8-hour Cu activity assigned to Cu^{64} by Van Voorhis.[5] An x-ray photograph of this activity obtained by Abelson[6] using a reflection type curved crystal spectrograph showed the x-rays to be characteristic of Ni. A photograph of this activity was also taken by the authors[7] using the 110 planes of a quartz crystal curved to a radius of 8 inches in a transmission type spectrograph. X-rays characteristic of Cu as well as Ni were observed (Fig. 1). The photographic procedure is shown in Fig. 2. After deuteron activation of metallic Cu the sample was placed in a strong magnetic field in front of the spectrograph. A series of four exposures was made along with a decay curve. The first exposure extended over 4 hours during which time the intensity of the 38.5-minute Zn^{63} dropped to 1/100 the intensity of the 12.8-hour Cu^{64}. This exposure showed no x-rays. Ni and CuK lines appeared on the second (Fig. 1) photograph which was exposed for 36 hours. A third exposure for 40 hours showed no lines. After aging the sample for a few weeks, an exposure of 42 days showed CuK x-rays to be associated with the 250-day Zn^{65}. The results thus show conclusively that Cu x-rays are associated with the 12.8-hour Cu^{64} activity which is also a β-emitter. An internally converted gamma-ray in Cu arising from a genetically related isomer would account for the Cu x-rays. However, since there is no other evidence of such an isomer in Cu, it is assumed that the Cu x-rays are excited in the sample by the β-activity.

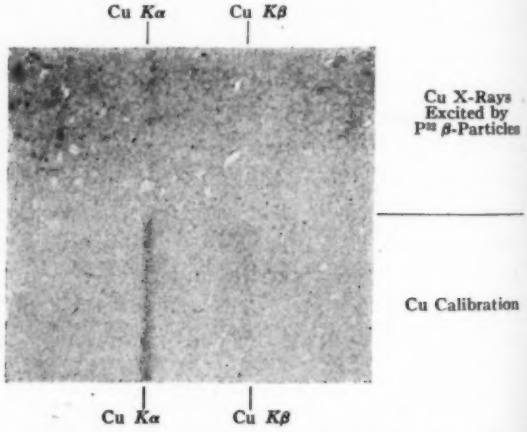

FIG. 3. Photograph of x-rays excited in Cu by P^{32} β-particles.

[5] S. N. Van Voorhis, Phys. Rev. **50**, 895 (1936).
[6] P. Abelson, Phys. Rev. **56**, 753 (1939).
[7] J. E. Edwards, M. L. Pool, and F. C. Blake, Phys. Rev. **67**, 150 (1945).

III. CHARACTERISTIC X-RAYS EXCITED BY P^{32} BETA-PARTICLES

Evidence to support the above interpretation of the source of the Cu x-rays was obtained by photographing the characteristic x-rays excited by P^{32} β-particles in various substances.

A P^{32} sample was prepared with a beta-ionization intensity approximately equal to that of the Cu^{64} sample discussed in II. P^{32} β-particles have a maximum energy of 1.7 Mev while Cu^{64} β-particles have a maximum energy of 0.58 Mev. The P^{32} was wrapped in an inactive 0.001″ Cu foil, then photographed with the same spectrograph as used with the Cu^{64}. Figure 3 is the result of an exposure comparable to that given the Cu^{64} in Fig. 1, the exposure time being adjusted to compensate for period differences. Figure 3 shows Cu$K\alpha$ and $K\beta$ lines excited in the Cu foil by the P^{32} β-particles. This evidence shows that the Cu^{64} β-particles were capable of producing the Cu x-rays observed in Fig. 1.

Photographs of characteristic x-rays excited by P^{32} β-particles in Zr, Rh, and Ag are shown in Fig. 4. These photographs were made with mica crystal spectrographs with a crystal curvature of 8″. The exposures extended over a period of 21 days with P^{32} samples of about 6 millicuries. The Zr and Rh photographs, Fig. 4, were exposed at the same time. A 0.005″ Zr foil was placed on one side of a flat P^{32} sample and a 0.001″ Rh foil was placed on the opposite side, both foils being in contact with the P^{32}. The assembly was placed in a magnetic field and photographs of the radiation from the two opposite sides were taken. The photograph taken from the Rh side of the sample shows that the Zr radiation was able to pass through the P^{32} sample and the Rh foil with sufficient intensity to produce ZrK lines in addition to the Rh lines. Rh lines did not appear on the Zr photograph because the Zr foil was thick enough to absorb most of the Rh radiation.

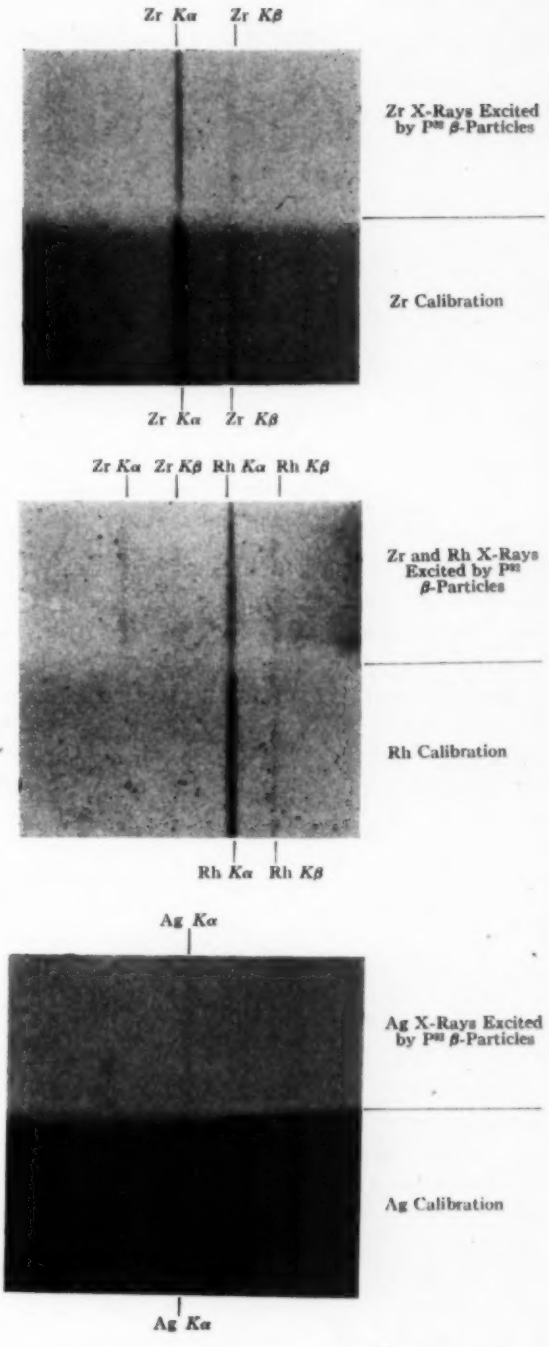

FIG. 4. Photographs of x-rays excited in Zr, Rh, and Ag by P^{32} β-particles.

IV. ABSORPTION CURVES OF X-RAYS EXCITED BY P^{32} BETA-PARTICLES

(a) Experimental Procedure

The experimental arrangement for making absorption measurements on the total radiation excited by P^{32} β-particles in various elements is shown in Fig. 5. A is a box made entirely of the target element to be used. The boxes had inside dimensions of $2'' \times 1\frac{1}{2}'' \times 1\frac{1}{4}''$ with a thickness in each case sufficient to stop all of the electrons. The opening in the bottom of the box was provided with a tube also made of the same target

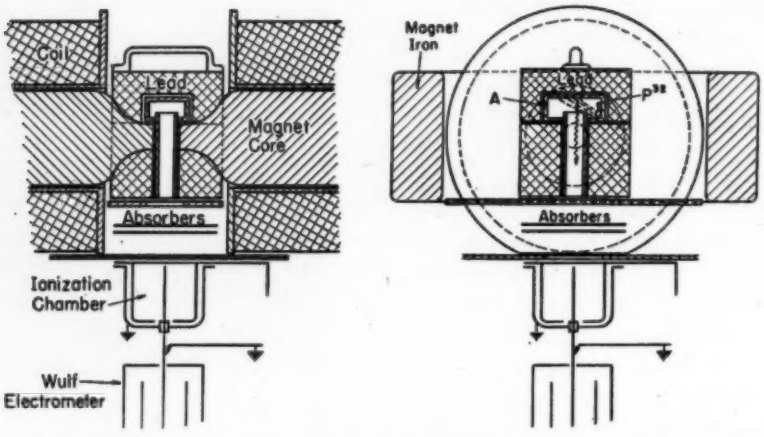

FIG. 5. Experimental arrangement for absorption study of x-rays excited by P^{32} β-particles. Two cross-sectional views at right angles. (A) is the metal target box.

material. Electrons which enter this tube from the box are then stopped in the same target material in the area of the magnet pole faces. The box and tube were surrounded by 1.5″ of Pb.

Measurements on the radiation from the target box were made by absorbing the radiation in an ionization chamber. The aluminum inner cup of the chamber had a diameter of 9 cm and a length of 9 cm. The window was aluminum 13.12 mg/cm² thickness and it was filled with Freon to a pressure of 20 lb./in.² gauge. The ionization currents were measured with a Wulf unifilar electrometer. The magnetic field was maintained constant at a point considerably above that necessary to prevent any electrons from reaching the ionization chamber.

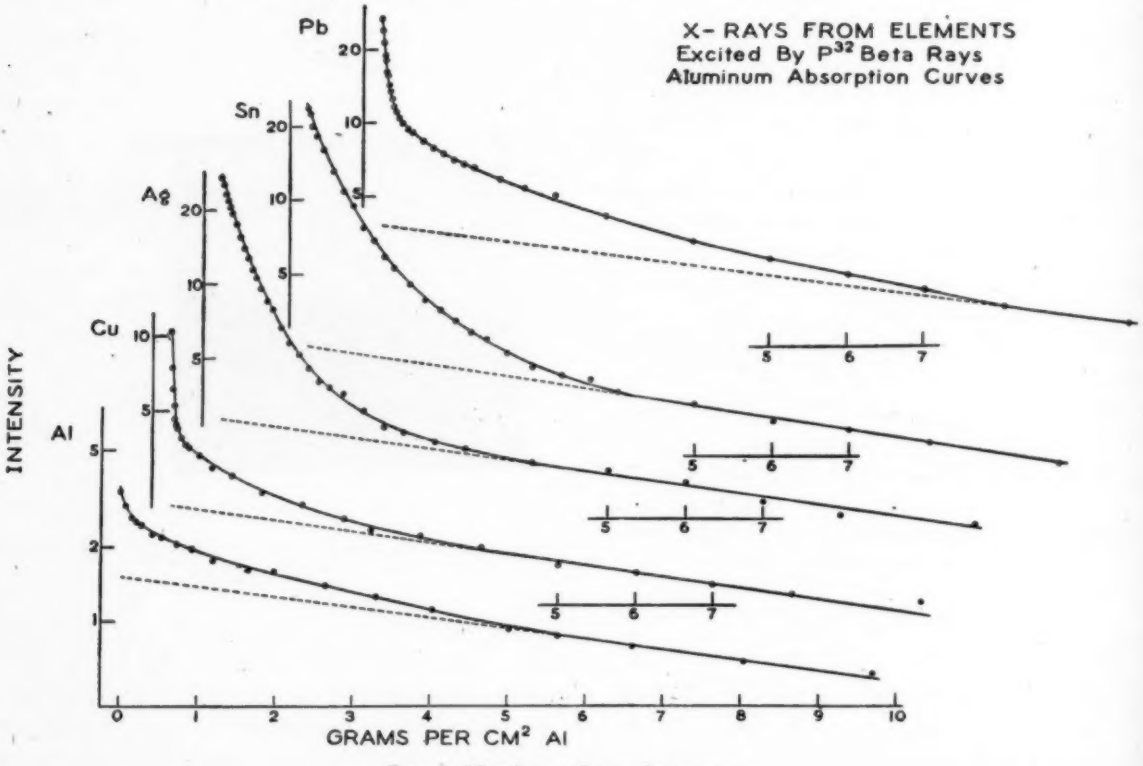

FIG. 6. Aluminum absorption curves.

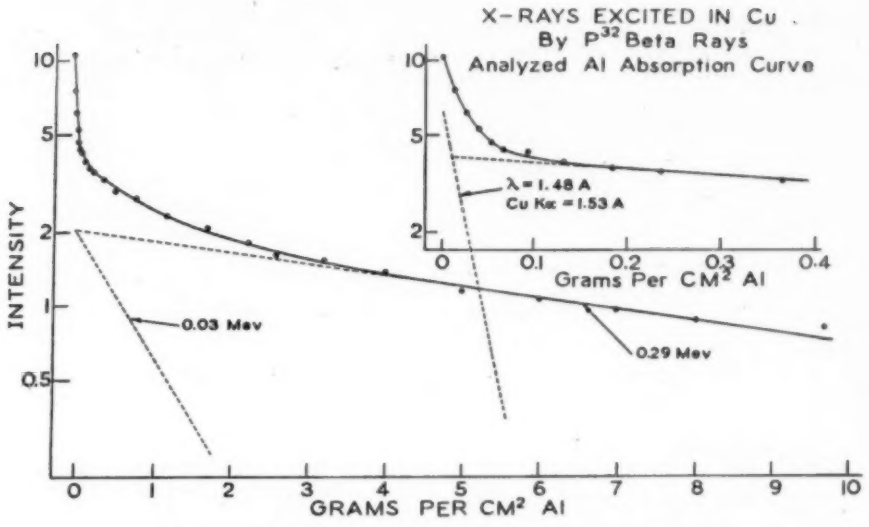

FIG. 7. Analyzed curve for Cu radiation (absorption in Al).

Virtually all of the radiation entering the ionization chamber originates in the target areas bombarded by the β-particles. P^{32} emits no monochromatic γ-ray. The weak inhomogeneous radiation (*innere bremsstrahlung*) originating in the P^{32} β-emitting nucleus must pass through at least 1″ of Pb to enter any effective area of the ionization chamber.

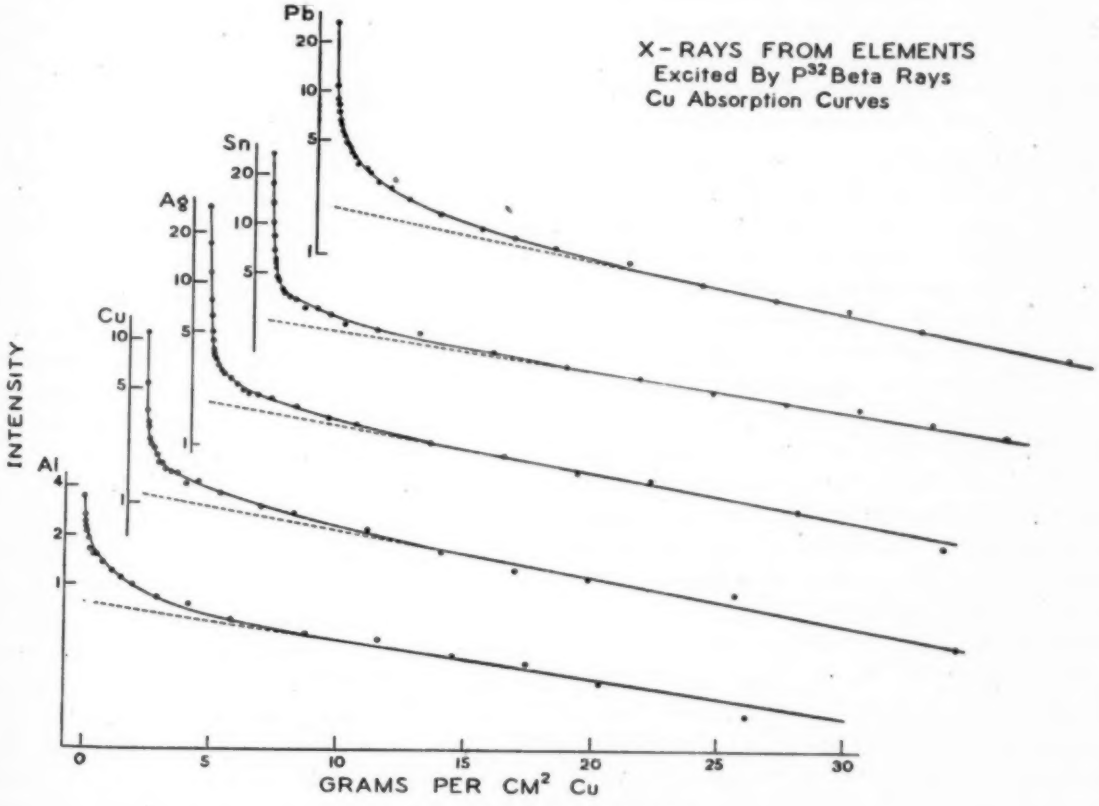

FIG. 8. Cu absorption curves.

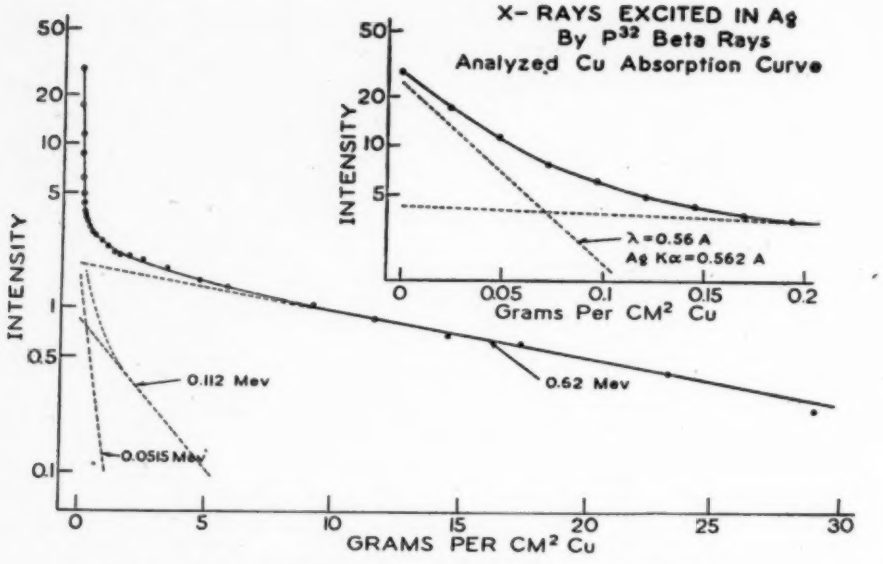

FIG. 9. Analyzed curve for Ag radiation (absorption in Cu).

(b) Results

Absorption curves in aluminum to a thickness of 10 g/cm² are shown in Fig. 6. This thickness was sufficient to absorb the major part of the characteristic radiation from the metal target boxes used. The curves were analyzed in the usual way by subtracting the general radiation background and were found to yield radiation energies corresponding to characteristic K radiation for the Cu, Ag, Sn, and Pb curves. The analyzed curve for the Cu radiation is shown in Fig. 7. Radiation energy in the region of the L lines of Pb was also found by analyzing the front end of the Pb curve. No appreciable amount of characteristic Al radiation could enter the ionization chamber. However, the curve for Al radiation in Fig. 6 shows a relatively high intensity for the soft components of the radiation. This apparent increase in intensity is due to a variation in the sensitivity of the ionization chamber with radiation wave-length. According to calculations the chamber was most sensitive to radiation in the region of 1 Angstrom.

Absorption curves in Cu to a thickness of 30 g/cm² are shown in Fig. 8. These curves show that the energy distribution of the hard part of the general radiation excited by β-particles is practically independent of the atomic number of the target material. These curves were analyzed to determine the average energy of the general radiation and the wave-length of the characteristic x-rays. Figure 9 shows an analyzed curve for x-rays excited in Ag. After subtracting the three exponential curves having absorption coefficients corresponding to energies of 0.62, 0.112, and 0.0515 Mev, the remaining curve gave an absorption coefficient very close to that expected for AgK radiation. The analysis of the general radiation into the three components is rather arbitrary and does not imply that only three components are present. The relative intensity of these three component curves has little significance since the sensitivity of the ionization chamber is not known for this harder radiation.

Absorption of the hard part of the radiation in lead gave similar curves for all target boxes. One of these curves for Ag radiation is shown analyzed into two exponential curves in Fig. 10.

(c) Discussion

Two experimental difficulties prevent accurate measurement of the relative intensity of the characteristic x-radiation from the various elements. (1) The sensitivity of the ionization chamber for the different radiation energies is not known. (2) The radiation which enters the chamber comes from the top of the target box and from the region of the magnet pole pieces. The radiation from the region of the pole pieces

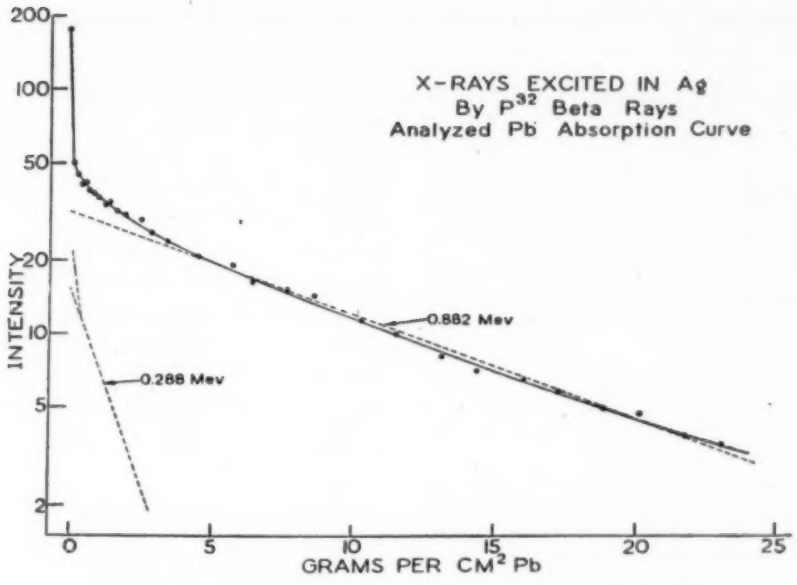

FIG. 10. Analyzed curve for Ag radiation (absorption in Pb).

is a variable factor depending upon the number of electrons reflected from the target box surfaces and is not easily determined.

The results of this investigation show that characteristic x-rays are associated with a β-particle source. The x-rays are excited in atoms outside the β-emitting atom. The intensity of the β-excited characteristic x-rays may be comparable with the intensity of x-rays arising from nuclear decay processes as was observed in the K-capture decay of Cu^{64}.

The authors are grateful for the support received from Mr. Julius F. Stone, The Ohio State University Development Fund, The Ohio State University Research Foundation, and The Graduate School.

Isotopic Constitution of Tellurium, Silicon, Tungsten, Molybdenum, and Bromine*

DUDLEY WILLIAMS AND PHILIP YUSTER
University of California, Los Alamos Scientific Laboratory, Los Alamos, New Mexico

(Received November 20, 1945)

The relative abundances of the isotopes of tellurium, silicon, tungsten, molybdenum, and bromine have been redetermined by means of a mass spectrograph of the Nier type. The results are as follows: *Tellurium.* Samples in the form of tellurium hexafluoride were employed and the ions TeF_5^+ and TeF_3^+ were used in measuring relative abundances.

Isotope	130	128	126	125	124	123	122	120
Relative abundance	100	92.3	54.2	20.2	13.3	2.47	7.05	0.26.

The existence of isotope 120 was confirmed. With the assumption of a packing fraction of -4, the above values for relative abundance lead to a value of 127.64 ± 0.01 for the chemical atomic weight. *Silicon.* Samples in the form of silicon tetrafluoride were employed and the ions SiF_4^+ and SiF_3^+ were used. The results are as follows:

Isotope	28	29	30
Isotopic abundance	100	5.07	3.31.

With Aston's values for the isotopic weights, the above values for isotopic abundances give 28.086 for the chemical atomic weight. *Tungsten.* The isotopic constitution of tungsten has been re-investigated with a view to obtaining more exact data on relative abundance. Relative isotopic abundances were measured for the W^+ ion obtained by electronic bombardment of tungsten hexacarbonyl vapor. The existence of isotope 180 has been confirmed. The estimates of isotopic abundances obtained by electrometrical methods are:

Isotopic	186	184	183	182	180
Relative abundance	92.7	100	47.0	86.2	0.44.

On the basis of a packing fraction of $+2$, these estimates lead to a value of 183.88 for the chemical atomic weight. *Molybdenum.* The isotopic constitution of molybdenum has been re-investigated. The values for isotopic abundance as determined electro-metrically from Mo^+ and Mo^{++} ions produced by electronic bombardment of molybdenum hexacarbonyl are:

Mass number	100	98	97	96	95	94	92
Relative abundance	40.5	100.0	39.8	69.5	66.1	38.4	66.8.

These values are in closer agreement with values reported by Valley than with values obtained by Aston or Mattauch. *Bromine.* Values for the relative abundance of the bromine isotopes have been obtained from measurements on Br_3^+, Br^+, and Br^{++} ions formed by electronic bombardment of bromine vapor. The relative abundances are in essential agreement with the values reported by Blewett:

Mass number	79	81
Relative abundance (present study)	100	97.9 ± 0.4
Relative abundance (Blewett)	100	97.5 ± 2.5.

No new isotopes of bromine were observed.

THE development of nuclear physics has made necessary a more exact knowledge of the isotopic constitution of the elements. Most of the early work in the field of mass spectroscopy was concerned primarily with the detection of isotopes and the accurate measurement of masses and only incidentally with the accurate determination of isotopic abundances.[1] With the exception of the apparatus described by Dempster[2] the instruments used employed photographic methods of detection. Relative abundances were based on photometric measurements.

During recent years several instruments have been designed with a view to obtaining more accurate information on relative abundance. These spectrometers employ electrical methods of detection and measurement.[3-5] With these instruments the accuracy of measurement of normal ratios of abundance is approximately one percent, and data on numerous elements have been reported by Nier, Bleakney, Valley, and others.[6]

The work reported in the present paper is concerned chiefly with data on the relative abundance of the isotopes of several elements not previously investigated by methods utilizing electrical methods of measurement.

* This article has been prepared by the Editor from four reports which were submitted by the authors after clearance by the War Department.

[1] F. W. Aston, *Mass Spectra and Isotopes* (Edward Arnold and Company, London, 1942), Part II.

[2] A. J. Dempster, Phys. Rev. **20**, 631 (1922).

[3] M. B. Sampson and W. Bleakney, Phys. Rev. **50**, 456 (1936).

[4] A. O. Nier, Phys. Rev. **52**, 933 (1937).

[5] A. O. Nier, Rev. Sci. Inst. **11**, 212 (1940).

[6] F. W. Aston, Summary of Work in *Mass Spectra and Isotopes* (Edward Arnold and Company, London, 1942), Part III.

APPARATUS AND PROCEDURE

The spectrometer used in the present study was designed by Nier and was similar in most essentials to the one mentioned above.[5] The general principles on which the operation of this type of instrument is based have been discussed by Barber[7] and Stephens and Hughes.[8] These authors have shown that if a slightly divergent beam of ions having the same momentum enters a homogeneous magnetic field between two V-shaped pole pieces in a direction normal to one boundary of the field and after deflection leaves the field in a direction normal to the other boundary of the field, re-focusing of the ion paths will occur. The nature of the re-focusing is such that the source of the ions, the apex of the V, and the point of re-focusing lie on a straight line. In the present spectrometer the beam of ions entering the magnetic field from the entrance slit is mono-energetic; hence, the ions of a given mass can be focused at the exit slit by giving the appropriate energy to the ions entering the field, provided the proper geometry connecting entrance slit, the apex of the V, and the exit slit is realized. The radius of curvature of the collected ion beam and the mass of the ion are given by the following familiar relationship:

$$m/e = 4.82 \times 10^{-5} r^2 H^2 / V, \qquad (1)$$

where m/e is in atomic mass units/electronic charge, r is the radius in cm, H is the magnetic field intensity in gauss, and V is the energy of the ions in electron volts. In operating the instrument, H is held constant at some appropriate value and the various isotopes are brought into focus by adjusting V.

The potentials used for accelerating the ions were obtained from a potentiometer connected to a 2000-volt electronically regulated power supply. In most of the present work the energies of the ions were between 1000 and 2000 electron volts.

The magnet used in the spectrometer was a large electromagnet with wedge-shaped 60° pole pieces. The separation of the pole pieces was $\frac{9}{16}$". The current for the coils of the magnet was supplied from a constant-current power supply with electronic regulation. The radius of the circle described by the collected ion beam in the magnetic field was 15 cm.

The collector for the ion current was located behind the exit slit of the spectrometer. A small negative potential applied to a diaphragm near the collector served to minimize the effects of secondary electron emission. The collector was connected to the grid of an FP-54 electrometer tube in a conventional DuBridge-Brown Circuit employing a grid resistance of 40,000 megohms. A high sensitivity galvanometer equipped with an Ayrton shunt was used with the amplifier. With a scale distance of two meters the amplifier-galvanometer system had a maximum sensitivity of 3×10^{-16} amp./mm. When the amplifier tube housing was evacuated with a forepump, the stability of the amplifier used at maximum sensitivity was usually adequate. Potentials from a Leeds and Northrup potentiometer could be applied in the grid circuit of the amplifier for purposes of calibration.

A two-stage mercury diffusion pump and a Welch Duo-Seal forepump were used in evacuating the spectrometer tube. With liquid nitrogen as a trap refrigerant, this combination was capable of producing a vacuum of 10^{-8} mm of mercury as measured by a Distillation Products ion gauge. Under normal operating conditions the pressure was not allowed to rise above 2×10^{-7} mm of mercury.

During operation a volatile compound of the element being investigated was admitted to the spectrometer source through a variable leak from a separate system. Ions were produced by electronic bombardment of the gas essentially in the manner described by Nier[5] except that the required voltages were obtained from a vacuum tube power supply.

In making relative abundance measurements on two isotopes A and B, galvanometer deflections produced by the two ion beams were measured. Deflections in the order AB, BA, AB, etc., were observed. After completion of these observations, the observed galvanometer deflections were reproduced by the application of known voltages from the potentiometer. These voltages were then compared to measure isotopic abundance. The chief advantage of this method of measuring abundance over the null method,

[7] N. F. Barber, Proc. Leeds Phil. Soc. **2**, 427 (1933).
[8] W. E. Stephens and A. L. Hughes, Phys. Rev. **45**, 123 (1934); W. E. Stephens, Phys. Rev. **45**, 513 (1934).

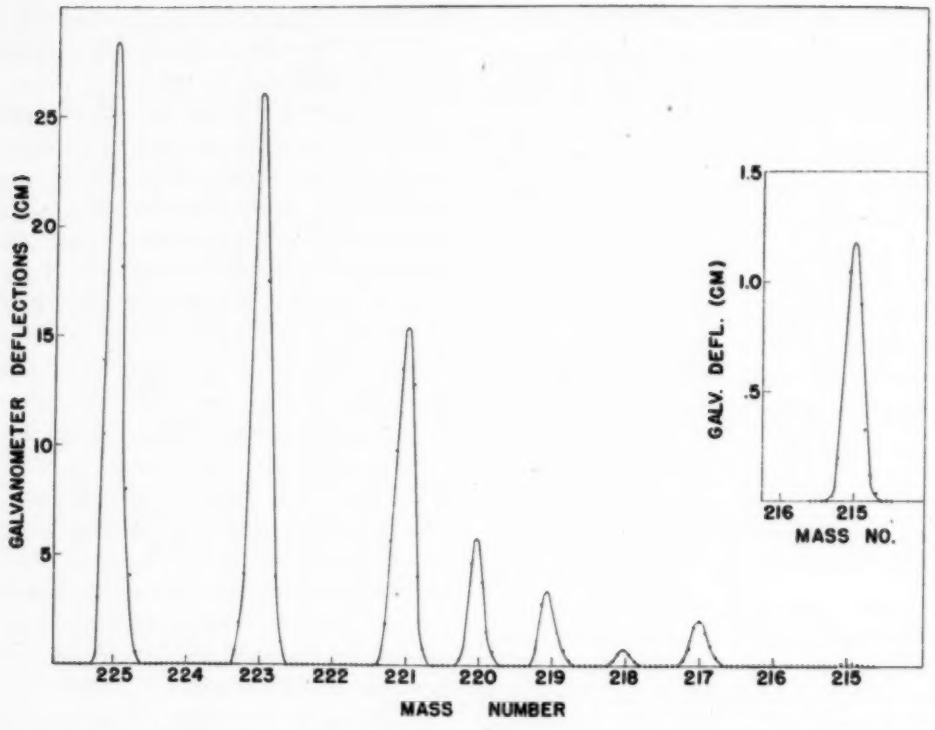

FIG. 1. Mass spectrum in the vicinity of the TeF_5^+ ion. The peak at mass position 225 corresponds to a beam current of 1.5×10^{-11} ampere.

in which the voltage produced in the grid resistor by the collected ion beam is balanced out by applied voltages from a potentiometer, lies in the fact that in the shorter time required for making observations the ion currents do not change as much as in the longer observation times required for null-method measurements. The chief disadvantage lies in the possibility of variations in grid resistance produced by large ion currents. Tests show that for ion currents of the magnitude actually used the grid resistance remains constant to within less than one percent. Experience with the present instrument seems to indicate that the deflection method of measurement when combined with immediate calibration gives more reliable and more reproducible results than the null method.

TELLURIUM

The isotopic constitution of tellurium has long been of interest on account of the anomalous position of its atomic weight in reference to that of iodine in the periodic table. Previous work by Aston,[9] Bainbridge,[10] Dempster,[11] and Bainbridge and Jordan[12] led to values of the abundance ratio of the isotopes presented in the last column of Table III.

The material used in the present work was tellurium hexafluoride. Samples were prepared in a vacuum system by a method involving a reaction between powdered tellurium and anhydrous cobaltic fluoride. Owing to the simple isotopic constitution of fluorine, results obtained with any of the ions formed are immediately

TABLE I. Relative abundance of ions formed by bombardment of tellurium hexafluoride with 100-volt electrons.

Ion	Relative abundance	Ion	Relative abundance
TeF_6^+	weak	TeF_2^+	6.3
TeF_5^+	100.0	TeF^+	9.1
TeF_4^+	5.5	Te^+	12.7
TeF_3^+	9.3		

[9] F. W. Aston, Phil. Mag. **42**, 241 (1921); **45**, 942 (1923); **49**, 1197 (1925); Proc. Roy. Soc. **A132**, 487 (1931).
[10] K. T. Bainbridge, Phys. Rev. **39**, 1021 (1932).
[11] A. J. Dempster, Phys. Rev. **50**, 186 (1936).
[12] K. T. Bainbridge and E. B. Jordon, Phys. Rev. **50**, 282 (1936).

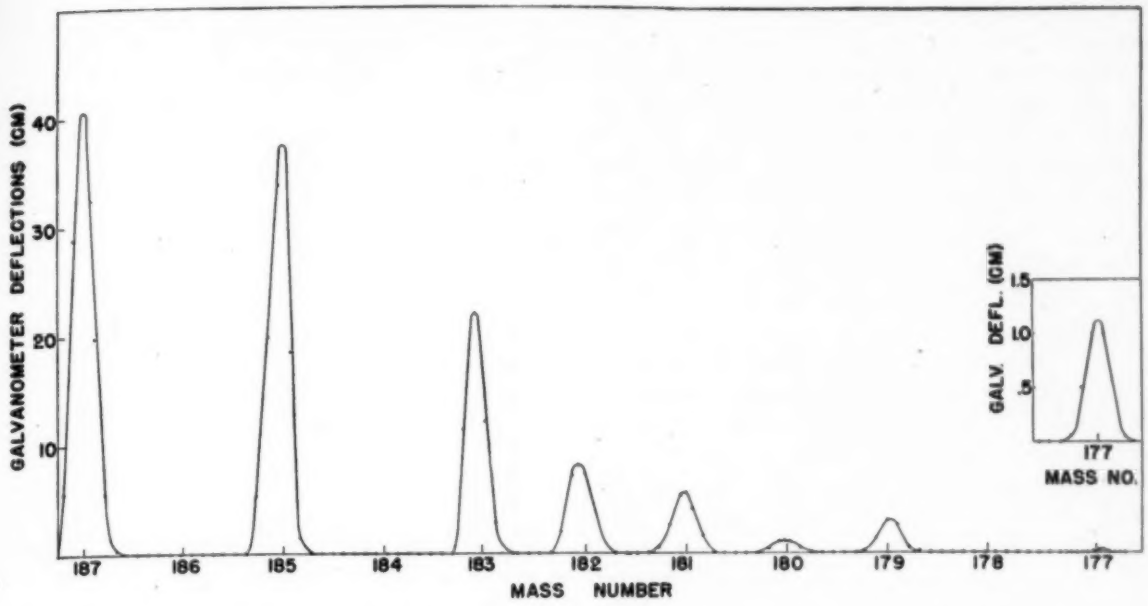

FIG. 2. Mass spectrum in the vicinity of the TeF_3^+ ion. The peak at mass position 187 corresponds to a beam current of 1.5×10^{-12} ampere.

interpretable. The relative abundances of the ions produced by electronic bombardment are given in Table I. The estimates given in the table are probably accurate to ten percent.

Owing to the large relative abundance of the TeF_5^+ and TeF_3^+ ions formed, these ions were chosen for study in measuring isotopic abundances. The mass spectrum observed in the vicinity of the TeF_5^+ ion is shown in Fig. 1. In obtaining the data represented in this figure the exit slit was made just wide enough to receive the total ion beam for the peaks shown. The indicated resolution obtained is adequate for making abundance measurements. The inset shows the peak observed at mass number 215 where the amplifier was operated at highest sensitivity. No peaks were observed at 226, 224, 222, or 216.

In Fig. 2 are shown the results obtained for the TeF_3^+ ion. Here again the resolution seems to be adequate for making dependable abundance estimates. The inset in this figure shows the 177 peak as observed with the amplifier operating at highest sensitivity.

In Table II are given the relative abundances of the tellurium isotopes as measured from the peaks observed for the ions TeF_5^+ and TeF_3^+. Each value in the table represents the average of at least four ratios. Two complete sets of values are given for TeF_5^+; these two sets were obtained from data taken under different conditions of pressure, collector slit width, etc. The values obtained from these measurements on TeF_5^+ are in fair agreement with each other and with the measurements on TeF_3^+. As indicated in the table, most of the figures on abundance were obtained by direct comparison of each peak with the peak produced by the most abundant isotope

TABLE II. Measured isotopic abundance of tellurium isotopes. Relative abundance measured from indicated ion (all measurements in terms of 130 except as indicated).

Isotope	TeF_5^+ I	TeF_5^+ II	TeF_3^+	Average
130	100	100	100	100
128	92.5	92.5	92.0	92.3
126	54.5	54.2	53.8	54.2
125	20.5	20.15	19.8	20.15
124	13.6	13.4	13.0	13.3
123	2.52	2.51	2.38	2.47
122	7.25	7.14	6.77	7.05
120	0.261	—	—	0.261
124*	13.3	13.4	13.2	13.3
123*	2.47	2.51	2.42	2.47
122*	7.12	7.14	6.89	7.05
120*	0.256	—	—	0.256

* Using 125/130 = 20.15 and taking ratios to 125, the above abundances were obtained.

130. However, in order to obtain an additional check on the rarer isotopes 124, 123, 122, and 120, their abundances were re-measured in terms of 125. The results of these measurements are given in the lower part of Table II. The agreement between these values and the ones obtained by direct comparison with 130 is satisfactory. A search for other isotopes was made. The upper limit for abundances of 131, 129, 127, and 121 relative to 130 can be set at 1/20,000.

The final estimates of abundance based on the measurements described above are summarized in Table III for comparison with the values obtained by Bainbridge from a comparison of his own measurements on 124, 123, and 122 with Aston's earlier estimates on the more abundant isotopes. The uncertainties indicated for the values obtained in the present study are based on variations in the individual determinations and do not include systematic errors arising from changes in the grid resistance of the electrometer tube circuit, which may be as large as one percent.

The values in the column headed "Atomic percentage" imply an accuracy greater than justified by the data and were used only in computing the atomic weights. In this computation a packing fraction of -4 was assumed for all isotopes. The resulting value for the chemical atomic weight is 127.64 ± 0.01. The uncertainty indicated includes only the uncertainties in the abundance measurements and not uncertainties in packing fraction. The value obtained from the present work is slightly larger than the accepted value for the International Atomic Weight 127.61.

TABLE III. Relative abundance of the isotopes of tellurium.

	Present study		Aston and Bainbridge values
Isotope	Relative abundance	Atomic percentage	Atomic percentage
130	100.00	34.51%	33.1
128	92.3±0.3	31.85	32.8
126	54.2±0.2	18.70	19.0
125	20.2±0.2	6.98	6.0
124	13.3±0.4	4.59	4.5
123	2.47±0.05	0.85	1.6
122	7.05±0.18	2.43	2.9
120	0.256±0.017	0.09	*W*

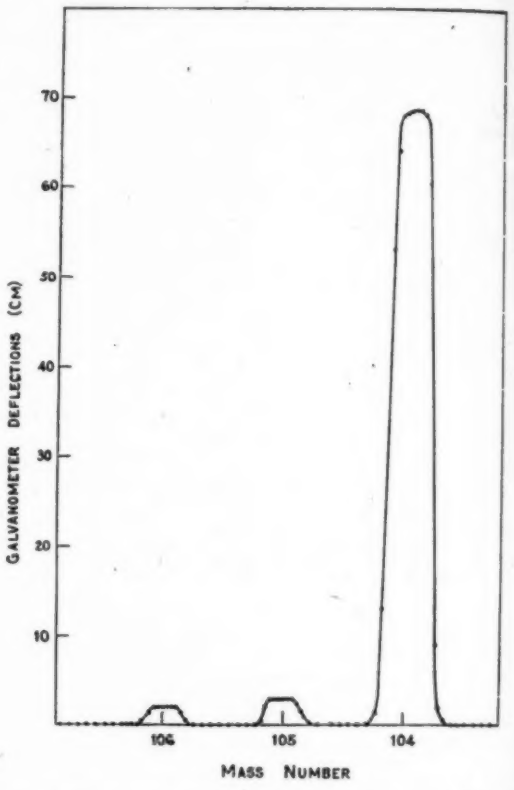

FIG. 3. Mass spectrum in the vicinity of the SiF_4^+ ion. The peak at mass position 104 corresponds to a beam current of 5×10^{-12} ampere.

SILICON*

Aston[13] was the first to study the isotopic composition of silicon. Much valuable information on the isotopic constitution of silicon has also been obtained from studies of the band spectrum of silicon nitride. Mulliken[14] confirmed the existence of isotope 30. Later McKellar[15] made an estimate of relative abundances of silicon isotopes from photometric measurements of the violet bands of silicon nitride. The atomic percentages obtained from these measurements are given in the last column of Table V.

* Subsequent to the submission of the reports on which the present paper is based, Ney and McQueen (Phys. Rev. **89**, 41 (1946)) have published measurements with a mass spectrograph of the abundance ratio of the isotopes of silicon. The values presented in the present paper are in remarkable agreement with the results of Ney and McQueen. (Ed.)

[13] F. W. Aston, Phil. Mag. **40**, 628 (1920); **49**, 1198 (1925); Proc. Roy. Soc. **A132**, 491 (1931); Nature **137**, 613 (1936); **138**, 1094 (1936).

[14] R. S. Mulliken, Nature **113**, 423, 489 (1924).

[15] A. McKellar, Phys. Rev. **45**, 761 (1934).

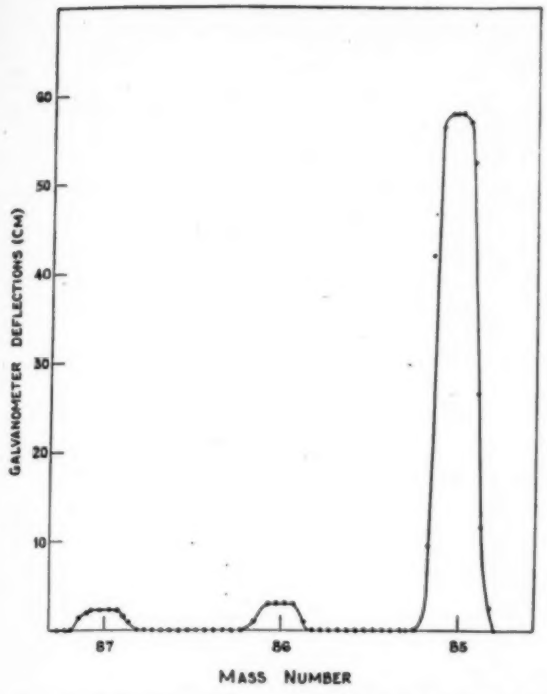

FIG. 4. Mass spectrum in the vicinity of the SiF_3^+ ion. The peak at mass position 85 corresponds to a beam current of 7.5×10^{-12} ampere.

The material used in the present study was silicon tetrafluoride and was prepared under vacuum by a reaction between elementary silicon and anhydrous cobaltic fluoride. When the silicon tetrafluoride vapor was subjected to electronic bombardment, peaks corresponding to ions of the types SiF_4^+, SiF_3^+, SiF_2^+, SiF^+, and Si^+ were observed. However, most of the actual measurements were made on SiF_4^+ and SiF_3^+. These ions were the most abundant, and the resolution obtained for them was satisfactory.

In Fig. 3 is shown the mass spectrum obtained in the vicinity of SiF_4^+ ion. In taking the data represented in this figure, the collector slit was wide enough to receive the total ion current for each peak. The peaks are well resolved. Examination of this region before and after the sample was studied showed no evidence of background at any place in the region.

Figure 4 shows the mass spectrum obtained in the vicinity of the SiF_3^+ ion. Here, again, resolution is adequate and there are no evidences of impurities. The SiF_3^+ ion was the most abundant ion formed under the conditions under which the source was operated.

In Table IV are given the results obtained on isotopic abundance in three independent sets of measurements. The first set of measurements was made on the SiF_4^+ ion and the other two were made on the SiF_3^+ ion under different conditions of pressure and source "tuning." The agreement between the values obtained is fair. A search for other isotopes was also made; none was found. The upper limits of abundances of 27 and 31 relative to 28 can be set at 1/20,000.

In Table V the values for isotopic abundances obtained in this study are summarized. The indicated uncertainties for relative abundances are based on the actual spread in the values obtained from the present measurements. There is also a possibility of systematic errors amounting to as much as one percent of the values listed. The source of this possible error has been discussed above. In the last column of Table V McKellar's values for atomic percentage are listed for comparison with the present values. Agreement between the two sets is poor.

In calculating the chemical atomic weight from the present data, Aston's values of 27.9869 and 28.9864 were used for the two lighter isotopes. A value of 29.9862 was assumed for the third isotope. With these values for the masses, the present values for abundance give a value of 28.086 for the chemical atomic weight. This value is in fair agreement with the international value of 28.06.

TABLE IV. Measured isotopic abundance of silicon isotopes.

	Relative abundance measured from indicated ion			
Isotope	SiF_4^+	SiF_3^+ I	SiF_3^+ II	Average
28	100	100	100	100
29	5.10	5.07	5.05	5.07
30	3.32	3.30	3.31	3.31

TABLE V. Relative abundance of silicon isotopes.

	Present study		McKellar's value
Isotope	Relative abundance	Atomic percentage	Atomic percentage
28	100	92.27	89.6
29	5.07±0.02	4.68	6.2
20	3.31±0.01	3.05	4.2

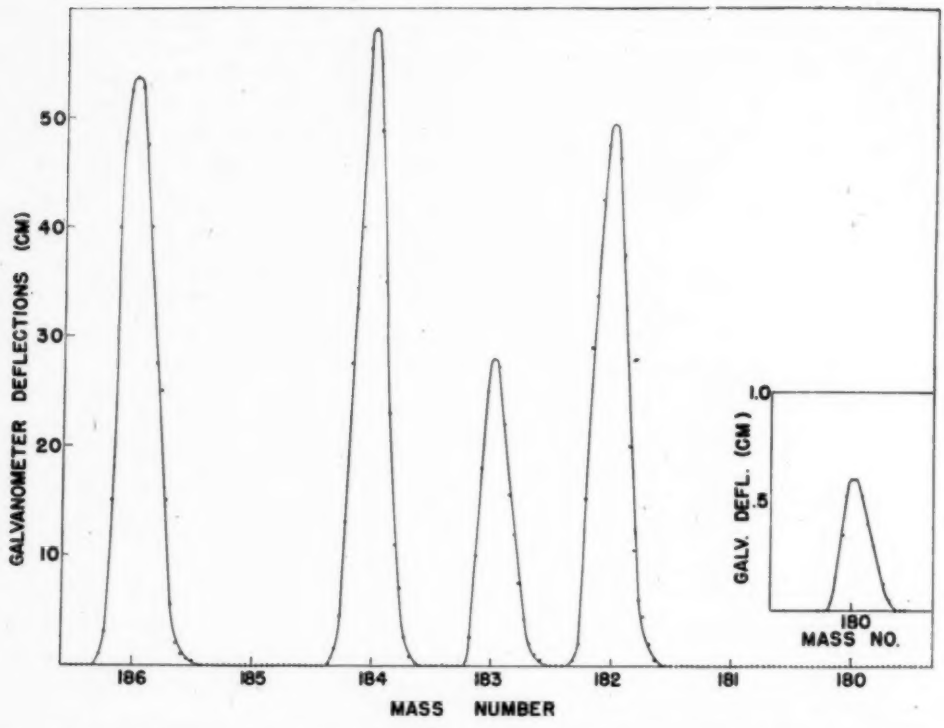

FIG. 5. Mass spectrum in the vicinity of the W^+ ion. The peak at mass position 184 corresponds to a beam current of 7.5×10^{-12} ampere.

TUNGSTEN

Early measurements of the abundance ratio of the isotopes of tungsten were by Aston[16] and by Dempster.[17] The values they obtained are shown in the last column of Table VI. The material used was tungsten hexacarbonyl, which in spite of its low vapor pressure gave satisfactory results.

Tungsten hexacarbonyl undergoes thermal decomposition into metallic tungsten and carbon monoxide at approximately 400°C. Hence, it was not surprising that the most abundant ion formed during electronic bombardment at 100 volts was the metallic ion. Rough estimates indicate that more than half of the positive ions formed were singly charged tungsten ions. However, other species of ions representing all stages of dissociation from $W(CO)_6^+$ to W^+ were observed. As there was evidence that the CO groups themselves decomposed, it was impossible to obtain interpretable data on any singly charged ions except W^+ because of overlapping. It was also impossible to obtain interpretable data on W^{++} because these peaks were overlapped by peaks produced by multiply charged ions of other species.

The mass spectrum observed in the vicinity of the singly charged tungsten ion is shown in Fig. 5. The peaks shown in this figure are sufficiently well resolved to permit accurate determination of isotopic abundances. There is no indication of background arising from impurities. The inset at mass position 180 shows this peak as observed with the amplifier operating at highest sensitivity. No minor peaks of com-

TABLE VI. Relative abundance of tungsten isotopes as determined from tungsten caronyl.

Isotope	Measured abundance from W^+ ion under different conditions of pressure and source "tuning" W^+ I	W^+ II	Average	Atomic percentage	Aston-Dempster values
186	92.9	92.6	92.7	28.41	29.8
184	100.0	100.0	100.0	30.64	30.1
183	47.0	47.1	47.0	14.40	17.3
182	86.2	86.2	86.2	26.41	22.6
180	0.438	0.443	0.440	0.13	0.2

[16] F. W. Aston, Proc. Roy. Soc. **A115**, 507 (1927); **A132**, 491 (1931).
[17] A. J. Dempster, Phys. Rev. **52**, 1074 (1937).

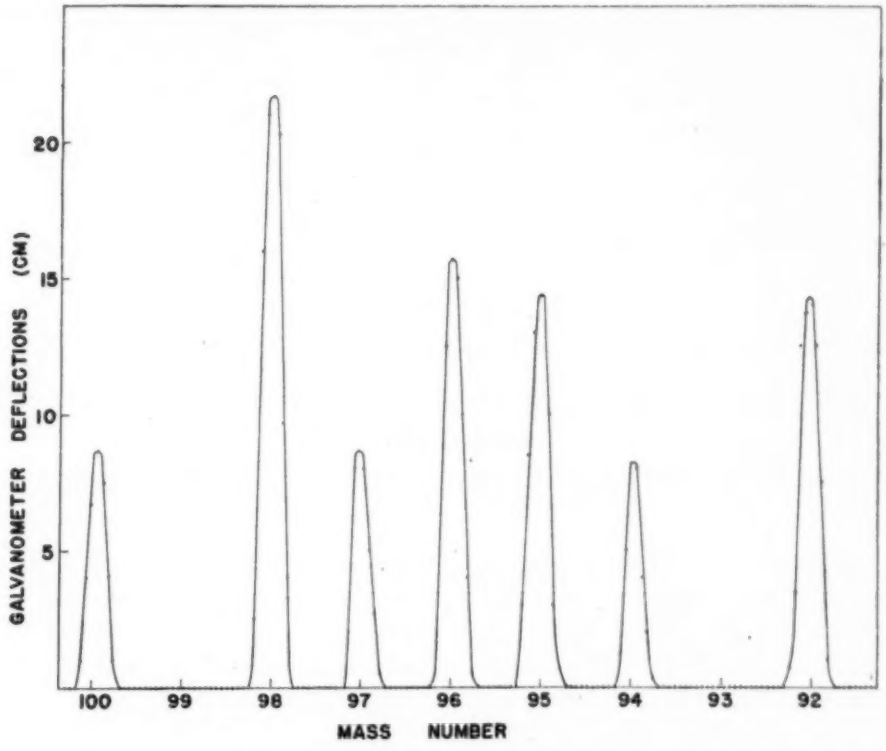

FIG. 6. Mass spectrum in the vicinity of the Mo^+ ion. The peak at mass position 98 corresponds to a beam current of 1×10^{-11} ampere.

parable magnitude were observed at other mass positions.

The results obtained on isotopic abundance are given in Table VI. Data are shown for two different conditions of pressure and spectrometer "tuning." Agreement between the two sets of data is fair. However, it would have been desirable to obtain data on another ion for purposes of comparison. It is believed that the values for isotopic abundance are accurate to ±2 percent. In the last column are shown the atomic percentages of the various isotopes as determined by Aston and Dempster. Agreement is good for isotopes 186 and 184 and rather poor for 183 and 182. In the case of the rare isotope 180, there is excellent agreement between the present results and Dempster's original estimate of its abundance as one percent of that of 183.

A search was made for isotopes of mass 179, 181, 185, and 187. No peaks were observed at these mass positions, although peaks of 1/10,000 that at mass position 184 could have been detected.

The packing fraction for tungsten has been measured by Aston,[18] who obtained a value of +1.7, and more recently by Dempster,[19] who reported a packing fraction of approximately +2. On the basis of a packing fraction of +2, the data obtained in the present study lead to a value of 183.88 for the chemical atomic weight. This value is in fair agreement with the currently accepted value of 183.92.

MOLYBDENUM

Previous measurements on the relative abundance of the molybdenum isotopes were made by Aston,[20] de Gier and Zeeman,[21] Mattauch and Lichtblau,[22] and Valley.[23] Their values will be found in Table VIII.

[18] F. W. Aston, Proc. Roy. Soc. **A132**, 491 (1931).
[19] A. J. Dempster, Phys. Rev. **53**, 64 (1938); **53**, 869 (1938).
[20] F. W. Aston, Proc. Roy. Soc. **A130**, 308 (1931).
[21] J. de Gier and P. Zeeman, Proc. Roy. Acad. Amst. **39**, 327 (1936).
[22] J. Mattauch and H. Lichtblau, Zeits. f. physik. Chemie **42**, 288 (1939).
[23] G. E. Valley, Phys. Rev. **57**, 1058 (1940).

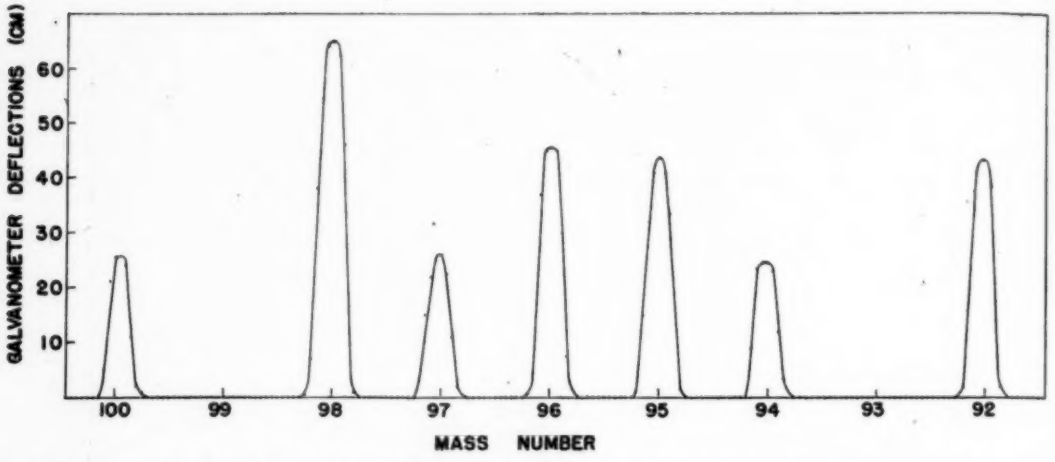

FIG. 7. Mass spectrum in the vicinity of the Mo^{++} ion. The peak at mass position 98 corresponds to a beam current of 2.5×10^{-13} ampere.

The material used in the present work was molybdenum hexacarbonyl vapor. As in the case of tungsten hexacarbonyl, it was found that bombardment of the vapor by 100-volt electrons produced the singly charged metallic ion (Mo^{+}) in greater abundance than other singly charged positive ions. The quantity of doubly charged mercury ions produced in vapor from the diffusion pump was not sufficient to introduce difficulties in measuring the Mo^{+} peaks. In fact, with liquid nitrogen as a trap refrigerant, even the magnitude of the peaks due to singly charged mercury ions was small compared to the molybdenum peaks. However, in order to be certain that no spurious effects were caused by doubly charged mercury ions, abundance measurements on molybdenum were repeated for the Mo^{++} ions.

The mass spectrum observed in the vicinity of the singly charged molybdenum ion is shown in Fig. 6. Resolution seems to be adequate for abundance measurements. No background is visible at mass position 99 which can be attributed to $(Hg^{198})^{++}$ nor was a peak observed at mass position 101 where $(Hg^{202})^{++}$ ions would appear if present in measurable quantity. The mass spectrum in the vicinity of the doubly charged molybdenum ion is shown in Fig. 7. Here, again, the resolution is satisfactory and no spurious background effects are apparent.

The data obtained for isotopic abundances are given in Table VII. Each value shown in the table represents the average of at least four careful determinations. Agreement between the data obtained from measurements on Mo^{+} and Mo^{++} is fair. The final values for isotopic abundance are shown in Table VIII for purposes of comparison with the results of other investigations. It is believed that the abundances obtained in this study are accurate to ±1 percent. If isotopes other than those listed in the table exist, they are present to less than 1/10,000 of the abundance of isotope 98.

It will be noted from Table VIII that the values for relative abundance as determined in

TABLE VII. Relative abundance of molybdenum isotopes as determined from molybdenum carbonyl.

	Measured abundance from indicated ion		
Isotope	Mo^{+}	Mo^{++}	Average
100	40.4	40.5	40.5
98	100.0	100.0	100.0
97	40.0	39.7	39.8
96	69.8	69.2	69.5
95	66.5	65.7	66.1
94	38.4	37.6	38.0
92	66.8	66.4	66.6

TABLE VIII. Relative abundances of molybdenum isotopes.

	Aston	Mattauch	Valley	Present study
100	42.6	33.8	38.4	40.5
98	100	100	100	100
97	41.7	34.2	40.0	39.8
96	77.4	66.1	68.9	69.5
95	67.4	64.2	66.8	66.1
94	43.5	34.3	39.0	38.0
92	61.7	61.0	61.8	66.6

the present study are in fair agreement (within the stated limits of error) with Valley's results for all isotopes except 100 and 92. In the case of isotope 100, the difference amounts to approximately 5 percent; for isotope 92 the difference is 7 percent. These differences are well beyond the limits of experimental error and could be accounted for by the presence of impurities. However, the close agreement between the results obtained for Mo^{+} and Mo^{++} ions in the present work would seem to preclude the possibility of large amounts of impurities. The large differences between the present results and Valley's results for isotopes 100 and 92 indicate that further work on molybdenum would be desirable.

The packing fraction for molybdenum has been measured by Dempster[24] and by Graves.[25] The value obtained by Graves is -5.5. Use of this value for the packing fraction in connection with the abundances obtained in the present study gives a value of 95.90 for the chemical atomic weight. The International Atomic Weight is 95.95.

BROMINE

Early experiments[26] indicated that bromine consists of the two isotopes 79 and 81 in practically equal proportions. Even careful photometric measurements[27] failed to reveal any differences in the intensity of the two observed lines. However, Blewett[28] by methods involving electrical measurements determined the ratio of 81 to 79 as 0.975 ± 0.025. Blewett's measurements were made on the peaks produced by Br^{+} and Br^{-} ions, and measurements on Br^{++} and Br^{--} ions served as a check.

The present study was undertaken with the purpose of obtaining more accurate data on relative abundance. Since the two bromine isotopes are so nearly equal in abundance, instrumental errors produced by small variations in the grid resistor with ion current are negligible and high precision is readily obtainable. As the resolving power of the spectrometer used in this work was higher than that of the instrument used by Blewett, it was possible to make measurements on the Br_2^{+} peaks as well as on the Br^{+} and Br^{++} peaks.

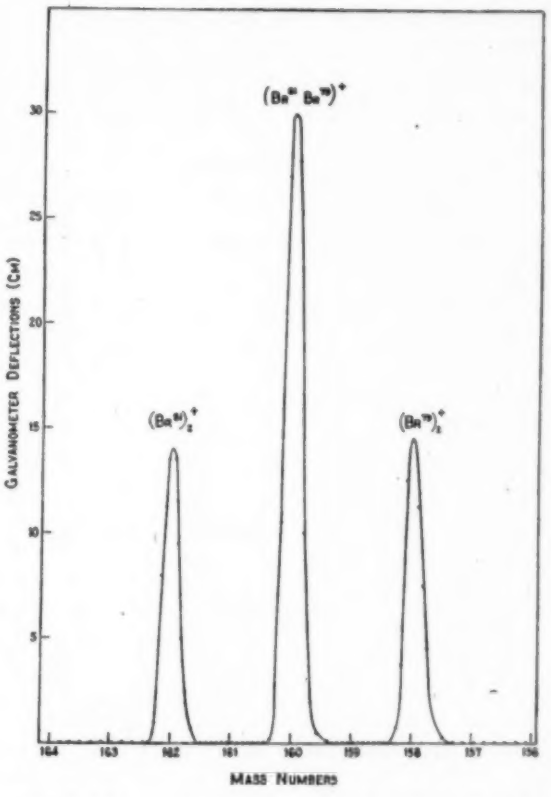

FIG. 8. Mass spectrum in the vicinity of the Br_2^{+} ion. The peak at mass position 160 corresponds to a beam current of 1.5×10^{-11} ampere.

There are obvious advantages in determining isotopic abundance from measurements of the Br_2^{+} peaks. If N_{79} and N_{81} are the numbers of atoms of Br^{79} and Br^{81} present in a given sample, the numbers of molecules of type $(Br^{79})_2$, $(Br^{79}Br^{81})$, and $(Br^{81})_2$ are

$$\frac{N_{79}^2}{2(N_{79}+N_{81})}, \quad \frac{N_{79}N_{81}}{N_{79}+N_{81}}, \quad \text{and} \quad \frac{N_{81}^2}{2(N_{79}+N_{81})},$$

respectively. Hence, the ratio of atomic abundance will be equal to the square root of the measured ratio of $(Br^{79})_2^{+}$ and $(Br^{81})_2^{+}$ peaks. The effects of random errors of measurement are reduced accordingly. Abundances determined in this manner can be checked by comparisons of $(Br^{79})_2^{+}$ and $(Br^{81})_2^{+}$ peaks with the $(Br^{79}Br^{81})^{+}$ peak. With the spectrometer used, these measurements could all be performed satisfactorily.

Two samples of bromine were used in the

[24] A. J. Dempster, Phys. Rev. **53**, 64 (1938).
[25] A. C. Graves, Phys. Rev. **55**, 863 (1939).
[26] F. W. Aston, Phil. Mag. **40**, 631 (1920).
[27] F. W. Aston, Proc. Roy. Soc. **A132**, 489 (1931).
[28] J. P. Blewett, Phys. Rev. **49**, 900 (1935).

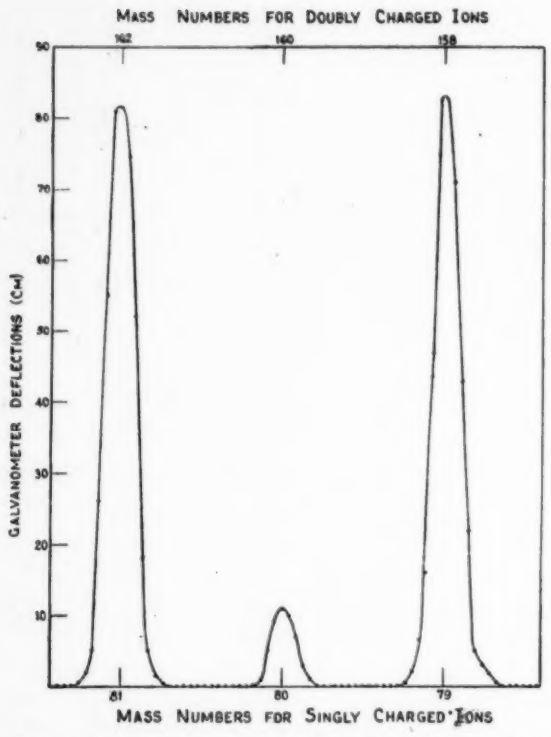

FIG. 9. Mass spectrum in the vicinity of the Br^+ and Br_2^{++} ions. The peak at mass position 79 corresponds to a beam current at 1×10^{-11} ampere.

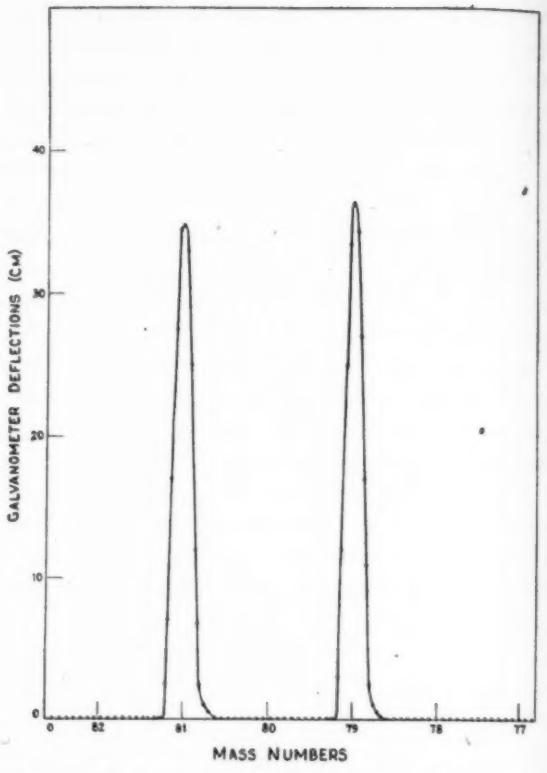

FIG. 10. Mass spectrum in the vicinity of the Br^{++} ion. The peak at mass position 79 corresponds to a beam current of 1.5×10^{-12} ampere.

present work. One of these was prepared under vacuum by a reaction between anhydrous cobaltic fluoride and potassium bromide. The other was a Baker's product, which was subjected to prolonged pumping at dry ice temperatures in order to remove possible traces of HBr. No peaks attributable to HBr were observed in ions from either sample.

The mass spectrum obtained in the vicinity of the Br_2^+ ions is shown in Fig. 8. The spectrum has the general appearance to be expected on the basis of previous results. The peaks are sufficiently well resolved for satisfactory abundance measurements, and no background effects could be detected.

In Fig. 9 is shown the spectrum obtained in the vicinity of the Br^+ ion. Large peaks were observed at mass positions 79 and 81, while a small peak was observed at mass position 80. Since ions of the type Br_2^{++} have the same m/e as the Br^+ ions, it was suspected that the peak at mass position 80 was actually due to ions of the type $(Br^{81}Br^{79})^{++}$. Accordingly, the observed magnitudes of the $(Br^{79})^+$ and $(Br^{81})^+$ peaks were subjected to appropriate corrections for $(Br^{79})_2^{++}$ and $(Br^{81})_2^{++}$ before abundances were calculated.

In order to check the above explanation of the small peak shown in Fig. 9 as well as to obtain further data on abundance, the spectrum in the region of the Br^{++} ion was carefully investigated. As the diatomic ion of equal m/e is Br_2^{++++} and as the probability of the formation of such an ion is slight, only two peaks were to be expected in this region. In Fig. 10 the observed mass spectrum is shown. The only peaks observed corresponded to ions of the type $(Br^{79})^{++}$ and $(Br^{81})^{++}$.

TABLE IX. Determinations of relative abundance of bromine isotopes. Weighted mean value for ratio 81/79 $=0.979\pm0.004$.

Type of ion	Peaks compared	Number of determinations	Ratio 81/79
Br_2^+	162, 158	80	0.980 ± 0.002
Br_2^+	162, 160	28	0.974 ± 0.002
Br_2^+	160, 158	28	0.982 ± 0.004
Br^+	81, 79	12	0.978 ± 0.002
Br^{++}	81, 79	16	0.974 ± 0.002

In Table IX is a summary of the results obtained from measurements on various ionic species. Values obtained from the data on different types of ions are in fair agreement. The final value for the abundance of Br^{81} relative to Br^{79} is 0.979 ± 0.004. No isotopes except 79 and 81 were detected. If isotopes 78, 80, or 82 exist, their abundance is less than 1/10,000 that of isotope 79.

The most recent figure[29] for the packing fraction of bromine is -7.4. In connection with this value the data obtained in this study give a value of 79.908 for the chemical atomic weight. The accepted international value is 79.916.

[29] F. W. Aston, Nature **141**, 1096 (1938).

ACKNOWLEDGMENT

The writers wish to express their appreciation to Dr. K. T. Bainbridge for his helpful discussion of the manuscript and to Mr. R. J. Watts for assistance in connection with electronic equipment.

PHYSICAL REVIEW VOLUME 69, NUMBERS 11 AND 12 JUNE 1 AND 15, 1946

Note on the Lifetime of Metastable States*

MARCELLUS L. WIEDENBECK**
Department of Physics, University of Notre Dame, Notre Dame, Indiana
(Received February 27, 1946)

The available data on approximately forty γ-emitting metastable states of isomeric nuclei has been compared with the present theories. Nearly all of the points lie near two straight lines when log λ (sec.$^{-1}$) is plotted against log E (Mev). These lines fall close to the theoretical curves of Bethe calculated for electric 2^4 and 2^5 pole radiation.

INTRODUCTION

SINCE the original proposal of the existence of metastable states by von Weizsacker,[1] several theories have been developed which relate the lifetime of a metastable state against γ-emission to the energy of this state. Included in these are the calculations on the liquid droplet model by Bethe,[2] Lowen,[3] Flügge,[4] Fierz,[5] and Koyenuma.[6] Calculations of the lifetime energy relationship have also been worked out on the basis of an alpha-particle moving in a potential well by Hebb and Uhlenbeck[7] and by Segrè.[8] Several of these theories have recently been discussed by Berthelot.[9] In addition, a correction of the earlier formulae has been proposed by Hebb and Uhlenbeck to take into account the additive decay probability brought about by internal conversion. This correction factor $[1+(N_e/N_\gamma)]$, where N_e/N_γ is the ratio of the number of conversion electrons emitted to the number of γ-rays emitted, becomes extremely important at low energies and approaches unity for high energies. It should be noted, however, that the lifetime relationships are meant merely as approximations and should, therefore, be expected to give only the order of magnitude of the lifetime as a function of the energy. In addition to this, the important ratio N_e/N_γ has been calculated only for low atomic numbers.

EXPERIMENTAL DATA

In Fig. 1 we have plotted the log of the decay constant *vs.* log of the energy of the metastable state for the states thus far studied. This includes nuclei in which the ground state is stable as well

* Some of these results have been presented at the St. Louis meeting of the American Physical Society, November 30, 1945.

** Now at the University of Michigan.

[1] C. F. von Weizsacker, Naturwiss. **24**, 813 (1936).
[2] H. A. Bethe, Rev. Mod. Phys. **9**, 226 (1937).
[3] I. S. Lowen, Phys. Rev. **59**, 835 (1941).
[4] S. Flügge, Ann. d. Physik **39**, 373 (1941).
[5] M. Fierz, Helv. Phys. Acta **16**, 365 (1943).
[6] N. Koyenuma, Zeits. f. Physik **117**, 358 (1941).
[7] M. H. Hebb and G. E. Uhlenbeck, Physica **5**, 605 (1938).
[8] E. Segrè, given by A. C. Helmholtz, Phys. Rev. **60**, 415 (1941).
[9] A. Berthelot, Ann. d. Physique **19**, 117 (1944).

as those which are unstable. Although all of the points do not fall on the lines, most points fall into two general regions about the lines which have been drawn. Such a spread should, of course, be expected on two accounts. First, the value of N_e/N_γ is a function of the atomic number Z, second, the data were obtained by many different experimenters, using various methods for determining the energy of the metastable level. From the various reports one sometimes finds considerable experimental deviations in the results obtained. Notable deviations from the two major regions may be found in the cases of 43^{99} (6.6 hr. period), Cd* (48.7 min. period), and Sr^{85} (70 min. period). These three points (dotted in diagram) fall midway between the regions. As such, they cannot be assigned to either region with any degree of certainty. The line $L=4$ corresponds to an electric 2^4 pole (or magnetic 2^3 pole) radiation and can be empirically represented by the equation:

$$\lambda = 42E^{3.67}.$$

Correspondingly, the line $L=5$ for electric 2^5 pole radiation can be represented by:

$$\lambda = 45.8\times 10^{-5}E^{3.67}.$$

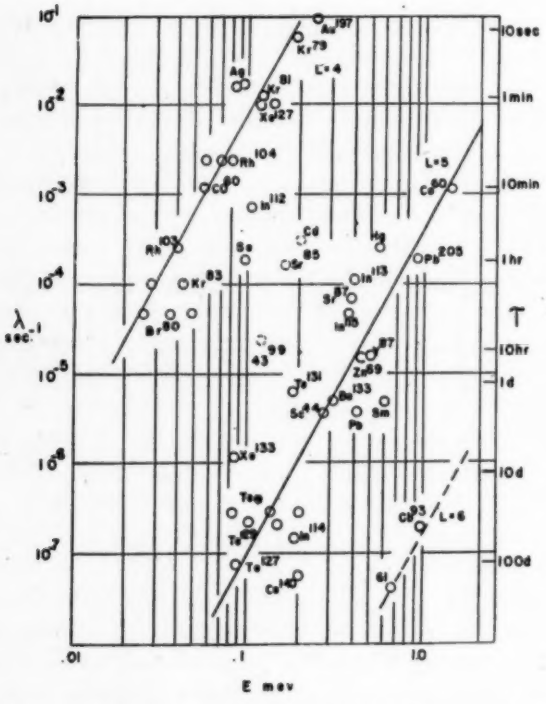

FIG. 1. Log λ *vs.* log E. $L=4$ and $L=5$ correspond to electric 2^4 and 2^5 pole radiation, respectively.

Two points fall considerably below the line $L=5$ and may possibly represent transitions in which the spin change is 6 units; these are owing to Cb^{93*} (half-life$\sim$40 days) and element 61 (half-life$\sim$200 days). This is highly uncertain at the present time.

In a few cases several γ-ray energies are reported for a given activity. These may arise from a cascade process in the decay of the metastable state to an intermediate level. As such, it is not immediately possible to determine which is the metastable transition energy. These energies are thus plotted on the same horizontal line in Fig. 1. In fact, Columbium might well belong to the group $L=5$ since two γ-ray energies are reported; namely, 0.15 Mev[10,11] and 0.94 Mev.[10] A second case of interest is $Cobalt^{60}$ (half-life 10.7 minutes) which emits γ-rays of energy 0.056 and 1.5 Mev. The first of these points falls on the curve for $L=4$ while the second falls on the curve $L=5$.

COMPARISON OF EXPERIMENTAL DATA WITH THEORY

In Fig. 2 we have plotted several of the life-time-energy relationships along with the experimental line $L=4$ from Fig. 1. Line 1 represents Bethe's uncorrected formula for a spin change $L=3$; line 2—Bethe's value with $L=4$ corrected for internal conversion; line 3—experimental; line 4—Bethe's uncorrected value with $L=4$; line 5—Lowen's value corrected for internal conversion; line 6—Lowen's uncorrected value; line 7—Flügge's value; line 8—Hebb and Uhlenbeck's value calculated on the alpha-particle model; line 9—Bethe's uncorrected value for $L=5$.

Figure 3 shows similar relationships for a spin change of 5 units.

From these diagrams one can clearly see that the corrected values of Bethe and Lowen correspond to the data most closely. It may also be noted that the internal conversion correction of

[10] W. N. Moquin and M. L. Pool, Phys. Rev. **65**, 60 (1944).

[11] R. Sogane, S. Kojima, G. Miyamoto, and M. Ikawa, Phys. Rev. **57**, 1180 (1940).

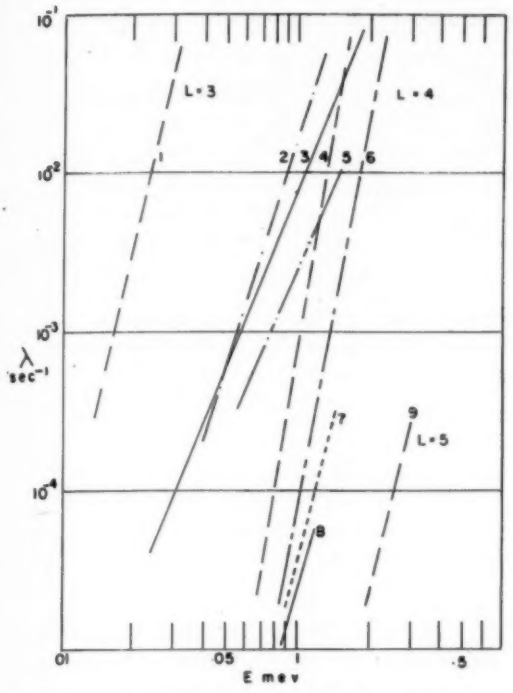

FIG. 2. Comparison of experimental data with several of the theories.

1. Bethe—uncorrected with $l=3$.
2. Bethe—corrected with $l=4$.
3. Experimental.
4. Bethe—uncorrected with $l=4$.
5. Lowen—corrected with $l=4$.
6. Lowen—uncorrected with $l=4$.
7. Flügge with $l=4$.
8. Hebb and Uhlenbeck with $l=4$.
9. Bethe—uncorrected with $l=5$.

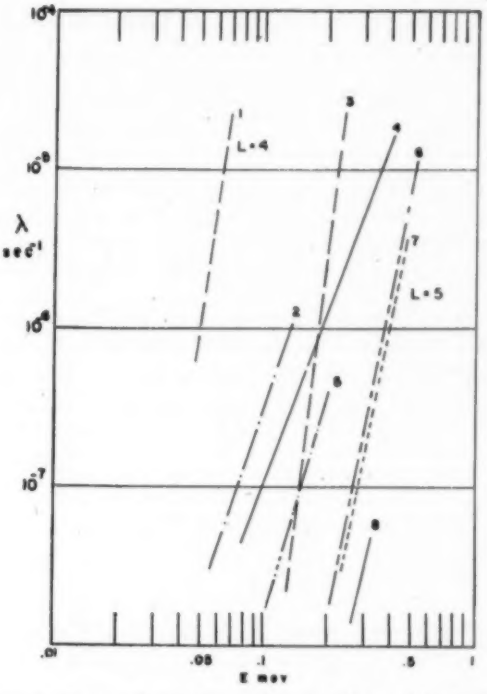

FIG. 3. Comparison of experimental data with theory.

1. Bethe—uncorrected with $l=4$.
2. Bethe—corrected with $l=5$.
3. Bethe—uncorrected with $l=5$.
4. Experimental.
5. Lowen—corrected with $l=5$.
6. Lowen—uncorrected with $l=5$.
7. Flügge with $l=5$.
8. Hebb and Uhlenbeck with $l=5$.

Hebb and Uhlenbeck not only increases the agreement in absolute value but also changes the directions of the curves so as to make the experimental and theoretical curves nearly parallel.

The spin change in such a transition can be obtained independently in some cases by determining the conversion coefficient[12–14] and the ratio of K conversion to L conversion. This has been done for several such transitions by Helmholtz.[15]

It has been possible to determine the multipole order of the transitions with a good degree of accuracy for four isotopes ($Zn^{69}(L=5)$, $Kr^{83}(L=4)$, $Sr^{87}(L=5)$, $Ag^{*}(L=4)$). In four other cases the transition order can only be assigned as probable ($Sc^{44}(L=5)$, $Te^{127}(L=5)$, $Te^{129}(L=5)$, $Te^{131}(L=5)$). In all cases these isotopes fall on the correct line in Fig. 1. However, it is not possible to distinguish between electric 2^l pole and magnetic 2^{l-1} pole radiation.

Thus far, no metastable state with $L=3$ has been studied. One might expect, however, that they should occur quite frequently. If such metastable states of reasonably long lifetime exist, it is seen that their energy is extremely low ($\sim$10 to 20 kv) and hence will not be accompanied by conversion. With the extension of techniques to study periods of 10^{-2} second and less, one could obtain conversion electrons which could easily be detected.

[12] M. H. Hebb and E. Nelson, Phys. Rev. **58**, 486 (1940).
[13] S. M. Dancoff and P. Morrison, Phys. Rev. **55**, 122 (1939).
[14] G. Goertzel and I. S. Lowen, Phys. Rev. **67**, 203 (1945).
[15] A. C. Helmholtz, Phys. Rev. **60**, 415 (1941).

The β-Radiations of Uranium X_1*

SWAMI JNANANANDA
The Harrison M. Randall Laboratory of Physics, University of Michigan, Ann Arbor, Michigan
(Received January 12, 1946)

An investigation of the distribution with momentum of the β-rays of uranium X_1 has been made by analyzing them with the magnetic electron lens spectrometer. The results are recorded by an electrical counter detection and mechanical recorder in the range between $H\rho<650$ and $H\rho>1875$. The lower limit of the range is limited by the window of the detecting device. The results of the experimental records $N/H\rho$ are plotted against $H\rho$ and the plot represents the normalized energy spectrum. In the continuity of the spectrum there is a clear evidence of three distinct peaks. The energy values of these peaks which represent three groups of β-rays due to internal conversion agree with those obtained by Meitner. The spectrogram shows that the end point of the continuous UX_1 β-ray spectrum is at $H\rho$ 1617 (189.9 kev), a value which agrees with those that are obtained by absorption method but differs considerably from Marshall's value obtained by the method of the expansion chamber. The present value, unlike that of Marshall, gives a point on the Sargent diagram nearly on the curve of allowed transitions.

1. INTRODUCTION

THE disintegration of uranium X shows β-activity with an emission of soft γ-rays which give rise to a few homogeneous groups of β-rays due to internal conversion. These β-groups were investigated by von Bayer, Hahn, and Meitner.[1] Their energy spectrum, showing well-defined lines—each indicating the energy limit of one of these groups—was measured by Meitner.[2]

In the decay process of uranium X_1, of the total β-ray emission, the characteristic β-rays are only a part, the essential portion, whose emission leads to a change in the nuclear charge and thus in the atomic number of the element, being the actual disintegration β-particles. These nuclear β-rays have velocities that vary over a wide range as first demonstrated by Chadwick.[3] An investigation of the distribution of these disintegration electrons as a function of energy or $H\rho$ should prove very useful in finding the upper limit of the kinetic energy carried by them. This datum is important, since it gives the total disintegration energy of this radioactive material.

2. EARLY EXPERIMENTS WITH UX_1 BY ABSORPTION METHODS AND THEIR RESULTS

The earliest experiments with uranium X, by absorption methods, were done mainly for finding the absorption coefficients of the uranium X β-rays in different materials. From the data and the absorption curves, obtained by Levin,[4] Schmidt,[5] and Fajans and Gohring,[6] it is possible to have some information concerning the maximum energy of the UX_1 disintegration electrons. It is of course difficult to interpret these curves with the degree of certainty necessary for precisely ascertaining the range. It may, however, be estimated and this, by the range/momentum law of Marshall and Ward,[7] may give the end point half-way between $H\rho$ 1400 and 1850. The value of the absorption coefficients for UX_1 β-rays in aluminum so found, on applying the empirical relation of Chalmers,[8] gives the end point of $H\rho$ 1640. Thus in the former there is some uncertainty, while the latter result involves an empirical rule. This method is an indirect one, but the results of its application in most of the other cases used, on comparing with those obtained by magnetic analysis, are found to be satisfactory.

3. THE USE OF AN EXPANSION CHAMBER TO INVESTIGATE UX_1 β-RAYS

An expansion chamber is also employed for the study of β-rays. In this method, the tracks of the β-particles are photographically recorded and from the curvature of the tracks produced by a

* This investigation was carried on at George Holt Physics Laboratories, The University of Liverpool, England.

[1] von Bayer, O. Hahn, and L. Meitner, Physik. Zeits. **14**, 873 (1913).
[2] L. Meitner, Zeits. f. Physik **17**, 54 (1923).
[3] J. Chadwick, Verh. d. D. Phys. Ges. **16**, 383 (1914).
[4] M. Levin, Physik. Zeits. **8**, 585 (1907).
[5] H. W. Schmidt, Physik. Zeits. **10**, 6 (1909).
[6] K. Fajans and O. Gohring, Physik. Zeits. **14**, 877 (1913).
[7] J. Marshall and A. G. Ward, Can. J. Res. **A15**, 39 (1937).
[8] J. A. Chalmers, Proc. Camb. Phil. Soc. **28**, 319 (1932).

magnetic field, a continuous distribution with velocity is found. For the investigation of the UX β-radiations, this method has been applied by Lecoin[9] and subsequently by Marshall.[10] Lecoin in his experiment used a thin UX source in an expansion chamber and as he found no UX peak in the distribution he obtained, he came to the conclusion that the end point was below $H\rho$ 1115 (100 kev). Marshall,[10] employing an expansion chamber containing hydrogen or helium at atmospheric pressure with ethyl alcohol vapor, with particular regard to momentum values below $H\rho$ 2000, has investigated the distribution with momentum of the UX_1 β-rays. He has found that these rays extend at least to $H\rho$ 1950, a value which differs very much from the one obtained from the mass absorption coefficient for UX_1 β-rays in aluminum by Chalmer's relation.[8]

In the cloud-chamber experiments, the measurements involve the selection of the tracks unaffected by scattering and in the absence of definite and strictly quantitative criterion for rejecting those β-ray tracks whose curvatures have been appreciably affected by scattering, the precision of the results is probably somewhat questionable. With high energy β-particles, an experiment employing a cloud chamber with air replaced by light gas may give satisfactory results provided a large number of particles are registered and the selection of the tracks which have not been appreciably affected by scattering is not faulty. The evidence obtained from the cloud-chamber experiment is liable to be less reliable, especially when the variation of the efficiency of registration of tracks with velocity during the time of expansion is not carefully investigated.

4. DIRECT METHODS OF ANALYSIS AND THE UX_1 ENERGY SPECTRUM

An investigation of the UX_1 β-rays by one of the two direct methods in vogue which gives the entire energy spectrum, showing the end point, should therefore prove very fruitful. Of these two, the first consists in analyzing the β-rays with the usual semi-circular focusing in a magnetic field and detecting the results by an electrical method. The second consists in analyzing them with the magnetic electron lens or with the electrostatic lens selective focusing and recording the results by the devices of detection and automatic registration.

A detailed and reliable record of the energy spectrum of UX_1 is important for considering its actual form and end point which gives the total disintegration energy. With improved data obtained in this way, the form of the continuous spectrum can be ascertained and the position of the end point on the original Sargent[11] diagram can be determined to test the other results and especially the latest one obtained by the cloud-chamber method[10] which has given an end point far to the right of the curve of allowed transitions.

5. EXPERIMENTAL ARRANGEMENT

In the present experiment, a thick magnetic electron lens β-ray spectrometer has been employed with a source of UX_1 of adequate strength and purity to investigate the energy spectrum from $H\rho < 650$ to $H\rho > 1875$, the lower end of the region being limited by the window of the detecting device.

The spectrometer, as explained elsewhere in detail,[12] is designed on the geometrical model of electron trajectories in a standard field, obtained from the determinants of their parameters and radial displacements. The design admits about 5 percent of 4π in solid angle of β-rays from the source into the field of the selective focusing action. The spectrometer, with a source holder on one end and an electrical counter on the other and with different component parts assembled together, is mounted in the body of a magnetic electron lens system, as shown in Fig. 1. This system is comprised of seven air-core, multi-layer straight solenoids, each 5 cm long, connected together in series and mounted on a cylindrical brass tubing about 12 cm in diameter and 50 cm in length. The spectrometer is fixed in the part of the lens body where the magnetic field is nearly homogeneous and axially symmetrical so that the lens system and the spectrometer are perfectly coaxial. The electron lens system with the spectrograph mounted in it is so adjusted as to let its axis be in alignment with the earth's magnetic lines of force.

[9] M. Lecoin, J. Phys. Rad. 9, 81 (1938).
[10] J. S. Marshall, Proc. Roy. Soc. A173, 391 (1939).
[11] B. W. Sargent, Proc. Roy. Soc. A139, 659 (1933).
[12] S. Jnanananda, Liverpool University, Ph.D. thesis, 1943.

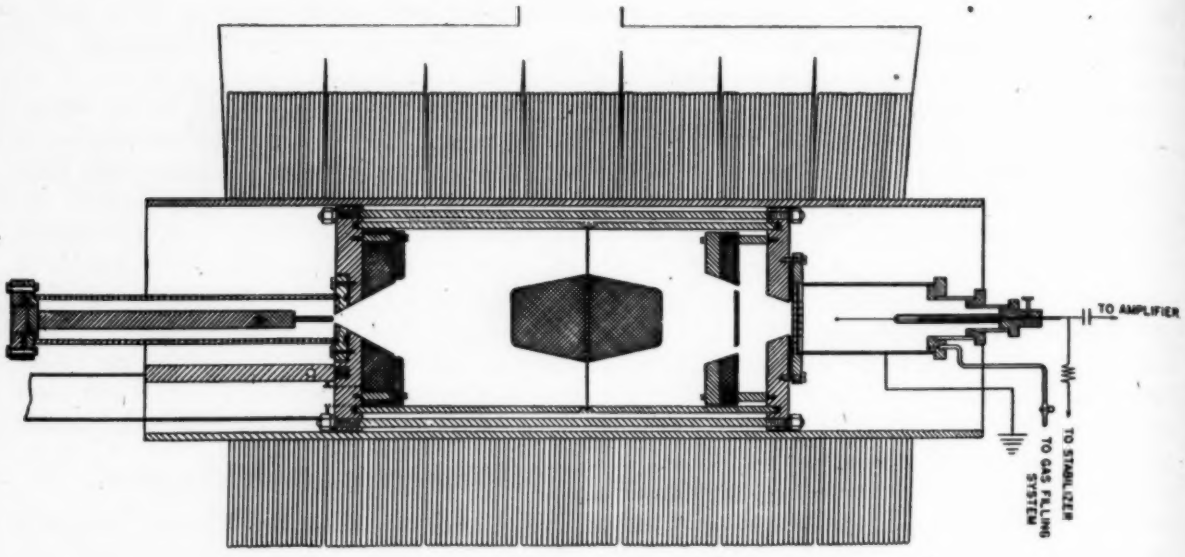

FIG. 1. Thick magnetic electron lens beta-ray spectrometer.

The spectrometer and the source chamber are exhausted to a pressure of nearly 10^{-5} mm of mercury by means of a single stage apiezon oil diffusion pump backed by a rotary pump.

Electrical power for the solenoids is supplied from 110-volt accumulators. The variation of the magnetizing current is effected by potentiometer control and the current at each variation is measured by a calibrated shunt connected to an ammeter. The current is constant to within one in at least two thousand parts during each short interval of operation at the end of which the necessary records are made.

The electrical counter, fixed at the end of the spectrometer, opposite to the source holder chamber, is used to detect the β-ray spectrum. Power necessary for the operation of the counter is applied from a neon valve stabilizer. This counter is provided with an amplifier, a scale of sixteen, and a thyratron operated mechanical recorder. This equipment is provided with H.T. of 230 volts from an eliminator.

6. CALIBRATION OF THE MAGNETIZING COIL CURRENT IN TERMS OF $H\rho$

In a magnetic electron lens β-ray spectrometer, the position of the source and that of the focal region, where an electrical counter is placed, are fixed so that β-rays of a particular velocity are focused at the effective region of the counter by the action of its corresponding field of force of the magnetic electron lens. This definite field of force can be determined by calibrating the magnetizing current in terms of $H\rho$ of a measured β-line. The calibration has been done by experimentally determining the magnetizing coil current which corresponds to the peak of the accurately measured[13] F-line of thorium B. It has been found that a magnetizing current of 2.4 amp. corresponds to the peak of the chosen reference line at $H\rho$ 1385.6.

7. EXPERIMENTAL PROCEDURE

A circular foil of platinum, 3 mm in diameter, with one of its surfaces having a deposit of uranium X_1 uniformly spread on it, is mounted and fixed on the tip of a brass rod. This brass rod, with its source carrying end, is screwed on a holder which is fixed in the source chamber so that the center of the foil lies on the axis of the spectrometer and the platinum surface with the

TABLE I. Relative strengths of the source used for different energy ranges.

Relative strength	Momentum range ($H\rho$)
11.9	From 600 to about 860
10.0	From 860 to about 1000
1.4	From 1000 to about 1150
1.3	From 1150 to about 1300
1.1	From 1300 to about 1560
1.0	From 1560 to about 1875

[13] C. D. Ellis, Proc. Roy. Soc. **A138**, 318 (1932); K. C. Wang, Zeits. f. Physik **87**, 633 (1934).

active deposit of UX_1 at the very threshold in front of the entrance aperture. After these arrangements, the spectrometer with the source chamber is exhausted to the limiting pressure.

Then the effect in the counter without the focusing action of the magnetic electron lens has been recorded. The counter record has been taken as a measure of the intensity of the source. With such counter records, the relative intensities of the source used at different times have been estimated. Also for a magnetizing coil current of 1.5 amp., the different sum total effects in the counter, for the different times the active source is used for investigation, have been recorded to verify the results obtained by the former method. There has been a fair agreement between the estimations of the intensities of the source obtained by these two methods. The mean value of the results of these two kinds of estimations is taken as the actual relative strength of the source, each time it is used for investigation. In this way, accidental errors and those arising out of statistical fluctuations are minimized in the determination of the relative intensities of the source. After the estimation of the relative intensity of the source, the magnetizing current has been applied and has been gradually raised at precisely regular intervals in steps of 12.5 ma from the lower limit up to the upper limit of the momentum range. At each step of the coil current and at the end of each interval, the counter reading corresponding to the magnetizing current applied during that interval has been recorded. In this way the spectrum of UX_1, with the source in different strengths at various ranges, has been measured by means of counter records (Table I).

Each one of the series of counter records which corresponds to one of the ranges, given in Table I, has been individually corrected for decay. The different spectrometrical data thus obtained with different relative strengths of the source have been reduced to those of the intensity of the source which is arbitrarily taken as a standard.

TABLE II. Data on three line groups.

Number of the line	Origin	Relative intensity	log $H\rho$	$H\rho$	Energy (kev)
I	L_1	10	2.96561	924	70.3
II	M_1	6	3.01069	1025	85.3
III	N_1	1	3.01977	1047	89.9

From these corrected series of counter impulse frequency records of the source of standard strength and their corresponding values of the magnetizing coil current in terms of $H\rho$, obtained by the experimental determination of the coil current corresponding to the F-line of thorium B at $H\rho$ 1385.6, the $N/H\rho$ values have been obtained for the entire measured momentum range $(600<H\rho-1875<H\rho<2000)$ of the β-particles of this source of the chosen standard strength. These values of $N/H\rho$ are plotted against those of their corresponding $H\rho$.

8. THE SECONDARY AND THE PRIMARY β-RAY SPECTRUM OF UX_1

The plot shown in Fig. 2 represents the curve of the distribution with momentum of the UX_1 β-rays. In the continuity of the spectrum there is a clear evidence of three distinct β-groups. The data of these three groups are given in Table II and for comparing them with those that are obtained by Meitner,[2] the two data are given in Table III.

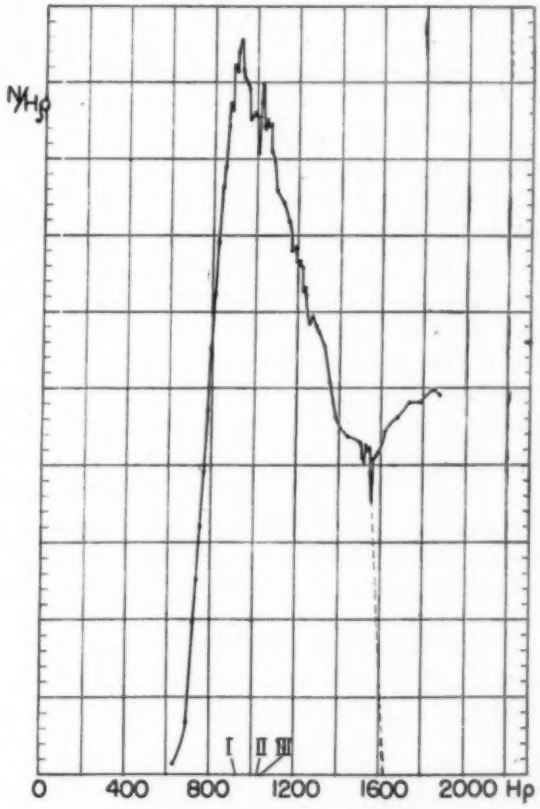

FIG. 2. Energy spectrum of uranium X_1.

From Table III, it is obvious that the present energy values of the β-lines agree with those of the same lines obtained by Meitner. The $N/H\rho$-values, plotted in the graph (Fig. 2), are not corrected for the relative absorption of the β-particles by the counter window. The β-particles of below $H\rho$ 650 are greatly cut off by the counter window. So, the low energy end-point of the continuous spectrum cannot be ascertained. The influence of the counter window on β-particles of over $H\rho$ 900 is, in consideration of the thickness of the window, so trivial that the values of the relative intensities of the β-lines given in the Table II, within the limits of experimental errors, may be regarded as being inappreciably affected.

An inspection of the distribution curve in Fig. 2 shows that it rises up to a maximum with three distinct off-shoots, representing three homogeneous groups of β-rays due to internal conversion. It then falls down at first abruptly, then gradually with a series of kinks beginning from $H\rho$ 1170 to $H\rho$ 1270 which indicates groups of weak energy lines. The curve then sinks down abruptly to a minimum, representing the end point of UX_1, from whence it rises again first abruptly and then gradually. The first part of the curve up to the second minimum represents the energy spectrum of UX_1 β-rays with its upper end point overlapped by the low energy part of the (UX_2+UZ) continuous β-spectrum. A line projected in the direction of the upper end at the second minimum intersects the momentum axis. This point of intersection indicates the upper limit of the continuous UX_1 β-ray spectrum at $H\rho$ 1617 (189.9 kev.).

The value of the end point at $H\rho$ 1617, obtained thus by the present spectrometric method, agrees with the mean value of $H\rho$ 1625, obtained from effective range measurements in aluminum of Levin,[4] Schmidt,[5] and Fajans and Gohring[6] by the range/momentum law of Marshall and Ward.[7] It also agrees with the value of $H\rho$ 1640 obtained

TABLE III. Comparison with Meitner's data.

Number of the line	Meitner's data $H\rho$	Meitner's data Kev	Present data $H\rho$	Present data Kev
I	927	71.0	924	70.3
II	1028	86.2	1025	85.3
III	1057	90.7	1047	89.9

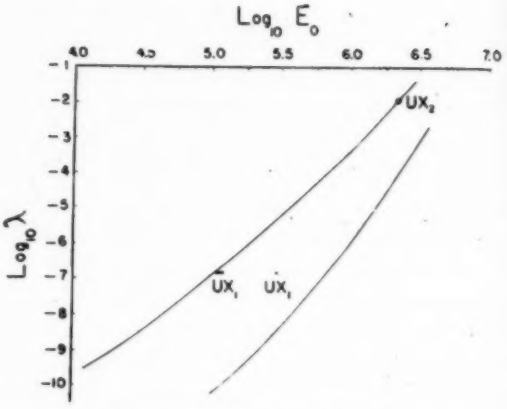

FIG. 3. The Sargent diagram.

from absorption coefficient found for the UX_1 β-rays (about 500 cm Al) by the empirical relation of Chalmers.[8] The present value, however, differs very much from the value $H\rho$ 1950 (265 kev) of Marshall obtained by expansion chamber method.

In this connection it is interesting to note that in almost all cases where the upper end points of continuous spectra have been measured by the three methods, there has been agreement between the values obtained by absorption measurements and those obtained by the magnetic spectral analysis while in most of the cases the results from cloud-chamber measurements have differed from those obtained by the other mentioned methods.

The present value of the end point of the continuous UX_1 β-spectrum, unlike Marshall's value, gives a point on the Sargent diagram, shown in Fig. 3, nearly on the curve of allowed transitions. The present value of UX_1 on the Sargent diagram is indicated by ▲ and the value obtained by absorption measurements by a dot. Marshall's value for the same is indicated also by a dot which is definitely away from the curve of allowed transitions.

It is a pleasure for the author to express his thanks to Sir James Chadwick for the kind interest and many valuable suggestions made during the work. The author also takes this opportunity to express his deep gratitude to Sri Maharaja Sir Narendra Saha Bahadur, the ruling chief of Tehri-Garhwal State (India), who by continued interest in the author's activities has enabled the author to follow philosophic and scientific pursuits and made this work possible.

Production of Mesotrons in the Stratosphere

INGRAM BLOCH
*Department of Physics, The University of Chicago, Chicago, Illinois**
(Received February 27, 1946)

The intensity of the vertically moving ionizing penetrating cosmic-ray particles in the stratosphere is derived as a function of altitude, magnetic latitude, and energy, the purpose being to test the validity of the initial assumptions: that all the cosmic-ray mesotrons have the same mean life at rest of 2.15μsec. and are produced, nine at a time, by primary protons in the fields of air nuclei, that the cross section of an air nucleus for mesotron production by a proton is independent of the proton's energy and is equal to 2.5×10^{-25} cm^2, and that the kinetic energy of a primary proton is divided equally among the total energies of the mesotrons it produces. Comparison of theory and experiment shows that the multiplicity of mesotron production by protons is approximately nine for proton energies above 7×10^9 ev, for a differential energy spectrum of protons, of the form $N_0\mathcal{E}^{-2.9}$, that for proton energies below 7×10^9 ev the multiplicity of mesotron production is lower than nine and the power law energy spectrum is modified, that mesotrons with mean lifetimes much less than 2.15×10^{-6} sec. probably must be postulated to account for the soft component in the stratosphere, and that, as mesotrons are produced, nuclear particles are knocked forward, taking a small fraction of the available energy.

I. INTRODUCTION

THE purpose of this paper is to determine to what extent the observed energy, latitude, and altitude dependence of the penetrating component of cosmic radiation is compatible with the assumption that mesotrons are produced in multiples by primary protons in the fields of atomic nuclei.

That some of the cosmic-ray primaries might be protons was first suggested by Compton and Bethe[1]; later, Johnson[2] concluded from measurements of the east-west asymmetry of the hard component at low altitudes that protons were the primaries of practically all the mesotrons present at sea level. Then Schein, Jesse, and Wollan[3] discovered that there were only very few electrons of energies between 10^9 and 10^{12} ev at very high altitudes, almost conclusively demonstrating that practically all the ionizing primaries of energies greater than about 10^9 ev are protons. According to Schein,[4] only mesotrons of very low energies (about 10^8 ev) are produced by non-ionizing radiation.

The primary differential energy spectrum $p_0(\mathcal{E})=N_0\mathcal{E}^{-2.9}$ used by Euler and Heisenberg[5] is also used here. Its validity, at least for high energies, is indicated by the fact that the energy distribution of many high energy cosmic-ray phenomena seems to follow approximately such a law. Its validity for low energies will be discussed in a later section.

It is assumed that the cross section of an air nucleus for mesotron production by a proton is independent of proton energy for proton energies above about 2.5×10^9 ev; the value of the cross section used, $\sigma=2.5\times10^{-25}$ cm^2, was obtained from the approximate formula,

$$\sigma=\pi r_0^2 Z^{\frac{1}{3}},$$

where Z is the atomic number of air (approximately 8), and r_0, the range of nuclear forces, is 1.4×10^{-13} cm.[6] It is shown in a later section that this assumption is very nearly valid for proton energies above 3×10^9 ev.

Schein, Jesse, and Wollan; Schein, Iona, and Tabin; and Schein and Stroud[7] have measured the number of coincidences involving a counter or counters above a block of lead or paraffin and two or more of a set of counters arranged in a horizontal plane below the block; these measurements were made at high altitudes, and a coincidence of

* Now at Box 1663, Santa Fe, New Mexico.
[1] A. H. Compton and H. A. Bethe, Nature **134**, 734 (1934).
[2] T. H. Johnson, Rev. Mod. Phys. **11**, 208 (1939).
[3] M. Schein, W. P. Jesse, and E. O. Wollan, Phys. Rev. **59**, 615 (1941).
[4] M. Schein, private communication.
[5] H. Euler and W. Heisenberg, Ergeb. d. Exakt. Naturwiss. **17**, 1 (1938).
[6] J. Tabin, Phys. Rev. **66**, 86 (1944).
[7] W. G. Stroud and M. Schein, Phys. Rev. **67**, 62 (1945).

the sort described was attributed to multiple production of mesotrons by a proton. The relative frequencies of two-, three-, and fourfold coincidences in the lower set of counters led Schein to the conclusion that the average multiplicity (i.e., the number of mesotrons produced by a single proton) was in the neighborhood of nine. In the present derivation, multiplicity is set at nine and is assumed to be independent of proton energy for energies above about 2.5×10^9 ev (the geomagnetic cut-off energy at Chicago). Other evidence regarding the multiplicity is discussed in Part III.

Further postulates on which the ensuing analysis is based are that, in the process of mesotron production, the kinetic energy of the primary proton is divided equally among the total energies (rest plus kinetic) of the mesotrons and that the latter all proceed in the direction in which the proton was traveling when it produced them (as indicated by the observed east-west asymmetry of the hard component in moderate altitudes).

The only part of the hard component considered herein is that part which moves vertically. If the direction of motion of each primary proton is perpetuated throughout the path of each mesotron produced by that proton, the derivation of the intensity of the hard component moving in any given direction proceeds in much the same way as the derivation carried out here for vertically moving particles. The soft (nonpenetrating) component of cosmic radiation is not treated here at all; hence no definite conclusion is reached as to whether it is necessary to postulate the existence of rapidly decaying (lifetime of the order of 10^{-9} sec.), so-called "transverse" mesotrons of the type considered by Moeller and Rosenfeld[8] in the theory of nuclear forces. The only mesotrons dealt with here are those whose mean life at rest is $2.15\pm0.07\mu$ sec.[9]; however, considerations mentioned in Section III, 4, make it appear likely that transverse mesotrons are needed to account for the soft component in the stratosphere. The soft component at lower altitudes is, according to Stanton,[10] satisfactorily accounted for by the observed long-lived mesotrons.

[8] M. Moeller and L. Rosenfeld, Kgl. Danske Vid. Sels. Math.-Fys. Medd. **17**, No. 8 (1940).
[9] N. Nereson and B. Rossi, Phys. Rev. **64**, 199 (1943).
[10] H. E. Stanton, Phys. Rev. **66**, 48 (1944).

Derivations of the dependence of the intensity of the mesotron component upon altitude, energy, and latitude have previously been made by Euler and Heisenberg[5] and Rathgeber,[11] and, more recently, by Swann,[12] and Hamilton, Heitler, and Peng.[13] Euler and Heisenberg and Rathgeber assumed that the cosmic-ray mesotrons are all produced by the soft component; this assumption is now pretty well ruled out by the absence of electrons at very high altitudes.[3] Swann made extensive calculations on the assumption that the primaries are heavy charged particles each of which splits up into a number of mesotrons of equal energy. He did not perform the integration over the production region which is here carried out in Section II, 4, and hence could not predict the mesotron distribution at very high altitudes. Hamilton, Heitler, and Peng used primary protons each of which produces many mesotrons in a series of single production processes, multiplicity and effective cross section of an air nucleus being functions of energy. As will be seen in Section III, 4, this picture is not compatible with the results recently obtained by Schein and his collaborators.[7]

II. THEORY

1. Proton Flux as a Function of Altitude

According to the assumptions, the differential proton spectrum at the top of the atmosphere is

$$p_0(\mathcal{E})=N_0\mathcal{E}^{-2.9},$$

where $\mathcal{E}$ is kinetic energy in ergs. Let z_0 be altitude in centimeters; if the stratosphere is assumed to be isothermal, air density at altitude z_0 in the stratosphere is given by

$$\rho(z_0)=\rho_0\exp(-az_0),$$

where

$$\rho_0\equiv1.970\times10^{-3}\text{ g cm}^{-3},$$

and

$$a\equiv1.550\times10^{-5}\text{ cm}^{-1}.$$[14]

Thus, if $p(\mathcal{E},z_0)d\mathcal{E}dz_0$ is the number per cm² sec. unit solid angle of vertically moving protons in dz_0 at z_0 with energies in $d\mathcal{E}$ at $\mathcal{E}$,

$$p(\mathcal{E},z_0)=p_0(\mathcal{E})\exp[-\alpha\exp(-az_0)],$$

[11] H. D. Rathgeber, Phys. Rev. **61**, 207 (1942).
[12] W. F. G. Swann, J. Frank. Inst. **236**, 111 (1943).
[13] J. Hamilton, W. Heitler, and H. W. Peng, Phys. Rev. **64**, 78 (1943).
[14] These values are obtained from tables in Humphreys *Physics of the Air*, and are valid for $T=219°$K.

and

$$\frac{\partial p}{\partial z_0}=p_0(\mathcal{E})a\alpha \exp(-az_0)\exp[-\alpha\exp(-az_0)],$$

where

$$\alpha\equiv\frac{6.03\times10^{23}\times2\sigma\rho_0}{29a}=13.2,$$

$\sigma=2.5\times10^{-25}$ cm² being the proton absorption cross section of an air nucleus.

These results will be seen to depend on the assumption that the protons in question lose no energy by ionizing the air; for protons of energy greater than 10^9 ev, in the stratosphere, ionization loss is practically negligible.

2. Spectrum of Mesotrons at Point of Production

Let $q_0(E_0, z_0)dE_0dz_0$ be the number of vertically moving mesotrons per cm² sec. unit solid angle produced in dz_0 at z_0 with total energies (rest plus kinetic) in dE_0 at E_0. Then, if $\phi(E_0, \mathcal{E})dE_0$ is the number of mesotrons with initial total energies in dE_0 at E_0 produced by a single proton with kinetic energy $\mathcal{E}$,

$$q_0(E_0, z_0)=a\alpha\exp(-az_0)\exp[-\alpha\exp(-az_0)]\int_{\mathcal{E}_0}^{\infty}p_0(\mathcal{E})\phi(E_0, \mathcal{E})d\mathcal{E}; \quad (1)$$

here $\mathcal{E}_0$ is the lowest proton energy present, or the lowest energy at which mesotrons can be produced. It is assumed that the mesotrons travel in the same direction as the proton which produced them.

3. Spectrum of Mesotrons Produced at a Given Height, z_0, as a Function of Altitude, z

A mesotron produced at z_0 with energy E_0 loses energy by ionizing the air. Let E be its energy at height z:

$$dE/dz=\gamma p(z)=\gamma p_0e^{-az},$$

or

$$E=E_0-\frac{\gamma p_0}{a}[\exp(-az)-\exp(-az_0)], \quad (2)$$

where γ is rate of energy-loss in ergs g^{-1} cm². γ is here assumed, for mathematical simplicity, to be independent of energy; its value is taken to be 4.0×10^{-6} erg g^{-1} cm².[15]

[15] B. Rossi and K. Greisen, Rev. Mod. Phys. **13**, 245 (1941).

While they are losing energy, the mesotrons are disintegrating at a rate which depends on their energy. Let $q(E, z)dE$ be the number of mesotrons at height z with energies in dE at E; then, if t is the time in the earth's frame of reference and τ is the mesotrons' mean life in the earth's frame of reference, for mesotrons of a given downward velocity $v(=c\beta)$,

$$\partial q(E, z')/\partial t=-q/\tau,$$

where z' is the changing altitude of the moving mesotrons. If τ_0 is the mesotrons' mean life in their own frame of reference,

$$\partial q(E, z')/\partial z'=q/v\tau=q(1-\beta^2)^{\frac{1}{2}}/v\tau_0.$$

Since

$$E=\mu c^2/(1-\beta^2)^{\frac{1}{2}}\cong\mu cv/(1-\beta^2)^{\frac{1}{2}}, \quad (3)$$

where μ is the rest mass of a mesotron,

$$\frac{dq}{q}=\frac{\mu c}{E\tau_0}dz. \quad (4)$$

If the expression for E is substituted from Eq. (2) and the resulting expression is integrated, the following equation is obtained for the number of vertically moving mesotrons per cm² sec. erg unit solid angle at altitude z which were produced at altitude z_0:

$$q(E, z_0, z)=q_0(E+G[y-y_0], z_0)\times\left(\frac{y_0}{y}\frac{E}{E+G(y-y_0)}\right)^{\mu c/[a\tau_0(E+Gy)]}, \quad (5)$$

where

$$y\equiv e^{-az}, \quad y_0\equiv e^{-az_0},$$

and

$$G\equiv\gamma\rho_0/a.$$

4. Mesotron Spectrum as a Function of Altitude

Let $q(E, z)dE$ be the number per cm² sec. per unit solid angle of the vertically moving mesotrons at height z with energies in dE at E.

$$q(E, z)=\int_z^{\infty}q(E, z_0, z)dz_0=\int_0^{y}\frac{1}{ay_0}\left(\frac{y_0}{y}\frac{E}{E+G(y-y_0)}\right)^{\mu c/[a\tau_0(E+Gy)]}q_0(E+G[y-y_0], z_0)dy_0. \quad (6)$$

Substitution for $q_0(E+G[y-y_0], z_0)$ from Eq. (1)

TABLE I. Calculated differential mesotron spectrum q at 90° magnetic latitude, expressed in terms of N_0, the number of protons at the top of the atmosphere per cm² sec. erg unit solid angle at one erg energy. q is given for 8 energies and 8 altitudes.

E (Total energy, ergs)	Kinetic energy, electron-volts	y	0	0.02	0.05	0.10	0.15	0.16	0.17	0.18
		z(altitude in cm)	∞	2.52 $\times 10^5$	1.93 $\times 10^5$	1.49 $\times 10^5$	1.22 $\times 10^5$	1.18 $\times 10^5$	1.14 $\times 10^5$	1.11 $\times 10^5$
		Pressure in cm Hg	0	1.88	4.70	9.40	14.1	15.0	16.0	17.0
5.6×10^{-4}	2.52×10^{8}	$\frac{10^{-7}q}{N_0}=0$		4.89	8.37	9.15	7.43	7.02	6.63	6.24
2×10^{-3}	1.16×10^{9}	$\frac{10^{-6}q}{N_0}=0$		1.66	2.90	3.33	2.93	2.92	2.71	2.59
2×10^{-2}	1.25×10^{10}	$\frac{10^{-5}q}{N_0}=0$		3.10	6.50	8.32	8.98	9.02	9.05	9.04
2×10^{-1}	1.26×10^{11}	$\frac{q}{N_0}=0$		4.16	8.28	11.8	13.3	13.4	13.6	13.7
2	1.26×10^{12}	$\frac{10^{5}q}{N_0}=0$		5.28	10.5	15.1	17.0	17.2	17.4	17.6
2×10^{1}	1.26×10^{13}	$\frac{10^{6}q}{N_0}=0$		6.65	13.3	19.0	21.5	21.8	22.0	22.2
2×10^{2}	1.26×10^{14}	$\frac{10^{9}q}{N_0}=0$		8.37	16.7	23.9	27.0	27.4	27.7	28.0
2×10^{3}	1.26×10^{15}	$\frac{10^{11}q}{N_0}=0$		1.05	2.10	3.01	3.40	3.45	3.49	3.52

yields

$$q(E,z)=\alpha\int_0^y e^{-\alpha y_0}\left(\frac{y_0}{y}\frac{E}{E+G(y-y_0)}\right)^{\mu c/[a\tau_0(E+Gy)]}\left\{\int_{\mathcal{E}_0}^{\infty}p_0(\mathcal{E})\phi(E+G[y-y_0],\mathcal{E})d\mathcal{E}\right\}dy_0.$$

In the case under consideration, each proton produces 9 mesotrons, each having total energy equal to $\frac{1}{9}$ of the kinetic energy of the proton, or

$$\int_{\mathcal{E}_0}^{\infty}p_0(\mathcal{E})\phi(E_0,\mathcal{E})d\mathcal{E}=9p_0(9\{E+G[y-y_0]\})\frac{d\mathcal{E}}{dE_0}$$
$$=81N_0\{9[E+G(y-y_0)]\}^{-2.9}.$$

Hence,

$$q(E,z)=9^{-0.9}\alpha N_0\int_0^y e^{-\alpha y_0}\left(\frac{y_0}{y}\frac{E}{E+G(y-y_0)}\right)^{A(E,y)}[E+G(y-y_0)]^{-2.9}dy_0, \tag{7}$$

where

$$A(E,y)\equiv\frac{\mu c}{a\tau_0(E+Gy)}.$$

The substitution $u=\alpha y_0$ yields

$$q(E,z)=\left(\frac{E}{y}\right)^{A}\frac{N_0\alpha^{-A}}{(E+Gy)^{A+2.9}9^{0.9}}\int_0^{\alpha y}e^{-u}u^{A}\left(1-\frac{Gu}{\alpha E+\alpha Gy}\right)^{-A-2.9}du$$
$$=\left(\frac{E}{y}\right)^{A}\frac{N_0\alpha^{-A}}{9^{0.9}(E+Gy)^{A+2.9}}\int_0^{\alpha y}e^{-u}\sum_{n=0}^{\infty}\frac{u^{A+n}}{n!}\left(\frac{G}{\alpha(E+Gy)}\right)^{n}(A+2.9)\cdots(A+n+1.9)du$$
$$=\left(\frac{E}{y}\right)^{A}\frac{N_0\alpha^{-A}}{9^{0.9}G^{A+1}D'^{A+1}(E+Gy)^{1.9}}\sum_{n=0}^{\infty}\frac{(A+2.9)\cdots(A+n+1.9)}{n!D'^{n}}\Gamma(A+n+1,\alpha y), \tag{8}$$

where

$$D' \equiv \frac{\alpha(E+Gy)}{G},$$

and $\Gamma(m, h)$, the incomplete gamma-function of m and h, is defined as

$$\Gamma(m, h) \equiv \int_0^h t^{m-1}e^{-t}dt.$$

The differential mesotron spectrum, $q(E, z)$, has been computed for eight values of energy (E) and seven altitudes (z) in the stratosphere, at four magnetic latitudes (λ). No account has been taken of variation of mesotron intensity with temperature or longitude. The computed values of q for the magnetic pole are tabulated in Table I; introduction of the latitude effect is discussed in the next section.

5. Latitude Effect

The equation

$$\mathcal{E}^* = 2.39\times10^{-2}\cos^4\lambda$$

defines the cut-off proton energy $\mathcal{E}^*$ for any magnetic latitude. Mesotrons with energies greater than $E_0^* \equiv \mathcal{E}^*/9$ will be unaffected in intensity by action of the earth's magnetic field; at any altitude z, there will be no mesotrons of energy less than $E^* \equiv E_0^* - Ge^{-\alpha z} = E_0^* - Gy$. Therefore, once $q(E, z)$ has been determined for $\lambda = 90°$, its determination for other latitudes is already accomplished except for the energy range $E_0^* > E > E^*$. In this energy range, for any height z and energy E, there will be a height z_0^* such that a mesotron of energy E_0^* originating at z_0^* will arrive at z with energy E. $y_0^* \equiv \exp(-\alpha z_0^*)$ is obtained thus:

$$E_0^* - E = G(y - y_0^*),$$

or

$$y_0^* = y - (E_0^* - E)/G.$$

Since all the mesotrons of energy E at height z must have been produced at height z_0^* or higher, the differential spectrum for this energy range can be obtained from Eq. (8), provided the upper limit of integration is made y_0^* instead of y:

$$q(E, z) = \int_0^{y_0^*} \frac{1}{ay_0}\left(\frac{y_0}{y}\frac{E}{E+G(y-y_0)}\right)^{\mu c/[\alpha r_0(E+Gy)]} q_0(E+G[y-y_0], z_0)dy_0$$

$$= \left(\frac{E}{y}\right)^A \frac{N_0\alpha^{-A}}{9^{0.9}G^{A+1}D'^{A+1}(E+Gy)^{1.9}} \sum_{n=0}^{\infty} \frac{(A+2.9)\cdots(A+n+1.9)}{n!D'^n}\Gamma(A+n+1, \alpha y_0^*). \quad (9)$$

6. Integral Mesotron Spectrum

Let $Q(E, z)$, the integral mesotron spectrum, be defined as

$$Q(E, z) \equiv \int_E^{\infty} q(E'', z)dE''.$$

If $E_1, E_2 \cdots E_i \cdots$ are a sequence of energies such that $E_i > E_{i-1}$ and $\lim_{i\to\infty} E_i = \infty$, and if

$$Q_i(z) \equiv \int_{E_i}^{E_{i+1}} q(E'', z)dE'',$$

then

$$Q(E_j, z) = \sum_{i=j}^{\infty} Q_i(z).$$

For any altitude and any latitude, if $E > E_0^*$, $q(E, z)$ can, over some energy ranges, be quite closely approximated in the form

$$q(E, z) = \bar{q}(z)E^k,$$

where $k \cong -2.9$. If this expression is valid for $E_i \leqslant E \leqslant E_{i+1}$, then

$$Q_i(z) = \bar{q}(z)\int_{E_i}^{E_{i+1}} E''^k dE'',$$

or

$$Q_i(z) = \frac{1}{k+1}[q(E_{i+1}, z)E_{i+1} - q(E_i, z)E_i]. \quad (10)$$

$$Q(E_j, z) = \sum_{i=j}^{\infty} Q_i(z)$$

was computed for the first four of the eight energies for which $q(E, z)$ was found. $Q_i(z)$ was obtained by Eq. (10) for $E \geqslant E_0^*$; for $E < E_0^*$, graphical means were employed.

7. Integral Spectrum for All Penetrating Particles

The integral mesotron spectrum, $Q(E, z)$, accounts for only part of the penetrating ionizing particles observed under absorbers. In addition

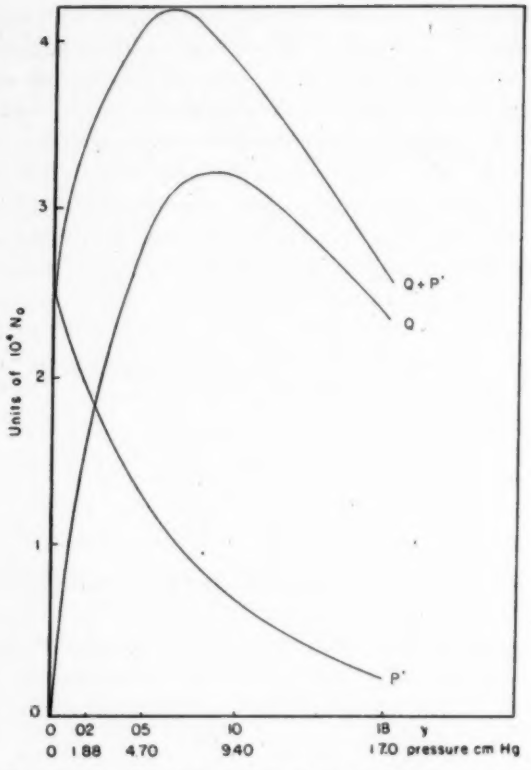

FIG. 1. Calculated intensity of the ionizing cosmic-ray particles which can penetrate 18 cm of Pb at 52° magnetic latitude, plotted against y (defined in Section II, 3) and pressure in the stratosphere. P' = proton curve; Q = mesotron curve; $Q+P'$ = total hard component. Intensities are expressed in terms of N_0, the number of protons at the top of the atmosphere per erg cm² sec. unit solid angle at one-erg energy.

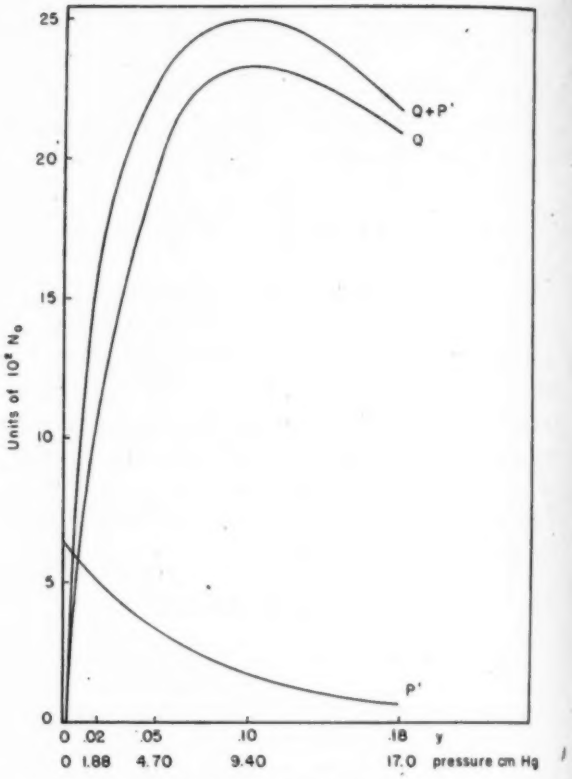

FIG. 2. Calculated intensity of the ionizing cosmic-ray particles which can penetrate 18 cm of Pb at the magnetic equator, plotted against y (defined in Section II, 3) and pressure in the stratosphere. P' = proton curve; Q = mesotron curve; $Q+P'$ = total hard component. Intensities are expressed in terms of N_0, the number of protons at the top of the atmosphere per erg cm² sec. unit solid angle at one-erg energy.

to mesotrons, protons are present; their differential spectrum is

$$p(\mathcal{E}, z) = N_0 \mathcal{E}^{-2.9} \exp\left[-\alpha e^{-ay}\right] = N_0 \mathcal{E}^{-2.9} e^{-\alpha y} \quad \text{for } \mathcal{E} \geqslant \mathcal{E}^*;$$
$$p(\mathcal{E}, z) = 0 \quad \text{for } \mathcal{E} < \mathcal{E}^*.$$

The integral proton spectrum is

$$P(\mathcal{E}, z) \equiv \int_{\mathcal{E}}^{\infty} p(\mathcal{E}'', z) d\mathcal{E}'',$$

or

$$P(\mathcal{E}, z) = \frac{N_0}{1.9} \mathcal{E}^{-1.9} e^{-\alpha y} \quad \text{for} \quad \mathcal{E} \geqslant \mathcal{E}^*;$$
$$P(\mathcal{E}, z) = \frac{N_0}{1.9} \mathcal{E}^{*-1.9} e^{-\alpha y} \quad \text{for } \mathcal{E} < \mathcal{E}^*. \tag{11}$$

For comparison of theory with experiment, it is necessary that $Q(E, z)$ be added to $P'(E, z)$, the number of protons that can penetrate the same thickness of, say, lead as can a mesotron of energy E. If $\mathcal{E}'(E)$ is defined as the kinetic energy a proton must have in order to penetrate as much lead as can a mesotron of total energy E,

$$P'(E, z) = P[\mathcal{E}'(E), z],$$

and can be computed from Eq. (11), with the aid of Table II.[15] Graphs of P', Q, and $P'+Q$ *vs.* y appear in Figs. 1 and 2, and a graph of $\log(P'+Q)$ *vs.* $\log E$ appears in Fig. 3.

TABLE II. Kinetic energy, $\mathcal{E}'$, needed by a proton if it is to penetrate the same amount of lead as a mesotron of total energy E. Energies in ergs.

E(ergs)	5.6×10^{-4}	2×10^{-3}	2×10^{-2}	2×10^{-1}	2	20
$\mathcal{E}'$(ergs)	6.41×10^{-4}	2.09×10^{-3}	1.93×10^{-2}	1.99×10^{-1}	2	20

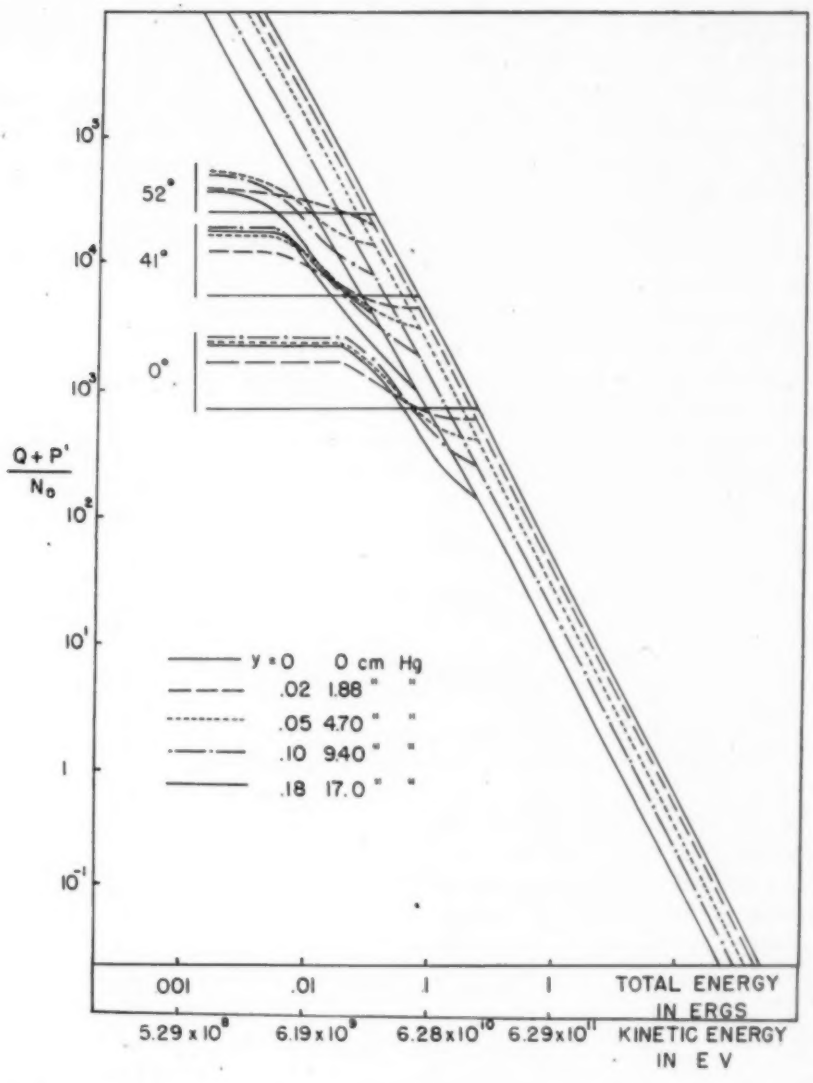

FIG. 3. Logarithmic graph of the calculated integral spectrum of mesotrons plus equally penetrating protons (expressed in terms of N_0, the number of protons at the top of the atmosphere per erg cm^2. Unit solid angle at one-erg energy) *vs.* E, total energy in ergs, at five different atmospheric pressures and four different magnetic latitudes.

8. Intensity of Cosmic Rays Underground

To any distance D underground there corresponds an energy E^* such that a mesotron of total energy E^* at the bottom of the stratosphere ($z=1.11\times10^6$ cm) has only its rest energy when it reaches depth D. If D is expressed in meters of water equivalent, then

$$E^*=4.0\times10^{-4}(D+10).$$

The total number of mesotrons present at depth D is thus

$$N(D)=Q(E^*, 1.11\times10^6)f,$$

where f is a factor introduced to take account of decay. Let $E^{*\prime}$ be the energy at sea level of a mesotron with energy E^* at $z=1.11\times10^6$. Table III lists, for three values of D, the corre-

TABLE III. Depth D below the ground, expressed in meters of water equivalent; energy E^* which a vertically moving mesotron must have at the bottom of the stratosphere if it is to penetrate to depth D; energy $E^{*\prime}$ which a vertically moving mesotron has at the surface of the ground if it had energy E^* at the bottom of the stratosphere; $T(D)$, time required for a high energy mesotron to reach depth D from the surface of the ground; and $\tau(E^{*\prime})$, mean life of a mesotron with energy $E^{*\prime}$.

D Meters water equivalent	E^* ergs	$E^{*\prime}$ ergs	$T(D)$ seconds	$\tau(E^{*\prime})$ seconds
89.1	3.85×10^{-2}	3.55×10^{-2}	8.91×10^{-8}	4.82×10^{-4}
163.2	6.81×10^{-2}	6.49×10^{-2}	1.63×10^{-7}	8.79×10^{-4}
245.4	1.01×10^{-1}	9.77×10^{-2}	2.45×10^{-7}	1.32×10^{-3}

sponding values of E^*, $E^{*\prime}$, $\tau(E^{*\prime})$ (mean life at energy $E^{*\prime}$), and $T(D)$ (time required for a mesotron to reach depth D from sea level in a medium of density = 3.3). Since $\tau_0 = 2.15 \times 10^{-6}$ sec., it is seen that decay in the ground is altogether negligible, for $T(D) \ll \tau_0$ for all D; this is true even if the density of the ground is as low as 2. It is also evident that $\tau(E^{*\prime})$ is large compared to $\frac{1}{3} \times 10^{-4}$ sec., the time required for a mesotron to reach sea level from the bottom of the stratosphere. Thus, the effect of decay may be altogether neglected. This is especially true because the foregoing comparisons of transit-times with mean lives were made for the shortest mean lives of the lowest energy mesotrons under consideration. Therefore, $f = 1$, and

$$N(D) = Q(E^*, 1.11 \times 10^6).$$

The fact that $Q(E^*, z)$ has effectively reached the asymptotic value at $z = 1.11 \times 10^6$ indicates that, at this height, the number of protons is already negligible. Certainly below ground the number of protons is extremely small compared to the number of mesotrons, and the high energy mesotrons produced below the stratosphere will be few compared to the number present at the bottom of the stratosphere. So the total intensity of vertically moving penetrating cosmic-ray particles at any depth, D, underground is simply $Q(E^*, 1.11 \times 10^6)$.

In Table IV are given the values of $Q(E^*, 1.11 \times 10^6)$ for 3 values of D.

III. DISCUSSION

1. Total Number of Penetrating Particles as a Function of Altitude

Schein, Jesse, and Wollan; Schein, Iona, and Tabin; and Schein and Stroud[7] measured the intensity of the penetrating component of cosmic radiation in the stratosphere. They measured, as a function of altitude, the total number of vertically-moving ionizing cosmic-ray particles which penetrated 18 cm of lead without producing secondaries in the lead. This number proved to be approximately the same as the number which penetrated 8 cm of lead without producing secondaries. Measurements were also made of the number of ionizing penetrating particles each of which, in a block of paraffin or lead, produced several ionizing penetrating secondaries. It will be assumed that the particles which produced secondaries were primary protons. Approximately the same number of multiple production processes occurred in 6 cm of paraffin as in 10 cm of paraffin or in 7 or 18 cm of lead. In Fig. 4, experimental and theoretical curves of mesotron, proton, and total penetrating intensity at 52° magnetic latitude are shown.

It can be seen that the theoretical and indicated experimental proton curves, having been

TABLE IV. Calculated numbers of mesotrons per cm² sec. unit solid angle at three depths D underground (meters water equivalent). Numbers are expressed in terms of N_0, the number of protons at the top of the atmosphere per erg cm² sec. unit solid angle at one-erg energy.

D (meters H_2O equivalent)	$Q(E^*, 1.11 \times 10^6)$
89.1	$31.62 N_0$
163.2	$10.97 N_0$
245.4	$5.25 N_0$

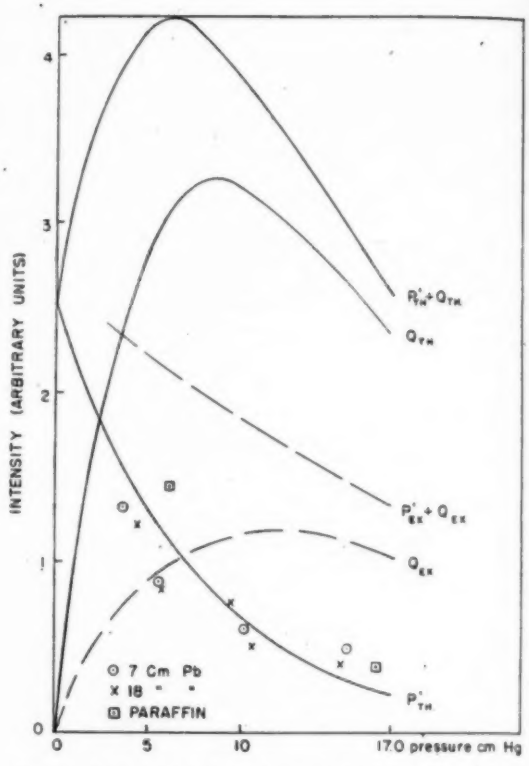

FIG. 4. Observed (broken) and calculated (solid) curves of mesotron (Q) and proton plus mesotron ($Q+P'$) intensity, and theoretical curve and experimental points of proton (P') intensity, plotted against pressure in the stratosphere. The relative scales are so adjusted that the theoretical and indicated experimental proton curves meet at the top of the atmosphere.

adjusted to meet at the top of the atmosphere, fit quite closely throughout the stratosphere. Thus the indication is that the assumed proton absorption cross section of an air nucleus (2.5×10^{-25} cm^2) is approximately correct for proton energies in the neighborhood of 6×10^9 electron volts (the average energy of the primaries at geomagnetic latitude 52°N) and that this cross section is in fact practically independent of energy above 6×10^9 ev since the experimental proton curve is in first approximation exponential.

The theory predicts approximately 3.5 times too many mesotrons near the maximum of the mesotron curve, and the theoretical rate of decay of these mesotrons is too rapid. This discrepancy could obviously be removed if a lower effective multiplicity than nine were assumed for mesotron production by a proton of approximately 6×10^9 ev energy. This possibility will be discussed in Section III, 4.

2. Absolute Number of Primaries

Bowen, Millikan, and Neher[16] have estimated, from ionization chamber measurements of the total cosmic-ray intensity, that there are 0.09 primaries per cm^2 sec., with energies between 6.7×10^9 ev and 15×10^9 ev at the top of the atmosphere. From this can be computed N_0, the number of primaries per erg cm^2 sec. unit solid angle with one-erg energy. Integration of the differential spectrum $N_0\mathcal{E}^{-2.9}$ from 6.7×10^9 ev to 15×10^9 ev gives $N_0=6.56\times10^{-6}$.

N_0 for the same proton spectrum can also be calculated from comparison of the theoretical integral mesotron spectrum with the underground intensity of mesotrons. The values obtained by Wilson,[17] using vertical counter telescopes,* for $N(D)$ at three depths, reduced to number of particles per cm^2 sec. unit solid angle, are given in Table V; with these values are tabulated the theoretical values as derived in Section II, 8. Since the theoretical values are proportional to N_0, equation of theoretical and experimental values permits calculation of N_0.

TABLE V. Depth D (meters water equivalent); $N(D)$, observed number of mesotrons per cm^2 sec. unit solid angle at depth D; $Q(E^*, 1.11\times10^9)$, calculated number of mesotrons at depth D per cm^2 sec. unit solid angle; values of N_0, the number of protons at the top of the atmosphere per erg cm^2 sec. unit solid angle at one-erg energy, obtained by equation of calculated and observed numbers of mesotrons at each depth.

D	$N(D)$	$Q(E^*, 1.11\times10^9)$	N_0
89.1	2.11×10^{-4}	$31.62N_0$	6.69×10^{-6}
163.2	7.72×10^{-5}	$10.97N_0$	7.05×10^{-6}
245.4	3.52×10^{-5}	$5.25N_0$	6.70×10^{-6}

[16] I. S. Bowen, R. A. Millikan, and H. V. Neher, Phys. Rev. **53**, 217 (1938).

The agreement between the values of N_0 obtained by the two methods is very satisfactory, although, as will be seen in Section III, 4, the value of N_0 given by Bowen, Millikan, and Neher may be somewhat too small. The indication is that from about 7×10^9 ev to at least 5×10^{11} ev the differential primary spectrum can be represented as $N_0^{-2.9}$ and the multiplicity is approximately nine, although the facts given here do not rule out the possibility of a different primary spectrum combined with a multiplicity which depends on energy.

3. Latitude Effect

Schein, Jesse, and Wollan[18] have measured the intensity of the hard component of cosmic rays

TABLE VI. Observed and calculated values of the ratio of the intensity of the hard component at 52° magnetic latitude to intensity at 41° magnetic latitude, at various atmospheric pressures.

Pressure (cm Hg)	$\frac{(Q+P')_{52°}}{(Q+P')_{41°}}$ (Experimental)	$\frac{(Q+P')_{52°}}{(Q+P')_{41°}}$ (Theoretical)
0	—	4.68
1.88	—	3.02
4.70	1.2	2.88
9.40	1.2	2.19
17.0	1.1	1.70

[17] V. C. Wilson, Phys. Rev. **53**, 337 (1938).

* Wilson's counter telescope was equivalent to a rectangular parallelepiped such that any ionizing particle which passed through both the top and bottom faces was counted. The data are given in terms of counts per minute, and must be expressed in terms of particles per cm^2 sec. unit solid angle. Let F be the factor by which counts per second must be divided to obtain particles per cm^2 sec. unit solid angle. F is approximately given by the formula

$$F=4\int_0^{\tan^{-1}L/h}\int_0^{\tan^{-1}W/h}\cos\theta\cos\phi(L-h\tan\theta)\times(W-h\tan\phi)d\theta d\phi,$$

where $L=71$ cm is the length of the parallelepiped, $W=9$ cm is the width, and $h=34.5$ cm is the height. In this case, $F=196$ cm^2. Strict accuracy would require the use of an F somewhat smaller than this value (leading to larger values of N_0), because an obliquely moving particle must start with a higher energy than a vertically moving particle to reach the same depth, and hence a larger fraction of the obliquely moving mesotrons are cut out by the ground. This correction may be as large as 25 percent.

[18] M. Schein, private communication.

as a function of altitude at magnetic latitudes 41° and 52°N. The values they obtained for the ratio of intensity at 52° to intensity at 41° at various pressures appear in Table VI; also tabulated are the theoretical values of this ratio.

The excessively large theoretical values of this ratio will be reduced (1) if the multiplicity of mesotron production is uniformly greater than nine, (2) if the multiplicity is an increasing function of proton energy, increasing rapidly in the neighborhood of 6.7×10^9 ev (the magnetic cut-off energy for 41°), or (3) if the integral proton spectrum falls off with increasing energy less rapidly than $\mathcal{E}^{-1.9}$ in the neighborhood of 5×10^9 ev.

The first possibility can be discarded, in the light of the measurements of proton and mesotron intensity discussed in Section III, 1. These same measurements indicate that multiplicity may increase with energy in the energy range around 5×10^9 ev; however, this assumption is not sufficient in itself to give the correct latitude effect, for even if multiplicity is zero for proton energies less than 7×10^9 ev and nine for energies greater than 7×10^9 ev, the theoretical latitude effect is still far too big, and, as was seen in Section III, 2, the multiplicity is probably not much greater than nine even at very high energies. Hence, it seems necessary to assume that the integral proton spectrum falls off less rapidly than $\mathcal{E}^{-1.9}$ between 3×10^9 ev and 7×10^9 ev.

4. Indications from Other Experiments

The foregoing facts seem to show that the differential proton spectrum is $N_0\mathcal{E}^{-2.9}$ for energies greater than about 7×10^9 ev, and falls off less rapidly with increasing energy for energies less than 7×10^9 ev. Furthermore, it appears that the multiplicity of the process of mesotron production by protons is about nine for proton energies greater than about 7×10^9 ev, and is an increasing function of energy for lower proton energies.

In addition, the fact that the knee of the curve of total intensity *vs.* latitude occurs at about 40° magnetic latitude at sea level, and at slightly higher latitudes at higher altitudes,[19,20] indicates that, for proton energies below about 3×10^9 ev, the integral proton spectrum is nearly constant and the multiplicity is not more than three or four.[21] It is known[22] that the sun's magnetic field prevents charged particles with energies less than approximately 3×10^9 ev from reaching the earth at all. It is probably significant, too, that, in the measurements referred to in Section III, 1, Schein and his collaborators found very few mesotrons which could penetrate 8 but not 18 cm of lead (i.e., few mesotrons of kinetic energy between about 1.2×10^8 ev and 2.5×10^8 ev).

If the primary spectrum is $N_0\mathcal{E}^{-2.9}$ above 7×10^9 ev, the underground measurements indicate that the multiplicity must be approximately nine in this range. If account is taken of the possibility that some of the energy present in the primaries goes into neutrinos which do not contribute to the total intensity curves of Bowen, Millikan, and Neher[16] (see Section III, 2), the number of primaries at the top of the atmosphere, as computed from the total intensity measurements, comes out larger by about 50 percent. In that case, agreement between their results and those obtained underground would require a multiplicity of about 13 for primary energies in the neighborhood of 5×10^{11} ev. If account is taken of the correction for oblique rays to the value of N_0 calculated from Wilson's results (see footnote on calculations of solid angle × area for counter telescopes, Section III, 2), the estimated multiplicity at high energies will be somewhat reduced, to a value of eleven or so.

Millikan, Neher, and Pickering[23] found that the total vertical intensity at the equator in the first radiation unit from the top of the atmosphere (2 cm Hg pressure) is greater, by a factor of about eight, than the intensity of the primaries as computed from the total ionization in the atmosphere. This fact indicates that, for primaries of about 3×10^{10} energy (the average energy of primaries at the equator), multiplicity of mesotron production is approximately eight.

The large (about 20 percent)[24] positive excess of the hard component supports the supposition

[19] A. H. Compton and R. N. Turner, Phys. Rev. **52**, 799 (1937).
[20] H. Carmichael and E. G. Dymond, Proc. Roy. Soc. **171A**, 321 (1939).
[21] L. W. Nordheim, Phys. Rev. **56**, 502 (1939).
[22] P. S. Epstein, Phys. Rev. **53**, 862 (1938).
[23] R. A. Millikan, H. V. Neher, and W. H. Pickering, Phys. Rev. **61**, 397 (1942).
[24] D. J. Hughes, Phys. Rev. **57**, 592 (1940).

that, at lower energies, multiplicity is not more than about five. While the soft component has not been considered at all in this treatment, it does not seem possible that, with so low a multiplicity for production of low energy mesotrons, there will be enough mesotrons decaying to account for the observed soft component, unless it is postulated that there are also rapidly decaying "transverse" mesotrons.[8] If these transverse mesotrons are produced in approximately the same numbers as the "pseudoscalar" mesotrons (those for which $\tau_0 = 2.15 \times 10^{-6}$ sec.) they must constitute a portion of the hard component which is at all points nearly proportional to the proton intensity. The experimental results discussed in Section III, 1, can perhaps be accounted for on the assumption that a large fraction of the energy of the primary protons goes into the production of rapidly decaying mesotrons.

The theory of Hamilton, Heitler, and Peng,[13] although it seems very satisfactory in many respects, appears to meet serious difficulties when used to determine the energy and altitude dependence of the intensities of mesotrons and protons separately. The measurements cited in Section III, 1, show that the proton absorption cross section of an air nucleus is nearly independent of energy and is much smaller than the cross section used by Hamilton, Heitler, and Peng for production of low energy mesotrons.

It seems worth while to note that energy and momentum are not simultaneously conserved in a process in which all or part of the *kinetic* energy of a primary goes to make up the *total* energies (rest plus kinetic) of any number of secondaries, unless some of the primary's kinetic energy is imparted to one or more other particles which existed before the inception of the process. Therefore, the sum of the total energies of the mesotrons produced by a given proton cannot be exactly equal to the original kinetic energy of the proton; furthermore, each mesotron production process is probably accompanied by the release of at least one neutron or proton from the nucleus in whose field the process occurs. This may be the natural explanation of the neutrons observed by Korff at high altitudes; since Bethe, Korff, and Placzek[25] concluded that most of these neutrons were probably produced with initial energies no greater than about 3×10^7 ev, it appears that the energy which goes into such particles does not significantly reduce the amount of energy left for mesotrons.

The author wishes to express his great appreciation for the aid and advice given him by Dr. Marcel Schein, of The University of Chicago, who suggested the problem and without whose help it could not have been completed, and by Dr. Frank Hoyt, of The University of Chicago, whose advice and instruction in theoretical physics have been invaluable. Thanks are also due Mr. T. J. Kinyon, of The University of Chicago, who performed nearly all the numerical computations employed in the derivation.

[25] H. A. Bethe, S. A. Korff, and G. Placzek, Phys. Rev. **57**, 573 (1940).

Partial Separation of the Oxygen Isotopes by Thermal Diffusion and the Deuteron Bombardment of O^{17} *,**

SHERRERD B. WELLES***
Sloane Physics Laboratory, Yale University, New Haven, Connecticut
(Received June 22, 1942)

With an eighteen-meter column, O^{18} has been enriched from the ordinary concentration of 0.2 percent to 17 percent and O^{17} from 0.04 percent to 0.8 percent. The former increase was determined by the mass spectrometer, the latter by the increased activity of F^{18} produced in the nuclear reaction $O^{17}(d, n)F^{18}$. The time rate of increase of the concentration of O^{18} was characterized by a step-wise nature, which arises from the staggering of the six three-meter tubes convectively coupled in series. A qualitative discussion of staggering is given.

THE apparatus consisted of six three-meter columns. The first three were constructed and used by E. F. Shrader for the separation of the chlorine isotopes.[1] They were all of the same dimensions, and consisted of an outer cold tube (I.D. 15.5 mm), cooled by a water jacket, and an inner hot tube (O.D. 6 mm). These tubes were of Pyrex glass and were kept concentric by means of groups of three, accurately ground, glass pins attached to the inner tube. The space between the tubes was 4.75 mm.

The inner tube was heated by means of a tungsten wire. This filament was centered by Lavite spacers at 15-cm intervals, and was kept under tension by a steel spring. The temperature of the inner tube was 373°C when 11.5 amperes were flowing through a 20-mil wire. About 770 watts are expended for each three-meter column. The tungsten filaments were at a temperature of 800°C and were in an atmosphere of nitrogen to afford good heat conduction and to prevent oxidation. An all-glass system for this was added to the original tubes and in five months of running no wire burned out. The differential expansion between the hot and cold tubes, which amounts to 2.5 mm, was taken care of by a thin brass sylphon bellows soldered in one end of the outer tube.

The other three tubes were of the Clusius and Dickel type.[2] In the first two, the inner diameter of the cold tube was 1 cm, and in the third it was 8 mm. The hot surface was a 15-mil platinum wire which was centered by cross wires attached by spot-welding. The wire was fastened to a 50-mil tungsten lead in a removable ground-glass joint fitting into the top of the tube. A copper weight, suspended from the end of the platinum wire, kept it straight and afforded electrical contact with a pool of mercury contained in a removable bottom. The expansion of the wire on heating was thus taken up by the lowering of the weight into the mercury. As there was no appreciable heating of the ground joints, they were kept tight with stopcock grease. About 300 watts per tube were required to keep the wire at a temperature of 700°C.

The columns were connected in series by convective coupling which produces the equivalent of a single column having a length equal to the sum of the effective lengths of each of the six tubes, i.e., 18 meters. Between the bottom of each column and the top of the next one are two connecting tubes, one at room temperature and the other heated to about 100°C. This procedure keeps the concentration at the top of one tube equal to that at the bottom of the preceding one. The oxygen was generated electrolytically at the rate of a half a liter per hour by passing a current of one ampere through five parts of distilled water and one part of concentrated sulphuric acid. Cylinders of platinum foil were used as electrodes. The gas was dried by being

* Part of a dissertation presented to the Faculty of the Graduate School of Yale University in candidacy for the Degree of Doctor of Philosophy, June, 1941.

** This paper was received for publication on the date indicated but was voluntarily withheld from publication until the end of the war.

*** Now at Air Technical Service Command, Cambridge Field Station, Cambridge, Massachusetts.

[1] E. F. Shrader and E. Pollard, Phys. Rev. **59**, 277 (1941).

[2] K. Clusius and G. Dickel, Zeits. f. physik. Chemie **B44**, 397 (1939).

passed through glass wool, calcium chloride, sodium hydroxide, and phosphorous pentoxide. The oxygen passes continually through the "top" of the first column, and keeps the concentration of O^{18} there at a constant value. An end volume of 300 cc was connected convectively to the "bottom" of the last column. Gas could be removed from there for the purpose of testing the separation factor during the period of operation. It is exploded with pure methane in a bulb provided with electrodes to form CO_2 which can be frozen down into a break-seal tube. This tube is then sealed off and can be connected to the mass spectrometer.

Each sample drawn off into the explosion bulb had a volume of 6 cc at N.T.P.; with this a little more than 3 cc of CH_4 was mixed by heating a convective return tube. The amount of CO_2 obtained was of the order of 2 cc, which gave a satisfactory pressure in the reservoir of the mass-spectrometer. Because of the oxidizing effect on the filament of the ion source of the mass spectrometer when O_2 is introduced, it was necessary to use CO_2. This introduces a peak at mass 45 owing to $C^{13}O^{16}O^{16}$ whose intensity is 1 percent of the normal $C^{12}O^{16}O^{16}$. Hence $C^{13}O^{16}O^{16}$ mask $C^{12}O^{16}O^{17}$ whose intensity is only 0.08 percent for unenriched oxygen. Because of the instability of the mass spectrometer when measuring on full sensitivity, it was impossible to estimate the increase of peak owing to mass 45 as the concentration of O^{17} increased. Figure 1 gives the separation factor of $O^{16}O^{18}$ from $O^{16}O^{16}$ as a function of the time.

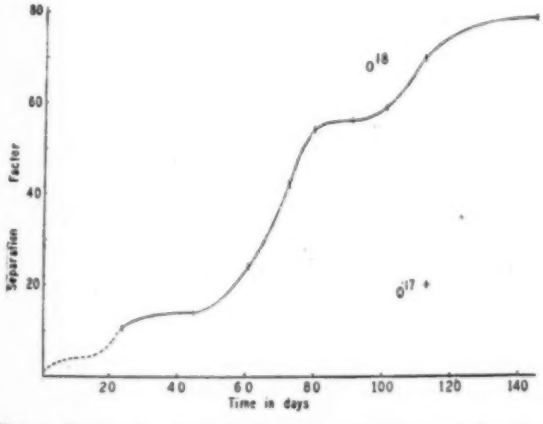

FIG. 1. Separation factor of O^{18} as a function of the time of operation.

The step-wise increase of the concentration of the rare isotope in the end volume may be explained quantitatively by setting up the equations of transport for each tube and introducing the effect of the convective coupling tubes which act as reservoirs between the diffusion tubes.[3] The phenomenon may also be explained from a graphical consideration. In Fig. 2 the rectangles at the bottom indicate the transport of each of two tubes. The transport T_2 of the heavy isotope

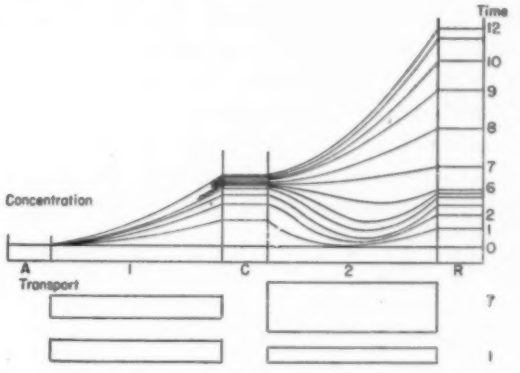

FIG. 2. Distribution of the concentration of a rare isotope in two thermal diffusion columns (1) and (2), connected by convective coupling pipes C. The time interval between successive curves is always the same. The step-wise rate of increase of concentration in the end volume reservoir (R) is apparent.

is given by the expression

$$T_2 = H\left\{c_2(1-c_2) - \frac{1}{2A}\frac{\partial c_1}{\partial z}\right\},$$

where H and A are constant in time and along the tube (the z direction) and c_2 is the relative concentration of the heavy isotope.[4] If c_2 is small and there is no concentration gradient, then the transport is equal to Hc_2. After the tubes have been in operation for a period of time, the concentration in the second tube will be larger than that in the first so the transports will be approximately equal only if the value of H for the second tube is proportionally smaller than that for the first tube. With these values of H, then at the beginning of operation, the transport of the first column will be greater than that of the second.

[3] L. Onsager, by private communication.
[4] W. H. Furry, R. C. Jones, and L. Onsager, Phys. Rev. 55, 1083 (1939).

Above the transport rectangles in Fig. 2 is plotted the concentration c_2 against the length down the tubes. Each curve is for a particular time, and the time interval between adjacent curves is the same. The concentration at A is kept constant by the continual flow of ordinary oxygen through the top of the apparatus. At time t_1, the concentration in the convective tube C will be greater than that in the reservoir R, because the transport of 1 is greater than that of 2, assuming the volumes of C and R are the same. The concentration of 2 near C will be larger than that near the middle, because of diffusion and convection from C. The rate of increase of the concentration in C will decrease because of the diffusion and convective flow into 2. There is no effect of this concentration wave on the transport of 2 until it reaches the end of 2. Until this time, the concentration of the end volume rises exponentially with time. When the concentration wave does reach the end volume, there is a rapid increase in concentration. Now the concentration of the whole tube is much higher than at the start, and consequently the transport is larger. The two tubes now begin to act as one and there is now another exponential decrease in the rate of increase of the end volume concentration. The addition of a third tube would introduce another wave and hence a third step in the concentration-time plot. Just such an effect is noticed in the separation of oxygen.

Clusius and Dickel separated air with several columns of different gap spaces, with several temperature differences, and different pressures.[2] From the factors they obtained, a rough idea of the performance of the hot wire columns used for oxygen alone can be calculated. The separation factor for the hot tubes of Shrader can be calculated for oxygen from their performance with chlorine.[1] The difference in the constants η, ρ, D, and α must be taken into account in each case, as well as the fact that α differs slightly in form for isotopic molecules and non-isotopic ones.

The operation of the columns can also be predicted upon the theory of Furry, Jones, and Onsager for the flat wall case.[4] The theoretical separation factors are always much larger than the actual ones, both because of asymmetry effects and because the flat wall assumption is a poor approximation to the hot wire columns. There is considerable uncertainty as to the value of α that should be used; that value determined from viscosity measurements is particularly unreliable in the temperature range used.[5] In addition the separation factor is quite sensitive to the value of the average temperature used in calculating the gas constants. The mean temperature $\frac{1}{2}(T_1+T_2)$ is certainly not correct for the hot wire case.

The expected equilibrium separation factors for the hot wire columns on the basis of the results of Clusius and Dickel are 4.2 and 4.7 for the 1 cm and 8 mm (I.D. of cold tube) tubes, respectively. It is interesting to note that the plateaus of Fig. 1 come at 4.15 (unobserved), $4.15\times3.65=15.2$, $4.15\times(3.65)^2=56.0$, etc., indicating that the separation factors of the hot wire tubes are approximately 3.65 and 4.15, respectively, about ten percent smaller than the expected values. In addition the time dependence is correct as may be seen from a calculation of the relaxation times. Thus the theory of staggering outlined above may be considered qualitatively verified.

In order to have the convective coupling tubes operate effectively, the flow of gas through them must be large enough so that there is no appreciable change in concentration between the points that they connect. The flow of gas in cc per second through the tubes is given by

$$v=\frac{\pi g M p \Delta T d^4}{2.1\times10^4 \eta T^2},$$

where M is the molecular weight of the gas, p is the pressure in atmospheres, ΔT is the difference between the temperature of the gas in the hot tube and that of the gas in the cold tube, d is the diameter of the tube, η is the viscosity, and T is the geometric mean between the temperature of the hot and cold gas.

It can easily be shown that the separation factor of the tubes is given by

$$\Delta S=\frac{c_1'}{c_1}\cdot\frac{c_2}{c_2'}=1+\frac{N_1}{Nc_1}-\frac{N_2}{Nc_2},$$

where c_1 and c_2 are the relative concentrations of species 1 and 2 in one tube and the primed

[5] M. Trautz and R. Heberling, Ann. d. Physik 10, 155 (1931).

quantities are for the other tube. N_1 and N_2 are the net forward transports of species 1 and 2, and $N=\rho v$, the mass of gas passing through a cross section of the tube per second. For ΔS to be less than 0.1 percent different from unity, the diameter of the convective tubes for the last columns can be as small as 5 mm for a $\Delta T=50°C$. Without departing too far from perfect coupling, the volume of the convective tubes should be as small as possible in order that the holdup of gas, and therefore the relaxation time, may be smaller.

DEUTERON BOMBARDMENT OF OXYGEN

Yasaki and Watanabe noticed a 114-minute activity from a tungsten oxide target which had been bombarded by deuterons.[6] F^{18} is known to emit positrons and the half-life is of this value.[7] There is, therefore, the question as by which isotope of oxygen the reaction is caused. There are two possibilities, either $O^{16}(d, \gamma)F^{18}$ or $O^{17}(d, n)F^{18}$. As both neutron and gamma-ray detection are difficult near the cyclotron, some other means of deciding between the two is advisable.

Yasaki and Watanabe were of the opinion that the reaction was not caused by the very rare O^{17} whose normal concentration is only 0.04 percent. W. L. Davidson[8] studied the reaction both by varying the energy of the incident deuterons and by calculating the cross section of the reaction, and found results which are characteristic of the (d, n) reaction. He concluded that the rare isotope is responsible.

A definite proof of the validity or falseness of this conclusion can be obtained by using two targets, one containing ordinary oxygen and the other containing an equal amount of oxygen enriched in the heavy isotopes. If, after bombarding each the same length of time and with the same intensity of beam, the enriched target showed an increased activity, the O^{17} is the isotope responsible. The only other reactions involving deuterons on oxygen which give radioactive products are $O^{16}(d, n)F^{17}$ (70 sec.), $O^{18}(d, p)O^{19}$ (31 sec.), and $O^{18}(d, \alpha)N^{16}$ (8 sec.). These will not interfere with the measurement of the 114-min. activity.

The tungsten targets, 1.7 cm in diameter and 1-mm thick, were cleaned by heating to a dull red and then applying sodium nitrite. After thorough washings and subsequent drying, the target was weighed. It was then placed in a quartz tube which contained oxygen at a pressure of approximately 18 cm of Hg. After two hours of heating at 700°C, the pressure had dropped to 4 cm. The increase in weight was about 40 milligrams. Each target was bombarded for 90 minutes by a 3.7-Mev deuteron beam of 0.9 microampere intensity. The activity was measured with a Lauritsen electroscope and for the enriched oxygen target was 20.4 times that for the ordinary oxygen one.

This factor is just what one would expect to obtain for the separation factor of O^{17} at the time the enriched oxygen was withdrawn. The rate of approach to equilibrium is much more rapid for O^{17} than for O^{18}, mainly because the equilibrium separation factor for the former is only the square root of that for the latter.

A careful measurement of the half-life of F^{18} gave 112 minutes. The energy of the emitted particles was in agreement with the accepted value, 0.7 Mev.[6] A magnetic analyzer checked the sign of the charge as being positive.

The Schumann-Runge bands in absorption of 17 percent (atomic) O^{18} heated to 800°C[9] failed to reveal bands caused either by the 18,18 molecule or by the 18,16 one. At this atomic concentration, the molecular concentration of 18,18 is only 4 percent of that of the 16,16 one, while the molecular concentration of 16,18 is only 10 percent. The failure to observe these bands is characteristic of work with absorption spectra, and it is estimated that a concentration of the order of 50 percent (atomic) would be necessary in order to determine (as well as detect) the alternating intensity ratio of the rotational lines of the enriched molecule.

The author wishes to express his appreciation to Professor W. W. Watson for his constant guidance, patience, and encouragement throughout this investigation. Acknowledgment is made to the George Sheffield Fund for the operation of the cyclotron.

[6] T. Yasaki and S. Watanabe, Nature **141**, 787 (1938).
[7] A. H. Snell, Phys. Rev. **51**, 143 (1937).
[8] W. L. Davidson, Jr., Phys. Rev. **57**, 1086 (1940).
[9] C. Füchtbauer and E. Holm, Physik. Zeits. **26**, 345 (1925).

PHYSICAL REVIEW VOLUME 69, NUMBERS 11 AND 12 JUNE 1 AND 15, 1946

Absorption of Slow Mesotrons in Lead, Iron, Aluminum, and Water

H. PAUL KOENIG
Physics Department, Laval University, Quebec, Canada

(Received February 5, 1945)

The absorption of slow mesotrons in lead, iron, aluminum, and water was measured by means of counters arranged in anticoincidence. In all cases, the statistical error in the number of mesotrons stopped by the absorbing layers was less than 3 percent. This accuracy was made possible by the high efficiency (about 99 percent) of the anticoincidence group of counters. The values obtained for the relative absorptions in the different substances were compared with those calculated from the theory of energy losses by collision. As is well known, the theory predicts a smaller absorption in heavier elements for a given superficial mass. The uncorrected experimental values did not agree with the theory. However, by taking into account the effect of scattering, which is of particular importance in heavy elements, the experimental data were brought into satisfactory agreement with the theory. For water, no reliable theoretical value could be calculated.

INTRODUCTION

IT is generally admitted that the hard component of the cosmic radiation at sea level is absorbed in different substances according to a mass-proportional law. It is also assumed that the absorption is essentially due to energy losses by collision. The theory of these losses indicates that the absorption should not be exactly proportional to the superficial mass of the absorber, but that there should be a slight dependence on the atomic number of the substance. However, the existing absorption measurements are not accurate enough to establish definitely whether these small discrepancies from the mass-proportional law exist or not.

In spite of the fact that many measurements of the absorption of the hard component in different materials have been published, there seems to exist no experiment in which the absorption in elements of widely different atomic number was measured with sufficient accuracy to test the above-mentioned point.

The lack of accurate data is due to the following reason. The absorption of mesotrons in matter is usually measured in two different ways. One may measure the intensity of a mesotron beam before and after the absorber is placed above the counter set or one may measure the intensity of the beam before and after the absorber is placed between the coincidence counters. Owing to the weak absorption of the hard component, very thick layers of matter are required to absorb more than a few percent of the radiation. For this reason when the absorber is placed above the counters, the divergence of the beam makes it necessary to employ inconveniently large volumes of the absorbing material. When the absorber is placed between the counters, a given thickness requires a smaller volume of absorber; but on the other hand the counters then have to be placed further apart, strongly decreasing the intensity of the beam. Moreover, the above mentioned methods are sensitive to variations in the intensity of the cosmic radiation. A quantitative analysis of the problem shows that for a light element the measurement of the absorption to within an accuracy of only ten percent would require an exceedingly long series of measurements.

There is another method that may be employed which involves the use of anticoincidence counters. In this experiment, one records directly the number of absorbed mesotrons instead of the difference in intensity with and without absorber. Hence the statistical error can only affect the small fraction of particles which is absorbed instead of the total number of particles in the beam.

A review of the available literature shows but one experiment performed by the anticoincidence method.[1] The accuracy attained in this experiment, however, was not sufficient for a quantitative test of the theory.

It was therefore considered worth while to

[1] M. A. Pomerantz and T. H. Johnson, Phys. Rev. 59, 143 (1941).

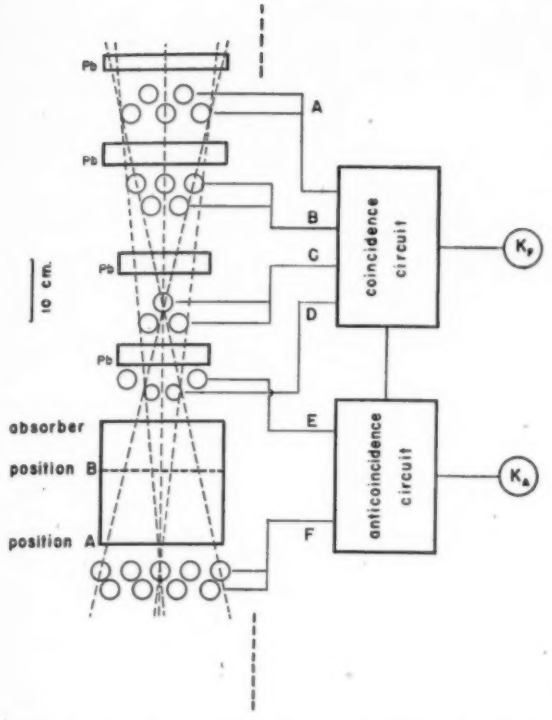

FIG. 1. Position of counters and absorbers in the first arrangements. Also showing connections to the recording circuits.

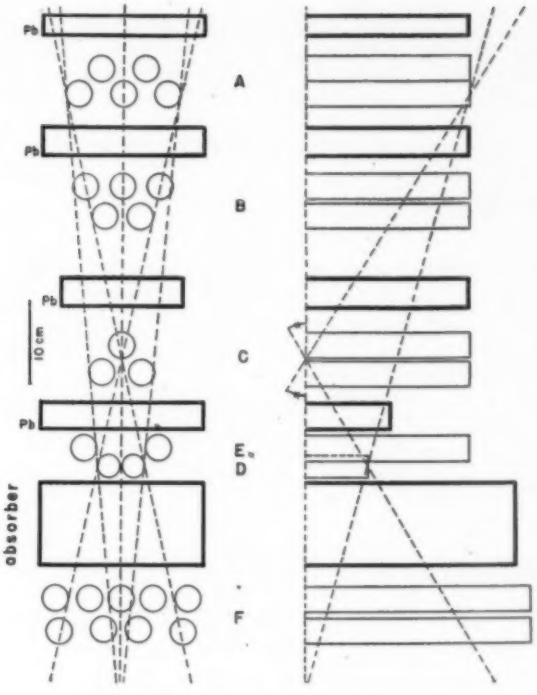

FIG. 2. Position of counters and absorbers in the second arrangement. Also showing the sections of the beam in two perpendicular planes.

undertake a new measurement of the absorption of mesotrons in different materials by the anticoincidence method. The precision attained was considerably higher than that achieved by any of the previous experimenters, owing chiefly to the high efficiency of the anticoincidence counter set and to the large number of particles recorded.

The geometrical arrangement of the counters and absorbers used in our experiment is shown in Fig. 1. The four groups of counters A, B, C, and D constitute a cosmic-ray "telescope" and define a beam of mesotrons. All counters within a given group are connected in parallel and each group is connected to one terminal of a fourfold coincidence set. This set actuates the mechanical recorder K_F when a coincidence ($ABCD$) occurs and in most cases this event corresponds to the passage of a charged particle in the telescope. The soft radiation is absorbed by 14 cm of lead distributed into several layers placed between the groups forming the telescope. In this way a beam of mesotrons is obtained which we believe to consist of 94 percent of mesotrons and 6 percent of electrons. These remaining electrons cannot be eliminated since they are in equilibrium with the hard component.

Referring to the diagram one sees that the absorber is placed immediately under the telescope and above the anticoincidence group F. The maximum thickness of absorber that can be conveniently used is limited by the fact that the area of group F must be sufficient to fill the solid angle defined by the telescope.

The purpose of the group F of counters is to detect the mesotrons which have not been stopped by the absorber. This group is connected to the anticoincidence unit. The anticoincidence unit always receives the signal of the occurrence of a fourfold coincidence ($ABCD$) and this signal will be transmitted to the mechanical recorder K_A except when accompanied by a simultaneous impulse from the group F. It is clear that K_A will record the number of particles stopped.

We will indicate by A the number of particles registered in K_A and by F the number of those registered by K_F. Thus, the above description makes it clear that the absorption increases

TABLE I. Measurements of absorption of slow mesotrons in lead, iron, aluminum, and water. The column headings have the following significance: t, thickness of material in cm; σ, mass per unit area in g/cm²; Abs. pos.; position of absorber; N_b, number of particles in the beam; N_s, number of stopped particles; R_s, percent of particles stopped; R(abs.) corr., percent absorption corrected for background; R(abs.) for 10 g/cm², percent absorption in 10 g/cm² of substance.

	t cm	σ g/cm²	Abs. pos.	N_b	N_s	R_s	R(abs.) corr.	R(abs.) for 10 g/cm²
				First arrangement				
Measurements with lead								
	2.43	27.7	A	78,400	2220	2.83	0.94±0.08	0.34±0.03
	9.87	112.5	A	156,174	9651	6.18	4.29±0.08	0.381±0.008
Background			A	178,736	3372	1.89		
	9.87	112.5	B	106,736	7291	6.84	4.89±0.09	0.435±0.009
Background			B	106,168	2070	1.95		
				Graphically extrapolated value:				*0.35±0.015*
Measurements with iron								
	10.2	80.2	A	84,500	4467	5.29	3.40±0.08	*0.424±0.008*
Background			A	178,736	3372	1.89		
Measurements with water								
	20.0	20.0	AR*	174,027	4918	2.83	0.97±0.05	*0.48±0.025*
Background			AR	277,138	5151	1.86		
				Second arrangement				
Background			B	235,800	2075	0.878		
Lead	9.87	112.5	B	57,800	2965	5.13	4.25±0.1	0.38±0.01
Iron	10.20	80.2	B	58,200	2559	4.40	3.52±0.09	0.44±0.01
Al	10.16	27.4	B	122,600	2627	2.14	1.26±0.015	0.465±0.004

* *AR* means that the absorber in position *A* is in a reservoir.

linearly with the fraction A/F. To obtain a true value of the absorption we need only measure A/F with the absorber and subtract the corresponding value of A_0/F_0 measured without the absorber.

In view of the fact that the absorbers used stopped only a small percentage of the mesotrons, experiments were performed to reduce the background A_0/F_0 to a minimum.

Two slightly different arrangements were employed. In the first (Fig. 1) the maximum permitted thickness of absorber was 20 cm and in this case the number of background coincidences A_0/F_0 was about 1.9 percent. In the second arrangement (Fig. 2) the anticoincidence counters were placed only 10 cm below the telescope. This arrangement reduced the maximum thickness of absorber but allowed a more favorable disposition of the anticoincidence counters, with a consequent decrease of A_0/F_0 to 0.9 percent. Finally two anticoincidence counters E were placed one on each side of the counters of group D in order to minimize the number of spurious fourfold coincidences caused by showers.

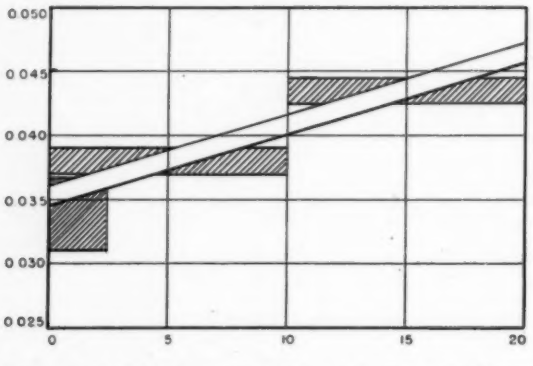

FIG. 3. Graphical extrapolation of the experimental results for the absorption in lead. Abscissae: distance in cm between the absorber and the counters F. Ordinates: percent absorption of mesotron beam in one g/cm².

The coincidence circuit used was of the conventional Rossi type and had a resolving time of about 16 microseconds. The anticoincidence circuit was of the same type as that employed in this laboratory in connection with a previous work.[2] The high voltage source included the usual pentode-stabilized circuit.[3] All the circuits were fed through a Raytheon stabilizer. The Geiger-Mueller counters used were of the self-quenching type and had a plateau of over 200 volts. Within a given group, the anodes of the

[2] F. Rasetti, Phys. Rev. **60**, 198 (1941).
[3] H. Victor Neher and W. H. Pickering, Rev. Sci. Inst. **10**, 53 (1939).

TABLE II. Most probable values of the mesotron absorption in lead, iron, aluminum, and water. The column headings have the following significance, R(abs.) for 10 g/cm², percent absorption in 10 g/cm² of substance from Table I; Arr., experimental arrangement; Av., average for arrangement 1 and 2; Av. (corr.), average corrected for divergence of the beam; σ(1 percent), mass per cm² (g/cm²) which absorbs one percent of the beam; σ(1 percent) corr., preceding values corrected for multiple scattering in absorber; Range (theor.), theoretical range for mesotrons of $p/\mu=1.257$ (adjusted for iron).

	R(abs.) for 10 g/cm²	Arr.	Av.	Av.(corr.)	σ(1%) g/cm²	σ(1%)corr. g/cm²	Range (theor.)
Lead	0.35±0.015	1	0.36±0.010	0.36±0.01	27.8	30.6±1	33.5
	0.38±0.01	2					
Iron	0.424±0.008	1	0.432±0.011	0.425±0.01	23.5	24.1±1	24.1
	0.44±0.01	2					
Al	0.465±0.004	2	0.465±0.004	0.453±0.004	22.1	22.4±1	21
Water	0.48±0.025	1	0.48±0.025	0.47±0.02	21.3	21.3±1	17

different counters were not connected together, but each one was coupled to the grid of the amplifying tube through a separate capacitor (10 micromicrofarads) and connected to the ground through a separate resistor (100 megohms). This type of coupling was necessary in the case of the anticoincidence counters in order to make sure that the discharge in one counter did not make the whole group insensitive.

The efficiency of the apparatus was periodically tested by disconnecting the anticoincidence counters from the high voltage source. In this case it is obvious that both mechanical recorders should count the same number of impulses.

The measurements with and without absorbers were performed alternatively for periods of one week in order to compensate for slow variations in the characteristics of the counters and the circuits.

EXPERIMENTAL RESULTS AND DISCUSSION

The measurements performed with the first arrangement (Fig. 1) in which the space available for the absorber was 20 cm were the following: (1) Absorption in 20 cm of water; (2) absorption in 10 cm of iron placed either in position A or in position B; (3) absorption in 10 cm of lead placed either in position A or in position B; (4) absorption in 2.5 cm of lead placed in position A.

The purpose of placing the absorber in two different positions was to obtain a measure of the importance of scattering compared to true absorption.

Several measurements were also performed with the second arrangement (Fig. 2) in which the maximum thickness of absorber that could be used was 10 cm. In this case the absorption in 10 cm of lead, iron, and aluminum was measured. The readings obtained from the recorders for both arrangements are summarized in Table I.

THE EFFECT OF SCATTERING

In order that the experimental data may be compared with the theoretical values they must be corrected for several perturbing factors. The most important of these is the effect of scattering which influences the apparent absorption in two different ways. A mesotron may be deflected from the beam by an elastic impact with the nucleus of the absorbing substance and hence will not be recorded by the anticoincidence counter. The multiple Coulomb scattering of mesotrons by nuclei has been calculated;[4] but it would be very difficult to evaluate, even approximately, the number of anticoincidences due to this effect because of the complicated geometrical conditions of the experiment. It was, therefore, considered more practicable to determine the effect of scattering empirically. This was done chiefly for lead, since the effect is much less important for the lighter elements. For this purpose, the apparatus in its first arrangement was used to measure the absorption in 2.5 cm of lead in position A, 10 cm of lead in position A,

[4] B. Rossi and K. Greisen, Rev. Mod. Phys. 13, 241 (1941).

and 10 cm of lead in position B. It is obvious that a much larger scattering angle is required in the A position than in the B position in order to deflect a mesotron out of the anticoincidence counters. Hence a rough consideration of the geometry of the experiment indicates that the effect of scattering should be much larger in the second case than in the first case.

Table I shows the results obtained for these three experiments. It appeared that the best way of utilizing them was to extrapolate graphically the value of the absorption per g/cm² of lead as a function of position as shown in Fig. 3. The abscissa indicates the distance of the lead absorber from the anticoincidence counter. The ordinate is the percentage absorption per g/cm² of lead. The horizontal length indicates the extension of the absorber, the vertical length the statistical error. A linear extrapolation was made and gave an absorption of 0.35 ± 0.015 percent for 10 g/cm² of lead for the ideal case of an absorber placed at zero distance from the group F. In the case of lead and iron, absorption measurements have been taken with the apparatus in both the first and the second arrangements. It is interesting to note that the results agree perfectly. This is particularly true in the case of lead where the extrapolated value of the absorption coincides with the value obtained in the second arrangement in which the geometry of the apparatus is such that the scattering is practically eliminated.

Because of this agreement, it has been deemed legitimate to consider both series of measurements as equally good and their average has been adopted as the most probable value of the absorption for the above mentioned substances (Table II).

Scattering will also affect the results through the lengthening of the path of the particle in the absorber. A correction for this effect was evaluated by using theoretical formulas given by Rossi and Greisen.[4] These authors give an expression for the square of the average scattering angle of a mesotron of initial momentum p_0, and possessing a momentum p after traversing a distance R (expressed in g/cm²) in an element of atomic number Z and of atomic weight A. They give:

$$\theta_m^2=16\pi\frac{\mu_e^2}{\mu^2}Nr_0^2\frac{Z^2}{A}\log\left(\frac{183}{Z^{\frac{1}{3}}}\right)\times\left[R\left(z,\frac{p_0}{\mu}\right)-R\left(z,\frac{p}{\mu}\right)\right]\frac{\log\left(\frac{1+y}{1+y_0}\frac{p_0}{p}\right)}{y_0+\frac{1}{y_0}-\left(y+\frac{1}{y}\right)}.$$

The symbols used in this formula have the following meaning: N is Avogadro's number; r_0 is the classical radius of the electron; μ_e is the mass of the electron; μ is the mass of the mesotron; and $y=[(p^2/\mu^2)+1]^{\frac{1}{2}}$. The masses are expressed in ev/c² and the momenta are expressed in ev/c. We now wish to calculate what thickness T of absorber corresponds to a path of length R, actually followed by the particle in its zig-zag motion through matter.

To do this we write:

$$dT=dR\cos\theta_m,$$

or

$$dT=dR\left(1-\frac{\theta^2m}{2!}+\frac{\theta^4m}{4!}+\cdots\right),$$

and since θ_m is generally small only the first two terms need be considered. Integrating, we have:

$$T\left(z,\frac{p}{\mu}\right)=R\left(z,\frac{p}{\mu}\right)-\int_0^{p_0/\mu}\frac{\theta_m^2}{2}\frac{dR}{d(p/\mu)}d\left(\frac{p}{\mu}\right).$$

The preceding integration has been performed for several values of the initial momentum p_0 ranging from $p_0/\mu=0$ to $p_0/\mu=3$ and for the substances on which our measurements have been made. It is interesting to note that T and R can be approximately expressed by the following linear relations:

Lead	$T=0.907R$,
Iron	$T=0.975R$,
Aluminum	$T=0.986R$,
Water	$T=1.0R$.

These correcting factors have been applied to the experimental values of the ranges that are listed in the fifth column of Table II. The corrected ranges are listed in the sixth column of the same table.

CORRECTION FOR THE DIVERGENCE OF THE BEAM

The purpose of this experiment was to obtain relative values of the absorption of slow meso-

trons in matter. Consequently the usefulness of our measurements would not be impaired by a slight divergence of the beam because this effect increases all the values of the absorption by a constant factor. This factor has been roughly evaluated from the geometry of the apparatus and found to be equal to 1.02. However, we thought it preferable to give our absorption measurements in terms of the actual thickness traversed and for this reason we have corrected them for the divergence of the beam. The true values are given in the fourth column of Table II.

THE EFFECT OF THE ELECTRONS IN EQUILIBRIUM WITH THE MESOTRON RADIATION

These absorption measurements have been made with a beam of mesotrons containing approximately six percent of electrons and it is important to make sure that the presence of these electrons in the apparatus does not affect our interpretation of the results. In this connection we must first note that these equilibrium electrons are produced by head-on collisions of the mesotrons with the electrons of the lead blocks placed in the telescope. Since only a few centimeters of lead are required for the radiation to attain equilibrium, we may safely assume that these equilibrium electrons are all produced in the layer placed immediately above the group D of counters. On the other hand, it can be shown that a mesotron which would be stopped in 10 cm of lead (our thickness of absorber) could not produce in the lead block above the group D an electron having more energy than 25×10^6 ev. The range of this electron in lead is only a few millimeters, and in all probability it could not emerge from the lead block in which it was produced. Consequently we may safely admit that within the precision of the experiment all the equilibrium electrons which had sufficient energy to emerge from the lead block in which they were produced must have been produced by energetic mesotrons which are not likely to be deflected out of the beam or stopped in the absorber. These mesotrons may reach the anticoincidence group alone or accompanied by their equilibrium electrons, but in both cases only one pulse will be given by the F group and the apparatus will behave normally.

CONCLUSION

We now wish to express the results of our absorption measurements in lead, iron, aluminum, and water, by means of four quantities which will be proportional to the ranges of the mesotrons in the above substances. To do this we make use of the fact that the absorption, in a thin absorber, is proportional to the thickness of absorber. We then calculate what thickness of absorber would stop a given (small) fraction, say 1 percent of the total radiation (see column 5, Table II).

The thickness of absorber thus calculated is such that it would stop all particles having a momentum less than a critical momentum p_c. Consequently, this thickness is equal (except for the correction due to scattering) to the range, in that absorber, of mesotrons of momentum p_c.

The thicknesses of lead, iron, aluminum, and water thus obtained from experimental measurement must be corrected for the multiple Coulomb scattering in the absorber, as previously explained. The corrected values for the experimental ranges are given in column 6, Table II.

On the other hand, the theoretical range-momentum curves[4] for different elements have the same shape and to a good approximation, differ only by a constant factor. Hence, to test the relationship between atomic number and range, we do not need to know p_c. It is only necessary to compare the corrected experimental values of the range with the theoretical values, for some convenient value of the momentum. If theory and experiment agree the two sets of values should be proportional. The theoretical and experimental values were made to agree for iron (see column 7, Table II).

Let us first consider the absorption in water. In this case, no satisfactory theoretical value of the energy loss is available. In fact, the calculations are based on a statistical model of the atom and cannot be expected to apply to hydrogen. Moreover, even if the correct value for hydrogen were known, it is by no means certain that the hydrogen in the water molecule would possess the same stopping power as in the free state. Hence a significant comparison between theory and experiment is possible only for lead, iron, and aluminum.

From the values in Table II one sees that the agreement is fairly good, but that there is a discrepancy which is definitely outside of the statistical error. The difference is in the sense that the experimentally observed absorption is less dependent upon the atomic number than should be expected according to the theory. There are several perturbing factors involved, and although an attempt has been made to evaluate their effects, one cannot be certain that they have all been accounted for with sufficient accuracy. In particular, it is possible that the electrons in equilibrium with the mesotrons affect the measured absorption to some extent. Moreover, there is some uncertainty in the number of mesotrons that are scattered out of the beam. In conclusion, we believe that the theoretical values are in approximate agreement with the experimental results and it appears probable that the discrepancies are not due to any fundamental inadequacy of the theory.

I wish to acknowledge my indebtedness to Dr. F. Rasetti for suggesting the problem and for valuable advice and discussion.

PHYSICAL REVIEW VOLUME 69, NUMBERS 11 AND 12 JUNE 1 AND 15, 1946

Performance of a Hot Wire Clusius and Dickel Column*,**

RALPH SIMON
*Sloane Physics Laboratory, Yale University, New Haven, Connecticut****

(Received June 8, 1942)

The separation factor for argon isotopes has been measured as a function of the gas pressure in a hot wire type of Clusius and Dickel column. The variation obtained is in accord with the predictions of the Furry, Jones, and Onsager theory. It is found empirically that the explicit expressions given by Furry, Jones, and Onsager for the flat, parallel wall case can be modified to give correct results for the extreme cylindrical case if the constants of the gas are evaluated at the proper mean temperatures. The existence of turbulence in the gas causes a slight, if any, decrease in the separation factor determined by extrapolation from the experimental data obtained under conditions of lamellar flow.

INTRODUCTION

IN 1938 Clusius and Dickel,[1] and subsequently Brewer and Bramley,[2] cascaded the small effect of thermal diffusion in separating isotopes by putting the gaseous isotopic mixture into the annular space between two concentric cylindrical surfaces, mounted vertically. By maintaining the inner surface at a higher temperature than the outer, convection currents are set up which carry the isotope that concentrates toward the hot surface to the top of the column, thus greatly increasing the transverse separation caused by the radial temperature gradient. Batteries of Clusius and Dickel columns coupled in series have since been used successfully to obtain large concentrations of important rare isotopes.[3]

The theory of the Clusius and Dickel method was first developed by Furry, Jones, and Onsager[4] in 1939 (hereinafter referred to as FJO) and also by Waldmann[5] and Debye.[6] FJO calculated explicit expressions for the vertical change in concentration from their general theory for the case of a temperature gradient between two flat,

* Part of a dissertation presented for the degree of Doctor of Philosophy at Yale University.

** This paper was received for publication on the date indicated but was voluntarily withheld from publication until the end of the war.

*** Now with the Signal Corps Engineering Laboratories, Bradley Beach, New Jersey.

[1] K. Clusius and G. Dickel, Naturwiss. **26**, 546 (1938); Zeits. f. physik. Chemie **B44**, 397 (1939).

[2] A. K. Brewer and A. Bramley, Phys. Rev. **55**, 590A (1939); J. Chem. Phys. **7**, 553L (1939).

[3] W. W. Watson, Phys. Rev. **57**, 562A (1940) and **57**, 899 (1940); E. F. Shrader, Phys. Rev. **58**, 475L (1940); S. B. Welles, Phys. Rev. **59**, 920A (1941); R. Fleischmann, Physik. Zeits. **41**, 14 (1940); A. O. Nier and J. Bardeen, J. Chem. Phys. **9**, 690 (1941).

[4] W. H. Furry, R. Clark Jones, and L. Onsager, Phys. Rev. **55**, 1083 (1939).

[5] L. Waldmann, Zeits. f. Physik **114**, 53 (1939).

[6] P. Debye, Ann. d. Physik **36**, 284 (1939).

parallel, vertical walls. Furry and Jones[7] extended the theory to the cylindrical case and published their results for two special cases.

The theoretical dependence, according to FJO, of the amount of separation of $C^{12}H_4$ and $C^{13}H_4$ on the gas pressure has been verified experimentally by Nier[8] and by Taylor and Glockler[9] using concentric metal cylinders. Measurements of this dependence have been reported for the extreme cylindrical case where the inner surface is an electrically heated wire.[10] The use of a hot wire permits the maintainance of much larger temperature gradients without excessive power inputs.

EXPERIMENTAL APPARATUS

An all-glass column was constructed so that the working length of the gas chamber was 200 cm. The gas chamber consisted of a 22-mm inner diameter glass tube cooled on the outside by a water jacket. The hot surface was a 20-mil tungsten wire heated by direct current to avoid vibration. Four sets of 20-mil nickel wire crosspieces were spot-welded onto the wire at .50-cm intervals to keep the wire centered in the column. The lower extremity of the wire hung freely under the tension of a 450-g cylindrical weight which consisted of a hollow copper tube filled with lead. Heating the wire in a vacuum at 1200°C for about thirty minutes served to straighten it and also to remove the oxide coating from its surface, thus greatly reducing radiant power loss needed to maintain a given temperature.

The gas chamber was terminated by two tapered ground-glass joints. The upper joint was fitted with a cap containing a sealed-in 75-mil tungsten lead. The cap was water-cooled to prevent the metal-to-glass seal and the stopcock grease used in the joint from becoming too hot. The lower ground-glass joint was fitted with a length of glass tubing surrounding the weight and terminating in a mercury cup deep enough to allow for as much as a 2.5-cm thermal extension of the wire. A copper lead from the bottom of the weight provided contact with the mercury. The lower joint was cooled sufficiently well by a flow of water through a lead pipe wrapped around the outside. Spot-welding of the wire to the leads was accomplished with the intermediate use of nickel.

TURBULENCE MEASUREMENTS

The FJO theory was derived on the assumption that the convective flow of gas is lamellar in the annular space between the two surfaces; i.e., the convection velocity, v, is entirely in the vertical, z, direction and is a function only of the radial distance, r, from the center of the wire, except, of course, at the very ends of the column. Preliminary experiments were undertaken to determine the range of stability of lamellar flow, following the method of Onsager and Watson.[11]

Dissipation of the power input necessary to maintain the wire at a given temperature is caused by the following, if the flow is lamellar:

(a) Radiation from the wire.
(b) Transverse conduction of heat through the gas.
(c) Conduction of heat through the spacers and leads.
(d) Heat losses at the ends of the column due to the convective flow.

Items (a) and (c) are obviously independent of the pressure of the gas in the column. Item (b) is independent of the pressure if the mean free path of the gas molecules is much smaller than the gap space between the wire and cold wall, a condition which was strongly satisfied for the pressures used. Item (d) is pressure dependent, but its contribution to the power loss will later be experimentally demonstrated to be negligible. Consequently, with a given power input, the temperature of the wire should remain constant as the gas pressure is increased until the critical Reynolds number for this type of flow is reached, above which the lamellar flow becomes unstable and breaks up into turbulence. The turbulent swirls provide an additional, pressure-dependent mechanism for direct transfer of heat from the wire to the cold wall. Hence, above the critical turbulence pressure, the temperature of the wire should decrease with increasing gas pressure and constant power input.

The critical pressures, p_c, were determined for

[7] W. H. Furry and R. C. Jones, Phys. Rev. **57**, 561A (1940).
[8] A. O. Nier, Phys. Rev. **57**, 30 (1940) and **57**, 358A (1940).
[9] T. I. Taylor and G. Glockler, J. Chem. Phys. **8**, 843 (1940).
[10] R. Simon, Phys. Rev. **61**, 388A (1942).
[11] L. Onsager and W. W. Watson, Phys. Rev. **56**, 474 (1939).

wire temperatures ranging from 400° to 1700°K. With a low gas pressure in the column, the desired initial wire temperature was obtained by adjusting the power input.[12] Once established, the power input was kept constant and changes in the temperature-dependent properties of the wire were recorded for increasing gas pressure. After going well beyond the critical pressure, readings were taken for decreasing pressure. The spacers and cooler spots on the wire in their vicinity introduce finite disturbances into the stream of gas which should cause general turbulence at the lowest possible Reynolds number, below which induced turbulence would be damped out. This fact was borne out experimentally as the readings for both increasing and decreasing pressure could be represented by the same curve in each case.

Figure 1 shows a typical set of curves obtained. The mean value of the pressures on each curve at which the line of zero slope intersects that with the negative slope was taken to be p_c. A slight downward trend of the "low pressure" line could be possibly detected only for the 1700°K run, which justifies the assumption that item (d) on the list of power losses is negligible. The results for nine runs are tabulated in Table I and plotted in Fig. 2.

In calculating the Reynolds numbers,[13] $R=v\rho L/\eta$, the flat-wall expression,

$$R=\frac{(2w)^3g}{18\sqrt{3}}\left(\frac{\rho}{\eta}\right)^2\frac{T_2-T_1}{T_2+T_1}, \tag{1}$$

TABLE I. Results of the turbulence experiments.

T_2(°K)	p_c(cm of Hg)	Reynolds number	Power input (watts)
400±20	57±2	109	9.6
500±20	47±1	76.0	15.0
600±20	40±2	47.7	28.6
700±20	38±1	35.4	46.2
900±20	49±2	37.1	101
1100±20	61±2	40.6	167
1300±20	67±7	34.0	270
1500±20	77±7	32.6	600
1700±20	80±5	26.1	1220

[12] The brightness temperature of the wire was measured by a Leeds and Northrup optical pyrometer. Below the visual temperature range temperatures were set by using the electrical resistance and thermal extension characteristics of tungsten. A thermocouple could not be used because it would conduct away heat rapidly enough to make the point of contact with the wire considerably cooler.

[13] O. Reynolds, Trans. Roy. Soc. London **A174**, 935 (1883).

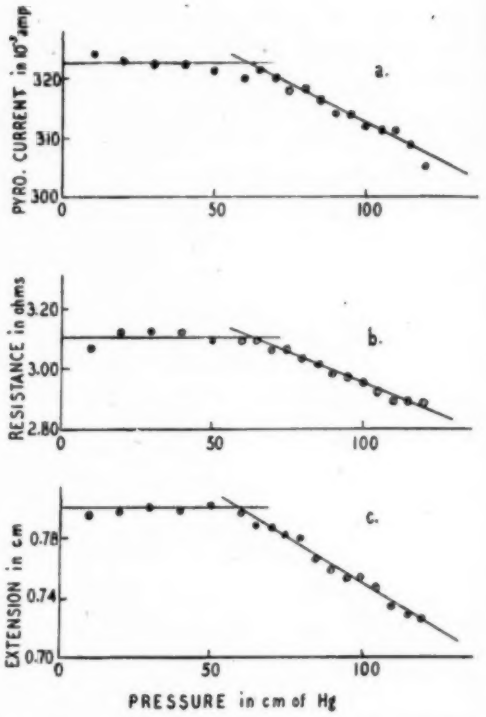

FIG. 1. Temperature dependent properties of the wire as functions of the pressure of the gas in the column for an initial wire temperature of 1100°K, which corresponds to the lines of zero slope. (a) Current through the filament of the pyrometer bulb at "matching" brightness. (b) Electrical resistance of the wire. (c) Thermal extension of the wire from its initial length at the cold wall temperature.

was used. The gap space $2w=b-a$ was substituted for the length dimension, L; where $a, b\equiv$radius of the wire, cold wall, respectively. The density of the gas (argon), ρ, was computed from the gas laws at the pressure p_c and at the temperature $\frac{1}{2}(T_2+T_1)$ in each case, where $T_2, T_1\equiv$temperature of the wire, cold wall, respectively. The viscosity, η, was calculated from Sutherland's formula,[14]

$$\eta=\eta_0\frac{T_0+C}{T+C}(T/T_0)^{\frac{1}{2}},$$

at $T=\frac{1}{2}(T_2+T_1)$ and with $C=140°$ and $\eta_0=2.10\times10^{-6}$ poise at $T_0=273$°K. The maximum convection velocity[11]

$$\frac{(2w)^2g}{18\sqrt{3}}\frac{\rho}{\eta}\frac{T_2-T_1}{T_2+T_1}$$

was used for v. g is the acceleration of gravity.

[14] W. Sutherland, Phil. Mag. **36**, 507 (1893).

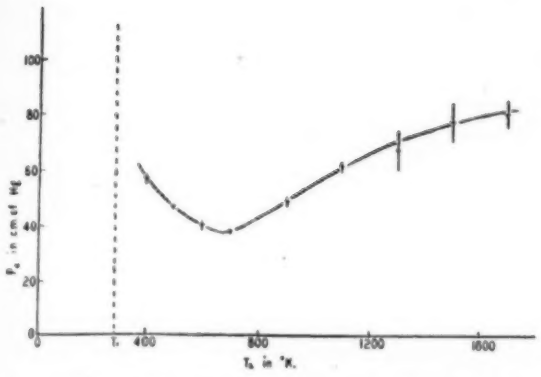

FIG. 2. The critical gas pressure, p_c, at which turbulence first appears in the column plotted *vs.* the hot wire temperature, T_2. T_1 is the constant cold-wall temperature.

The choice of $\frac{1}{2}(T_2+T_1)$ at which to calculate the gas constants in R is arbitrary because v_{max} does not occur in the column where $T=\frac{1}{2}(T_2+T_1)$. However, calculations of R at other temperatures between T_1 and $\frac{1}{2}(T_2+T_1)$ did not result in a more consistent set of Reynolds numbers. The Reynolds numbers obtained are only about 2 percent of those for pure pressure flow through pipes.

The curve of Fig. 2 is approximately represented by Eq. (1) if we assume a constant R and $\rho \propto p_c$. Turbulence first occurs at lower pressures for higher wire temperatures because of the increase in convection velocity with increased temperature gradient. However, the effect of increased velocity is soon overtaken by the effect of increased viscosity and decreased density near the hot wire with increasing temperature, which makes for stability of lamellar flow. Hence a minimum occurs at $T_2=650°\pm50°$K and the p_c *vs.* T_2 curve subsequently rises.

SEPARATION FACTOR MEASUREMENTS

The separation factor, f, of a thermal diffusion column is defined as the ratio of the relative particle concentrations of the two isotopes at the top of the column to that at the bottom; i.e., $f=(c_1/c_2)_{top}/(c_1/c_2)_{bottom}$, where the subscript 1 refers to the lighter isotope. According to FJO,[4] $\ln f=4A_d l$, where

$$A_d=\frac{A}{1+K_d/K_c}=\frac{H/2K_c}{1+K_d/K_c}. \tag{2}$$

and $2l$ is the length of the column. H, K_c, K_d are the coefficients of transport, remixing by convection, and remixing by diffusion, respectively. $A \propto \alpha D\eta/w^4\rho \propto 1/p^2$ and $K_d/K_c \propto (D\eta/w^2\rho)^2 \propto 1/p^4$, since D, the coefficient of self-diffusion of the gas, is proportional to η/ρ. The thermal diffusion constant, α, is given by

$$\alpha=\frac{105}{118}\frac{m_2-m_1}{m_2+m_1}R_T, \tag{3}$$

where the m's are the respective masses of the two isotopic molecules and $R_T(<1)$ represents a measure of the departure of the molecule from the hard-sphere model.[15] Hence, as a function of pressure, one may write

$$\ln f=(a'/p^2)/(1+b'/p^4). \tag{4}$$

The relation of Eq. (4) is experimentally verified if a straight line results from plotting $p^2/\ln f$ *vs.* p^4. Experimental values of the constants a' and b' may be determined from the slope and intercept of this line.

The same column was used for these measurements as for the turbulence measurements except that its length was reduced to 170 cm. No end-volumes were used other than the "dead" spaces at the top and bottom of the column, estimated to be about 30 cc each. At the end of each run small samples (about 3 cc) of the gas were removed from the top and bottom of the column in break-seal tubes. These were analyzed with a Nier-type 60° mass spectrometer[16] built by Professor W. W. Watson, obtaining the relative particle abundances of A^{36} to A^{40}.[17] No appreciable impurities with peaks at the same places as singly ionized masses 36 or 40 were found in the

TABLE II. Results of the separation factor measurements.

Temperature range	p(cm of Hg)	Separation factor, f	
	22.0±0.2	4.5	± 6.7%
$T_2=1500°$K	34.0±0.2	5.2	±11.8%
$T_1=293°$K	42.2±0.2	4.4	± 9.8%
	48.0±0.2	3.6	± 1.4%
	18.8±0.2	3.9	± 2.4%
$T_2=1100°$K	27.8±0.2	2.8	± 7.8%
$T_1=293°$K	36.0±0.2	2.4	± 4.5%
	40.8±0.2	1.7	± 8.2%

[15] R. Clark Jones, Phys. Rev. **58**, 111 (1940).
[16] A. O. Nier, Rev. Sci. Inst. **11**, 212 (1940).
[17] Argon has three stable isotopes of natural abundances: A^{36}—0.31 percent, A^{38}—0.06 percent, A^{40}—99.64 percent.

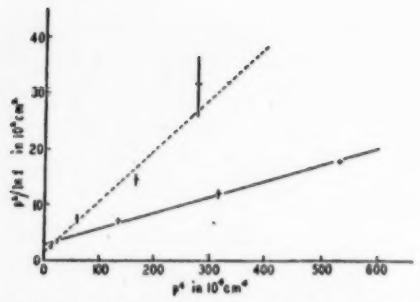

FIG. 3. Verification of the theoretical dependence of the separation factor on the gas pressure. Solid line—wire temperature of 1500°K. Broken line—wire temperature of 1100°K.

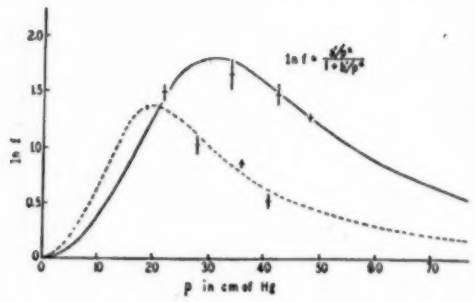

FIG. 4. Natural logarithm of the separation factor as a function of gas pressure with the constants a' and b' determined from FIG. 3. Solid line—wire temperature of 1500°K. Broken line—wire temperature of 1100°K.

spectrometer. A^{38} was neglected because:

a. The A^{38} peak could not be completely resolved from the large A^{40} peak.

b. The separation factor for A^{38} from A^{40} is only about the square root of that for A^{36} from A^{40}, since $f \propto e^{\alpha}$.

c. The presence of A^{36} does not invalidate any theoretical analysis based on a binary mixture.[18]

Preliminary runs were made to determine the time needed to attain equilibrium. The relaxation time was about thirty minutes for somewhere near the least favorable case. Consequently all runs were made from four to five hours long to be certain that equilibrium had been reached.

Table II summarizes the results of runs at four different pressures each for wire temperatures of 1100°K and 1500°K. The highest pressure used in each case was well below the critical turbulence pressure for the respective temperature. $p^2/\ln f$ is plotted against p^4 in Fig. 3. The theoretical variation is evidently well satisfied in the 1500°K case. The deviation of the 1100°K points from a straight line, which appear to be random, are ascribed to difficulties occasioned with some of the analyses. The slope and intercept of each line were calculated by the method of least squares with weights on each point inversely proportional to the actual error in $p^2/\ln f$. By substituting the values of the constants a' and b' thus determined into Eq. (4), the experimental variation of the separation factor with pressure is

$$\ln f = \frac{3.42\times10^3/p^2}{1+8.95\times10^5/p^4} \quad \text{for} \quad T_2=1500°\text{K}, \qquad (5)$$

and

$$\ln f = \frac{1.10\times10^3/p^2}{1+1.59\times10^5/p^4} \quad \text{for} \quad T_2=1100°\text{K}, \qquad (5')$$

where p is in cm of Hg. These relations are plotted in Fig. 4.

From Eq. (4) the maximum value of $\ln f$ is $a'/2b'^{\frac{1}{2}}$ and comes at a pressure for which $b'/p^4=1$. At maximum $\ln f$, $p^2/\ln f=2b'/a'$; hence the determination of optimum p and f can be made very simply graphically from an experimental plot such as Fig. 3. They correspond to the point on the straight line which has double the ordinate of the intercept.

COMPARISON WITH THE THEORY

FJO give explicit expressions for A and K_d/K_c for a gas of Maxwellian molecules and for a gas of hard spheres, derived on the assumption of a temperature gradient between two flat, parallel, vertical walls. The values obtained from either of these expressions, calculating the gas constants at $\frac{1}{2}(T_2+T_1)$ as suggested by FJO, are several times greater than the experimental ones. However, excellent agreement with experiment has been obtained by modifying the simpler expressions for the Maxwellian case[19] to read

$$A=H/2K_c=\frac{63}{4}\frac{\alpha}{gw^4}\left\langle\left(\frac{D\eta}{\rho}\right)\right\rangle_{Av} \qquad (6)$$

and

$$\frac{K_d}{K_c}=1890\frac{1}{g^2w^6}\left\langle\left(\frac{D\eta}{\rho}\right)^2\right\rangle_{Av}\ln\left(\frac{r_0}{w}\right). \qquad (7)$$

The $\langle\ \rangle_{Av}$ denotes that the gas constants are to be suitably averaged over the gas in the column. r_0 will be defined later.

One can obtain a simple expression for the temperature distribution in the column by using the inverse power repulsive model of intermolecular

[18] R. Clark Jones, Phys. Rev. **59**, 1019 (1941). Section on "Ternary and higher order mixtures."

[19] Equations (31) and (32) of reference 4.

force, $F=K/d^{\nu}$. For this model the thermal conductivity, $\lambda \propto T^{n}$, where $n=\frac{1}{2}(\nu+3)/(\nu-1)$. If Q is the heat flow per second per cm of length through any concentric cylindrical section of radius r in the gas chamber, $Q/2\pi r=-\lambda(dT/dr)$. Using $\lambda=\lambda_0(T/T_0)^n$ and integrating from a to r (T_2 to T), we obtain

$$T_2^{n+1}-T^{n+1}=\frac{(n+1)QT_0^n}{2\pi\lambda_0}\ln\left(\frac{r}{a}\right).$$

Eliminating QT_0^n/λ_0 by using

$$T_2^{n+1}-T_1^{n+1}=\frac{(n+1)QT_0^n}{2\pi\lambda_0}\ln\left(\frac{b}{a}\right),$$

we find the radial temperature distribution may be described by the relation

$$r=r_0\equiv e^{-\gamma x}, \tag{8}$$

where

$$x\equiv T^{n+1},\quad \gamma\equiv \ln\,(b/a)/(x_2-x_1)$$

and

$$r_0\equiv\exp\,[(x_2\ln b-x_1\ln a)/(x_2-x_1)].$$

T as a function of r, as given by Eq. (8), is plotted in Fig. 5. The mean qth power of the temperature, averaged over the gas in the column, is given by

$$\langle T^q\rangle_{Av}=\frac{1}{\pi(b^2-a^2)}\int_a^b T^q\cdot 2\pi r dr$$
$$=\frac{2\gamma r_0^{\,2}}{b^2-a^2}\int_{x_1}^{x_2} x^{q/(n+1)}e^{-2\gamma x}dx. \tag{9}$$

The inverse power model is adequate only if n is considered as a slowly varying function of temperature. However, since n has been assumed to be constant in the above derivation, a suitable mean value of n must be found for given hot-wire and cold-wall temperatures. This may be done very simply experimentally as follows:

The column was filled with a given amount of gas at the cold-wall temperature, $T_1=293°K$. The wire temperature, T_2, was then increased in steps to 1700°K and the gas pressure recorded. Within the limits of experimental error, the pressure was found to be a linear function of T_2 of the form $p=p_0[1+(T_2-T_1)/7.2T_1]$.[20]

From the gas laws one can calculate a temperature T' which would produce the same experimental change in pressure as a given T_2 if all of the gas were at T'. For $T_2=1100°K$, $T'=404\pm1°K$; and for $T_2=1500°K$, $T'=460\pm1°K$. The total mass of gas in the column equals

$$\int\int \rho\cdot 2\pi r dr dz=\int\int \frac{p}{R'T}\cdot 2\pi r dr dz=\text{constant},$$

where R' is the gas constant per gram. Since the maximum convection velocity is of the order of 10 cm/sec., p is not a function of r. The slight variation of p with z may be disregarded and, besides, p was measured at only one point in the column (at the bottom). Since the temperature gradient is determined by the transverse conduction of heat alone (except for comparatively small lengths at the top and bottom of the column), T is not a function of z. Consequently,

$$1/p\propto\int_a^b (1/T)\cdot 2\pi r dr.$$

Thus T' is the reciprocal of the mean reciprocal temperature.

Table III summarizes the results of numerical integration of Eq. (9) with $q=-1$ for $T_2=1500°K$ and $T_1=293°K$. By interpolating in Table III it is seen that the suitable mean value of n to use

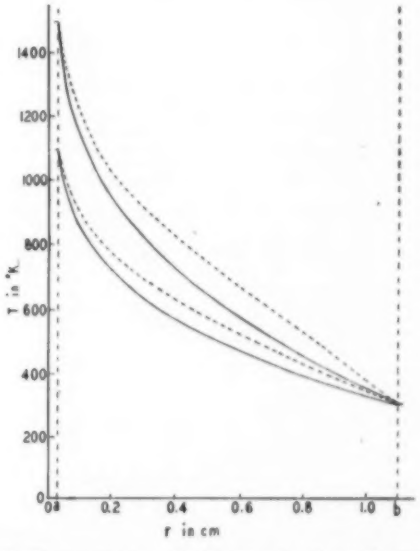

FIG. 5. Temperature of the gas in the volumn *vs.* the distance from the center of the wire for wire temperatures of 1500°K and 1100°K and for a cold-wall temperature of 300°K. a=radius of wire; b=radius of cold wall. Solid lines—for a gas of hard spheres ($n=\frac{1}{2}$). Broken lines—for a gas of Maxwellian molecules ($n=1$). Note that the gas as a whole is "colder" as the hard sphere case is approached.

[20] The initial pressure, $p_0=30$ cm of Hg, was low enough so that this line, when plotted on Fig. 2, fell entirely below the turbulence region.

TABLE III. Calculated values of T' for $T_2=1500°K$, $T_1=293°K$.

n	$T'(°K)$
0.5	447
0.6	455
0.7	463
1.0	487

for this temperature range is $\frac{2}{3}$. In the same manner it was found that the value of n appropriate for the range 293° to 1100°K is 0.7.

For $n=\frac{2}{3}$: $\nu=13$, $D=(6/5)f(\nu)\eta/\rho=1.37\eta/\rho$, and $R_T=(\nu-5)/(\nu-1)C(\nu)=0.597$.[21] For $n=0.7$: $\nu=11$, $D=1.40\eta/\rho$, and $R_T=0.529$.[21]

$\langle D\eta/\rho\rangle_{Av}\propto\langle(\eta/\rho)^2\rangle_{Av}\propto\langle T^{2(n+1)}\rangle_{Av}$. Equation (9) can be integrated exactly for $q=2(n+1)$ yielding

$$\langle T^{2(n+1)}\rangle_{Av}=\frac{b^2}{b^2-a^2}\left(x_1^2+\frac{x_1}{\gamma}+\frac{1}{2\gamma^2}\right)-\frac{a^2}{b^2-a^2}\left(x_2^2+\frac{x_2}{\gamma}+\frac{1}{2\gamma^2}\right).$$

Similarly, $\langle(D\eta/\rho)^2\rangle_{Av}\propto\langle T^{4(n+1)}\rangle_{Av}$. From Eq. (9),

$$\langle T^{4(n+1)}\rangle_{Av}=\frac{b^2}{b^2-a^2}\left(x_1^4+2\frac{x_1^3}{\gamma}+3\frac{x_1^2}{\gamma^2}+3\frac{x_1}{\gamma^3}+\frac{3}{2\gamma^4}\right)-\frac{a^2}{b^2-a^2}\left(x_2^4+2\frac{x_2^3}{\gamma}+3\frac{x_2^2}{\gamma^2}+3\frac{x_2}{\gamma^3}+\frac{3}{2\gamma^4}\right).$$

Table IV lists values of these mean temperatures for the two cases in question. Using the appropriate ones at which to calculate the gas constants in Eqs. (6) and (7) (ρ by the gas laws and η by Sutherland's formula), and also using Eq. (3) for the thermal diffusion constant α, one obtains:

$$\ln f=\frac{3.46\times10^3/p^2}{1+9.66\times10^5/p^4}\quad\text{for}\quad T_2=1500°K,\qquad(10)$$

and

$$\ln f=\frac{1.45\times10^3/p^2}{1+1.97\times10^5/p^4}\quad\text{for}\quad T_2=1100°K.\qquad(10')$$

When one considers the fact that any slight deviation from the cylindrical shape of the cold wall, such as might easily be expected for glass tubing, would produce appreciable changes in A and K_d/K_c which vary as w^{-4} and w^{-6}, respectively, besides introducing additional remixing due to temperature asymmetry, one finds the agreement between this semi-empirical theory and experiment is excellent. That agreement is markedly better between (10) and (5) than between (10′) and (5′) may be ascribed to the fact that the experimental relation (5′) is nowhere near as reliable as (5). (See Fig. 3.)

[21] From a table of values of $(6/5)f(\nu)$ and $C(\nu)$ in reference 15.

TABLE IV. Mean temperatures at which to evaluate the gas constants in Eqs. (6) and (7).

$T_2(°K)$	n	$(\langle T^{10/3}\rangle_{Av})^{3/10}$	$(\langle T^{20/3}\rangle_{Av})^{3/20}$	$(\langle T^{3.4}\rangle_{Av})^{1/3.4}$	$(\langle T^{4.4}\rangle_{Av})^{1/4.4}$
1500	2/3	613°K	736°K		
1100	7/10			490°K	564°K

In passing, it is to be noted that experiment yields only the relative magnitudes of the three constants H, K_c, and K_d. One is also interested in the value of the coefficient of transport, H, in order to be able to estimate the relaxation time and also to "match" the mass transports of the units of a multi-stage apparatus.[4] Knowing the appropriate mean value of n, one may calculate easily the coefficient of remixing by longitudinal diffusion since it is merely

$$K_d=\int_a^b\rho D\cdot2\pi r dr.$$

H can then be found from the values of $A=H/2K_c$ and K_d/K_c.

EFFECT OF TURBULENCE ON SEPARATION

Additional measurements of the separation factor were made for $T_2=1500°K$ at pressures above the critical pressure for turbulence. The results are: $f=1.63\pm0.07$ for $p=80.6$ cm of Hg, and $f=1.39\pm0.07$ for $p=96.2$ cm of Hg. Substituting these pressures into Eq. (5), one obtains $f=1.67$ and 1.44, respectively. Thus turbulence produces a slight, if any, decrease in the separation factor calculated by extrapolation from the experimental data obtained under conditions of lamellar flow.

To the author's knowledge, there exists no evidence that turbulence is definitely harmful to the separation process. It has been conjectured that turbulence is harmful since the FJO theory is based on the assumption of lamellar flow. The experiments of Groth[22] on xenon, with a similar

[22] W. Groth, Naturwiss. 27, 260 (1939).

hot tungsten wire apparatus, has been used as evidence that turbulence decreases separation.[11] For a column of 12-mm diameter and at atmospheric pressure Groth found that isotope separation increased with wire temperature but reached a maximum at 1000°. On the other hand, for a tube diameter of 5 mm, separation continued to increase up to the highest temperature used, 1750°. This behavior is to be expected if the 1100°K curve of Fig. 4 is correct. Since the $\ln f$ *vs.* p curves for various values of T_2 overlap and the maxima shift to higher pressures with increasing T_2, there is an optimum wire temperature for maximum separation for a given fixed pressure and gap space.

Although the geometry of the convective flow of the gas is not quite the same and hence the Reynolds number may have a different magnitude, one can, perhaps, approximately apply the author's experimental turbulence curve, Fig. 2, to Groth's case by adjusting for the differences in w and η/ρ according to Eq. (1). This procedure multiplies the ordinates of Fig. 2 by about 0.9 and shifts the minimum to the left, since the viscosity increases more rapidly with temperature for xenon than for argon, n being closer to unity for xenon.[15] Since the wire temperatures used by Groth are to the right of the minimum point, an increase in temperature at constant pressure would not produce turbulence. The gas in Groth's larger diameter column may well have been turbulent at all the temperatures he used, becoming less turbulent for higher wire temperatures.

Experiments performed by Bramley and Brewer[23] seem to show that turbulence is definitely advantageous to the separation process. However, they used systems of corrugations or baffles that produced well-defined swirls of gas in definite paths and not isotropic turbulence. This procedure may conceivably be a favorable mechanism for the thermal diffusion process.

The failure of turbulence to produce a marked decrease in separation may be caused by the fact that the pressures used were only slightly above the critical pressure for 1500°K, and hence the turbulent swirls were not violent enough to compete with the thermal diffusion process, which maintains the transverse concentration gradient.[24] Measurements made at still higher pressures would be indecisive, because the extrapolated separation factor would approach too close to unity to be able to distinguish with any accuracy a possible decrease in $\ln f$ due to turbulence.

Another possible explanation is that turbulence does introduce a new separating mechanism as borne out by the experiments of Bramley and Brewer. A theoretical investigation of this point would be desirable.

ACKNOWLEDGMENTS

The author is indebted to Professor William W. Watson for the indispensable assistance and encouragement he has given him throughout the progress of all phases of this work. He also wishes to express his appreciation to Professor Lars Onsager of the Yale Chemistry Department for valuable experimental suggestions and advice with the theory.

[23] A. Bramley and A. K. Brewer, Science **90**, 165 (1939); J. Chem. Phys. **7**, 972L (1939).

[24] There is no doubt that some turbulence existed in the gas for these runs because of the 1.3 percent and 4.8 percent greater power inputs at pressures of 80.6 cm and 96.2 cm of Hg, respectively, needed to maintain the wire at 1500°K than was required for the previous runs under lamellar flow conditions.

PHYSICAL REVIEW VOLUME 69, NUMBERS 11 AND 12 JUNE 1 AND 15, 1946

A New Method of Determining Electronegativity from Other Atomic Properties

WALTER GORDY
Department of Physics, Duke University, Durham, North Carolina

(Received March 18, 1946)

The relation,

$$x=0.31\left(\frac{n+1}{r}\right)+0.50,$$

where x represents the electronegativity of an atom according to Pauling's revised scale, n the number of electrons in its incompletely filled (valence) shells, and r its single bond covalent radius measured in Angstroms, has been found valid for all elements having x values available for comparison, except for Ag, Au, and Cu. This equation is used to extend the electronegativity scale to include a total of fifty-two elements. A chart is constructed to demonstrate the systematic relation of the values to the periodic table. Beginning with the definition of the electronegativity of a neutral atom in a stable molecule as the potential at a distance r (covalent radius) from its nucleus which is caused by the nuclear charge effective at that distance, a simple theoretical justification is offered for the existence of a linear relation between x and $(n+1)/r$. This relation, like Mulliken's, provides an "absolute" scale of electronegativity values.

INTRODUCTION

RIGID mathematical methods which attempt to express the properties of molecules in terms of the motion of individual electrons are almost hopelessly complicated for any except the simplest type of molecules. For this reason attempts to define and measure over-all properties or lumped constants of the atoms, such as electronegativity or atomic radii, which can be used in approximate but widely applicable calculations, are of great significance.

From thermal data Pauling[1,2] has established an approximate scale of relative electronegativity values for thirty-three elements. By qualitative theoretical considerations and from a comparison of results with Pauling's relative scale, Mulliken[3] has shown that the average of the ionization potential and electron affinity of an atom, $(I+E)/2$, is a measure of its electronegativity. Though it has a somewhat better theoretical basis, Mulliken's method is not as widely applicable as that of Pauling. However, the values that have been determined by his method have served the useful purpose of fixing the origin of the more extensive relative scale of Pauling so that it is no longer arbitrary.

Recently the author[4] has found an empirical relation, of the form

$$k=aN(x_Ax_B/d_{AB}^2)^{\frac{1}{4}}+b,$$

which applies to the bonds of a large number of diatomic and simple polyatomic molecules. In this equation x_A and x_B are the electronegativities of the atoms forming a given bond AB; N, k, and d_{AB} are the bond order, bond-stretching force constant, and bond length, respectively; and a and b are constants for certain broad classes of molecules. Pauling's values were used to establish the relation, which was then used to determine the electronegativities of several atoms not listed by Pauling and to extend some of his values to an additional place whenever the accuracy of the available data seemed to justify it. By means of a new relation, to be described here, the electronegativity scale is extended further to include a total of fifty-two elements.

ELECTRONEGATIVITY AS A FUNCTION OF ATOMIC RADIUS AND EFFECTIVE NUCLEAR CHARGE

I have examined the possibility of defining the electronegativity of a neutral atom of a stable molecule as the potential, $(Z_{eff})e/r$, where $(Z_{eff})e$ is the effective nuclear charge of the atom acting

[1] L. Pauling, *The Nature of the Chemical Bond* (Cornell University Press, Ithaca, New York, 1939), p. 64.
[2] L. Pauling, J. Am. Chem. Soc. **54**, 3570 (1932).
[3] R. S. Mulliken, J. Chem. Phys. **2**, 782 (1934); **3**, 573 (1935).
[4] W. Gordy, Phys. Rev. **69**, 130 (1946); J. Chem. Phys., in press.

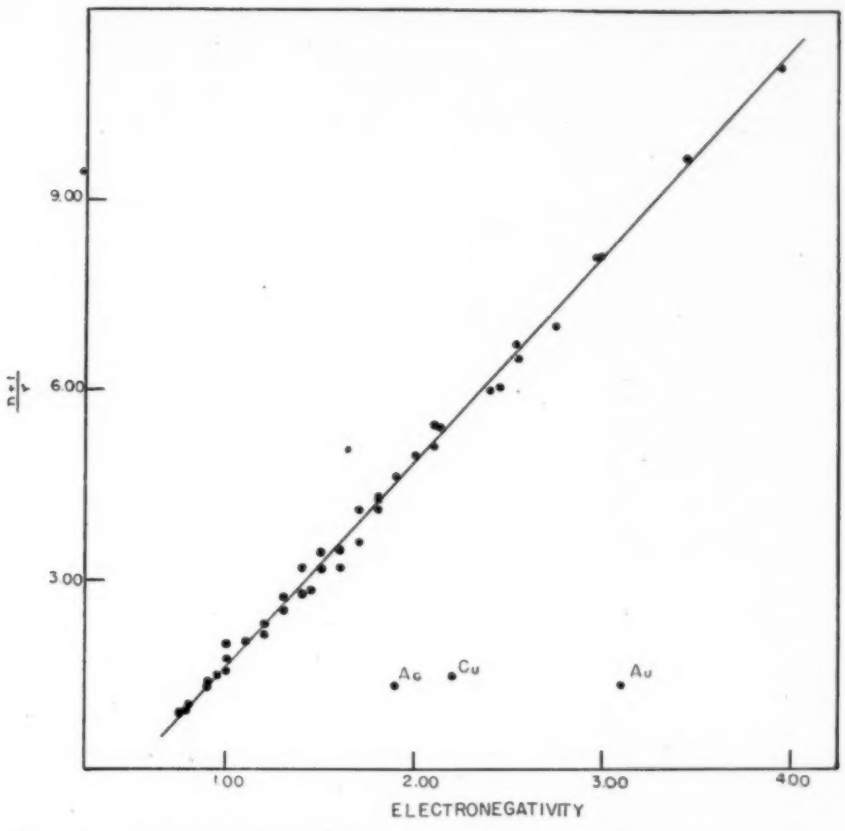

FIG. 1. A plot of electronegativity, x, as a function of $(n+1)/r$, for the elements listed in Table I except those in parentheses.

on a valence electron at a distance from its nucleus equal to its single bond covalent radius r.

If the simplifying assumption is made that all the electrons in the closed shells below the valence shell exert their full screening power, and that the screening constant[5] of one valence electron for another is 0.5, then,

$$Z_{eff}=n-0.5(n-1)=0.5(n+1),$$

where n represents the number of electrons in the incompletely filled (valence) shells. Similar assumptions[6] regarding screening constants have been used successfully in atomic spectra for certain non-penetrating orbits. Since the part of the orbit of a valence electron which is effective in forming a covalent bond—which contributes to the effective bonding cloud of an electron pair bond—would probably lie well outside the region of greatest electron density of the inner closed shells, the assumption of complete screening by all except the valence electrons would seem to be justified for the present purpose. It is at least justified for an approximate test of the proposed definition which expresses electronegativity as the potential at a point which is essentially outside the inner closed shell.

Substituting $0.5(n+1)$ for Z_{eff} in the proposed definition of electronegativity, x, gives

$$x=\frac{(Z_{eff})e}{r}=k\left(\frac{n+1}{r}\right), \qquad (I)$$

where k is the constant $0.5e$.

To test this theory, I have plotted x as a function of $(n+1)/r$. Results are shown in

[5] Pauling (reference 1, p. 65) uses 0.4 for the screening constant of a valence electron. This value is almost as satisfactory as the one assumed here. Because the same screening constant is used for all the valence electrons the results here are not particularly sensitive to changes in its value.

[6] A. H. Compton and S. K. Allison, *X-Rays in Theory and Experiment* (D. van Nostrand Company, New York, 1935), p. 37; L. Pauling and S. Goudsmit, *The Structure of Line Spectra* (McGraw-Hill Book Company, Inc., New York, 1930), Chap. III.

TABLE I. Electronegativities, covalent radii and number of valence electrons.

Atom	Single bond covalent radius r	Valence electrons n	Electronegativity[f] x	$0.31\left(\frac{n+1}{r}\right)+0.50$
Ag	1.53[a]	1	1.9	0.91
Al	1.26[a]	3	1.5	1.48
As	1.21[b]	5	2.0	2.04
Au	1.50[a]	1	3.1	0.92
B	0.88[b]	3	1.9	1.91
Ba	2.17[c]	2	0.9	0.93
Be	1.06[a]	2	1.45	1.38
Bi	1.40[a]	5	1.8	1.83
Br	1.14[b]	7	2.75	2.68
C	0.77[b]	4	2.55	2.52
Ca	1.78[d]	2	1.0	1.03
(Cb)	1.43[e]	5	(1.8)	1.76
Cd	1.48[a]	2	1.1	1.13
Cl	0.99[b]	7	2.97	3.00
(Cr)	1.25[e]	6	(2.2)	2.24
Cs	2.25[e]	1	0.75	0.78
Cu	1.35[a]	1	2.2	0.96
F	0.72[e]	7	3.95	3.94
Ga	1.26[a]	3	1.4	1.48
Ge	1.22[b]	4	1.7	1.77
H	0.37[e]	1	2.13	2.17
Hg	1.50[e]	2	1.0	1.12
I	1.33[b]	7	2.45	2.36
In	1.44[a]	3	1.4	1.36
K	1.96[e]	1	0.80	0.82
(La)	1.86[c]	3	(1.2)	1.17
Li	1.34[e]	1	0.95	0.96
(Ma)	1.31[d]	7	(2.4)	2.39
Mg	1.40[a]	2	1.2	1.16
(Mn)	1.18[e]	7	(2.6)	2.60
(Mo)	1.36[e]	6	(2.1)	2.09
N	0.74[e]	5	2.98	3.01
Na	1.54[e]	1	0.90	0.90
O	0.73[e]	6	3.45	3.47
P	1.10[b]	5	2.1	2.19
Pb	1.46[a]	4	1.5	1.56
(Po)	1.46[d]	6	(2.0)	1.98
Rb	2.11[e]	1	0.78	0.79
S	1.04[b]	6	2.53	2.58
Sb	1.41[b]	5	1.8	1.82
Sc	1.61[d]	3	1.3	1.27
Se	1.17[b]	6	2.4	2.35
Si	1.17[b]	4	1.8	1.82
Sn	1.40[b]	4	1.7	1.61
Sr	1.93[d]	2	1.0	0.98
Te	1.37[b]	6	2.1	2.08
Ti	1.45[e]	4	1.6	1.57
Tl	1.47[a]	3	1.3	1.34
(V)	1.30[e]	5	(1.9)	1.93
Y	1.75[d]	3	1.3	1.21
Zn	1.31[a]	2	1.2	1.21
Zr	1.58[e]	4	1.6	1.48

[a] L. Pauling, reference 1, p. 167. These values are for tetrahedral covalent radii.
[b] L. Pauling, reference 1, p. 154.
[c] N. V. Sidgwick, *The Covalent Link in Chemistry* (Cornell University Press, Ithaca, New York, 1933), pp. 83–85.
[d] These values are obtained from a smooth curve drawn through points determined by known values for other elements in the same period of the periodic table.
[e] V. Schomaker and D. P. Stevenson, J. Am. Chem. Soc. 63, 37 (1941).
[f] These electronegativity values, except those enclosed in parentheses, are taken from Table VIII of the author's paper (J. Chem. Phys., in press). Some are Pauling's values (reference 1), and some were determined by the author (reference 4). Those in parentheses are the rounded off values taken from column 4 of the present table.

Fig. 1. The values* used for x, r, and n are listed in Table I. With the exception of Ag, Au, and Cu the points fall closely along a straight line, the equation of which is

$$x=0.31\left(\frac{n+1}{r}\right)+0.50. \qquad \text{(II)}$$

For comparison with the x values the right-hand side of the equation is evaluated and the results listed in the last column of Table I. In this equation r, the single bond covalent radius, is measured in Angstrom units.

Ag, Au, and Cu are known to form compounds in which they contribute more than one electron to the formation of covalent bonds. Hence the most probable cause of their wide deviation is the assumption of screening constants of unity for all electrons except the one in the final shell. For all other elements the deviations are sufficiently small to be explained by inaccuracies in x and r.

Equation (II) has been used to compute electronegativity values for Cb, Cr, La, Ma, Mn, Mo, Po, and V. These are also listed in Table I, column 3.

Equation (I) defines the electronegativity of an element in an absolute sense rather than in terms of that of some other element. The scale determined by it nevertheless requires a small shift of origin to make its values proportional to those of Mulliken's[3] "absolute" scale. This is revealed by the form of Eq. (II), which yields values that are in direct proportion to those of Mulliken.

The electronegativity of a given atom, according to the above theory, would be greater for double or triple bonds—since they have smaller covalent radii—than for single bonds. This assumes that the effects of the decrease in covalent radius are not offset by increased screening factors of the valence electrons.

ELECTRONEGATIVITY CHART

Using the x values given in Table I, column 3,** I have plotted in Fig. 2 electronegativity as a

* Elements included in parentheses are not plotted in this graph. Their electronegativity values, also inclosed in parentheses, were determined from the graph.

** There is one exception. Because Pauling's value for Sn, 1.7, gives a noticeable departure from symmetry in the chart, I have used the value 1.6 given by Eq. (II).

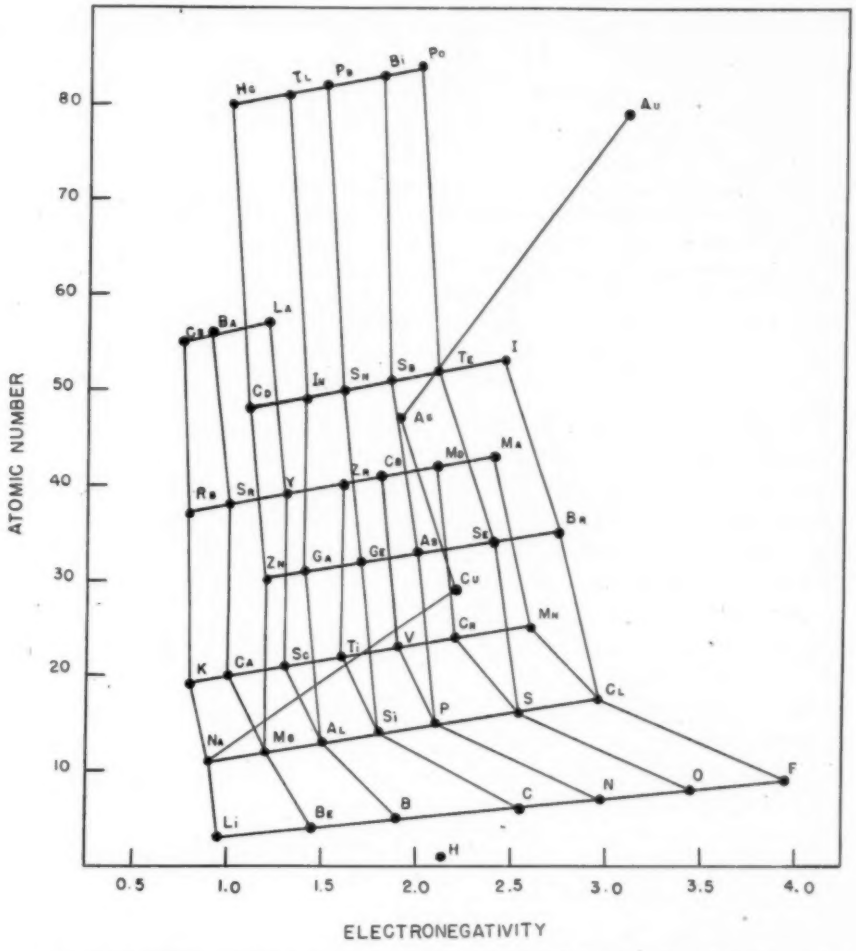

FIG. 2. Electronegativity chart. A plot of electronegativity as a function of atomic number, with lines connecting the elements of the same rows and of the same periods of the periodic table.

function of atomic number. It is seen that, with the exception of Ag, Au, and Cu, the electronegativities for a given period increase in an approximately linear fashion with atomic number —and hence with number of valence electrons— and that there are discrete jumps from period to period.

Pauling[7] has constructed a scale showing how electronegativities for the elements of the different periods of the periodic table bear a systematic relation to each other. In Fig. 2 the lines connecting the atoms having the same number of valence electrons show that the additional electronegativity values which I have determined also follow this systematic pattern.

I wish to thank Vida Miller Gordy for her assistance in the preparation of the manuscript.

[7] L. Pauling, reference 1, p. 65.

Relativistic Correction in Calculating the Magnetic Moment of the Deuteron

P. CALDIROLA
Istituto di Fisica dell' Università di Pavia, Pavia, Italy

(Received March 4, 1946)

This paper presents a study of the variation in the magnetic moment of protons and neutrons caused by their kinetic energy; it assumes that these particles satisfy the relativistic Dirac-Pauli equation, which is characteristic of a particle with spin ½, and that the particles possess a supplementary magnetic moment (not depending on charge). An hypothesis, formulated by Margenau about the variation law for magnetic moments, and the effect of the relativistic correction in calculating the deuteron magnetic moment are discussed.

IT is important in the study of nuclear forces to know the magnetic moments of elementary particles which compose atomic nuclei. One of the most interesting problems is to establish exactly how the magnetic moments of proton and neutron determine the magnetic moment of the deuteron. In this connection it is interesting —as Margenau[1] has first pointed out—to consider the fact that the field of force in a deuteron impresses a movement upon proton and neutron, whose magnetic moments may be changed by this movement. This change appears as a dependence of the magnetic moments on the kinetic energy of the particle, and it is calculated by Margenau assuming that the field of force in the deuteron be a central one and that the neutron and the supplementary proton magnetic moment (that is the part of the magnetic moment not contained in Dirac's equation) change, on account of the field of force, in accordance with the law characteristic of the magnetic moment of a particle obeying Dirac's equation. It is also possible, and results in a more coherent method, to take account of such a supplementary magnetic moment by supposing that proton and neutron satisfy, not the ordinary Dirac equation, but the equation corrected by Pauli.[2] Using this corrected equation, which we will call the Dirac-Pauli equation, and without prejudicing the relativistic invariance, a magnetic moment is introduced which is not necessarily dependent on the particle charge. We have solved this equation for the case of a particle moving in a central field of force and subjected to a constant magnetic field H, a case closely related to the deuteron problem.

Use is made of the assumption that every particle having spin ½ and rest mass M_0 satisfies the relativistic Dirac equation:

$$\left[\boldsymbol{\alpha}\cdot\left(\mathbf{p}-\frac{\epsilon}{c}\mathbf{A}\right)+\beta M_0 c\right]\Psi=-\left(\frac{h}{i}\frac{1}{c}\frac{\partial}{\partial t}+\frac{1}{c}V\right)\Psi, \quad (1)$$

where $\boldsymbol{\alpha}$ is the operator for v/c, $\mathbf{p}$ the operator with components $(h/i)(\partial/\partial x_i)$, $\mathbf{A}$ the vector potential, and $V(x_1, x_2, x_3)$ the potential energy of the static forces acting on the particle.

Pauli has shown that Dirac's equation may be modified without destroying its relativistic invariance—by adding to the operator that appears in the first member, the term

$$\lambda \sum_{(\mu<\nu)} \sigma^{\mu\nu}F^{\mu\nu} \quad (\mu, \nu=1, 2, 3, 4),$$

where λ is a constant factor, $F^{\mu\nu}$ the antisymmetrical tensor of the electromagnetic field, and $\sigma^{\mu\nu}$ the operators defined by means of the relations:

$$\sigma^{mn}=i\beta\alpha^m\alpha^n, \quad \sigma^{4n}=i\beta\alpha^n, \quad \sigma^{\mu\mu}=0,$$

$$(m, n=1, 2, 3).$$

In our case, in which only a magnetic field is present, the additional Pauli term becomes:

$$i\lambda\beta \sum_{(m\neq n)} \alpha^m\alpha^n F^{mn}=\frac{\lambda}{c}(\mathbf{S}\times\mathbf{H}),$$

where $\mathbf{S}$ is the vector operator having components:

[1] H. Margenau, Phys. Rev. **57**, 383 (1940).
[2] W. Pauli, *Handbuch der Physik*, first series, Vol. 24, p. 232.

$$S_1=\begin{vmatrix}0&1&0&0\\1&0&0&0\\0&0&0&-1\\0&0&-1&0\end{vmatrix},\quad S_2=\begin{vmatrix}0&i&0&0\\-i&0&0&0\\0&0&0&-i\\0&0&i&0\end{vmatrix},\quad S_3=\begin{vmatrix}1&0&0&0\\0&-1&0&0\\0&0&-1&0\\0&0&0&1\end{vmatrix}.$$

Therefore the Dirac-Pauli equation, which a particle with spin $\frac{1}{2}$ obeys when it is in a field of force derivable from the scalar potential function V and subjected to a magnetic field $\mathbf{H}$, must be written:

$$\left[\boldsymbol{\alpha}\cdot\left(\mathbf{p}-\frac{\epsilon}{c}\mathbf{A}\right)+\beta M_0c+\frac{\lambda}{c}\mathbf{S}\cdot\mathbf{H}\right]\Psi=-\frac{1}{c}\left(\frac{\hbar}{i}\frac{\partial}{\partial t}+V\right)\Psi. \quad (2)$$

The particle obeying such an equation has, as one easily verifies, a magnetic moment λ not directly associated with its charge; we will assume Eq. (2) as a characteristic equation describing proton and neutron ($\epsilon=0$). Since in our problem the magnetic field is constant and uniform and all forces acting on the particle are constant with time, Eq. (2) admits a solution of the type:

$$\Psi=u\exp\left(-\frac{i}{\hbar}Wt\right),$$

where u satisfies the equation

$$\left[\frac{-W+V}{c}+\boldsymbol{\alpha}\cdot\mathbf{p}+\beta M_0c+\Lambda\right]u=0, \quad (3)$$

provided

$$\Lambda=\frac{\epsilon}{c}\boldsymbol{\alpha}\cdot\mathbf{A}+\frac{\lambda}{c}\mathbf{S}\cdot\mathbf{H}=\frac{\epsilon H_0}{c}(x\alpha_2-y\alpha_1)-\frac{\lambda}{c}S_3H_0. \quad (4)$$

We will solve Eq. (3) by the perturbation method, assuming Λ to be a perturbing term. For the unperturbed system we have the ordinary Dirac equation:

$$\left[\frac{-W^0+V}{c}+\boldsymbol{\alpha}\cdot\mathbf{p}+\beta M_0c\right]u^0=0,$$

whose solutions are well known.

The action of the perturbing term yields a change of the eigenvalue given by:

$$\Delta W^0=-c\int_\infty\int\int\int\sum_1^4{}_k\, u_k{}^{0*}\Lambda u_k{}^0d\tau$$

$$=-\frac{\epsilon H_0}{2}\int_\infty\int\int\int[-u_1{}^{0*}i(x+iy)u_4{}^0+u_2{}^{0*}i(x-iy)u_3{}^0-u_3{}^{0*}i(x+iy)u_2{}^0+u_4{}^{0*}i(x-iy)u_1{}^0]d\tau$$

$$+\lambda H_0\int_\infty\int\int\int[u_1{}^{0*}u_1{}^0-u_2{}^{0*}u_2{}^0-u_3{}^{0*}u_3{}^0+u_4{}^{0*}u_4{}^0]d\tau,$$

where the integrations are easily carried out with the use of well-known relations for the spherical functions.

Then, assuming (see Margenau's work):

$$\kappa=\int_\infty\int\int\int F_+{}^2d\tau \quad (5)$$

and following a procedure quite similar to Margenau's, the result is ($j=l+\frac{1}{2}$):

$$\Delta W^0=\frac{2m-1}{2l+1}H_0\left\{(l+1)\mu_0-\frac{2(l+1)^2}{2l+3}x\mu_0+\lambda+\frac{\lambda}{2l+3}\kappa\right\}. \quad (6)$$

The magnetic moment is obtained from (6) by putting $m=l+1$ and dividing ΔW^0 by H. Thus

$$\mu=(j+\tfrac{1}{2})\mu_0+\lambda-\left[\frac{(j+\frac{1}{2})^2}{j+1}\mu_0-\frac{1}{2(j+1)}\lambda\right]\kappa. \quad (7)$$

The expression for κ may be easily evaluated for the limiting cases of high and low energy particles. Thus we have

Newton-approximation:

$$\mu=(j+\tfrac{1}{2})\mu_0+\lambda; \quad (8)$$

approximation for $v\ll c$:

$$\mu=(j+\tfrac{1}{2})\mu_0+\lambda-\left[\frac{(j+\frac{1}{2})^2}{j+1}\mu_0+\frac{1}{2(j+1)}\right]\bar{T}; \quad (9)$$

extreme-relativistic approximation:

$$\mu=\frac{1}{2(j+1)}[(j+\tfrac{1}{2})\mu_0+(2j+3)\lambda], \quad (10)$$

where $\bar{T}$ is the average kinetic energy, written in units M_0c^2:

$$\bar{T}=\int\int\int_{\infty}\frac{E-V+M_0c^2}{M_0c^2}(g^2+f^2)d\tau.$$

Quite analogously we may carry through the calculations for the case $j=l-\frac{1}{2}$. But the results can immediately be obtained from the preceding formulas on merely replacing l by $-(l+1)$.

For the applications, the case of a particle in an s-state, for which $l=0$, is important. From (9), putting $j=0$, we have for $v\ll c$:

$$\mu=\mu_0+\lambda+\tfrac{1}{3}\bar{T}(-2\mu_0+\lambda).$$

Then the change in magnetic moment due to the relativistic correction is

$$\Delta\mu=\tfrac{2}{3}\bar{T}\mu_0+\tfrac{1}{3}\bar{T}\lambda.$$

Observing furthermore that the proton's rest magnetic moment is

$$\mu_p=\mu_0+\lambda_p \quad \text{with} \quad \lambda_p=1.789\mu_0,$$

while that of the neutron is:

$$\mu_n=\lambda_n \quad \text{with} \quad \lambda_n=-1.935\mu_0,$$

we have, respectively, the following expressions for the relativistic corrections:

$$\Delta\mu_p\simeq-0.072\bar{T}\mu_0, \quad \Delta\mu_n\simeq-0.645\bar{T}\mu_0.$$

These corrections are not proportional—in contrast with Margenau's assumption—to the value obtained for the rest magnetic moments of the two particles.

In further investigation of this question we may observe that, if we had used the following equation instead of (2),

$$\left[\boldsymbol{\alpha}\cdot\left(\mathbf{p}-\frac{e}{c}\mathbf{A}\right)+\beta M_0c+\frac{\lambda}{c}\boldsymbol{\sigma}\cdot\mathbf{H}\right]\Psi=-\frac{1}{c}\left(\frac{h}{i}\frac{\partial}{\partial t}+V\right)\Psi, \quad (11)$$

with:

$$\sigma_1=\begin{vmatrix}0&1&0&0\\1&0&0&0\\0&0&0&1\\0&0&1&0\end{vmatrix}, \quad \sigma_2=\begin{vmatrix}0&i&0&0\\-i&0&0&0\\0&0&0&i\\0&0&-i&0\end{vmatrix},$$

$$\sigma_3=\begin{vmatrix}1&0&0&0\\0&-1&0&0\\0&0&1&0\\0&0&0&-1\end{vmatrix},$$

we should have obtained the following results:

Newton-approximation:

$$\mu=(j+\tfrac{1}{2})\mu_0+\lambda,$$

approximation for $v\ll c$:

$$\mu=(j+\tfrac{1}{2})\mu_0+\lambda-\left[\frac{(j+\frac{1}{2})^2}{j+1}\mu_0+\frac{j+\frac{1}{2}}{j+1}\right]\bar{T},$$

extreme-relativistic approximation:

$$\mu=\frac{1}{2(j+1)}[(j+\tfrac{1}{2})\mu_0+\lambda].$$

These results agree, as one may easily see, with Margenau's assumption that the magnetic moment of the elementary nuclear particles depends on their energy in accordance with the same law which describes the magnetic moment characteristic of the Dirac equation and which considers the moment as strictly bound up with the particle's charge. However, Eq. (11) is not invariant with respect to Lorentz transformations, because the ordinary vector σ that appears here is the spatial part of a 4-vector; it is not—as Lorentz invariance requires—a part of an antisymmetrical tensor of the second rank.

It is very interesting to discuss the deuteron magnetic moment in order to know the variation of the sum $\mu_p+\mu_n$. That is, after our hypothesis

$$\Delta(\mu_p+\mu_n)=\tfrac{1}{3}\bar{T}(\lambda_p+\lambda_n-2\mu_0)\simeq-0.72\bar{T}\mu_0,$$

while after Margenau

$$\Delta(\mu_p+\mu_n)=-\tfrac{2}{3}\bar{T}(\lambda_p+\lambda_n+\mu_0)\simeq-0.57\bar{T}\mu_0.$$

We will assume—following Margenau—that proton and neutron have, in the field of force acting in the deuteron (assuming the potential hole model), an average kinetic energy $\bar{T}\simeq0.012$. Then we have, respectively, on the two hypotheses

$$\Delta(\mu_p+\mu_n)\simeq-0.007\mu_0, \quad \Delta(\mu_p+\mu_n)\simeq-0.006\mu_0.$$

In conclusion, though the two hypotheses—Margenau's and our own—imply quite different laws for the variation in the magnetic moment of an elementary particle, yet they give about the same result in calculating the whole magnetic moment of the deuteron. Surely—as Margenau has remarked—the problem here considered will take on added interest when the neutron magnetic moment is known with greater accuracy.

The Magnetic Moments of Light Nuclei

R. G. SACHS
Ballistic Research Laboratory, Aberdeen Proving Ground, Maryland*
(Received January 16, 1946)

The sum of the magnetic moments of two nuclei which can be obtained from each other by interchanging neutrons and protons is shown to be related in a simple way to the probabilities of occurrence of each of the states of given spin and orbital angular momentum that can be combined to form the ground state. This result, which is independent of any nuclear model, has immediate application to the nuclei with equal numbers of neutrons and protons, in particular, to H^3, Li^6, B^{10}, and N^{14}. From the observed moments it is found that the ground state of B^{10} is a combination of about 50 percent ^3S and 50 percent ^3D function. The ground state of Li^6 contains at least 70 percent but no more than 90 percent of the ^3S term. It may contain as much as 30 percent of the ^3P term, or 15 percent of the ^1P term, or, finally, 10 percent of the ^3D term. The ground state of N^{14} contains at least 52 percent but no more than 84 percent of the ^3D function. It may contain as much as 48 percent ^1P function, but the ^3P term cannot contribute more than 24 percent or the ^3S more than 16 percent. All of these results are based on the assumption that the only terms contributing appreciably to the ground states of the nuclei are those found to be near the ground state in the Hartree approximation. It will be possible to obtain similar information concerning the ground states of other light nuclei if a technique for measuring the magnetic moments of radioactive nuclei is developed.

1. INTRODUCTION

THE magnetic moment constitutes a valuable source of information concerning the distribution of angular momentum between the orbital motion and spin in the ground state of a nucleus. In general, it is possible to guess from the observed moment which of the possible terms is predominant in the wave function of the ground state. However, the relative contribution of this term and the other possible terms usually cannot be obtained quantitatively because the relation between the magnetic moment and wave function involves cross products between the various terms. In addition the moment depends to some extent on the detailed functional properties of each term.

As has already been pointed out,[1] this difficulty can be overcome to a considerable extent by combining a measurement of the magnetic moment of one nucleus with a measurement of the magnetic moment of the nucleus which is obtained from the original one by replacing all of the protons by neutrons and all of the neutrons by protons. The latter nucleus will henceforth be referred to as the nucleus *conjugate* to the original nucleus. The sum of the moments of these two nuclei depends only on the relative probability of occurrence of each possible term in the ground state, as will be shown in the next section. This result depends on the assumption of equality of neutron-neutron and proton-proton forces and, in consequence, is not applicable to heavy nuclei for which the Coulomb interaction between protons becomes important.

One of the pair of conjugate nuclei will usually be radioactive, in which case application of the stated result will have to await development of a technique for the measurement of the magnetic moments of active nuclei. It can be hoped that such techniques will be forthcoming shortly.

There is one case in which the sums of the moments of conjugate nuclei have been obtained; that is, for the nuclei containing an equal number of neutrons and protons. These nuclei will be referred to as *self-conjugate*. For the self-conjugate nuclei, the sum of the moments is obviously just twice the moment of the nucleus. Magnetic moments have been measured for all of the stable self-conjugate nuclei (for the alpha-particle nuclei they are, of course, zero). The conclusions that can be drawn from them will be discussed in Section 3.

2. THE SUM OF THE MAGNETIC MOMENTS OF CONJUGATE NUCLEI

In the approximation that the Coulomb forces between protons can be neglected, that is, for light nuclei, it is generally assumed that the forces between neutrons and those between protons are the same. Then the only difference

* This work is in no way related to the author's work for the Ordnance Department.

[1] R. G. Sachs and J. Schwinger, Phys. Rev. 61, 732A (1942).

between each of a pair of conjugate nuclei is the number of neutrons and protons, so the role played by the neutrons in the one nucleus is the same as that played by the protons in the conjugate nucleus.[2] More explicitly, the wave function of the one nucleus can be obtained from that of the conjugate nucleus by identifying those variables in the one wave function which refer to the neutrons as the variables referring to protons in the other wave function, and by treating the proton variables in a similar manner.

Because of this symmetry between neutrons and protons, the sum of the magnetic moments of the pair of conjugate nuclei is the same as the sum of the moments of two hypothetical nuclei, one consisting entirely of protons and the other of neutrons.[3] The wave functions of these hypothetical nuclei have the same form as the wave functions of the original nuclei. The magnetic moment of a system consisting of one type of particle depends in a simple way on the total orbital angular momentum and the total spin, as is well known for the electronic magnetic moment of atoms. Thus the moments of each of the hypothetical nuclei can be expressed in terms of the relative probability of occurrence of each allowed combination of orbital and spin angular momentum. The sum of the moments of the two hypothetical nuclei can then be expressed in similar terms. Thus the same statement can be made for the sum of the moments of the original nuclei, since this is equal to the sum of the moments of the hypothetical nuclei.

In order to demonstrate this result quantitatively, we write the wave function of one nucleus as

$$\Psi_{JM}(r_1, r_2, \cdots r_n; r_{n+1}, \cdots r_{n+m}; s_1, \cdots s_n; s_{n+1}, \cdots s_{n+m}),$$

where $r_1 \cdots r_n$, $s_1 \cdots s_n$ refer to the space coordinates and the z components of the spins of the n neutrons, respectively, and the other r's and s's refer to the m protons. J is the total angular momentum of the nucleus and M is the projection of this angular momentum on the z axis. The wave function of the conjugate nucleus is the same but with the variables numbered from 1 to n now referring to protons and the other variables to neutrons. This wave function can be expressed as a sum of functions each of which refers to a state of given total orbital angular momentum, L, and given total spin, S:

$$\Psi_{JM} = \sum_{LS} c_{LS} \Phi_{JM}{}^{LS}. \quad (1)$$

The coefficients satisfy the normalization condition

$$\sum_{LS} |c_{LS}|^2 = 1. \quad (2)$$

The values of L and S which appear in these sums are those for which $L+S, L+S-1, L+S-2, \cdots$, or $|L-S|$ equals J.

The projection on the z axis of the magnetic moment of the nucleus consisting of n neutrons and m protons will be designated by $g_1 M$ and that of the conjugate nucleus by $g_2 M$. If the g-factors in units of the nuclear magneton for neutron and proton are g_n and g_p, respectively, the magnetic moment in the same units of the first nucleus is

$$g_1 M = \langle L^z{}_{n+1} + \cdots + L^z{}_{n+m} + g_n(s_1 + \cdots + s_n) + g_p(s_{n+1} + \cdots + s_{n+m}) \rangle_{JM}, \quad (3a)$$

where $L^z{}_j$ is the projection on the z axis of the orbital angular momentum of the jth particle. The bracket $\langle\ \rangle_{JM}$ is meant to indicate the average over the wave function Ψ_{JM}. The magnetic moment of the conjugate nucleus is

$$g_2 M = \langle L^z{}_1 + \cdots + L^z{}_n + g_p(s_1 + \cdots + s_n) + g_n(s_{n+1} + \cdots + s_{n+m}) \rangle_{JM}, \quad (3b)$$

and the sum of the moments is

$$GM = g_1 M + g_2 M = \langle L^z + (g_n + g_p) S^z \rangle_{JM}, \quad (4)$$

where L^z and S^z are the projections on the z axis of the total orbital and total spin angular momentum, respectively. Since $L^z + S^z = J^z$, the z component of the total angular momentum, this expression can be rewritten as

$$GM = \tfrac{1}{2}(1 + g_n + g_p) M + \tfrac{1}{2}(1 - g_n - g_p) \langle L^z - S^z \rangle_{JM}. \quad (5)$$

The average values of L^z and S^z, and therefore the average of their difference, can be calculated

[2] The difference between the masses of neutron and proton is neglected.

[3] A similar statement can be made for any of the properties of the nuclei which is the sum of operators referring individually to each of the particles in the nucleus.

TABLE I. Observed g-factors, values of $g-g_0$, and values of $(g_0-g)/0.0945$ for odd-odd, self-conjugate nuclei.

Nucleus:	H^2	Li^6	B^{10}	N^{14}
g	0.856	0.821	0.598	0.403
$g-g_0$	−0.022	−0.057	−0.280	−0.475
$\frac{g_0-g}{0.0945}$	0.23	0.60	2.96	5.03

by means of the usual vector sum rule. This gives

$$\langle L^z-S^z\rangle_{JM}=\frac{\langle(\mathbf{L}-\mathbf{S})\cdot\mathbf{J}\rangle_{JM}}{J(J+1)}\cdot M$$
$$=\frac{\langle|\mathbf{L}|^2-|\mathbf{S}|^2\rangle_{JM}}{J(J+1)}\cdot M.$$

Inserting this value into Eq. (5), the formula for G reduces to

$$G=\tfrac{1}{2}(1+g_n+g_p)$$
$$+\tfrac{1}{2}(1-g_n-g_p)\langle|\mathbf{L}|^2-|\mathbf{S}|^2\rangle_{JM}/J(J+1). \quad (6)$$

Thus it is seen that G is made up of two terms, one that is the same for all nuclei and another that is proportional to the average value of the difference of the squares of the orbital and spin angular momenta. The value of G then depends on the characteristics of the nuclear wave function only through the latter term. Since this term depends only on the total orbital and spin angular momenta, the average involved is determined by the relative probabilities of occurrence of states of given orbital angular momentum and spin in the ground state. These probabilities are given by $|c_{LS}|^2$, where the c_{LS} are defined by Eq. (1). In terms of the $|c_{LS}|^2$ the average under consideration is

$$\langle|\mathbf{L}|^2-|\mathbf{S}|^2\rangle_{JM}=\sum_{LS}|c_{LS}|^2[L(L+1)-S(S+1)].$$

Therefore Eq. (6) takes the form

$$G=\tfrac{1}{2}(1+g_n+g_p)+\tfrac{1}{2}(1-g_n-g_p)$$
$$\times\sum_{LS}|c_{LS}|^2\frac{L(L+1)-S(S+1)}{J(J+1)}, \quad (7)$$

where the sum is over all states that can be combined to form a state of total angular momentum J. This expression shows how a measurement of the quantity G can be combined with the accepted values of g_n and g_p to obtain information concerning the probability coefficients $|c_{LS}|^2$. It should be kept in mind that these coefficients also satisfy the normalization condition Eq. (2), so one of them may be expressed in terms of the others if it is convenient.

In order to investigate the use of the relation Eq. (7) in detail we now turn to those nuclei for some of which the necessary data are available, namely the self-conjugate nuclei.

3. APPLICATION TO SELF-CONJUGATE NUCLEI

It has been pointed out in the Introduction that for self-conjugate nuclei, i.e., those with an equal number of neutrons and protons, the G-factor for the sum of the moments reduces to twice the g-factor for the single nucleus. Therefore the magnetic moments of these nuclei are expressible in terms of the probabilities $|c_{LS}|^2$. If g is the gyromagnetic ratio of a self-conjugate nucleus, we find from Eq. (7) that

$$g=\tfrac{1}{4}(1+g_n+g_p)+\tfrac{1}{4}(1-g_n-g_p)$$
$$\times\sum_{LS}|c_{LS}|^2\frac{L(L+1)-S(S+1)}{J(J+1)}. \quad (8)$$

The result expressed by Eq. (8) is particularly useful because some of the odd-odd, self-conjugate nuclei, namely, H^2, Li^6, B^{10}, and N^{14}, are stable and their magnetic moments have been measured. Since the heavier odd-odd, self-conjugate nuclei are unstable, their moments have not been measured, but, of course, Eq. (8) applies equally well to them as long as the Coulomb energy can be neglected. The alpha-particle nuclei are also self-conjugate but, since their moments are all expected to vanish, no useful information can be obtained from them.

The observed g-factors for the nuclei under consideration are given[4] in Table I. The total angular momentum of each of these nuclei is $J=1$. On the basis of Russell-Saunders coupling, it has been surmised[5] that the ground state of each nucleus is a ^3S state. In this case we would have $g=g_0=\frac{1}{2}(g_n+g_p)=0.878$ for all of the nuclei if we take[4] $g_n=-3.822$ and $g_p=5.579$. The difference $g-g_0$ is given in the third row of Table I. From these differences it seems clear that

[4] These figures are taken from the summary of results given by S. Millman and P. Kusch, Phys. Rev. 60, 91 (1941).

[5] M. E. Rose and H. A. Bethe, Phys. Rev. 51, 205 (1937).

the deviation from Russell-Saunders coupling becomes increasingly important for the heavier nuclei. This fact has already been pointed out by Rose.[6]

According to Eqs. (8) and (2), the difference $g-g_0$ is

$$g-g_0=-0.0945\sum'_{LS}|c_{LS}|^2k_{LS}, \qquad (9)$$

with $k_{LS}=L(L+1)-S(S+1)+2$. The $\sum'_{LS}$ indicates the sum over all states except the ^3S state. The values of $(g_0-g)/0.0945=\sum'|c_{LS}|^2k_{LS}$ for each of the nuclei under consideration are given in the fourth row of Table I.

A large number of possible terms are included in the expansion of the wave function of the ground states for all of these nuclei except H^2. In order to make use of the results obtained thus far, it is desirable to indicate which of the terms are probably most important. In the Hartree approximation, it is found[7] that certain of the terms arise from one configuration and it seems likely that these would contribute most strongly to the wave function of the ground state. The resulting terms corresponding to unit total angular momentum are tabulated in Table II for each of the nuclei under consideration.* For the $^1P_1$, $^3P_1$, and $^3D_1$ terms the values of k_{LS} are 4, 2, and 6, respectively. Using the results given in the last row of Table I, we find the following linear relations between the $|c_{LS}|^2$ for the various nuclei:

H^2: $$6|c_{21}|^2=0.23, \qquad (10a)$$

Li^6: $$4|c_{10}|^2+2|c_{11}|^2+6|c_{21}|^2=0.60, \qquad (10b)$$

B^{10}: $$6|c_{21}|^2=2.96, \qquad (10c)$$

N^{14}: $$4|c_{10}|^2+2|c_{11}|^2+6|c_{21}|^2=5.03. \qquad (10d)$$

TABLE II. Low-lying terms with $J=1$ in the odd-odd, self-conjugate nuclei.

Nucleus:	H^2	Li^6	B^{10}	N^{14}
Terms:	$^3S_1$ $^3D_1$	$^3S_1$ $^3D_1$ $^1P_1$ $^3P_1$	$^3S_1$ $^3D_1$	$^3S_1$ $^3D_1$ $^1P_1$ $^3P_1$

[6] M. E. Rose, Phys. Rev. **56**, 1064 (1939).

[7] E. Feenberg and E. Wigner, Phys. Rev. **51**, 95 (1937). The terms for H^2 are taken from W. Rarita and J. Schwinger, Phys. Rev. **59**, 436 (1941).

* For Li^6 and N^{14} all terms that occur in the Hartree approximation are given in the table, but out of the many possible terms for B^{10} only the two lowest are given in order to avoid complicating the argument.

In addition the coefficients must satisfy Eq. (2) with the coefficient for the ^3S state, $|c_{01}|^2$, included in the sum.

Equation (10a) does not lead to a new result since it is on the basis of this relation, $|c_{21}|^2=0.038$, that the magnetic moment of the neutron was obtained.[4]

Equation (10c) gives, for B^{10}, $|c_{21}|^2=0.49$, so there appears to be a mixing of the ^3D state with the ^3S state to such an extent that the probability of each is about $\frac{1}{2}$. It should be borne in mind that this result is valid only if none of the other terms, such as the ^1P, ^3P, ^5P, ^5D, etc., contribute appreciably to the ground state, as is suggested by the Hartree model.

Rose[6] assumed that the ^1P and ^3P states would not make an important contribution to the ground states of Li^6 or N^{14}, but there seems to be no *a priori* reason for making such an assumption. It is true that, if the tensor spin-orbit interaction is responsible for the mixing of terms, only the D state would occur in first order if the S state were dominant. However, it turns out that in N^{14}, for example, the D state occurs with a much higher probability than the S state. It follows that the P state may also occur with a high probability since the tensor force will mix P and D states.

On this basis we assume that all three of the coefficients in Eqs. (10b) and (10d) are to be treated on an equal footing. Considering first Eq. (10b), it is seen that the largest possible values of each of the coefficients is obtained by setting the other two equal to zero. Thus we find for Li^6

$$|c_{10}|^2\leq 0.15, \quad |c_{11}|^2\leq 0.30, \quad |c_{21}|^2\leq 0.10. \qquad (11)$$

Since Eq. (10b) can also be written in the form

$$|c_{10}|^2+|c_{11}|^2+|c_{21}|^2=0.10+\tfrac{1}{3}|c_{10}|^2+\tfrac{2}{3}|c_{11}|^2,$$

it follows that the sum of the squares of the three coefficients must be greater than or equal to 0.10 or, in virtue of Eq. (2), the contribution of the ^3S state, $|c_{01}|^2$, cannot be greater than 90 percent. Equation (10b) can also be written in the form

$$|c_{10}|^2+|c_{11}|^2+|c_{21}|^2=0.30-|c_{10}|^2-2|c_{21}|^2,$$

which shows in a similar way that the contribution of the ^3S state cannot be less than 70 percent. Therefore we see that the ground state of Li^6 is predominately a ^3S state, with a mixture

of at least 10 percent and at most 30 percent of the other three states. The individual contributions of the other three states are limited by the conditions Eq. (11).

For N^{14}, Eq. (10d) shows that there must be an appreciable contribution from the ^3D state. As a consequence it is convenient to rewrite the equation with the coefficient $|c_{21}|^2$ eliminated in favor of the ^3S coefficient, $|c_{01}|^2$, by means of the normalization condition Eq. (2). In this way Eq. (10d) becomes

$$2|c_{10}|^2+4|c_{11}|^2+6|c_{01}|^2=0.97. \quad (12)$$

The largest possible value of each of the coefficients is obtained, as for Li^6, by setting the other two equal to zero:

$$|c_{10}|^2\leq 0.48, \quad |c_{11}|^2\leq 0.24, \quad |c_{01}|^2\leq 0.16. \quad (13)$$

Also as for Li^6, it is easy to show that the sum of the squares of these three coefficients can be no less than 0.16 and no greater than 0.48. Therefore, it follows that the contribution of the ^3D state must be at least 52 percent and may be as large as 84 percent. Thus the ground state of this nucleus is either predominantly a ^3D state or it is an almost equal mixture of ^3D and ^1P states. The contribution of the ^3S state cannot be greater than 16 percent.

Again it must be emphasized that this discussion is subject to the condition that the only states which contribute to the ground state are those found to be near the ground state on the basis of the Hartree model.

4. CONCLUSION

In this discussion no attempt has been made to predict theoretically what the magnetic moments of nuclei *should* be on the basis of a particular nuclear model. Rather, an attempt has been made to show how the observed moments can be used to give information about the structure of the wave functions of the ground states. In the present state of our experimental knowledge of magnetic moments, the results obtained here are particularly applicable to the odd-odd nuclei consisting of equal numbers of protons and neutrons. The conclusions that can be drawn concerning the nuclei of this type which are stable are given in Table III. When a technique is developed for the measurement of the moments of radioactive nuclei, it will be possible to obtain similar information concerning the structure of the ground states of those light nuclei for which the moments of the conjugate pair are observed.

TABLE III. Percentage contributions of Russell-Saunders terms to the ground states of the stable, odd-odd, self-conjugate nuclei as found from the observed gyromagnetic ratios. (The values for H^2 are included for completeness.)

Term:	^3S	^3D	^1P	^3P
Nucleus				
H^2	(96%)	(4%)	—	—
Li^6	70–90%	0–10%	0–15%	0–30%
B^{10}	51%	49%	—	—
N^{14}	0–16%	52–84%	0–48%	0–24%

It should be remarked that the additivity of the magnetic moments of the neutron and proton has been assumed here. Since current ideas concerning nuclear forces make it seem quite possible that these moments are altered by the interaction with other particles in the nucleus, it is conceivable that the assumption of additivity is not valid. In this case marked deviations from the results obtained here would be expected.

The author had profitable discussions of this paper with Dr. U. Fano.

The Pressure Broadening of Spectral Lines

H. M. FOLEY*
University of Michigan, Ann Arbor, Michigan
(Received February 7, 1946)

The Fourier integral expression for the intensity distribution in a pressure broadened line is derived from the quantum radiation theory with an adiabatic collision approximation. The phase shift approximation to the solution is obtained with the actual distribution of phase shifts taken into account. It is shown that in general there is a shift in line position as well as a line broadening both proportional to the pressure. The ratio of the shift to the broadening depends only on the power of the intermolecular distance with which the interaction decreases. Experimental values of this ratio in foreign gas broadening are on the average consistent with the inverse sixth power. The predicted line widths are slightly larger than those given by Weisskopf. Good agreement with the observed line width is found for most of the alkali metals absorption lines. Calculated line widths and shifts are given for the vibration-rotation lines of linear polar molecules. A method for treating non-adiabatic collisions is given. The conditions for which the Lorentz line form transforms to the Margenau-type line form are indicated. It is shown that the Jablonski wave mechanical treatment of translational motion leads to the same line forms as the Fourier integral method under the proper physical conditions.

INTRODUCTION

THE earliest treatment of the effects on spectral lines due to the interaction of radiating atoms and molecules is that of Lorentz.[1] A classical radiating oscillator is taken as the model for the radiating atom. The atoms or molecules are assumed by Lorentz to have a definite collision radius, and each radiating system periodically suffers a sudden disruption to the radiation mechanism. The collision either stops the radiating process or changes the phase by an arbitrary amount. The Fourier integral analysis of the wave train yields the observed frequency distribution of spectral intensity. The result is the well-known dispersion line form

$$I(\omega)=\frac{c}{\pi}\frac{n\pi a^2\bar{v}}{(n\pi a^2\bar{v})^2+(\omega-\omega_0)^2}$$

with a half-width, in angular frequency units, of $2n\pi a^2\bar{v}$ with n the number of atoms per cc, a the collision radius, and $\bar{v}$ the mean velocity of the atoms.[1]

This result agrees with the experimental data in that the dependence of line width on pressure is found to be linear up to pressures of several atmospheres. In many cases, particularly for self-broadening, a dispersion type of line form is found. The theory furnishes no values of the collision radius nor, consequently, of the spectral line half-widths.[2]

Weisskopf[3] has extended the ideas of Lorentz by taking as the model for the radiating atom a classical oscillator whose frequency varies in time according to the collision perturbations on the system. The intensity distribution is given by

$$I(\omega)=\left|A\int_{t_i}^{\infty}\exp\left[-i\int_{t_i}^{t}\omega'(x)dx+i\omega t\right]dt\right|^2, \quad (1)$$

where

$$\begin{aligned}\omega'(t)&=[E_i(t)-E_f(t)]/h\\&=\omega_0+[P_i(t)-P_f(t)]/h,\end{aligned} \quad (2)$$

with $P_i(t)$ and $P_f(t)$ the collision perturbations of the initial and final radiation states of the atoms and $E_i(t)$ and $E_f(t)$ the corresponding total energies of these states. The time t_i corresponds to the initial time of the radiation process. Under conditions such that the duration of the collision is small compared to the interval between collisions, the main effect of the perturbations is to produce phase shifts in the oscillation. Weisskopf has evaluated the expression for the intensity distribution with the assumption that all phase shifts with magnitudes greater than unity are equivalent to arbitrary phase shifts, and the effects of smaller phase shifts are negligible. A

* Now at Columbia University, New York City.
[1] H. A. Lorentz, Proc. Amst. Acad. Sci. 8, 591 (1906).
[2] H. Margenau and W. W. Watson, Rev. Mod. Phys. 8, 22 (1936).
[3] V. Weisskopf, Zeits. f. Physik 75, 287 (1932).

Lorentz-type line form is obtained, with the collision radii given directly from the force law. With interaction energies varying as the inverse third and inverse sixth powers of the separation distance, the values of the collision radii are, respectively,

$$a=(2\beta/\bar{v})^{\frac{1}{3}} \quad \text{and} \quad a=(3\pi\beta/8\bar{v})^{1/5}$$

where β is defined by

$$[P_i(t)-P_f(t)]/\hbar=\beta/R^p. \tag{3}$$

The phase shift approximation, as will be shown later, is valid for low densities and high velocities of the gas molecules. This assumption, namely, that the effects of the small phase shifts can be neglected and that the larger phase shifts are equivalent to arbitrary shifts, brings about the result that the shift of line centers, an important feature of the pressure effect, is not contained in the solution.

A very different type of solution has been given by Kuhn and London.[4] Their method consists essentially in taking as the intensity distribution, not the Fourier integral transform of the oscillations of varying frequency, but the frequencies which occur instantaneously in the oscillations. The intensity given to any frequency is proportional to the fraction of time that this frequency occurs in the oscillations. If the particles move with uniform velocity, the intensity for any frequency is proportional to the volume in space in which that time varying frequency is emitted. Thus if the frequency scale ω is measured from the unperturbed line position, we have for the inverse sixth-power law

$$I(\omega)d\omega\approx R_\omega^2 dR_\omega=\beta d\omega/2\omega^{\frac{1}{2}}. \tag{4}$$

This result of Kuhn and London has the obvious defect of giving a divergent intensity at the line center.

Margenau[2, 5] has improved this result by taking into account the additive effect of all the perturbing atoms that interact simultaneously with the emitting atom. Thus, for N perturbing atoms, the intensity for any frequency is proportional to the volume in the $3N$-dimensional configuration space corresponding to the perturbation energy difference $\hbar\omega$. Margenau's expression for the normalized line form is

$$I(\omega)=\frac{2\pi}{3}\beta^{\frac{1}{2}}\frac{n\exp[-\pi\lambda/\omega]}{\omega^{\frac{1}{2}}} \text{ with } \lambda=4\pi^2\beta n^2/9 \tag{5}$$

and n the density. This formula indicates a line width and shift of peak intensity which are proportional to the square of the density.

The expressions of Kuhn and London and of Margenau represent essentially "static" solutions in which the particles are considered to be held in fixed positions. All effects due to the translational motion are neglected. This formulation is valid for conditions of low velocity and high density. How this line form transforms into the dispersion form of Lorentz at high velocities and low densities will be indicated later.

A rather different but quite rigorous approach to the pressure broadening problem has been given by Jablonski.[6–8] The gas is considered to be analogous to a very large molecule, and the stationary states of intermolecular motion, subject to the Van der Waals interaction, are computed. The interaction force depends on the state of internal motion of the interacting atoms or molecules, with the result that, in general, the translational wave functions for different states of internal motion are not orthogonal. Thus, subject to the assumption that the interaction forces are additive and that the effect of the intermolecular motion on internal states is an adiabatic perturbation, the matrix elements for optical transition contain as a factor the products of the "overlap" integrals of the translational wave functions of all the perturbing atoms or molecules. The probability amplitude for an optical transition from an initial state of the emitting (or absorbing) atom of energy E_i and translation energies of interatomic motion $e(n_1)\cdots e(n_K)\cdots e(n_N)$ to a final state with energy E_f of internal motion and with translational energies $e(n_1')\cdots e(n_K')\cdots e(n_N')$ is

$$A(i\to f)=S_{if}\prod_{K=1}^{N}\int_0^{R_0}dR_K R_K^2 L_{eK}(R_K)L_{eK'}(R_K), \tag{6}$$

where $L_{eK}(R_K)$ is the radial wave function of the K perturber. This transition corresponds to the

[4] H. Kuhn and F. London, Phil. Mag. **18**, 983 (1934).
[5] H. Margenau, Phys. Rev. **48**, 755 (1935).
[6] A. Jablonski, Acta Phys. Polonica **6**, 371 (1937).
[7] A. Jablonski, Physica **7**, 541 (1940).
[8] A. Jablonski, Phys. Rev. **68**, 78 (1945).

emission (or absorption) of radiation of frequency

$$\omega=\frac{\Delta E}{\hbar}=\omega_0+\frac{i}{\hbar}\sum_{K=1}^{N}[e(n_K)-e(n_K')].$$

Jablonski has calculated an expression for the line form which is essentially the same as that of Kuhn and London. With *WKB* radial wave functions, each "overlap" integral has the form

$$\frac{1}{R_0}\int_0^{R_0}dR\cos\left\{\frac{1}{\hbar}\int_0^{R}[p(R)-p'(R)]dR+\eta-\eta'\right\}, \tag{7}$$

with $p(R)$, $p'(R)$ the momenta in initial and final states, and η, η' the phases in these states. In analogy with the Frank-Condon principle for discrete vibrational transitions, Jablonski has evaluated the integral at the points where $p(R)=p'(R)$, as the integral oscillates slowly at these values of R. This assumption is obviously equivalent to that of Kuhn and London, and in fact, Jablonski arrives at their formula on averaging the expressions for a single perturber over all possible transitions. It is clear that in any line broadening theory, a treatment which considers only a single perturbing atom and then averages over all transitions of this system will always yield a line form which diverges at the center, since, for a large vessel, the perturber will spend an infinitesimal fraction of time within the effective range of the forces.

Jablonski considers that the fact that the intensity distribution calculated by this method does not agree with the Lorentz-Weisskopf formula indicates that the Fourier integral method is fundamentally incorrect. However, it will be shown that the wave mechanical treatment does, in fact, yield both of these formulas under the assumption of physical conditions proper for each.

DERIVATION OF THE CLASSICAL FOURIER INTEGRAL

In this section a derivation will be given of the Fourier integral expression for the intensity distribution assumed by Lorentz and Weisskopf. The quantum theory of radiation is employed in calculating the probability of radiation emission by a system of interacting atoms or molecules. The treatment of the intermolecular motion is classical in that classical orbits are assumed. Thus the coordinates of the colliding particles become known functions of the time. In the Hamiltonian of the system, these coordinates appear not as dynamical variables but as time dependent parameters. The molecular interaction becomes a function of the time and may be treated as a time dependent perturbation on the system. The justification of this treatment lies in the fact that when the velocity of a "packet" representing the molecular motion is determined to good accuracy, the positions may be known, for all except the very light molecules, to one or two A. The ranges of the interaction forces which are important in line broadening are many times this packet size.

The Hamiltonian is taken to be of the form

$$H=H_1(p_l, q_l)+H_2(p_l, q_l, Q_i(t))+H_3(p_l, q_l, p_s, q_s)+H_4(p_s, q_s). \tag{8}$$

Here H_1 is the energy function of the variables of the internal motion of the isolated molecules, H_2 is the term representing the interaction of the molecules, and contains the molecular coordinates $Q_i(t)$. H_3 is the interaction with the radiation field, and H_4 is the energy of the charge-free radiation field. The terms H_2 and H_3 are treated as perturbations. The eigenfunction solutions of the unperturbed Hamiltonian consist of products of wave functions of the atomic systems and of the radiation field oscillators. When the complete wave function is expanded in terms of these eigenfunctions and inserted in the wave equation, the usual set of equations for the growth of the states is obtained. The state equations which do not involve optical transitions are of the form

$$\dot{a}_n=-(i/\hbar)V_m^n(t)a_m(t)\times\exp[-i(E_m-E_n)t/\hbar], \tag{9}$$

where $V_m^n(t)$ is the matrix element of H_2, that is, of the intermolecular interaction. For adiabatic collision conditions the solution is

$$a_n(t)=\frac{V_m^n(t)a_m(t)}{E_m-E_n}\exp\left[-\frac{i}{\hbar}(E_m-E_n)t\right] \quad \text{for } V(0)=0. \tag{10}$$

The equations containing optical transition

matrix elements are of the form

$$\dot{a}_f = S_i^f a_i \exp\left[-\frac{i}{\hbar}(E_i - E_f - \hbar\omega_s)t\right] - \frac{i}{\hbar} V_n^f(t) a_n(t) \exp\left[-\frac{i}{\hbar}(E_n - E_f)t\right],$$

in which S_i^f is the ordinary matrix element for the spectral transition. The increase of the coefficient a_f corresponds to the emission (or absorption) of a radiation quantum of frequency ω_s. The insertion of expression (10) into the state equations involving the optical matrix element permits an explicit solution for the probability amplitude for emission of a quantum of frequency ω_s

$$A_{\omega_s}(T) = \exp\left[-\frac{i}{\hbar}\int_0^T P_f dt\right]\int_0^T dt S_f^i \times \exp\left[-\gamma_N t - \frac{i}{\hbar}\int_0^t (P_i(t) - P_f(t)dt + i\omega t\right], \quad (11)$$

in which γ_N is the natural line width, and P_i and P_f are the instantaneous interaction energies in the initial and final states, respectively. For foreign gas broadening these terms are the second-order Van der Waals interactions. For self-broadening the collisions may produce a resonance interaction of like molecules as well as the Van der Waals interactions. In this case of first-order resonance splitting of the levels, it may be shown that the expression for the spectral intensity consists of the sum of two terms similar to that of Eq. (11), in which, however, the P_i or P_f values are now the resonance splitting, with the symmetric level in one term and the antisymmetric in the other. With the neglect of natural line width* and the extension of the radiation time interval to infinity, the Eq. (11) is identical with the Fourier integral formula of Lorentz and Weisskopf.[1] From the derivation it is clear that this expression may be described as the Fourier integral of the optical matrix element between the adiabatic, or instantaneous solutions of the time dependent wave equation. For the self-broadening case the instantaneous solution is that which diagonalizes the energy matrix of $H_2(t)$, i.e., the symmetric and antisymmetric combinations of the wave functions of the resonating states.

PHASE SHIFT SOLUTION OF THE FOURIER INTEGRAL

The Fourier integral amplitude may be written as

$$A(\omega) = N\int_0^\infty dt \exp\left[-i\int_0^t P(x)dx + i\omega t\right],$$

in which $P(t)$ is the difference of $P_i(t)$ and $P_f(t)$ in angular frequency units, and the frequency is measured from the unperturbed line position. N is a normalization factor. The intensity distribution is given by

$$I(\omega) = N\int_0^\infty dt_1 \int_0^\infty dt_2 \times \exp\left[-i\int_{t_2}^{t_1} P(x)dx + i\omega(t_1 - t_2)\right]$$

or, with $t_1 - t_2 = \tau$ and $t_2 = t_0$,

$$I(\omega) = N\int_{-\infty}^{+\infty} d\tau \int_0^\infty dt_0 \exp\left[-i\int_{t_0}^{t_0+\tau} P(x)dx + i\omega\tau\right] = \Re N\int_0^\infty d\tau \int_0^\infty dt_0 \exp\left[-i\int_{t_0}^{t_0+\tau} P(x)dx + i\omega\tau\right], \quad (12)$$

in which $\Re$ signifies that only the real part of the integral is to be taken.

Now the function

$$\bar{y}(\tau) = \int_0^\infty dt_0 \exp\left[-i\int_{t_0}^{t_0+\tau} P(x)dx\right], \quad (13)$$

in which the integral in t_0 is extended over the complete interval of the radiation process, is a measure of the average correlation of the function

$$\exp\left[-i\int_0^\tau P(x)dx\right]$$

over the interval τ. τ is the time interval over

* As is well known the natural line width is extremely small for optical transitions, about 10^{-4} cm^{-1}, and even smaller still, about 10^{-7} cm^{-1}, for infra-red lines.

which the correlation is to be determined. Thus the radiation intensity may be expressed as the Fourier amplitude of this correlation function.

For time intervals which are large compared to the collision duration, the integral

$$\int_{t_0}^{t_0+\tau} P(x)dx$$

is simply the sum of the phase shifts of the collisions occurring in this interval. The phase shift approximation consists in the assumption that the duration of the collisions is vanishingly small, so that this integral may be expressed as the sum of an integral number of collision phase shifts for all values of τ. It will be shown later that this approximation is valid for low densities and high velocities of the gas molecules. Thus we have

$$\int_{t_0}^{t_0+\tau} P(x)dx = \sum_{i=1}^{n} \alpha_i$$

for n phase shifts in the interval. If the mean time between collisions is τ_0, the expected number of collisions in the interval τ is τ/τ_0, and the probability of n collisions is given by $(\tau/\tau_0)^n(e^{-\tau/\tau_0}/n!)$. The average value of the correlation function for all cases with n collisions becomes

$$\int dt_0 \exp\left[-i\sum_{i=1}^{n}\alpha_i\right] = \prod_{i=1}^{n}\int_{-\infty}^{+\infty} d\alpha p(\alpha) \times(\cos\alpha - i\sin\alpha) = (A-iB)^n, \quad (14)$$

in which $p(\alpha)d\alpha$ is the distribution in phase shifts, and A and B are, respectively, the average values of $\cos\alpha$ and $\sin\alpha$. The forces may be considered to be "cut off" at a collision distance ρ_0, corresponding to τ_0, and the phase shifts cut off at a corresponding value α_0. This cut-off distance is only a device for convenience and is eventually to be extended to infinity to include all phase shifts. The correlation function is thus given by

$$\bar{y}(\tau) = \sum_{n=0}^{\infty}\frac{e^{-\tau/\tau_0}}{n!}\left(\frac{\tau}{\tau_0}\right)^n(A-iB)^n = \exp\left[\frac{A-iB}{\tau_0}\tau - \frac{\tau}{\tau_0}\right]. \quad (15)$$

The intensity formula is

$$I(\omega) = \Re N\int_0^{\infty} d\tau \exp\left[\frac{A-1}{\tau_0}\tau - i\frac{B-\omega}{\tau_0}\tau\right] = \frac{(1-A)/\pi\tau_0}{[(1-A)/\tau_0]^2+[(B/\tau_0)-\omega]^2}. \quad (16)$$

This expression for the line shape yields a half-width $2(1-A)/\tau_0$ and a shift of the line center B/τ_0, both of which are proportional to n, that is, to the density.

For the evaluation of the constants in this formula we shall assume the interaction energy to be of the form $V=\beta\hbar/R^p$. For the phase shifts, we have

$$\alpha = \int_{-\infty}^{\infty}\frac{V_i-V_f}{\hbar}dt = \int_{-\infty}^{\infty}\frac{\beta_i-\beta_f}{(\rho^2+v^2t^2)^{p/2}}dt = \frac{\gamma}{v\rho^{p-1}},$$

with v the relative velocity. In addition to the distribution in velocities $f(v)dv$, there may be a distribution in force law constants g_k, corresponding to the various excitation states of the colliding molecules. The total number of collisions per second producing phase shifts larger than the minimum cut-off value α_0 is

$$\frac{1}{\tau_0} = n\sum_k\int_0^{\infty} dv f(v) g_k \pi \rho_{0k}^2 v,$$

where n is the density of particles. ρ_{0k} is the collision distance corresponding to a phase shift α_0 for a collision between particles of relative velocity v and with a force law β_k/R^{p_k}. The probability for a phase shift for this case is

$$p(\alpha)d\alpha = \frac{D\gamma_k^{2/(p_k-1)}g_k f(v)v^{(p_k-3)/(p_k-1)}}{\alpha^{(p_k+1)/(p_k-1)}(p_k-1)},$$

in which D is a normalization factor. On averaging all types of collisions and velocities the expression for the half-width becomes

$$8\pi n\sum_k g_k\frac{\gamma^{2/(p_k-1)}}{p_k-1}\langle v^{(p_k-3)/(p_k-1)}\rangle_{Av} \times\int_0^{\infty}\frac{d\alpha\sin^2\alpha}{|\alpha|^{(p_k+1)/(p_k-1)}}, \quad (17)$$

for the case in which all phase shifts have positive sign. For resonance broadening phase shifts with positive and negative signs occur with equal probability and the integration is then extended

TABLE I. Ratio, R, of shift to half-width.

p:	5	6	7
R:	0.500	0.363	0.288

over the complete range of the distribution. Similarly the line center shift is given by

$$2\pi n \sum g_k \frac{\gamma^{2/(p_k-1)}}{p_k-1}\langle v^{(p_k-3)/(p_k-1)}\rangle_{kv} \times \int_0^\infty \frac{d\alpha \sin\alpha}{|\alpha|^{(p_k+1)/(p_k-1)}}, \quad (18)$$

and the same conditions hold for the range of integration of α as with the half-width. In these expressions the cut-off distance has been allowed to become infinite. The phase shift integrals may be evaluated in terms of gamma-functions. It is to be emphasized that both the shift and broadening expressions are found in the same low density approximation to the solution of the Fourier integral. If the phase shift distribution $p(\alpha)$ is an even function of α, as it is in the resonance broadening case, there will be no shift in the line position. In other cases such as the foreign gas broadening, the phase shifts have predominantly one sign (i.e., either positive or negative) and hence the shift is not zero. For foreign gas broadening in atomic spectra, the phase shifts in most cases have only one sign, which may be either positive or negative. It is of considerable interest that in this case the ratio of the shift to broadening is independent of the pressure, in the phase shift approximation, and, for the case of one sign in the phase shifts, depends only on the form of the interaction law between molecules. For an inverse power law β/R^p this ratio is

$$\text{Ratio} = \tfrac{1}{2}\cot\left\{\frac{p-3}{2(p-1)}\pi\right\}.$$

The values are given for a few cases in Table I.

The half-width obtained by Weisskopf is

$$2\pi n\langle v^{(p-3)/(p-1)}\rangle_{kv}\gamma^{2/(p-1)}.$$

Our formula shows the same dependence on the variables of the system, but the half-width is greater than that given by Weisskopf by a factor which, for the important cases of inverse third- and sixth-power laws, has the values 1.57 and 1.21, respectively. For the more slowly decreasing force laws the neglect of small phase shifts is more important, hence the greater discrepancy with the Weisskopf formula for the third-power force law.

NON-ADIABATIC EFFECTS

The Fourier integral expression for the intensity distribution in a spectral line is valid under conditions such that the collisions induce no transitions among states defined by the instantaneous solutions of the Hamiltonian equation

$$H(t)\psi_n(t) = E_n(t)\psi_n(t). \quad (19)$$

An expression for the probability of non-adiabatic transitions which serves as an indication of the validity of the adiabatic assumption in any particular case will be derived here. Resonance transitions which are necessarily also non-adiabatic were discussed previously and are excluded from consideration.

The complete wave function describing the molecular system may be expanded in terms of these instantaneous solutions

$$\Psi(t) = \sum_n a_n(t)\exp\left[-\frac{i}{\hbar}\int_0^t E_n(t)dt\right]\psi_n(t).$$

This function must satisfy the wave equation

$$H(t)\Psi(t) = -(\hbar/i)(\partial\Psi/\partial t),$$

leading to the equation for the rate of growth of the amplitude for any state

$$\dot{a}_k = -\sum_n a_n(t)\left[\psi_k^*, \frac{\partial\psi_n}{\partial t}\right] \times\exp\left[-\frac{i}{\hbar}\int_0^t (E_n-E_k)dt\right],$$

in which the first bracketed expression is

$$\int dq\psi_k^*\cdot(\partial\psi_n/\partial t)$$

integrated over all coordinates of the wave functions. The time-dependent term in the Hamiltonian is contained in the collision interaction and may be treated as a perturbation. The solutions of Eq. (29) may then be given as

$$\psi_n(t) = {}_0\psi_n + \sum_i \frac{H_i^n(t)}{E_i-E_n}\,{}_0\psi_i.$$

${}_0\psi_i$ is a solution of the time independent zero-order Hamiltonian and H_i^n is the matrix element of the collision interaction. If the system is initially in state m, the probability amplitude for transition to state k during the collision becomes

$$a_k = \frac{-i\omega_{km}}{E_k - E_m} \int_{-\infty}^{\infty} H_m^k(t) \exp\left[i\omega_{km}t\right] dt$$

with

$$\omega_{km} = (E_k - E_m)/\hbar.$$

For the usual case of dipole-dipole interaction, we have

$$H_m^k(t) = \beta_{km}/(\rho^2 + v^2t^2)^{\frac{1}{2}}.$$

The probability amplitude for this case is given by

$$a_k = \frac{\beta_{km}\pi K^2}{\rho^3(E_k - E_m)} H_1(iK), \qquad (20)$$

in which $K = \rho\omega_{km}/v$ and $H_1(iK)$ is the first-order Hankel function with imaginary argument. In any particular case of line broadening this formula indicates whether non-adiabatic transitions are numerous enough to play an important part in the radiation process. It will be found that for most cases of atomic line spectra, the level separations are so large that the probability of such transitions is negligible. Exceptions are found in cases of "quenching" collisions. In molecular infra-red spectra, cases of non-adiabatic transitions may occur due to a near coincidence of the rotational levels of a foreign molecule with those of the radiating molecule. Generally the level to which such a transition takes place does not radiate in the same spectral region as the original state, so that when such a non-adiabatic "jump" occurs, the radiation process ceases. This fact furnishes an approximate method for including the non-adiabatic effects in the preceding treatment. The termination of the radiation process is equivalent to an arbitrary phase shift and may be treated as such by introducing into the phase shift distribution $p(\alpha)$, a probability for arbitrary phase shifts equal to the total probability for non-adiabatic transitions.

FOREIGN GAS BROADENING IN ATOMIC SPECTRA

The calculation of the line broadening and line shift produced by a foreign gas requires the determination of the electronic dispersion interaction in both levels involved in the optical transition. For the ground states, fairly accurate values of the interaction can be obtained by the use of the polarizability,[9] but for the excited states only rough estimates can be given. Thus the lack of accurate knowledge of the atomic Van der Waals forces precludes any close experimental verification of the theory of line widths. For the inverse sixth-power interaction law, our analysis, taking the distribution of collision phase shifts into account, yields, as has been shown, a twenty percent greater line width than that of Weisskopf. This author[3] has estimated upper and lower limits to the foreign gas broadening in a number of cases by his method. These estimates are so uncertain, however, that our increase in predicted line width is not very significant. The

TABLE II. Experimental ratios of shift to half-width in foreign gas broadening.

Spectral line	Perturber	Ratio	Reference
Hg 2537	A	0.39	a
	N_2	0.45	a
	O_2	0.47	a
Na 5890	A	0.35	b
	N_2	0.44	
K 7665	N_2	0.47	c
		0.37	d
7699	N_2	0.50	c
		0.44	d
4044	N_2	0.50	c
4047	N_2	0.57	c
Hg 2537	CO_2	0.25	a
2537	H_2O	0.22	a
2537	H_2	0.16	a
Na 5890	H_2	0.23	b
K 7665	A	0.36	d
7699	A	0.42	d
Rb 4216	He	0.33	
4202	He	0.23	
4216	Ne	0.17	
4202	Ne	0.22	e
4216	A	0.56	
4202	A	0.39	
Cs 4555	He	0.30	
4555	Ne	0.23	
4555	A	0.42	f
4555	N_2	0.62	
3876	He	0.62	
3876	Ne	0.37	
3876	A	0.77	
3876	N_2	0.32	

[a] C. Fuchtbauer, G. Joos, and O. Dinkelacher, Ann. d. Physik **71**, 204 (1923).
[b] H. Margenau and W. W. Watson, Phys. Rev. **44**, 92 (1933).
[c] H. Margenau and W. W. Watson, Phys. Rev. **44**, 748 (1933).
[d] G. F. Hull, Phys. Rev. **50**, 1148 (1936).
[e] T-Z Ny and S-Y Chen, Phys. Rev. **52**, 1158 (1937).
[f] C. Fuchtbauer and F. Gossler, Zeits. f. Physik **87**, 89 (1933).

[9] H. Margenau, Rev. Mod. Phys. **8**, 1 (1939).

linear dependence of line breadth and line shift on pressure is observed at low pressures in all cases.

For the ratio of shift to half-width, the situation is somewhat more favorable. It was shown above that this ratio is independent of the strength of the interaction and, in fact, depends only on the power of the separation distance which occurs in the interaction law. The observed ratios of shift to half-widths are given for a number of cases in Table II. These ratios show such a spread in values that it cannot be said that the inverse sixth-power law is confirmed. The experimental uncertainties in the determination of the half-widths are large and the values found by different investigators are not always consistent. The average of the ratios given in Table II is 0.375, which is very close to the value for the theoretical sixth-power law. It is believed that the ratio of shift to broadening is sufficiently sensitive to the form of the force law to permit a determination of the law by careful experiments.

SELF-BROADENING IN ATOMIC SPECTRA

The line widths of the first members of the principal series of the alkali metals have been examined by several investigators.[10–13]

Houston[14] has discussed these cases of resonance broadening with special reference to the question as to whether the component lines of such multiplet transitions are equally broadened. The calculations of this author are based on a method due to Fursow and Wlassow,[15] in which the probability per collision for the transfer of the excitation energy of the emitting atom to the normal state atom is obtained. This transfer of excitation energy is regarded as a damping in the oscillation of the radiating atoms which leads to a spectral distribution following the dispersion law with a half-width equal to the "decay constant" of the oscillation. The results of Houston are given in Table III. The ratio of line widths of the doublet components is unity in all cases, according to these calculations.

TABLE III. Half-widths of alkali resonance lines.

Reference			Observed		Calculated (this paper)		Calculated (Houston)	
		J	$10^7\Delta\nu n$	Ratio	$10^7\Delta\nu n$	Ratio	$10^7\Delta\nu n$	Ratio
11	Na	1/2	0.712	1.55	0.71	1.42	0.49	1.00
		3/2	1.10		1.01		0.49	
10	K	1/2	3.2	1.0	0.91	1.42	0.63	1.00
		3/2	3.2		1.29		0.63	
12	Rb	1/2	0.55	1.75	0.52	1.38	0.65	1.00
		3/2	0.96		0.72		0.65	
13	Cs	1/2	0.84	1.72	0.95	1.52	0.71	1.00
		3/2	1.45		1.44		0.71	

It appears to the writer that the method of averaging the transfer probabilities which take place between the degenerate sub-levels of the initial state and those of the resonant state resulting from the collision over all possible transitions is incorrect. The transfer probabilities from any sub-level of the initial state should be summed over all final states and then averaged over the initial levels. This process, if employed in the calculations of Houston, leads to line width ratios of the doublet components in agreement with those calculated by the phase shift method derived below.

From Eq. (17) the half-width of a resonance broadened line is

$$\Delta\nu_{\frac{1}{2}}=4\pi^2 n\beta_{\text{av}}, \tag{21}$$

in which β_{av} is the average absolute value of the coefficient in the resonance interaction β/R^3. These coefficients are given by the roots of the $2(2J+1)(2J'+1)$ secular equations of the interaction of an excited atom with an atom in the ground state. J is the angular momentum quantum number of the ground state and J' that of the excited state. Half of these $2(2J+1)(2J'+1)$ degenerate states are symmetric and half are antisymmetric with respect to exchange of the two atoms. Only the symmetric states may combine optically with the final state of the radiation process in which both atoms are in the ground states. Therefore, in computing the average value of β_i, we shall sum these coefficients over all the symmetric states and divide by the total number of states, since all states have equal probability of occurrence. We shall employ the root mean square value of β_i, as this quantity is readily obtained by summing the diagonal elements of the matrix of the square of the interac-

[10] P. E. Lloyd and D. S. Hughes, Phys. Rev. **52**, 1215 (1937).
[11] K. Watanabe, Phys. Rev. **59**, 151 (1940).
[12] Shang-Ui Ch'eng, Phys. Rev. **58**, 844 (1940).
[13] C. Gregory, Phys. Rev. **61**, 465 (1942).
[14] W. V. Houston, Phys. Rev. **54**, 884 (1938).
[15] W. Fursow and A. Wlassow, Phys. Zeits. Sowjetunion **10**, 379 (1936).

tion energy. This sum is

$$\sum_i \sum_j V_j^i V_i^j = \sum_i \sum_j (V_j^i)^2 \qquad (22)$$

for symmetrical matrices. The matrix elements are of the form

$$V_j^i = \frac{e^2}{R^3}[X_1(m_i', m_i)X_2(m_j, m_j') + Y_1(m_i', m_i)Y_2(m_j, m_j') - 2Z_1(m_i', m_i)Z_2(m_j, m_j')], \qquad (23)$$

in which the X, Y, Z are the coordinates of the optical electrons in the two atoms denoted by the subscripts 1 and 2, respectively. This matrix element connects the state of the system in which the first atom is excited and has a magnetic quantum number m_i' and the second atom is in the ground state with a magnetic quantum number m_j, with the state in which the first atom is in the ground state and the second atom is excited and the quantum numbers are m_i and m_j', respectively. After the computation of expression (22) and division by the number of states, the value of the line half-width is obtained. The half-width is given by

$$\Delta\nu_{\frac{1}{2}} = 2\sqrt{3}\pi^2 n \frac{he^2}{m\Delta E_{JJ'}}\left(\frac{2J+1}{2J'+1}\right)^{\frac{1}{2}} f_{JJ'}, \qquad (24)$$

in which $f_{JJ'}$ is defined in the usual manner

$$f_{JJ'} = \frac{2m}{3h^2}\frac{\Delta E_{JJ'}}{2J+1}\sum_{m'}|X(Jm, J'm')|^2.$$

For the alkali doublets the ratio of the half-widths of the $\frac{3}{2}$ and $\frac{1}{2}$ components is approximately $\sqrt{2}$. In Table III the experimental half-widths are compared with those calculated from Eq. (24) and with those calculated from Houston's formula. Except in the case of potassium, the agreement we obtain appears to be quite satisfactory. The experimental value for potassium differs from those of the other elements by such a large factor, although essentially the same interaction is present, that it surely seems to be in error.

LINEAR MOLECULES

In order that an interaction be effective in line broadening, it is necessary, in the adiabatic approximation, that there be a difference in the perturbations on the two levels of the optical transition. It may be shown that in the calculation of the second-order "electronic dispersion" forces, the summation over the matrix elements for any vibration-rotation state in a particular electronic level leads to the same result. The denominators of these terms contain the energy differences between the state being perturbed and states of different electronic quantum numbers. Thus all the levels in the same electronic state will have very nearly the same "dispersion" interaction energies. The effect of the dispersion forces in vibration or rotation spectra is therefore negligible.

For polar molecules the interaction between the permanent dipoles is a first- or second-order effect depending on the presence of resonance in the collision. A molecule of angular momentum quantum number l will show resonance interaction with another molecule in state $l\pm1$, regardless of whether the two molecules are in the same vibrational state.* The mean value of the resonance interaction is zero. We shall approximate the mean absolute value by the root mean square value which has been shown by Margenau[5] to be

$$\langle V^2\rangle_{Av}^{\frac{1}{2}} = \left(\frac{2}{3}\right)^{\frac{1}{2}} \frac{l+1}{[(2l+1)(2l+3)]^{\frac{1}{2}}}\cdot\frac{\mu^2}{R^3}, \qquad (25)$$

in which μ is the dipole moment and l is the smaller of the angular momentum quantum numbers of the interacting molecules. Either the initial or the final level of the optical transition may undergo resonance. For a vibration band spectrum, both the symmetric and antisymmetric states of the resonance splitting will combine optically with the final state of the transition and the expression (25) may be used directly as the average β_i in Eq. (21).

For non-resonating collisions of polar molecules the second-order perturbation solutions of Eq. (10) are identical with those given by London.[16]

$$V_{Av} = \frac{2\mu^4 I}{3h^2R^6} \times \frac{l_1(l_1+1)+l_2(l_2+1)}{(l_1+l_2)(l_1+l_2+2)(l_1-l_2-1)(l_1-l_2+1)}, \qquad (26)$$

* This assumes that the convergence of the rotation levels in the excited vibration state is negligible.

[16] F. London, Zeits. f. Physik 63, 245 (1930).

TABLE IV. Calculated half-width in cm^{-1} for one atmosphere pressure at 25°C.

HCl		HCN				
		Half-widths cm^{-1}				
l	Half-width cm^{-1}	l	Sec. order	Resonance	Total	Shift cm^{-1}
0	0.39	0	0.32	0.54	0.86	+0.12
1	0.60	1	0.39	0.92	1.31	+0.14
2	0.72	2	0.44	1.33	1.87	+0.14
3	0.70	3	0.48	1.69	2.17	+0.14
4	0.58	4	0.50	1.98	2.48	+0.13
5	0.42	5	0.53	2.20	2.73	+0.12
6	0.27	6	0.54	2.35	2.89	+0.10
7	0.158	7	0.54	2.41	2.95	+0.065
8	0.080	8	0.55	2.41	2.96	+0.040
9	0.038	9	0.56	2.34	2.90	+0.010
10	0.016	10	0.55	2.24	2.79	−0.018
		11	0.54	2.06	2.60	−0.043
		12	0.53	1.87	2.40	−0.067
		13	0.51	1.67	2.17	−0.082
		14	0.50	1.46	1.96	−0.10
		15	0.48	1.25	1.73	−0.11
		16	0.44	1.05	1.49	−0.11
		17	0.42	0.87	1.29	−0.12
		18	0.38	0.71	1.09	−0.11
		19	0.36	0.56	0.92	−0.11
		20	0.32	0.44	0.76	−0.10
		21	0.30	0.34	0.64	−0.10
		22	0.26	0.26	0.52	−0.088

where V_{k_1} is the mean interaction energy between molecules in states denoted by l_1 and l_2. It is the difference in the interaction between the two levels involved in the transition which produces the phase shifts in pressure broadening. In contrast to the "dispersion interaction" in foreign gas broadening in atomic spectra, this difference in perturbations may be either positive or negative depending on the quantum numbers of the colliding particles. Hence, as will be shown for certain of the fine structure lines of a band, the shift in position may be positive while in others it is negative.

The infra-red band spectra of linear molecules are a favorable case for the comparison of line broadening theory with experiments, as they are among the few cases in which the interaction forces may be evaluated with any accuracy. With expressions (25) and (26) we obtain the phase shift probability distribution for both resonance and non-resonance cases. Since the effects of these types of interactions, when they occur in different collisions, enter linearly in the total phase shift distribution, we may calculate the half-widths produced by each type of collision and simply add these contributions to obtain the total half-widths. All possible collision interactions must be taken into account, with probabilities assigned according to the thermal distribution in states. Molecules in states near the maximum of the Maxwell-Boltzmann distribution encounter molecules in states differing by one unit of angular momentum very often, and these lines will show the greatest broadening. The shifts in line positions, due to the second-order interaction, show a rather interesting behavior. The lines near the edge of the band are moved toward the band center, and those near the center, closer than the most intense lines, move away from the band center. The molecules in states corresponding to the most intense region of the band encounter other molecules with lower quantum numbers about as often as those in higher states. For these molecules the phase shift distribution is nearly symmetrical and there will be no shift in line position. Actually these second-order interactions, proportional to the fourth power of the dipole moment, are negligible in almost all cases. Only in the case of HCN, which has a very strong polarity, are the shifts within the range of experimental detection. The calculated half-widths in cm^{-1} for one atmosphere pressure at 25°C are given in Table IV for HCl and HCN. For HCN the second-order effects are negligible, and only the resonance broadening values are given in the table. Actually the effects of quadrupole and exchange forces determine a lower limit on the collision radius of 3–5A, and a consequent lower limit on the broadening per atmosphere of 0.04–0.10 cm^{-1}. Therefore the widths given for the lines at the edge of the HCl band are not very significant. For HCN the resonance, second-order, and total half-widths are given. The calculated shift per atmosphere is also shown.

PROPERTIES OF THE GENERAL SOLUTION OF THE FOURIER INTEGRAL FOR FOREIGN GAS BROADENING

The statistical problem in the determination of the Fourier integral intensity distribution may be reduced to the calculation of the correlation function (13). For very small values of τ, this expression may be written approximately as

$$\int dt_0 \exp\left[-iP(t_0)\tau\right]. \qquad (27)$$

The integral in t_0 is to be interpreted as the

average over all interactions occuring in the radiation process. Thus, for small values of τ, this expression becomes

$$\int dPD(P)e^{-iP\tau}, \tag{28}$$

in which $D(P)$ is the distribution in the function $P(t)$. For large values of τ the expression (15) becomes the correct approximation for the correlation function. If the correlation function (28) is inserted in the intensity expression (12) and the integration over τ is extended to infinity, the exponential factor takes on the properties of a so-called delta-function, $\delta(P,\omega)$, and the resulting intensity distribution is $I(\omega)=D(P)$ which is identical with that of Margenau. Thus the use of the correlation approximation (15) over the complete interval yields the phase shift line form, and the use of expression (28) leads to the "static" distribution. The exact correlation function transforms from (15) to (28) at values of τ of the magnitude of the duration of a collision producing unit phase shift.

In Table V are given the values of the half-width and the shift of peak intensity for these two cases. χ is the ratio of the volume enclosed by the collision radius for unit phase shift to the volume corresponding to the average distance between molecules. This quantity serves as a criterion as to which approximation is the more accurate for any condition of density, temperature, and strength of interaction. As conditions change such that χ increases through the value of unity, the dependence of line width on density goes from the first power to the second power. The two formulas give the same width and shift for values for χ of 1.51 and 1.48, respectively. Preliminary calculations, employing higher approximations to the correlation function, indicate fairly good agreement of the half-width and line shifts with the phase shift values, for χ less than unity, and with the "static" values for χ greater than unity.

THE WAVE MECHANICAL TREATMENT OF INTERMOLECULAR MOTION

In the formulation of Jablonski, the probability amplitude for any particular combination of translation transitions (6) is to be squared, summed over all transitions from these initial states, and averaged over the distribution in initial translational states, subject to the conditions on the total energy change of the system

$$\Delta E=\omega\hbar=E_i-E_f+\sum_{i=1}^{N}(e_i-e_i'), \tag{29}$$

in which the summation is extended over all the perturbing particles. With the WKB approximation to the radial wave functions, each "overlap" integral may be written in the form

$$\int_{\rho}^{R_0} dR\frac{c^2}{p(R)}\cos\left\{\int_{\rho}^{R}\frac{m}{\hbar}\frac{\Delta e-\Delta U(R)}{p(R)}dR\right\} \tag{30}$$

in which $p(R)$ is the classical radial component of momentum, Δe is the translation energy difference for the perturber in the initial and final states, and $\Delta U(R)$ is the difference in potential energy in initial and final states. The effects due to the extension of the wave functions into the "non-classical" region $R<\rho$ are neglected. At the edge of the container, the boundary conditions are of the form

$$\frac{p(R_0)\cdot R_0}{\hbar}-\frac{l\pi}{2}+\eta_{el}=\tfrac{1}{2}(2n+1)\pi$$

for both initial and final states. The argument of the cosine in the integrand of (30) satisfies the asymptotic condition

$$[p(R_0)-p'(R_0)](R_0/\hbar)+\eta_{el}-\eta_{e'l'}=m\pi, \tag{31}$$

in which primed quantities refer to the final state of the transition. We now introduce the variable

$$dt=\frac{mdR}{p(R)}=\frac{mdR}{(2m)^{\frac{1}{2}}[e-U(R)-(l^2\hbar^2/2mR^2)]^{\frac{1}{2}}}$$

and employ the classical approximation for the angular momenta $l^2\hbar^2=m^2v^2\rho^2$. The boundary Eq.

TABLE V. Half-widths and shift of peak intensity.

Approximation	Half-width	Shift
Phase shift $\chi\ll1$	$8.53\omega_0/\chi$	$3.10\omega_0/\chi$
Static $\chi\gg1$	$5.63\omega_0$	$2.10\omega_0$

$\omega_0=4\pi^2\beta n^2/9$ $\quad\chi=\frac{4}{3}\pi n\left(\frac{3}{8}\pi\frac{\beta}{v}\right)^{3/5}$

(31) at $R_0=T/v$ becomes

$$\omega_i T_i-\int_0^{T_i}\frac{\Delta U_i}{\hbar}dt=m\pi \tag{32}$$

with $\omega_i=\Delta e_i/\hbar$ for each perturber. The overlap integral expressed in the new variable is

$$c^2\int_0^{T_i}dt_i\cos\left[\omega_i t_i-\int_0^{t_i}\frac{\Delta U_i(t)}{\hbar}dt\right]. \tag{33}$$

The phase at the boundary in the integrand,

$$\alpha_i'=\int_0^{T_i}\frac{\Delta U_i(t)}{\hbar}dt,$$

is exactly half the phase shift for such a collision which would appear in the Fourier integral expression for the intensity.

If conditions are such that the effective range of forces is large compared to the average distance between molecules, that is, if the overlap integrals for perturbing molecules with ρ comparable with the particle separation show phase values larger than unity, then the procedure employed by Jablonski in calculating the integral (30) is correct, and the static type of solution is obtained. Jablonski has obtained the Kuhn-London line form by considering only a single perturber, but it is clear that the averaging over all possible simultaneous transitions, subject to condition (29), is completely equivalent to the calculation of Margenau and leads to the line form given by that author.

Under conditions such that the effective range of the forces is small compared to the molecular separation, the effect of the interaction forces is simply the introduction of the phase into the integrand (33), and the integrand is a harmonically oscillating function over the range of integration. The result of this calculation will yield the same formula for the intensity distribution as would be obtained in the phase shift approximation to the Fourier integral.

As an example of this calculation, we shall show that the wave mechanical treatment leads to the Lorentz line form for the same conditions that were assumed in that calculation. We assign a definite cut-off radius to the interaction forces, but we assume that the forces inside this radius are sufficiently great that the phases of expression (33) are arbitrarily large. Then this integral becomes simply

$$\int_0^{T_i}dt_i\cos(\omega_i t_i-\alpha_i)=\frac{\sin\alpha_i}{\omega_i}=\frac{\sin\omega_i T_i}{\omega_i} \tag{34}$$

with the use of the boundary condition (32). Of the total number of molecules in the container, N, only a fraction of them, N', will have angular momenta, or collision distances, sufficiently small to enable them to come within the range of the forces. For the other molecules the translational wave functions in the upper and lower states of the radiation process form identical sets of orthogonal functions, and no change in energy is permitted in the transition. Therefore we need only concern ourselves with the N' molecules which may actually collide with the radiating molecule. Leaving off numerical factors, the expression (34) becomes

$$A(\omega)=\prod_{i=1}^{N'}\frac{\sin\omega_i T_i}{\omega_i}, \tag{35}$$

with

$$\omega=\sum_{i=1}^{N'}\omega_i. \tag{36}$$

The intensity distribution is obtained by averaging $|A(\omega)|^2$ over all combinations of simultaneous transitions. The distribution in the parameter $T_i=R_0/v$ is taken to be $e^{-T_i/T_0}/T_0$ in which $T_0=R_0/\bar{v}$ and $\bar{v}$ is the average velocity. To obtain the intensity distribution, the expression

$$\prod_{i=1}^{N'}\int_0^{\infty}dT_i\frac{\sin^2\omega_i T_i}{\omega_i^2}\frac{e^{-T_i/T_0}}{T_0}=\prod_{i=1}^{N'}\frac{T_0^2}{1+4\omega_i^2T_0^2}$$

must be averaged over all values of the ω_i. The assumption of arbitrarily large phases allows each perturber to make any energy transition. The intensity is given by

$$I(\omega)\approx\prod_{i=1}^{N'}\int_{-\infty}^{\infty}\frac{d\omega_i}{1+4\omega_i^2T_0^2}$$

with the condition (36). This N'-fold integration may be performed in successive steps, and leads to

$$I(\omega)\approx[1+(2\omega T_0/N')^2]^{-1}.$$

The number of molecules in the container which may collide with the radiating atom is

$N'=2\pi nR_0a^2$ with n the density. Thus the line form is given by

$$I(\omega)=A/[(n\pi a^2\bar{v})^2+\omega^2] \qquad (37)$$

which is the Lorentz formula, with frequencies measured from the line center.

Under the two extreme physical conditions the wave mechanical and classical treatments lead to the same expressions for the line form.

The writer wishes to express his gratitude to Professor D. M. Dennison for his continued interest and advice in this study, and to Professor G. E. Uhlenbeck for several helpful suggestions.

PHYSICAL REVIEW VOLUME 69, NUMBERS 11 AND 12 JUNE 1 AND 15, 1946

Self-Broadening in the 14μ Band of HCN

H. M. FOLEY*
University of Michigan, Ann Arbor, Michigan
(Received February 7, 1946)

The intensity distribution in the positive branch of the 14μ HCN band has been measured at pressures of 2.5 cm, 16 cm, 40 cm, and 58 cm. Because of the large permanent dipole moment of this molecule, there is considerable line broadening at these pressures. The overlapping of lines, slit width effects, and finite thickness of the absorbing layer of gas are taken into account in relating the theoretical line widths to the intensity distribution. The two constants giving the effective slit width and the absolute vibration intensity are determined from the low pressure lines, and these constants with the theoretical line widths determine the intensity distribution throughout the band. Reasonably good agreement is found at all pressures, and no systematic disparity of theory and experiment is indicated. The predicted shifts in the lines, which are just within the limits of detection, are in qualitative agreement with the observed values. The absolute value of the dipole strength of this vibration transition is determined.

IN a preceding paper,[1] formulas were developed for the width and shifts of the lines of the infra-red vibration bands of polar molecules. Table IV of reference 1 gives the widths and half-widths per atmosphere of the rotational lines for bands of HCl and HCN.

Inasmuch as the polar molecules are among the few cases in which the interactions important in line broadening may be calculated accurately, it has appeared worth while to determine experimentally the intensity distribution at various pressures in a band of such a molecule. Hydrogen cyanide gas was chosen for several reasons. Since it is a linear molecule, the spectrum is especially simple. It has a very large dipole moment (2.65×10^{-18} c.g.s. e.s.u.), which indicates that considerable broadening will occur at moderate pressures. The spectrum is not complicated by the lines due to an isotope, as is the case with HCl. The positive branch of the 14μ band was chosen for measurement, as there are no interfering bands of atmospheric H_2O or CO_2 in this region. The line positions in the band have been measured previously by Barker and Choi.[2]

The infra-red spectrometer employed was that described by Hardy.[3] The writer was very kindly permitted the use of the instrument by Professor E. F. Barker. The grating used was of the echelette type, ruled with 700 lines to the inch. This spectrometer is equipped with a KBr fore prism to remove the higher order spectra of short wave-lengths.

Measurements of the absorption of the gas were made at pressures of 2.5 cm, 16 cm, 40 cm, and 58 cm of mercury, with absorption cell lengths of 12 cm, 2.5 cm, 1 cm, and 1 cm, respectively. The total amount of gas through which the radiation passed was thus roughly constant. 58 cm was the highest pressure that could be maintained at

* Now at Columbia University, New York City.
[1] H. M. Foley, Phys. Rev. 69, 616 (1946).
[2] E. F. Barker and K. N. Choi, Phys. Rev. 42, 777 (1932).
[3] J. D. Hardy, Phys. Rev. 38, 2162 (1931).

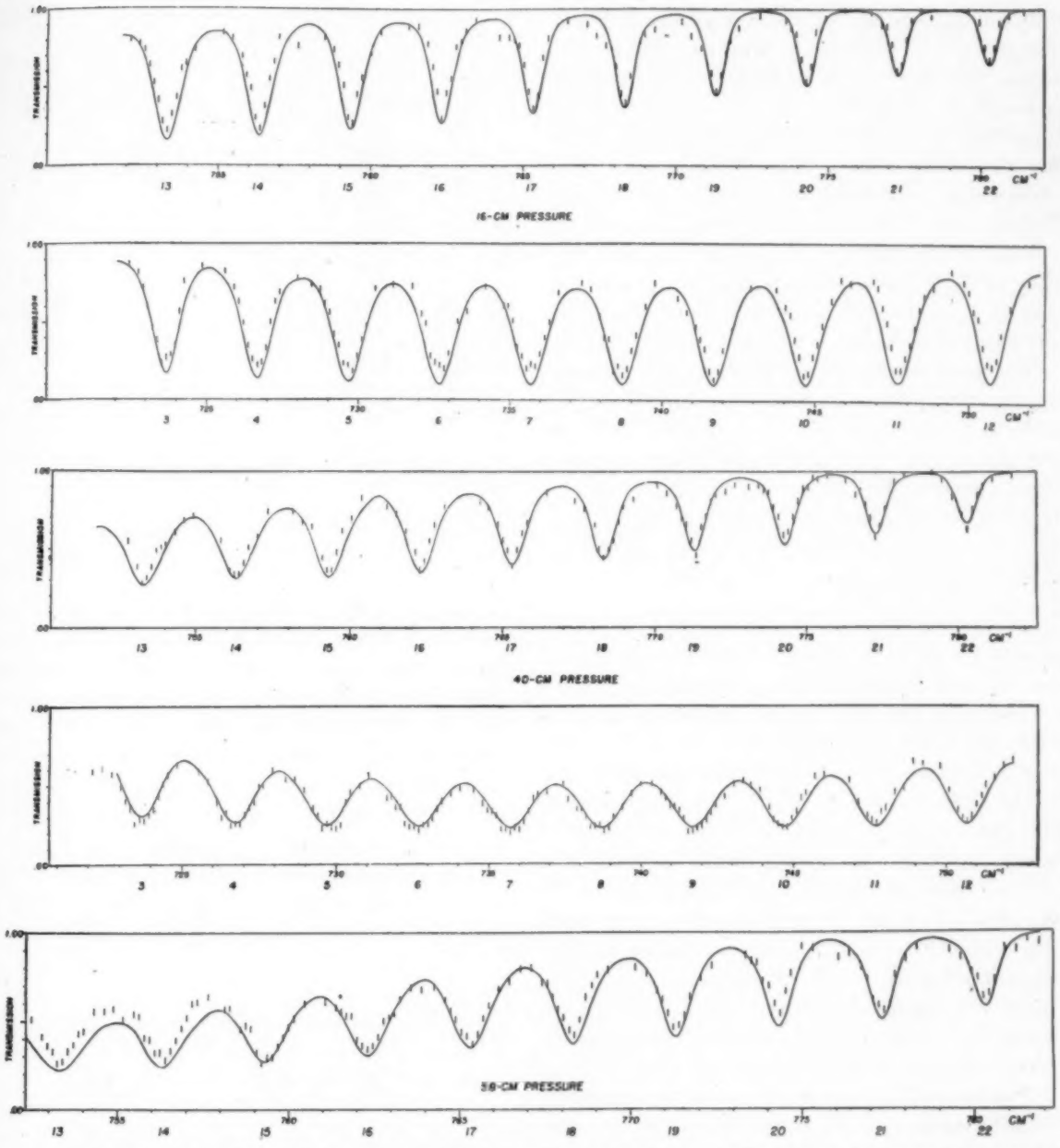

FIG. 1. Distribution of intensity of absorption in HCN. Experimental points and curve calculated from pressure broadening theory are shown. Absorption lines are numbered according to rotational quantum numbers of initial states.

room temperature, as this is very nearly the vapor pressure of the gas. Values of the percent transmission were measured at intervals of fifteen or thirty seconds of angle of the grating in the region covered by the lines with $l=3$ to $l=22$ inclusive, where l is the rotational quantum number of the initial state of the transition. The strong absorption of the Q branch of the band overlaid the first three lines of this branch. At the 58-cm pressure, the absorption for the lines with $l=13$ was so heavy that significant data could not be obtained in this region. An apparent polymerization of the HCN gas in the cell made it difficult to maintain the higher pressures and may have affected the results slightly.

After a number of trials, a slit width of 0.2

mm was chosen as the smallest practical width. The intensity falling on the thermopile was then so low that an abnormally high amplification had to be employed, with a consequent increase in the unsteadiness of the galvanometer deflections. Several readings were taken at each point. The observed transmissions for the pressures of 16 cm, 40 cm, and 58 cm are plotted in Fig. 1. Each value is represented by a line segment, the length of which indicates the uncertainty in the observed transmission, as judged from the deviations in the readings.

The analysis of the data is rather complicated, as the finite thickness of the absorbing layer, the diffusing effects of the spectrometer, and the overlapping of the rotational lines must be taken into account. The observed transmission is a function of the form

$$T(\nu_0)=\int_{-\infty}^{\infty} d\nu\rho(\nu-\nu_0)e^{-\alpha(\nu)d}, \qquad (1)$$

in which $\alpha(\nu)$ is the absorption coefficient of the gas per unit length and is compounded from the overlapping line absorption intensities. d is the absorption cell path length. $\rho(\nu-\nu_0)$ is the function describing the distribution in intensity due to the spectrometer slit width and aberrations. If the slits are the sole source of this diffusion of energy and are of equal width, the function $\rho(\nu-\nu_0)$ is triangular in form with a base-width equal to twice the slit width in frequency units. Equation (1) may be considered as an integral equation for $\alpha(\nu)$ and solved stepwise over the band. For strong absorptions this is not a feasible procedure, however, as $\alpha(\nu)$ can then be determined only with poor accuracy.

For the comparison of the theoretical intensity distributions with the data, we shall integrate Eq. (1) throughout the region of observation. The agreement with the observed absorption will serve as the test of the line broadening theory. This is a more complete comparison of the theory with the observed distribution in intensity than is obtained by determining only the observed half-widths, as the overlapping absorption from "tails" of the lines is of considerable importance at the higher pressures.

In addition to the theoretical half-widths of Table IV of reference 1, two other constants are necessary for the integration of Eq. (1). These are the width of the function $\rho(\nu-\nu_0)$ and the absolute intensity constant of this vibration transition.

TABLE I. Data obtained from pressure broadening of HCN lines.

l	Tm	(Abs. ×Min.)	$\frac{(\text{Abs.}\times\text{Min.})}{\log_{10} T_m}$	$\frac{(\text{Abs.}\times\text{cm}^{-1})^2}{4n\delta\nu_0 d(l+1)e^{-\epsilon_l/kT}}$	Shift per atmosphere
			2.5-cm pressure		
3	0.355	0.760	1.67	2.10×10^{-5}	+0.34 cm^{-1}
4	0.370	0.800	1.85	2.11	+0.06
5	0.340	1.085	2.32*	2.91*	0.00
6	0.355	0.980	2.18	2.14	+0.16
7	0.331	0.950	1.98	1.91	+0.07
8	0.31	0.993	1.95	2.08	+0.26
9	0.32	1.12	2.26	2.83*	+0.16
10	0.305	1.29	2.50*	4.29*	+0.29
11	0.38	0.820	1.95	1.91	+0.36
12	0.43	0.651	1.78	1.44	+0.09
13	0.45	0.560	1.61	1.24*	0.00
14	0.455	0.675	1.97	2.51	−0.06
15	0.55	0.460	1.77	1.54	−0.16
16	0.59	0.384	1.67	1.50	−0.13
17	0.62	0.420	2.02	2.54	0.00
18	0.66	0.346	1.92	2.60	−0.03
19	0.63	0.340	1.69	3.78*	−0.03
20	0.76	0.232	1.95	2.65	−0.24
21	0.75	0.197	1.58	2.14	+0.06
22					0.00
			4-cm pressure		
20	0.56	0.36	1.43	1.89	
21	0.61	0.34	1.58	2.56	
22	0.71	0.22	1.48	1.75	
Averages			1.86 min.	2.07×10^{-5} n in cm Hg	

Because of the presence of the finite absorption and the slit effects, in general no very simple relation between the observed intensity distribution and the theoretical line strengths and line widths can be given. Dennison,[4] however, has given several useful relationships of the parameters determining the line shape for the case of narrow, intense, non-overlapping lines. The absorption coefficient is taken to be of the form

$$\alpha(\nu)=c\delta/\pi(\delta^2+\Delta^2\nu), \qquad (2)$$

with c the total intensity of the line, and $\Delta\nu$ the frequency measured from the line center. δ is equal to half the width listed in Table IV of reference 1. Dennison shows that the total absorption obtained by integrating Eq. (1) over the line is

$$\text{Abs.}=2(c\delta d)^{\frac{1}{2}} \qquad (3)$$

for lines which satisfy the condition

$$cd/\pi\delta\gg1.$$

For these lines he also obtains the result

$$\text{Abs.}/\log_{10} T_m=2.42a, \qquad (4)$$

in which T_m is the transmission at the line center.

[4] D. M. Dennison, Phys. Rev. **31**, 503 (1928).

a is the half-width of the function $\rho(\nu-\nu_0)$, when taken to be of Gaussian form

$$\rho(\nu-\nu_0)=\exp\left[-\Delta\nu^2/2.77a^2\right]/2(2.77\pi)^{\frac{1}{2}}a.$$

It is also shown that the result (3) is quite insensitive to the choice of $\rho(\nu-\nu_0)$ as a Gaussian or triangular function. The theoretical line strengths are given by

$$c_l=n\nu_l(l+1)\alpha\exp\left[-l(l+1)h^2/2IkT\right], \quad (5)$$

in which α is a constant independent of l and contains the transition matrix element. Thus the constants a and α, together with the δ_l from Table IV of reference 1 determine the intensity distribution at all pressures. a and α may be determined from a study of a set of narrow lines showing considerable absorption. In Table I is given the data obtained from the nineteen lines at 2.5-cm pressure and three of the narrowest lines, at 4-cm pressure. In the second and third columns are given the line center transmission and the total absorption. From column four the effective slit width given by Eq. (4) is determined. The numbers appearing in this column are by no means constant in value, but no systematic trend is observable. From the fifth column, the value of α may be determined, using Eqs. (3) and (5). The quantities marked with an asterisk were omitted from the averages because the corresponding values either of Abs. or T_m differed from those of neighboring lines in a very irregular manner. The value 18.70×10^{-40} g cm^2 for the moment of inertia was employed, and is taken from Barker and Choi.

It was now possible to calculate the transmissions at all points in the spectrum with the use of Eq. (1). A triangular form was taken for $\rho(\nu-\nu_0)$ with a base width of 1.0 cm^{-1}, as determined from Eq. (4). The integrations were carried out by summations, using five intervals over the 1 cm^{-1} integration region. Thus the predicted values of transmission were calculated at 0.2 cm^{-1} intervals throughout the region from $l=3$ to $l=22$ for the pressures of 16, 40, and 58 cm Hg. The calculated curves are shown in Fig. 1.

The agreement at 40-cm pressure is considered to be good. In the cases of the lines at 16-cm and 58-cm pressure, the form of the theoretical curves agree well with the distribution of experimental points, but in general the observed transmission is somewhat greater than the theoretical values. This may be due to the difficulty in maintaining pressure described above. The general agreement of theory and experiment, considering the variation across the band as well as the dependence on pressure, is sufficiently good that it may be stated that, in this case, the effect of pressure on the intensity distribution has been completely accounted for.

In the theoretical treatment no correction to the intensities due to vibration-rotation was made. Inasmuch as the lines in this band show almost no convergence, it appears that this effect is small.

The accuracy with which the position of the centers of the lines is determined is approximately 0.1 cm^{-1}. From Table IV in reference 1 it is clear that, with respect to line shifts, no very exact quantitative agreement of theory and experiment can be expected. From a plot of the line positions at the observed pressures, an approximate determination of the shift per atmosphere was made. These numbers appear in Table I. The values of Table I, while not agreeing line for line with the theoretical values of Table IV, suffice to show the existence of the effect predicted by the theory, namely the shift of all rotational lines towards the intense part of the band. The lines in the most intense region, $l=8$ to $l=11$, show an abnormal position shift. These lines suffer the greatest broadening and hence the positions are determined with the least accuracy.

From the quantity α, the absolute value of the "dipole moment" of the vibration can be calculated. Adjusting the expression given by Dennison[3] for diatomic band intensities to this case, we have

$$\alpha=(8\pi^3/3hc)D^2/\textstyle\sum_l(2l+1)\exp\left[-W_l/kT\right].$$

From the observed value of 6.45×10^{-23} cm^2 for α, we obtain for the effective dipole moment

$$D=1.47\times10^{-19}\text{ e.s.u.}$$

It is believed that this is the first case of the evaluation of the dipole moment of a "bending vibration" of a molecule.

Dispersion of the Velocity and Anomalous Absorption of Sound in Hydrogen

ELLEN SWOMLEY STEWART*
Rowland Physical Laboratory, The Johns Hopkins University, Baltimore, Maryland
(Received March 13, 1946)

The velocity and absorption of sound in hydrogen were measured at frequencies of 3.855 Mc and 6.254 Mc and pressures of 1.00, 0.83, 0.67, and 0.50 atmos., with all observations made at 25°C. Dispersion of the velocity from 1321.9 m/sec. to 1382.0 m/sec. and anomalous absorption which were observed are interpreted as caused by molecular absorption induced by loss of the rotational degrees of freedom. Calculations place the inflection point of the dispersion curve at 10.95 Mc and the peak of the absorption curve at 10.0 Mc from velocity data, and at 16.1 and 14.8 Mc from absorption data. The relaxation times for pressures of 1 atmos. from the two sets of data are 1.9 and 1.7×10^{-8} sec. The f/p law is not strictly obeyed.

INTRODUCTION

THE so-called molecular dispersion and absorption of sound in gases was first inferred by Herzfeld and Rice[1] from considerations advanced by Rice regarding the velocity of chemical reactions in gases. As first postulated by these authors: "A slow rate of exchange between external and internal degrees of freedom keeps the internal degrees from taking up the whole amount of heat, and therefore acts as if the effective specific heat were decreased, and the velocity of sound increased with increasing frequency." The well-known results of G. W. Pierce[2] on CO_2 were already at hand to serve as a partial test of the theory. Bourgin[3] followed with another approach to the problem, and Kneser[4] derived useful equations and gave new experimental results, using the Pierce piezoelectric oscillator.

With the exception of the results presented in the present paper, and the indications obtained by Stewart, any dispersion in the velocity may be explained in terms of a lag of equilibrium between the translational and vibrational states of the molecule activated by the sound wave. Evidence of dispersion due to such a lag between translational and rotational states has hitherto not been found, though looked for, especially in hydrogen.

Richards and Reid[5] reported a dispersion in hydrogen in the 400-kc region, but Wallmann[6] later showed that there was no dispersion between 385 kc and 1.48 Mc. Roy and Rose,[7] from theoretical considerations, predicted that any dispersion in hydrogen should come above 1.5 Mc, and found experimentally that it did not occur up to 1.465 Mc. Van Itterbeck and his co-workers,[8] who have made extensive studies of hydrogen at 300 kc and 600 kc, found at times a small increase in the velocity over the classical value. However, they were never able to reproduce the effect, and finally determined that it did not exist at their frequencies. Their work on velocity is significant because it illustrates the wide variation in different samples of hydrogen and indicates the great care that must be taken to secure pure gas. They did find an anomalous absorption which they ascribed to molecular absorption because of the loss of the rotational degrees of freedom. This absorption they studied as a function of temperature and pressure and determined a relaxation time.

The present study was instigated by Stewart's[9] measurements in this laboratory on impure hydrogen, which indicated a dispersion in the frequency region between four and eight megacycles. The purpose of the present work was to

* At present Instructor in Physics, Connecticut College, New London, Connecticut.

[1] K. F. Herzfeld and F. O. Rice, Phys. Rev. **31**, 691 (1928).

[2] G. W. Pierce, Proc. Am. Acad. Sci. **60**, 271 (1925).

[3] D. G. Bourgin, Nature **122**, 133 (1928); Phys. Rev. **42**, 721 (1932).

[4] H. O. Kneser, Ann. d. Physik [5] **11**, 761 (1931).

[5] W. T. Richards and J. A. Reid, J. Chem. Phys. **2**, 206 (1934).

[6] M. H. Wallmann, Ann. d. Physik [5] **21**, 671 (1934).

[7] R. S. Roy and M. E. Rose, Proc. Roy. Soc. **A149**, 511 (1935).

[8] A. Van Itterbeck and P. Mariens, Physica **4**, 609 (1937); A. Van Itterbeck and L. Thys, Physica **5**, 889 (1938); A. Van Itterbeck and R. Vermaelen, Physica **9**, 345 (1942).

[9] J. L. Stewart, Dissertation, Johns Hopkins University (1943); Rev. Sci. Inst. **17**, 59 (1946).

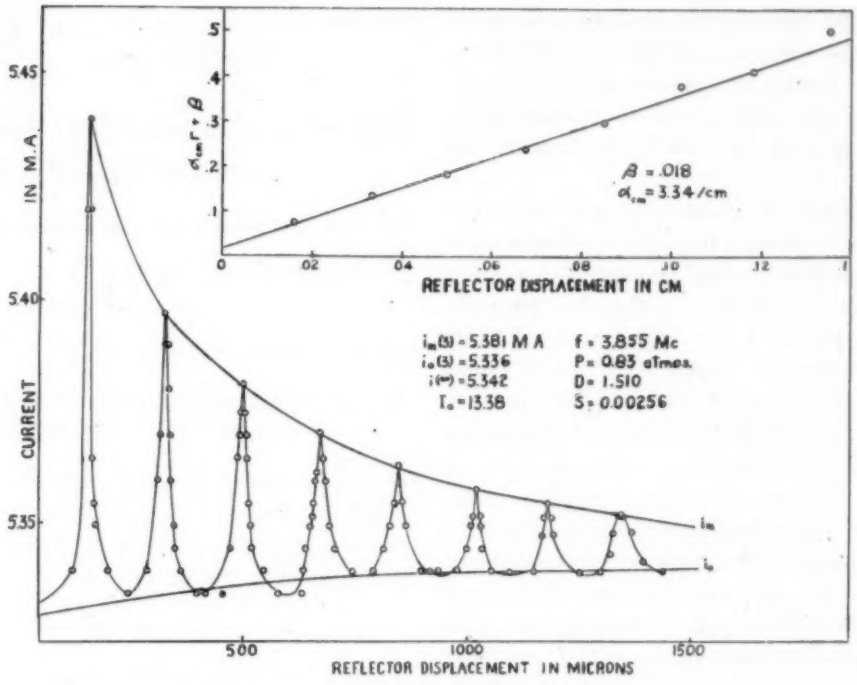

FIG. 1. Graph of peak structure and $(\alpha_{cm}r+\beta)$ *vs.* r for $\alpha=3$/cm and $\beta=0.02$.

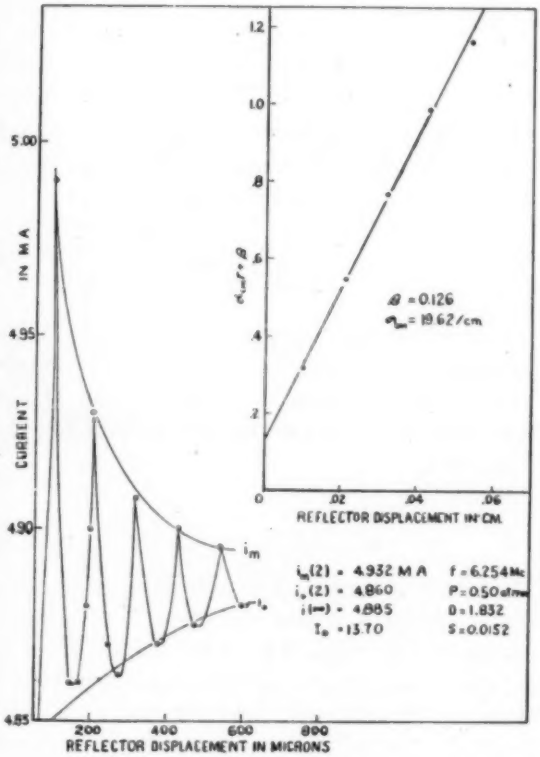

FIG. 2. Graph of peak structure and $(\alpha_{cm}r+\beta)$ *vs.* r for $\alpha=20$/cm and $\beta=0.13$.

determine whether such a dispersion and the associated increased absorption did occur in pure hydrogen at frequencies above four megacycles. A preliminary report of the results has been made.[10]

THEORY

The acoustic interferometer circuit, of the type used in this work, was developed and first analyzed by Hubbard[11] for the measurement of ultrasonic absorption and reflection coefficients. Alleman[12] modified the treatment to include dissipative losses in emission as well as reflection at the source. The present paper employs a new treatment developed by Hubbard[13] for the case in which the absorption coefficient is large.

With the interferometer crystal in the resonant circuit, the current in the thermocouple-cross in the circuit is a function of the amplitude of vibration of the crystal, which, in turn, is a function of the reflector displacement, as shown in Fig. 1 and Fig. 2. These figures illustrate the

[10] E. S. Stewart, J. L. Stewart, J. C. Hubbard, Phys. Rev. **68**, 231 (1945).
[11] J. C. Hubbard, Phys. Rev. **38**, 1011 (1931); **41**, 523 (1932).
[12] R. S. Alleman, Phys. Rev. **55**, 87 (1939).
[13] J. C. Hubbard (to be published).

resonance of the fluid column and the associated damping of the vibration of the crystal. Since this damping results in current peaks, the determination of the positions of these peaks gives a simple method of measuring the velocity of sound.

The calculation of absorption and reflection coefficients for hydrogen from these data is more difficult. According to the theory[11,12] a certain function, ϕ, of the current in the thermocouple cross has the property that the reciprocal of its values for successive peaks, $1/\phi_m$, is a linear function of $\tanh(\chi_m/2)$; where $\chi_m/2=\alpha r_m+\beta$. Here α is the amplitude coefficient of absorption per cm for particle velocity, r the distance of reflector from source, and $e^{-\beta}=\gamma$, the amplitude coefficient of reflection between gas and solid (source or reflector). Absorption coefficients measured hitherto by this method have been small enough to allow the approximation, $\tanh(\chi/2)\doteq(\chi/2)$. From the slope of the $\chi/2$ *vs.* m curve and the half-width of a peak, the absorption and reflection are evaluated. In the present work the value of α was so great that the above approximation is not valid. Moreover, approximations made in the previous work using peak width data are no longer valid, necessitating a restudy of the whole procedure of evaluating α and β from the data.

As a result of this the following method for calculating the absorption and reflection coefficients has been developed.[13] We define $\sigma_0=i_0/I_0$ and $\sigma_m=i_m/I_0$ in which (Fig. 1) i_0 is the current at the minima of the reaction curve, i_m is the value at the maxima, and I_0 is the value of the current when the interferometer and crystal are replaced by their equivalent capacity.

From Alleman's[12] paper we have

$$P=\sinh\chi/(\cosh\chi-\cos\delta), \tag{1}$$

TABLE I. Velocity of sound in pure hydrogen at 25°C.

f(Mc)	p(atmos.)	$\bar{V}$(m/sec.)	S.D. (m/sec.)	S.D. (%)	Number of determinations
3.855	1.00	1321.9	1.08	0.082	6
	0.83	1329.8	2.59	0.15	7
	0.67	1340.7	4.03	0.30	6
	0.50	1349.9	4.08	0.31	6
6.254	1.00	1365.0	3.28	0.24	6
	0.83	1366.0	3.82	0.28	4
	0.67	1373.4	5.91	0.43	5
	0.50	1382.0	3.59	0.26	8

where

$$\chi=2(\alpha r+\beta), \quad \delta=\frac{r-n\lambda/2}{\lambda/2}\cdot 2\pi.$$

Hubbard[11] showed that, S and D being constants,

$$\sigma=(1+SP)/(1+SP+D). \tag{2}$$

For reaction peaks $r=n\cdot\lambda/2$, so $\delta=0$ and

$$P=P_m(n)=\sinh\chi/(\cosh\chi-1)$$
$$=1/[\tanh(\alpha r+\beta)]. \tag{3}$$

Similarly for troughs $r=(n-\frac{1}{2})\cdot\lambda/2$, $\delta=\pi$, and

$$P=P_0(n-\tfrac{1}{2})=\sinh\chi/(\cosh\chi+1)$$
$$=\tanh(\alpha r+\beta). \tag{4}$$

If curves are drawn through the experimental points $i_0(n-\frac{1}{2})$ a hypothetical value of $P_0(n)$ can be found at $r=n\cdot\lambda/2$ by interpolating for $i_0(n)$. Then from (3) and (4)

$$P_m(n)=1/P_0(n). \tag{5}$$

Using (2) we obtain the equations

$$SP_m(n)=\frac{\sigma_m(n)}{1-\sigma_m(n)}D-1, \tag{6}$$

$$SP_0(n)=\frac{\sigma_0(n)}{1-\sigma_0(n)}D-1. \tag{7}$$

For the case of high absorption, i_0 and i_m rapidly approach the same limiting value $i_0(\infty)=i_m(\infty)=i(\infty)$ and from (6) or (7)

$$S=\frac{\sigma(\infty)}{1-\sigma(\infty)}D-1. \tag{8}$$

D can be separated from S by squaring (8) and equating to the product of (6) and (7), and S is then calculated from (8). After S and D have been found $P_m(n)$ can be determined for each value of n.

According to (3)

$$\tanh^{-1}(1/P_m)=\alpha_{cm}r+\beta. \tag{9}$$

Therefore, if $\tanh^{-1}(1/P_m)$ is plotted against r, the intercept is β and the slope is α_{cm}. This is shown in Fig. 1 and Fig. 2 for two different α's. α_λ, the exponential amplitude absorption coefficient per wave-length, is $\alpha_{cm}\cdot\lambda$. The exponential intensity absorption coefficients are $\mu_{cm}=2\alpha_{cm}$ and $\mu_\lambda=2\alpha_\lambda$. The exponential intensity reflection coefficient $\beta^*=2\beta$.

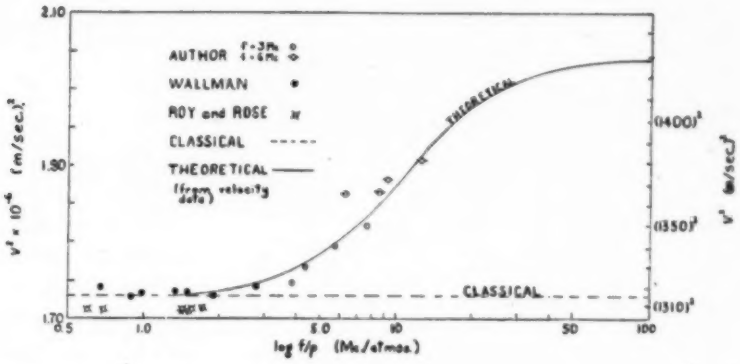

FIG. 3. V^2 against log (f/p) for hydrogen at 25°C.

DESCRIPTION OF APPARATUS AND EXPERIMENTAL PROCEDURE

The apparatus used in this work consists of three parts: the interferometer, the electrical circuits, and the gas-handling system.

The interferometer is that described by Stewart.[9] It is a variable-path, constant-pressure interferometer designed for high frequency work, with the piston surface kept parallel to the crystal to an accuracy of two light fringes. The path is varied by a micrometer screw whose motion is communicated to the piston through a bellows. The micrometer screw was driven by a small, reversible Telechron motor.

A conventional oscillator-amplifier combination was used to drive the interferometer crystal in the usual resonant circuit, and a thermocouple-galvanometer combination was used to detect and measure the r-f current.

The interferometer was part of a vacuum system that was evacuated before the gas was admitted and contained a trap to which refrigerants could be applied.

Since it has been shown that the velocity in hydrogen depends a great deal on the purity of the gas, every attempt was made to obtain and maintain a high degree of purity. The gas used was said to have a purity of 99.9 percent. In spite of all the precautions taken while transferring the gas from the tank to the vacuum system, some impurities not removed by a liquid nitrogen trap contaminated the gas as evidenced by low values for the velocity. Finally liquid hydrogen, applied after the trap had been cooled with liquid nitrogen, was used. Both the gas and liquid hydrogen were supplied by the CY Laboratory, Johns Hopkins University.

Before making the velocity and absorption measurements, the resonance circuit was tuned to the natural frequency of the crystal so the crevasse came below the peak of the resonance curve. With the oscillator driving the crystal in its crevasse, the piston was moved away from the crystal, and galvanometer deflections were recorded as a function of micrometer readings (Fig. 1 and Fig. 2). The galvanometer and thermocouple combination had been calibrated with direct current, making it possible to convert galvanometer readings into currents through the thermocouple. With full power (approximately 1.5 volts across the crystal) the deflection of the first peak at one atmosphere pressure was about three centimeters. Because of the large absorption, at reflector distances of a few wave-lengths the deflections fell off to one or two millimeters. It was necessary to read these deflections to one-tenth of a millimeter.

The frequency of the crevasse was measured by beating the oscillator against a calibrated precision signal generator concurrently checked by a 10-kc, crystal-controlled multivibrator. The temperature of the gas was measured by a calibrated thermometer with tenth-degree graduations.

Velocities, which were measured at 25°C, were calculated by

$$V=f\lambda. \tag{10}$$

As it was suspected that these measurements were made in a region of molecular absorption, the velocities were not reduced to 0°C by the classical temperature correction because it does not hold in such regions. Measurements were made at frequencies of 3.855 and 6.254 Mc.

The absorption and reflection coefficients were

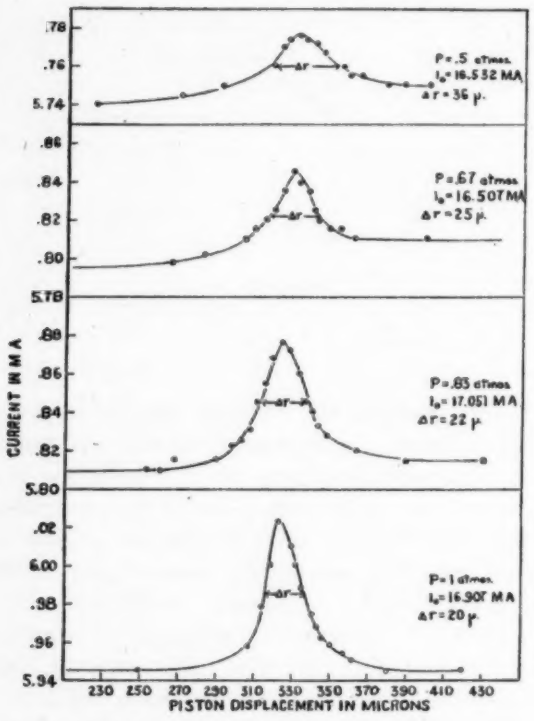

FIG. 4. Structure of the second peak at four pressures, $f=3.855$ Mc, illustrating the increased displacement from the crystal, the increased width at half-height, and the decreased current.

calculated according to the method outlined in the section on theory. To obtain the best values of $\sigma_0(n)$, $\sigma_m(n)$, and $\sigma(\infty)$ smooth curves were drawn through the maxima and minima of the current-displacement graphs (Fig. 1 and Fig. 2), and values of $i_0(n)$ and $i_m(n)$ were taken from these curves at half-wave-length intervals. The value of $i(\infty)$ was also estimated from these curves.

DISCUSSION OF RESULTS

Velocity Measurements

Table I gives the mean values obtained for the velocity of sound in hydrogen at frequencies of 3.855 and 6.254 Mc and pressures of 1.00, 0.83, 0.67, and 0.50 atmos. at 25°C. Figure 3 shows these data graphically as the conventional plot of V^2 against log (f/p) and in addition gives the classical value,* the theoretical dispersion curve, and the experimental values of Wallmann[6] and Roy and Rose[7] reduced to 25°C by the classical temperature correction

$$V_{25}=V_t\left(\frac{273.2+25}{273.2+t}\right)^{\frac{1}{2}}. \tag{11}$$

This applied since their measurements were not made in a dispersion region.

There is a definite change in velocity with both frequency and pressure. To determine whether such changes were significant an analysis based on Fisher's[14] discussion of the significance of means was made. This involved the calculation of the standard deviation (S.D.) of the mean velocity for each frequency and pressure, the calculation of the "t" function for the differences of the means, and finally the determination from Fisher's tables of the probability (P) of this occurring by chance. An example is the following: For the difference of the means at $p=1$ atmos., $f=3.855$ and 6.254 Mc, it was found that "t"$=11.25$ and $P=10^{-9}$. Consequently the change in velocity cannot be caused by chance but is physically significant; that is, a dispersion does exist. Likewise it was found that the differences in the velocities at 1 and 0.5 atmos., $f=3.855$ Mc, and at 1 and 0.5 atmos., $f=6.254$ Mc, were significant. It should be noted that V_{25} for 3.855 Mc and 1 atmos. is 0.6 percent higher than the classical value of 1315.8 m/sec.

From Fig. 3 it is seen that V^2 against $\log f/p$ does not give the conventional dispersion curve in that the dependence on f is not the same as the dependence on $1/p$. It was thought that this discrepancy might be caused by differences in the magnitude of the acoustical reaction when the effect of halving the pressure is compared with doubling the frequency. However this was disproved by measurements made on the same filling of gas ($p=1$ atmos., $f=3.855$ Mc) at two different powers (deflections of first peak 0.135 and 0.017 ma). The difference in velocities in

TABLE II. Velocity of sound in dry, CO_2-free air at 0°C.

f(Mc)	p(atmos.)	$\bar{V}$(m/sec.)	S.D. (m/sec.)	S.D. (%)	Number of determinations
3.855	1.00	331.7	0.22	0.07	3
	0.50	332.4	0.25	0.08	2
6.254	1.00	333.2	0.35	0.10	3

* This was calculated using $\gamma=1.404$, $p=76$ cm, $\rho=8.23\times10^{-5}$ g/cm³, and $t=25$°C.

[14] R. A. Fisher, *Statistical Methods for Research Workers*, (Oliver and Boyd Ltd., Edinburgh, 1944), ninth edition, pp. 122–128, 169.

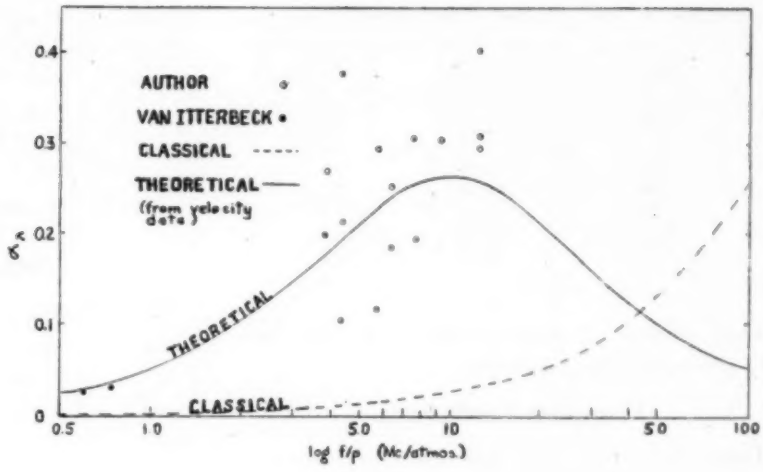

FIG. 5. The molecular and classical absorption coefficients (amplitude per wavelength) against log (f/p) for hydrogen at 25°C.

these two cases was only 0.47 percent and the greater velocity was obtained for the lower acoustic reaction, the opposite of the observed effect.

Next an attempt was made to determine the causes of the errors in the means for a given f and p. Two sources of error are involved in each mean—the measurement of length in the individual samples and the possible variations in the amounts of impurities in the different fillings of gas. Each $\lambda/2$ was an average over several peaks, the number depending on the pressure of the gas and decreasing with decreasing pressure. The standard deviations of $\bar{\lambda}/2$ for the different runs were calculated. In each case the S.D. of the mean V was less than the S.D. of the mean of the $\bar{\lambda}/2$'s used to calculate the velocity. For example:

TABLE III. Exponential reflection and absorption coefficients of hydrogen at 25°C.

f(Mc)	p(atmos.)	β	α_{rm} (exp)	α_λ (exp)	α_λ (class)	α_λ (mol)
3.855	1.00	0.31	6.09	0.209	0.010	0.199
		0.07	8.49	0.281		0.271
	0.83	0.02	3.40	0.117	0.011	0.106
		0.04	6.43	0.222		0.211
		0.20	11.19	0.386		0.375
	0.67	0.02	3.83	0.133	0.015	0.118
		0.51	8.90	0.309		0.294
	0.50	0.22	6.17	0.216	0.020	0.196
6.254	1.00	0.05	9.22	0.201	0.016	0.185
		0.17	12.35	0.269		0.253
	0.83	0.07	14.86	0.324	0.019	0.304
	0.67	0.03	14.84	0.327	0.024	0.303
	0.50	0.21	15.44	0.342	0.032	0.308
		0.16	14.80	0.328		0.296
		0.25	19.62	0.434		0.402

f/p(Mc/atmos.)	$\bar{V}$(m/sec.)	S.D.$(\bar{V})$%	S.D.$(\bar{\lambda}/2)_{hi}$%
3.855	1321.9	0.08	0.28
12.508	1382.0	0.26	0.67

Consequently any error due to differences in the gas measured must be less than the error due to measurement of length. The reason for the increase in the standard deviation as pressure decreased lies in the measurement of $\lambda/2$ as shown in Fig. 4. As the peaks became broader with decreasing pressure, the center of the peak was less accurately determined. Also the magnitude of the deflections decreased, decreasing the number of peaks that could be measured.

Measurements were also made on dry, CO_2-free air (Table II). With the same power as for hydrogen, at atmospheric pressure, ***one hundred*** peaks were measured in air with the same accuracy as that of *ten* measured in hydrogen. In addition the air peaks were sharper making the determination of the peak position more precise. The difference between the acoustical reactions of air and hydrogen is due to two effects. First, the lesser mass of hydrogen makes the initial reaction (deflection of the first peak) less than for air. Second, the greater absorption of hydrogen causes the amplitude to fall off much more quickly. The small changes in the velocity in air with pressure and frequency which were observed are on the border of significance but because of the small number of measurements this is considered insufficient evidence for the existence of dispersion in air. However, it is interesting to see that the variations with f and

TABLE IV. f_w and τ, from velocity measurements.

f(Mc)	p(atmos.)	f_w(Mc)	τ(sec.)	τ_{sl}(atmos.-sec.)
3.855	1.00	16.1	1.65×10^{-8}	1.7×10^{-8}
	0.83	12.0	2.21	1.8
	0.67	11.0	2.41	1.6
	0.50	12.1	2.19	1.1
6.254	1.00	7.3	3.64	3.6
	0.83	8.7	3.05	2.5
	0.67	9.5	2.79	1.8
	0.50	10.9	2.44	1.2

$1/p$ are similar to those in hydrogen but have only one-tenth the magnitude.

Absorption Coefficients

Table III gives the experimental values of the amplitude absorption coefficient α_{cm} and $\alpha_\lambda=\alpha_{cm}\cdot\lambda$, the classical absorption per wavelength, and the molecular absorption per wavelength, which is the experimental absorption minus the classical. This last quantity is plotted in Fig. 5 together with the theoretical molecular absorption, the classical absorption, and experimental values from Van Itterbeck and Vermaelen.[15] The experimental values vary considerably and give only the order of magnitude. However they establish that there is a variation with f/p although they are not accurate enough to establish whether the variation with f differs from that with $1/p$.

There are two sources of error. First, there was considerable inaccuracy in the current measurements. The deflections of the last few peaks were only two or three millimeters and the oscillator-amplifier combination sometimes lacked stability. The measurements at 6.254 Mc, where the oscillator was more stable, are more consistent than those at 3.855 Mc. Second, the values of α and β also depend on the particular peak (n) used to calculate D and S.

The classical amplitude absorption coefficient was evaluated from

$$\alpha_\lambda(\text{class})=\frac{2\pi^2 f}{\rho V^2}\left[\frac{4}{3}\eta'+\frac{\gamma-1}{C_p}K\right], \qquad (12)$$

using $V=1316$ m/sec., $\rho=8.23\times10^{-5}$ g/cm^3, $\eta'=1.146\eta$, $\eta=8.935\times10^{-5}$ poises, $\gamma=1.404$, $C_p=3.424$ cal./g°, $K=4.275\times10^{-4}$ cal./cm° sec., $p=1$ atmos., and $t=25$°C.

[15] A. Van Itterbeck and R. Vermaelen, reference 8, p. 351.

Both the classical and the experimental velocity were used in determining the classical absorption coefficient. The difference was much less than the experimental accuracy of the absorption measurements. The classical absorption was plotted in Fig. 5 to show its magnitude relative to that of the molecular absorption.

Reflection Coefficients

The extremely great absorption of hydrogen makes necessary the development of a more sensitive and more stable detector in order to use the method of calculation employed in this paper. This is evidenced by the results in Table III. The value of β, the exponential amplitude reflection coefficient, due to heat conduction was calculated from Herzfeld's[16] formula to be 0.03 at 4 Mc and 25°C.

The present results are very satisfactory in the sense that the measured values of β are without exception positive and in many cases are of the same order of magnitude as the result predicted. It should be noted however that the mean value of β is several times the predicted value. The large values of β accompanied by large α may be caused by poor alignment of the crystal. Further work should show whether this is the case or whether an extension of the Herzfeld theory must be made for high frequencies.

Application of Relaxation Theory

As in the case of CO_2 and other examples of dispersion the present results may be interpreted as caused by molecular absorption. According to the theory, dispersion in the velocity of sound occurs at frequencies where the periodicity of the change in energy in the sound wave is comparable to the time required to establish equi-

TABLE V. f_m and τ, from absorption measurements.

f(Mc)	p(atmos.)	α_λ(mole)	f_m(Mc)	τ(sec.)	τ_{sl}(atmos.-sec.)
3.855	1.00	0.199	8.5	2.7×10^{-8}	2.7×10^{-8}
	0.83	0.106	20.7	1.2	1.0
	0.83	0.211	8.8	2.7	2.3
	0.67	0.118	24.4	1.0	0.7
	0.50	0.196	17.3	1.4	0.7
6.254	1.00	0.185	15.3	1.6	1.6
	1.00	0.253	8.4	2.9	2.9

[16] K. F. Herzfeld, Phys. Rev. **53**, 899 (1938).

librium between the inner and outer degrees of freedom. At frequencies below this region energy flows into and out of the inner degrees, the molecule has all of its classical degrees of freedom, and the velocity of sound is classical. At frequencies above the dispersion region energy has not time to enter the inner degrees, the molecule exhibits only its outer degrees of freedom, and the velocity of sound is correspondingly increased. In the dispersion region the energy partially enters the inner degrees and then emerges out of phase with the wave, resulting in dissipation of energy. Thus in the dispersion region the velocity is between the two limiting velocities and a high absorption, called the molecular absorption, is present.

It is characteristic of this process that the increase in absorption commences at lower frequencies than the increase in velocity. This was observed for hydrogen. (Compare Fig. 3 and Fig. 5.) Also the f/p law should be obeyed by velocities in the case of molecular absorption, but in the present work this is only roughly true. As was shown in the discussion of velocity results, the scattering of the points is believed to be due to other causes than impurities in the gas.

Since at 300°K hydrogen is in the lowest vibrational state, the increase in velocity must be caused by the loss of its rotational degrees of freedom. Such a loss would increase the ratio of specific heats from 1.40 to 1.67 (approximately) and hydrogen would behave like a monatomic gas with only translational degrees of freedom. This would correspond to a velocity change from $V_0=1316$ m/sec. to $V_\infty=1435$ m/sec. at 25°C.

The dispersion formula may be written

$$f_w^2=f^2(V_\infty^2-V^2)/(V^2-V_0^2), \qquad (13)$$

where f_w is the inflection point of the V^2 against $\log f/p$ curve, V_0 is the velocity of sound for all degrees of freedom, V_∞ is the velocity for the translational degrees of freedom only, and V is the velocity at any frequency f. Table IV gives the values of f_w which were calculated for each experimental point. Using the average, $f_w=10.95$ Mc±8 percent, the complete theoretical dispersion curve was calculated according to (13). This is given in Fig. 3 together with the experimental results and shows that V_∞ should be reached in the 40–50 Mc region.

According to Kneser[17] the amplitude absorption coefficient per wave-length for molecular absorption is given by

$$\alpha_\lambda=\frac{\pi(Q^2-1)n}{1+Q^2n^2}; \quad \begin{matrix} Q=V_\infty/V_0 \\ n=f/f_w. \end{matrix} \qquad (14)$$

This has a maximum value

$$\alpha_\lambda(\max)=\pi/2(Q-1/Q) \qquad (15)$$

at the frequency

$$f_m=f_w/Q. \qquad (16)$$

For each experimental value of α_λ, f_m was found using a combination of (14) and (16),

$$f_m=\frac{f}{2\alpha_\lambda}\{\pi(Q-1/Q)\pm[\pi^2(Q-1/Q)^2-4\alpha_\lambda^2]^{\frac{1}{2}}\}. \qquad (17)$$

It can be seen from Fig. 5 and Table III that there were values of α_λ larger than $\alpha_\lambda(\max)=0.264$, calculated from (15). These substituted in (17) gave imaginary values for f_m and therefore are not included in Table V. These large α_λ's, as was mentioned in the discussion of reflection coefficients, are probably caused by malaligment of the crystal.

From the absorption data $f_m=14.8$ Mc±13 percent and $f_w=16.1$ Mc. f_m from the velocity data is 10.0 Mc. Since the velocity measurements are more accurate than the absorption measurements, the latter value for f_m was used in (14) to obtain the theoretical absorption curve shown in Fig. 5.

The relaxation time for equilibrium to be established between the translational and rotational degrees of freedom is given by

$$\tau=\frac{1}{2\pi f_w}\frac{C}{C_a}=\frac{1}{2\pi f_m}\frac{V_0}{V_\infty}\frac{C}{C_a}, \qquad (18)$$

in which C is the total specific heat per mole and C_a is that caused by translation. Since Van Itterbeck[8] has shown that τ is inversely proportional to pressure the quantity

$$\tau_{at}=\tau\cdot p \qquad (19)$$

was also calculated (Tables IV and V). The

[17] H. O. Kneser, Ann. d. Physik [5] 16, 337 (1933).

average value for τ_{at} from the velocity measurements is 1.9×10^{-8} atmos.-sec. and from the absorption data is 1.7×10^{-8} atmos.-sec. Van Itterbeck gives 2.0×10^{-8} atmos.-sec. at 15°C and 1 atmos. from absorption measurements made at 600 kc.

The failure of these data to fit the f curve is now interpreted as caused by two assumptions in the Kneser theory of vibrational dispersion which are not applicable to the case of rotational dispersion. Since the relaxation times for adjustment between the unequally spaced rotational levels obviously are unequal, the curve should be a step curve, to which the f curve is a first approximation. The deviations from the f/p law are believed to be caused by the failure of the assumption that the number of favorable collisions is proportional to the pressure and are presumably caused by the effect of three-body collisions. A more rigorous interpretation of this dispersion, in the light of the above discussion, will be the topic of a subsequent paper.

ACKNOWLEDGMENT

The author wishes to express her grateful appreciation to Professor J. C. Hubbard for his continued help and guidance during the progress of this research.

PHYSICAL REVIEW VOLUME 69, NUMBERS 11 AND 12 JUNE 1 AND 15, 1946

Theory of Long Period Magnetic Relaxation

CHARLES KITTEL
Department of Physics, Massachusetts Institute of Technology, Cambridge, Massachusetts
(Received March 11, 1946)

A discussion is given of the long period changes in magnetization in a mild steel specimen subjected to alternating stresses while in a weak magnetic field. The magnetization changes appear to occur with two time constants, of the order of three months and five years. A formal treatment of the phenomena is given along the lines of the time-dependent barrier potential used by Snoek in discussing other magnetic relaxation processes. The increase in the potential barrier is pictured as caused by the mechanical relaxation of local strains.

INTRODUCTION

DURING the war there was built up by physicists attached to the Naval Ordnance Laboratory, Washington, D. C., and to the Director of Scientific Research, British Admiralty, a body of experimental data relating to long period variations of magnetization of mild steel subject to alternating mechanical stresses while in a weak magnetic field. There has been little fundamental research, however, into the mechanisms involved. The existence of such time effects have been known for a very long time—see for example Ewing's book[1] or any manual on the compensation of ships' compasses. In view of the possible importance of the effects to our general understanding of ferromagnetism, it is desirable to summarize the main conclusions derived from the data and to indicate a phenomenological representation similar to that employed by Snoek[2] in discussing other magnetic relaxation processes.

The basic facts derived from observation at ordinary temperatures are given below. The applied fields involved are of the order of 0.5 gauss.

(*a*) After a period of the order of five years in a constant applied field the magnetization of a mild steel specimen subjected to alternating stresses *approximates* a state represented by infinite effective permeability, as was pointed out first by Dr. D. W. Ver Planck.

(*b*) When the applied field is changed suddenly, a considerable fraction of the magnetization changes practically instantaneously—this fraction is determined by the ordinary permeability and by the demagnetization coefficient.

[1] J. A. Ewing, *Magnetic Induction in Iron* (The Electrician Publishing Company, London, 1892).

[2] J. L. Snoek, Physica **5**, 663 (1938).

(*c*) Following a sudden change in the applied field, there is a slow change in magnetization with a time constant of the order of three months. This change does not proceed all the way to the condition of infinite effective permeability discussed in (*a*) above.

Dr. H. Iskenderian has shown that a single time constant of about three months, as proposed originally by the author, does not fit all of the data; subsequently Dr. H. R. Hulme and Mr. E. C. Holmberg of the British Admiralty showed that the remainder of the magnetization changed with a time constant of the order of five years.

The existence of a period of the order of five years is also evident in the work of R. L. Downdell[3] on the aging of magnet steels.

REPRESENTATION OF EXPERIMENTAL RESULTS

A phenomenological picture generally consistent with the above facts can be made along the following lines; it should be remembered that this picture is bound to be oversimplified.

Suppose that an initially demagnetized steel specimen is placed at time $t=0$ in a uniform constant applied field H_0. The specimen is subjected to alternating stresses with a frequency of the order of 60 cycles per minute while in the field; the magnitude of the stresses is not known but is probably of the order of 1/20 of the yield stress.

After a period of time which measurements suggest should be long in comparison with five years, the magnetization of the specimen will have reached a steady or equilibrium state in the field H_0. There are some measurements which suggest that for mild steel in fields of the order of 0.5 gauss the equilibrium state is characterized by nearly infinite effective permeability, so that

$$M_0^e = H_0/N, \tag{1}$$

where M_0^e is written for the total equilibrium magnetization (magnetic moment per unit volume) and N in the demagnetization coefficient in the direction of the field. It is supposed that the shape of the specimen is such that a demagnetization coefficient can be defined, at least approximately. Equation (1) is obtained from the well-known relation

$$M = H_0/[N+4\pi/(\mu-1)] \tag{2}$$

by letting $\mu \to \infty$.

It appears that the equilibrium magnetization is composed of three somewhat distinct parts which we shall denote by M_1^e, M_2^e, M_3^e, so that

$$M_0^e = M_1^e + M_2^e + M_3^e. \tag{3}$$

Here M_1^e is the ordinary induced magnetization which changes practically instantaneously when the applied field is changed, according to Eq. (2). We shall write

$$M_1^e/H_0 = c_1. \tag{4}$$

The second term M_2 represents the magnetization which increases to its equilibrium value M_2^e in a time of the order of three months, according to existing measurements. It would be tempting to try to describe the time variation of M_2 by an equation of the form

$$dM_2/dt = H_i/\tau_2, \tag{5}$$

where H_i is the internal field in the specimen after allowing for the demagnetizing field, but with this equation M_2 increases until H_i is zero, meaning that total equilibrium is reached with a time constant of three months. This contradicts the known existence of a five-year time constant. Instead of Eq. (5) we shall assume

$$dM_2/dt = (M_2^e - M_2)/\tau_2; \tag{6}$$

that is, the rate of change of M_2 is taken to be proportional to the difference between the equilibrium value M_2^e and the instantaneous value M_2; we specify further that

$$M_2/H_0 = c_2, \tag{7}$$

a constant.

The third term M_3 represents the magnetization which increases to its equilibrium value M_3^e in a time of the order of five years. We shall assume that the time variation of M_3 is governed by equations similar to those written above for M_2, so that

$$dM_3/dt = (M_3^e - M_3)/\tau_3 \tag{8}$$

and

$$M_3^e/H_0 = c_3. \tag{9}$$

Combining Eqs. (3), (4), (7), and (9) we get

$$M_0^e = M_1^e + M_2^e + M_3^e = (c_1+c_2+c_3)H_0, \tag{10}$$

[3] R. L. Downdell, Am. Soc. Metals Trans. **22**, 19 (1934); Trans. Am. Soc. Steel Treat. **5**, 27 (1924).

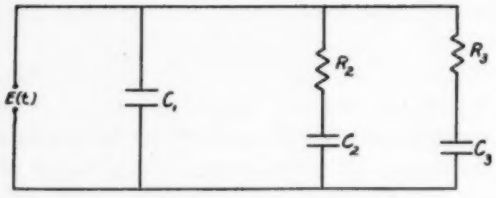

FIG. 1. Equivalent electrical circuit.

so that, by Eq. (1),

$$c_1+c_2+c_3=1/N. \tag{11}$$

To study the time variation of the total magnetization as the applied field H_0 is varied, we write

$$\begin{aligned} dM_0/dt&=(dM_1/dt)+(dM_2/dt)+(dM_3/dt)\\ &=(c_1dH_0/dt)+([c_2H_0-M_2]/\tau_2)\\ &\quad+([c_3H_0-M_3]/\tau_3). \end{aligned} \tag{12}$$

This equation is equivalent in behavior to the electric circuit shown in Fig. 1 if we make the following substitutions:

H_0 = voltage $E(t)$
M_i = charge Q_i
c_i = capacitance C_i
τ_i = time constant R_iC_i.

In terms of electrical quantities Eq. (12) becomes

$$\begin{aligned} dQ_0/dt&=C_1dE/dt\\ &\quad+(C_2E-Q_2)/\tau_2+(C_3E-Q_3)/\tau_3, \end{aligned} \tag{13}$$

an equation which has been studied in connection with dielectric relaxation. The solution in terms of magnetic quantities is

$$M_0(t)=\left[c_1H_0(t)+\int_0^\infty \varphi(\theta)H_0(t-\theta)d\theta\right], \tag{14}$$

where

$$\begin{aligned} \varphi(\theta)&=(c_2/\tau_2)\exp[-\theta/\tau_2]\\ &\quad+(c_3/\tau_3)\exp[-\theta/\tau_3] \end{aligned} \tag{15}$$

is the Boltzmann "memory function."

Before we discuss special solutions of Eq. (14) we must make some decision as to the values of the constants c_1, c_2, c_3. Now c_1 is determined from Eqs. (2) and (4), giving

$$c_1=[N+4\pi/(\mu-1)]^{-1}. \tag{16}$$

From Eq. (11),

$$c_2+c_3=(4\pi/N)/[N(\mu-1)+4\pi]. \tag{17}$$

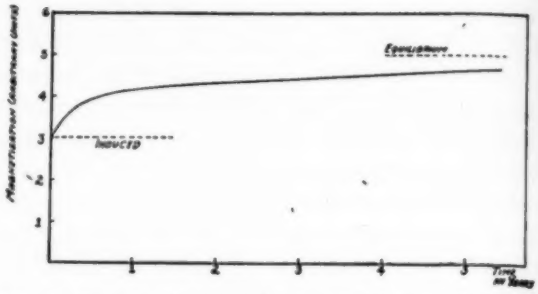

FIG. 2. Growth of magnetization following switching-on at $t=0$.

There is little information as to the relative importance of c_2 and c_3. In the case of a steel tube-like structure characterized by an equivalent volume permeability of about 4, and for which $N=2\pi$, giving $c_1=0.3/\pi$, there is evidence suggesting $c_2\sim c_3\sim 0.1/\pi$. The relative extent to which c_2 and c_3 share in satisfying Eq. (17) in other situations is not known.

Two solutions of Eq. (14) are of particular interest. The first is for the case of switching on the field at $t=0$; that is $H_0=0$ for $t<0$, while $H_0=h$ for $t>0$. Here the solution is $M_0(t)=0$ for $t<0$ and

$$\begin{aligned} M_0(t)&=h[c_1+c_2(1-\exp(-t/\tau_2))\\ &\quad+c_3(1-\exp(-t/\tau_3))], \end{aligned} \tag{18}$$

for $t>0$; for large t this approaches M_0^e. Figure 2 shows a plot of M_0 *vs.* t, for $\tau_2=3$ months, $\tau_3=60$ months, and is chosen so that $hc_1=3$, $hc_2=hc_3=1$, which corresponds to the situation discussed above for the ratio of the c's.

Another solution of interest is found by letting $H_0=he^{j\omega t}$, which gives, apart from transients,

$$\begin{aligned} M_0(t)/H_0(t)&=c_1+c_2/(1+j\omega\tau_2)\\ &\quad+c_3/(1+j\omega\tau_3). \end{aligned} \tag{19}$$

The magnetization lags the applied field. A plot of M_0 *vs.* H_0 gives a loop closely resembling a hysteresis loop.

THEORY

The existence of magnetic relaxation effects in iron with a time constant at room temperature of the order of minutes is well known. A review is given by Ewing[1] and by Becker and Doering.[4] A unified theory has been given by Snoek[2] which

[4] R. Becker and W. Doering, *Ferromagnetismus* (Edwards Brothers, Ann Arbor, Michigan, 1943).

accounts successfully for several different associated phenomena on the basis of domain theory. For a general discussion of domain theory Becker and Doering, and Bitter[5] may be consulted.

In order to eliminate non-essential features from the picture, Snoek supposes the magnetization at low field strength to be caused only by 180° reversals—that is, by the movement of boundaries separating domains magnetized in opposite directions. He assumes that the material is subject to "elastic after-effect" so that it can adapt itself locally to the condition of strain prevailing in the barrier layer itself. The loss of potential energy in the boundary layer in the course of adaptation of the material to local strain is thought of as a sort of supplementary potential hole coming gradually into existence after the barrier layer has moved from one spot to another. The characteristic time constant for the establishment of the potential hole is identified with the magnetic relaxation time constant.

The relaxation processes considered by Snoek are quite temperature dependent and are characterized by an activation energy of the order of one electron-volt per atom. His theory does not give any account of the effects of alternating stresses on the time constant. From the experimental standpoint nothing quantitative is known about the relative importance of thermal agitation and of alternating external stresses on the long period relaxation of barrier potentials. For convenience we shall proceed on the assumption that *elapsed time*, rather than *number of stress cycles*, is the significant independent variable. We shall apply Snoek's theory in a formal way to the long period relaxation processes, since it is attractive to try to associate them with long period mechanical relaxation of local strains. Furthermore, Snoek's theory can be generalized in a natural way to take account of the co-existence of several time constants. This is a very important point. In the discussion which follows the very short period effects (of the order of minutes) are omitted for the sake of compactness.

Changes in magnetization in a specimen may be discussed by considering the displacements of the boundaries separating domains magnetized in opposite directions. The displacement of such a boundary is determined by the potential function describing the strain energy of the boundary as a function of the position of the boundary, and also by the pressure exerted on the boundary by the applied magnetic field.

The strain potential will be written

$$V_0(x,t) = V_1(x) - \text{time-dependent terms.} \quad (20)$$

Here $V_1(x)$ is the potential energy due to the *permanent* part of the strain, while the time-dependent terms describe supplementary potentials with relaxation time constants of the order of three months and five years. The latter terms will be written $V_2(x,t)$ and $V_3(x,t)$, respectively; and their equilibrium values after a very long time at $x=x_1$ will be described by $V_2^e(x-x_1)$ and $V_3^e(x-x_1)$, so that

$$V_0^e(x) = V_1(x) - V_2^e(x-x_1) - V_3^e(x-x_1). \quad (21)$$

The V_2^e and V_3^e are bell-shaped curves (Fig. 3) of half-width comparable with the wall thickness.

It is supposed that the course of the supplementary potential V_2 is given by an equation somewhat similar to Eq. (6):

$$\partial V_2(x,t)/\partial t = [V_2^e(x-x_1) - V_2(x,t)]/\tau_2; \quad (22)$$

that is, the time rate of change of V_2 at a given point x (when the barrier wall is at x_1) is directly proportional to the difference between the equilibrium potential $V_2^e(x-x_1)$ and the instantaneous potential $V_2(x,t)$. The solution for the growth of V_2 at a new position x_1 for the barrier is given by

$$V_2(x,t) = V_2^e(x-x_1)[1-\exp(-t/\tau_2)]. \quad (23)$$

Similar equations hold for V_3.

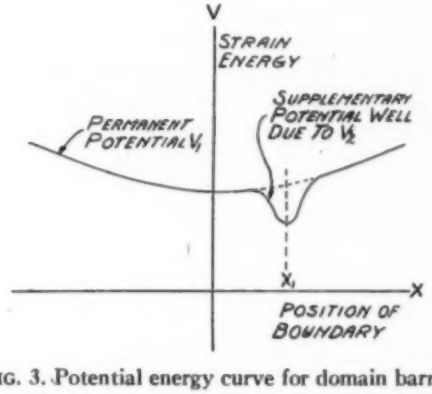

FIG. 3. Potential energy curve for domain barrier.

[5] F. Bitter, *Introduction to Ferromagnetism* (McGraw-Hill Book Company, Inc., New York, 1937).

TABLE I.

Approximate relaxation time	Probable cause
~5 years	Relaxation of local strains
~3 months	Relaxation of local strains
$\sim 10^{-2}-10^{2}$ second	Relaxation of local strains
$\sim 10^{-7}$ second	Eddy current damping of irreversible processes
$\sim 10^{-9}$ second	Eddy current skin depth less than domain dimensions.

Consider what happens to a boundary which has been at $x=0$ for a very long time, when a field H is applied suddenly. The pressure on the domain wall due to the field is $2M_sH$, where M_s is the saturation magnetization. The wall will move until the pressure is balanced by a force caused by the boundary strains. Since the force due to the boundary strains relaxes in the course of time, the wall will slowly creep farther out, thus increasing the macroscopic magnetization. All this time the wall is creating at its new positions new supplementary potentials, but these have no important influence on the qualitative aspects of the motion, and ultimately the wall will reach an equilibrium position determined by the fixed potential function $V_1(x)$.

Neglecting the effect of the new potentials created as the wall moves out, we treat the motion of the wall in the original set of potentials given by:

$$V_0(x,t)=V_1(x)-V_2^{e}(x)\exp(-t/\tau_2)-V_3^{e}(x)\exp(-t/\tau_3). \quad (24)$$

The instantaneous position of the wall is given by

$$\partial V_0(x_1)/\partial x \equiv V_1'(x_1)-V_2'(x_1,t)-V_3'(x_1,t)=2M_sHA, \quad (25)$$

where A is the area of the boundary wall. Since $x=0$ is the equilibrium position without a field we can write for small x, $V'(x)=xV''(0)$.

When the field is switched on the wall moves to x_1, where

$$x_1(t)\,V_0''(0,t)=2M_sHA. \quad (26)$$

Here x_1 is directly proportional to the macroscopic magnetization of the material, so that we can study the time variation of magnetization by studying the variation of x_1.

Immediately after the applied field is switched on the movement of x proceeds until limited by the combined effect of the three potential functions: the signs of V_1'', $-V_2^{e\prime\prime}$, and $-V_3^{e\prime\prime}$ are all positive. After a time comparable with τ_2 the effect of V_2^{e} practically vanishes and the magnetization has increased to approximately $M_1^{e}+M_2^{e}$. Finally after a time comparable with τ_3 the effect of V_3^{e} also vanishes and the equilibrium state M_0^{e} is reached, where $x_1(\infty)=2M_sHA/V_1''(0)$. Since the effective permeability is very high in the equilibrium state, the value of V_1'' must be small in comparison with $V_2^{e\prime\prime}$ or $V_3^{e\prime\prime}$.

If accurate values of the time constants of strain relaxation are required for any purpose, the calculation should be made including the effects due to the new potentials created by the barrier motion. Such calculations may be made by an extension of the method indicated by Snoek.

MAGNETIC RELAXATION SPECTRUM

The characteristic relaxation times for magnetization in iron may be summarized as in Table I. It should be emphasized that both the relaxation times and the assigned causes are only tentative.

ACKNOWLEDGMENTS

It is a pleasure to thank Professor Francis Bitter and Dr. D. W. Ver Planck for stimulating discussions of this subject. I am obliged to Dr. E. E. Schumacher of the Bell Telephone Laboratories for references to the metallurgical literature. This work was begun while the author was at the Naval Ordnance Laboratory, Washington, D. C.

The Magnetic Antenna*

LEIGH PAGE
Sloane Physics Laboratory, Yale University, New Haven, Connecticut
(Received November 2, 1941)

The theory of the magnetic antenna, consisting of a cylindrical rod of cemented magnetic powder around the center of which is wound a few turns of wire, is investigated. This antenna is shown to be more efficient than an electric antenna in receiving short electromagnetic waves of a few meters length. For such waves it exhibits an interesting selectivity.

(1) INTRODUCTION

THE magnetic antenna investigated in this paper consists of a rod in the shape of a right circular cylinder of radius a small compared with its length, composed of a permeable material of effective permeability μ and effective permittivity or dielectric constant κ. We shall be concerned with its efficiency as a receiver of plane electromagnetic waves of lengths ranging from a few centimeters up to several meters. The antenna is supposed to be oriented with its axis parallel to the magnetic vector of the incoming waves. Then the changing magnetic flux gives rise to an electromotive force in a few turns of wire wound around the center of the cylindrical rod. In developing the theory the antenna will be treated as if its length were infinite.

It was shown in a previous paper[1] that, in order to obtain practically the entire available permeability at the high frequencies under consideration, a permeable substance such as iron, which has also a large conductivity, must be used in the form of a cemented powder, the grains of which have radii of the order of magnitude of $(10)^{-4}$ cm. With such a powder effective permeabilities running up to 100 may be expected and effective permittivities up to 25, at realizable packing factors.

The primary object of this paper is to calculate the ratio of the flux of magnetic induction through a cross section of the cylindrical antenna at any specified wave-length to the flux in a cylindrical rod of the same cross section and the same effective permeability in a magnetostatic field of the same intensity as the magnetic field in the impinging wave. It is shown that the cylindrical antenna exhibits a sort of focusing action, caused presumably by internal reflections of the waves in the permeable medium, which gives rise, at a critical wave-length, to a resultant flux which is several times greater than that in a comparable magnetostatic field.

The ratio of the amplitude of the electromotive force produced in the coil encircling the magnetic antenna to that produced in an electric antenna employing the same length of wire is taken as a criterion of the relative efficiencies of the two types of antenna. Actually the electromotive force on the grid of the first tube in the amplifying system is a more significant quantity, and this is a considerable fraction of the electromotive force developed in the coil surrounding the magnetic antenna only if the capacity of the circuit is very small.

Heaviside-Lorentz symmetrical units are used except where otherwise indicated.

(2) THEORY

We introduce a set of right-handed rectangular coordinates with the Z axis along the axis of the cylindrical antenna, so oriented that the X axis is in the direction of propagation of the impinging plane wave. Then $\mathbf{E}$ and $\mathbf{H}$ in the incident wave are parallel, respectively, to the Y and Z axes. In addition we need the right-handed cylindrical coordinates r, ϕ, z, where $r^2=x^2+y^2$ and $\tan\phi=y/x$. Evidently the magnetic vector has the form

$$\mathbf{H}=\mathbf{k}H_0(r,\phi)e^{-i\omega t}, \tag{1}$$

where $\mathbf{k}$ is a unit vector along the Z axis and $\omega=2\pi\nu$ is the angular frequency.

If we put $\psi\equiv(\omega/c)\kappa$, $\chi\equiv(\omega/c)\mu$, where c is the

* This paper was received for publication on the date indicated but was voluntarily withheld from publication until the end of the war.

[1] Leigh Page, Phys. Rev. **60**, 675 (1941).

velocity of light *in vacuo*, and write

$$p \equiv (\psi\chi)^{\frac{1}{2}} r = \frac{2\pi r}{\lambda}(\kappa\mu)^{\frac{1}{2}},$$

where λ is the wave-length in empty space, the wave equation for H in cylindrical coordinates becomes

$$\frac{\partial^2 H}{\partial p^2} + \frac{1}{p}\frac{\partial H}{\partial p} + \frac{1}{p^2}\frac{\partial^2 H}{\partial \phi^2} + H = 0. \tag{2}$$

The solution of this gives us

$$H_z = \sum_{n=0}^{\infty} \{A_n J_n(p) + B_n N_n(p)\} \cos n\phi \tag{3}$$

for the amplitude of the Z component of the magnetic intensity, where $J_n(p)$ is the Bessel function and $N_n(p)$ the Neumann function of integral order n. The azimuthal component of the electric intensity and the radial component of the electric displacement are easily found from the field equations. Their amplitudes are

$$E_\phi = -i\left(\frac{\mu}{\kappa}\right)^{\frac{1}{2}} \frac{\partial H_z}{\partial p}, \quad D_r = i\frac{c}{\omega r}\frac{\partial H_z}{\partial \phi}. \tag{4}$$

Utilizing the recurrence formulae for the Bessel and Neumann functions, and putting $\beta \equiv (\mu/\kappa)^{\frac{1}{2}}$, we find

$$\begin{aligned} E_\phi = {} & i\beta\{A_0 J_1(p) + B_0 N_1(p)\} \\ & + \tfrac{1}{2} i\beta \sum_{n=1}^{\infty} \{A_n[J_{n+1}(p) - J_{n-1}(p)] \\ & + B_n[N_{n+1}(p) - N_{n-1}(p)]\} \cos n\phi. \end{aligned} \tag{5}$$

We shall distinguish the region inside the cylindrical antenna from that outside by primes. Thus

$$p' = (\psi'\chi')^{\frac{1}{2}} r = \frac{2\pi r}{\lambda}(\kappa\mu)^{\frac{1}{2}},$$

where κ is the effective permittivity and μ the effective permeability of the antenna, and

$$p = (\psi\chi)^{\frac{1}{2}} r = 2\pi r/\lambda.$$

In both these expressions, and everywhere else in this paper, λ represents the wave-length in free space outside the antenna.

The boundary conditions at the surface of the cylinder demand the continuity of H_z, E_ϕ, and D_r. Evidently if H_z is continuous for all values of ϕ, D_r is also. Now each B_n' must vanish because the Neumann functions become infinite for $p=0$. Hence, if we put $\alpha \equiv 2\pi a/\lambda$ and $\alpha' \equiv (2\pi a/\lambda)(\kappa\mu)^{\frac{1}{2}}$, the boundary conditions are

$$\begin{aligned} A_0 J_0(\alpha) + B_0 N_0(\alpha) &= A_0' J_0(\alpha'), \\ A_1 J_1(\alpha) + B_1 N_1(\alpha) &= A_1' J_1(\alpha'), \\ &\cdots\cdots\cdots \end{aligned}$$

from (3), and, with $\beta \equiv (\mu/\kappa)^{\frac{1}{2}}$,

$$\begin{aligned} A_0 J_1(\alpha) + B_0 N_1(\alpha) &= \beta A_0' J_1(\alpha'), \\ A_1[J_2(\alpha) - J_0(\alpha)] + B_1[N_2(\alpha) - N_0(\alpha)] & \\ = \beta A_1'[J_2(\alpha') - J_0(\alpha')], & \\ \cdots\cdots\cdots & \end{aligned}$$

from (5). Eliminating B_0, and making use of the identity

$$J_1(\alpha)N_0(\alpha) - J_0(\alpha)N_1(\alpha) = 2/\pi\alpha,$$

we have

$$A_0' = \frac{2}{\pi\alpha}\frac{1}{\beta J_1(\alpha')N_0(\alpha) - J_0(\alpha')N_1(\alpha)} A_0. \tag{6}$$

Also we find

$$\frac{B_0}{A_0} = -\frac{\beta J_1(\alpha')J_0(\alpha) - J_0(\alpha')J_1(\alpha)}{\beta J_1(\alpha')N_0(\alpha) - J_0(\alpha')N_1(\alpha)}. \tag{7}$$

Put

$$\begin{aligned} f_0 &\equiv \beta J_1(\alpha')J_0(\alpha) - J_0(\alpha')J_1(\alpha), \\ g_0 &\equiv \beta J_1(\alpha')N_0(\alpha) - J_0(\alpha')N_1(\alpha). \end{aligned}$$

Then

$$A_0' = \frac{2}{\pi\alpha g_0} A_0 = -\frac{2}{\pi\alpha f_0} B_0. \tag{8}$$

We shall not need the coefficients of higher index.

Next we turn our attention to the boundary condition at infinity. Without loss of generality we may suppose the magnetic intensity H_z^i in the incident wave to be of unit amplitude. Then

$$\begin{aligned} H_z^i &= e^{i(\omega/c)x} = e^{ip\cos\phi} \\ &= J_0(p) + 2iJ_1(p)\cos\phi \\ &\qquad + 2i^2 J_2(p)\cos 2\phi + \cdots, \end{aligned} \tag{9}$$

and the magnetic intensity H_z^r in the reflected wave is obtained by subtracting this from the total magnetic intensity given by (3). Hence

$$\begin{aligned} H_z^r = {} & \{(A_0 - 1)J_0(p) + B_0 N_0(p)\} \\ & + \{(A_1 - 2i)J_1(p) + B_1 N_1(p)\}\cos\phi \\ & + \{(A_2 - 2i^2)J_2(p) + B_2 N_2(p)\}\cos 2\phi + \cdots. \end{aligned} \tag{10}$$

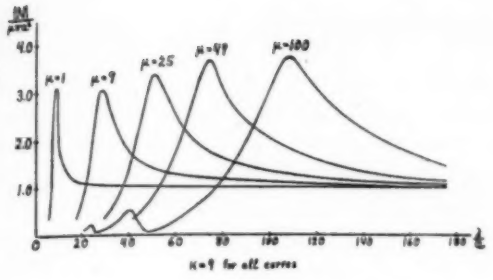

FIG. 1.

Since the reflected wave must be propagated *outward* from the antenna, it follows from the asymptotic expressions for $J_n(p)$ and $N_n(p)$ that

$$B_0=i(A_0-1), \quad B_1=i(A_1-2i), \quad B_2=i(A_2-2i^2), \quad \cdots. \tag{11}$$

Consequently

$$A_0'=\frac{2}{\pi\alpha}\frac{1}{(g_0^2+f_0^2)^{\frac{1}{2}}}e^{i\epsilon_0}, \quad \tan\epsilon_0\equiv\frac{f_0}{g_0}, \tag{12}$$

and similarly for the coefficients of higher index.

We are now ready to calculate the flux N of magnetic induction through a cross section of the cylindrical antenna. Since

$$H_z'=\sum_{n=0}^{\infty}A_n'J_n(p')\cos n\phi,$$

it follows that

$$N=\mu\int_0^{2\pi}\int_0^a H_z'rdrd\phi=\frac{2\pi A_0'}{(2\pi/\lambda)^2}\int_0^{\alpha'}J_0(p')p'dp'$$
$$=\mu\pi a^2[2J_1(\alpha')/\alpha']A_0'. \tag{13}$$

Putting in the value of A_0' given by (12), we obtain for the ratio of the flux at any specified wave-length to the flux in a cylindrical rod of the same cross section and the same effective permeability in a magnetostatic field of unit intensity

$$\frac{N}{\mu\pi a^2}=\frac{4}{\pi\alpha\alpha'}\frac{J_1(\alpha')}{(g_0^2+f_0^2)^{\frac{1}{2}}}e^{i\epsilon_0}, \quad \tan\epsilon_0\equiv\frac{f_0}{g_0}. \tag{14}$$

Here ϵ_0 represents the lag of the flux behind the magnetic intensity in the exciting wave.

Finally, the amplitude of the electromotive force per turn of wire around the magnetic antenna is $\mathcal{E}_m=(2\pi/\lambda)|N|$, whereas the amplitude of the electromotive force produced in an electric antenna employing a straight wire of the same length parallel to the electric vector in the incoming wave is $\mathcal{E}_e=2\pi a$. This gives for the efficiency of the magnetic antenna relative to a comparable electric antenna

$$\frac{\mathcal{E}_m}{\mathcal{E}_e}=\frac{|N|}{a\lambda}=\frac{1}{2}\mu\alpha\left(\frac{|N|}{\mu\pi a^2}\right). \tag{15}$$

(3) CALCULATIONS

We have calculated the modulus and the argument of the complex quantity (14) for a sufficient number of values of the ratio λ/a to draw fairly accurate curves, for a variety of values of κ and μ. As regards ϵ_0 nothing further will be said than to note that the lag increases with decreasing wave-length from the value zero at infinite wave-length.

A typical set of curves, in which the ratio of the modulus of N to $\mu\pi a^2$ is plotted against λ/a, is shown in Fig. 1. These curves are all for a permittivity $\kappa=9$. It is seen in each case that, as the wave-length decreases, the flux increases from the value $\mu\pi a^2$ at infinite wave-length to a maximum over three times as great, and then falls off rapidly to a value much less than $\mu\pi a^2$. The curve for $\mu=100$ is extended far enough to show the appearance of two much smaller subsidiary maxima. The height of the principal maximum, while very sensitive to change of the permittivity κ, seems to depend only in minor degree upon the value of the permeability μ. On the other hand, the critical wave-length λ_m at which the principal maximum occurs is very sensitive to change in μ. For constant κ, it is roughly proportional to the square root of μ.

The significant quantities revealed in these curves are the heights $|N|_m/\mu\pi a^2$ of the principal maxima, the ratios λ_m/a of the critical wave-lengths at which these maxima occur to the radius of the antenna, and the width of the peaks, which we define as the ratio $\Delta\lambda/\lambda_m$ of the wave-length interval $\Delta\lambda$ between the half-maxima on either side of a peak to λ_m. These quantities, together with the ratios of the critical wave-lengths $\lambda_m'=\lambda_m/(\kappa\mu)^{\frac{1}{2}}$ *inside* the antenna to a, are listed in Table I for all the cases for which curves have been computed. In the last column of the table is given the efficiency of the magnetic antenna at the critical wave-length relative to a comparable electric antenna. On account of the sharpness of the flux peaks, this is practically identical with the maximum value of $\mathcal{E}_m/\mathcal{E}_e$.

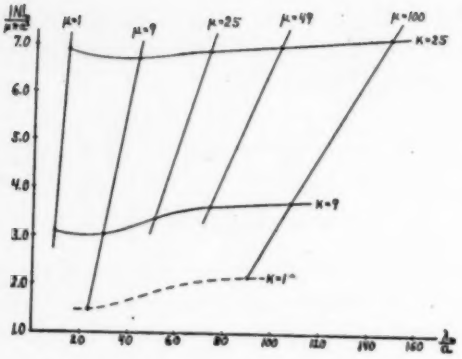

FIG. 2.

In Fig. 2 the dependence of the height and of the position of the principal maxima of the flux upon κ and μ is shown graphically. Each intersection represents a point listed in the table.

(4) CONCLUSIONS

The peculiar property of the cylindrical magnetic antenna of concentrating the flux in its interior at a critical wave-length many times the radius of the cylinder would seem to make it of value as a receiver of short electromagnetic waves. As is evident from Fig. 2, it is desirable that both the permittivity and the permeability of the antenna should be as large as possible. A high permittivity results in a high flux peak, and the critical wave-length at which this peak occurs increases with both κ and μ. It is probable that a permittivity of 25 and a permeability of 100 is realizable with suitable magnetic powders. Constructed of such material, a cylindrical antenna of 2-cm radius, used to receive electromagnetic waves of 3-meter wave-length, should develop an electromotive force 15 times as great as a comparable electric antenna. Furthermore, the magnetic antenna exhibits a selectivity which may be of value in certain applications. Particularly on the short wave side of the peak the response drops rapidly to a very low value.

A magnetic antenna in the form of a hollow cylinder has been investigated and flux curves similar to those in Fig. 1 have been computed. While a peak was obtained in the cases considered, it was considerably lower and occurred at a shorter wave-length than in the case of a solid cylinder of the same cross-sectional area. Therefore it was concluded that the solid cylinder is a more efficient receiving antenna than the hollow cylinder.

For the purpose of comparison with the cylindrical magnetic antenna it is interesting to consider the flux in a permeable slab bounded by parallel plane faces a distance $2a$ apart, when plane electromagnetic waves are incident normally on one surface. An easy analysis gives for the ratio of the amplitude of the flux at any wave-length λ to the amplitude of the flux at infinite wave-length the expression

$$\frac{\sin \alpha'/\alpha'}{(\cos^2 \alpha' + (\mu/\kappa) \sin^2 \alpha')^{\frac{1}{2}}},$$

where $\alpha' \equiv (2\pi a/\lambda)(\kappa\mu)^{\frac{1}{2}}$. For $\kappa < \mu$ this ratio is less than unity for all $\alpha' > 0$. However, for $\kappa > \mu$, peaks at which the ratio is greater than unity appear, as in the case of the cylinder. For instance, with $\kappa = 9\mu$, there is a peak at a value of α' a little less than $\pi/2$ at which the ratio is nearly 2.

TABLE I. Significant quantities revealed by curves of Fig. 1.

κ	μ	$\frac{\lvert N\rvert_m}{\mu\pi a^2}$	$\frac{\lambda_m}{a}$	$\frac{\Delta\lambda}{\lambda_m}$	$\frac{\lambda_{m'}}{a}$	$\frac{\mathcal{E}_m}{\mathcal{E}_s}$
1	9	1.44	24		8.0	1.2
1	100	2.15	90		9.0	7.8
9	1	3.1	9	0.5	2.9	1.1
9	9	3.0	29	0.8	3.2	3.0
9	25	3.4	51	0.7	3.4	5.2
9	49	3.6	74	0.6	3.5	7.6
9	100	3.7	108	0.6	3.6	10.8
25	1	6.9	14	0.18	2.7	1.6
25	9	6.7	43	0.22	2.9	4.4
25	25	6.9	73	0.22	2.9	7.5
25	49	7.0	103	0.22	2.9	10.5
25	100	7.2	149	0.22	3.0	15.1

Rapid and Direct Measurement of Vapor Pressure of Liquid Metals

A. H. WEBER AND SISTER GONZAGA PLANTENBERG, O.S.B.
Department of Physics, Saint Louis University, Saint Louis, Missouri
(Received March 2, 1946)

A rapid, direct method for determining the vapor pressure of liquid metals by measuring the force of impact of evaporated particles with a vacuum microbalance is described. The vapor pressure of Bi obtained by this method in a preliminary experiment is found to be in fairly good agreement with other measurements.

STUDIES in this laboratory of various properties of thin metallic films have led to the development of a rapid, direct method for measuring the vapor pressure of the liquid metal evaporated in vacuum to form these films. In the method devised the force of impact of a stream of vapor on a surface is measured directly. The procedure for the evaporation of the metal was practically identical with that used previously.[1,2] The stream of vapor striking the bottom of a glass bucket suspended from an helical quartz spiral was interrupted with a shutter and the elevation of the bucket was measured with a micrometer microscope.

THEORETICAL

By kinetic theory the vapor pressure p of a substance at Kelvin temperature T effusing as an ideal gas through an orifice of area dS into a solid angle $d\omega$ normal to dS is

$$p=\frac{dN}{dt}(2\pi mkT)^{\frac{1}{2}}\frac{\pi}{dS\,d\omega}\frac{N_0}{}; \qquad (1)$$

where dN/dt is the number of moles of the substance issuing per sec. from orifice, N_0 is Avogadro's number, k is Boltzmann's constant, and m is the mass of a particle.

The pressure p_c of an ideal gas condensing completely (*without reflection*) on a surface is

$$p_c=nkT/2, \qquad (2)$$

where n is the number of molecules/volume. Making the usual substitutions $n_c=nv/(6\pi)^{\frac{1}{2}}$, $v=(3kT/m)^{\frac{1}{2}}$ in Eq. (2) yields

$$p_c=n_c(\pi mkT/2)^{\frac{1}{2}}; \qquad (3)$$

where n_c = the number of molecules condensing/area per sec. Since $(n_c/N_0)A$ (A is the area over which condensation occurs) is the number of moles condensing/sec. it equals dN/dt in Eq. (1). Hence, putting

$$\frac{n_c}{N_0}A=\frac{p_cA}{\left(\frac{\pi}{2}mkT\right)^{\frac{1}{2}}N_0}, \qquad (4)$$

in Eq. (1) yields

$$p=2\pi p_cA/dS d\omega;$$

or

$$p=2\pi F/dS d\omega \qquad (5)$$

since $F=p_cA$, where F is the force of the condensing vapor on A.

EXPERIMENTAL

The apparatus is shown by Fig. 1 and is described in the accompanying legend. A micrometer microscope was placed to sight normal to the optical flat W, with its objective entering the recess shown. With the device shown by detail I, a calibrated rider (0.152_4 mg in vacuum) could be rested on and raised from the edge of the bucket B to calibrate the helical quartz spiral. The sensitivity of the microbalance under operating conditions was 4.20×10^{-7} g/micrometer-scale-division. The temperature of the liquid bismuth was measured with a tungsten-Kovar thermocouple with cold junction maintained at 0°C. The reference line chosen to measure the elongation and contraction of the quartz spiral appeared as a thin horizontal line produced by reflection of light from the bottom of the bucket.

A needed shutter (not shown by Fig. 1) entering through a side tube at 180° from I was used either to interrupt the vapor beam or to allow its

[1] A. H. Weber and S. C. Kirsch, Phys. Rev. **57**, 1042 (1940).
[2] E. Rudberg and J. Lempert, J. Chem. Phys. **3**, 627 (1935).

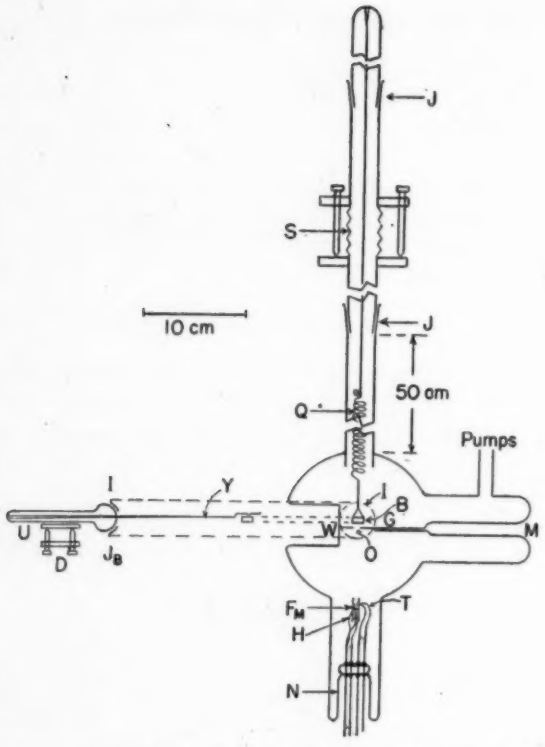

FIG. 1. Vacuum tube and microbalance. *J*, ground glass joints; J_B, ball and socket ground glass joint; *S*, bronze sylphon with screws for adjusting length and centering of spiral; *Q*, helical quartz spiral supported from above by a glass rod; *B*, glass bucket on the lower surface of which the metallic vapor particles condense; *O*, circular hole in glass plate *G*; *W*, optical flat (window); F_M, molybdenum furnace having orifice of area d*S* containing 99.8 percent c.p. Bi in upper cylindrical cavity; *H*, heating coil of 10-mil tungsten wire in lower cylindrical cavity; *N*, 50-mil lead-in wires; *T*, hot junction of tungsten-Kovar thermocouple; *I*, side tube entering at 90° from plane of Fig. 1 for glass rider-rod *Y* (used in manipulating rider on and off edge of bucket *B*); *M*, cylindrical recess through which illumination of reference line is produced; *U*, handle with rest *D*.

passage through the hole *O*. Thus readings taken with shutter "open" and "closed" after thermal equilibrium was established yielded directly the force of impact *F* of the vapor beam on the bucket bottom. The vapor pressure was calculated from Eq. (5).

RESULTS

Preliminary results for the vapor pressure of Bi are given in Table I.

Comparison of several Bi vapor pressure determinations is shown by Fig. 2. Curve 1 represents the data of Weber-Kirsch[1] in the temperature interval 876.1–911.4°K and extrapolated (dashed section) for the higher temperatures. The corresponding equation is

$$\log_{10} p_{mm} = -52.23(205/T)+9.03. \quad (6)$$

Curve 2 is obtained by extrapolating for the temperature range here considered the equation[3]

$$\log_{10} p_{mm} = -52.23(200/T)+8.87. \quad (7)$$

The vapor pressure as determined by Ko[4] in the temperature range 1100–1220°K is shown by curve 3 and is represented by

$$\log_{10} p_{mm} = -52.23(195/T)+8.56. \quad (8)$$

Since the vapor pressure of bismuth in the present investigation was obtained for one temperature only, no curves can be drawn to represent these results; hence the mean vapor pressure at 969.9°K of Table I is shown by a circle on Fig. 2. Values of the vapor pressure of bismuth at 969.6°K read from the curves of Fig. 2 are listed in Table II.

Two correction factors applying to measurement of vapor pressure of Bi by molecular effusion have not generally been taken into consideration; the effect of a short canal between the evaporating surface and the effusion orifice, and the diatomic character of Bi vapor. During the evaporation the surface of liquid Bi in the furnace is lowered. As the ratio of depth/diameter approaches unity,[5] the probability of the particles

TABLE I. Summarized date for vapor pressure of Bi. d$S=\pi(0.194\ \text{cm}^2)$, diameter of $O=0.716$ cm, distance from d*S* to $O=4.99$ cm, $T=969.6$°K.

Elevation of bucket by vapor beam (scale divisions)	$F\times10^3$ (dynes)	Vapor pressure p (mm-Hg)
19.0	7.82	0.0194
19.0	7.82	0.0194
14.0	5.76	0.0142
16.5	6.79	0.0167
12.0	4.94	0.0122
19.5	8.02	0.0198
15.0	6.17	0.0152
15.0	6.17	0.0152
16.0	6.58	0.0163
15.0	6.17	0.0152
18.0	7.41	0.0183
19.0	7.82	0.0194
18.0	7.41	0.0183
12.5	5.14	0.0127
		Mean 0.0166±0.0017

[3] Int. Crit. Tab. **3**, 205 (1926).
[4] C. C. Ko, J. Frank. Inst. **217**, 173 (1934).
[5] R. Fraser, *Molecular Rays* (Cambridge University Press, New York, 1931), p. 16.

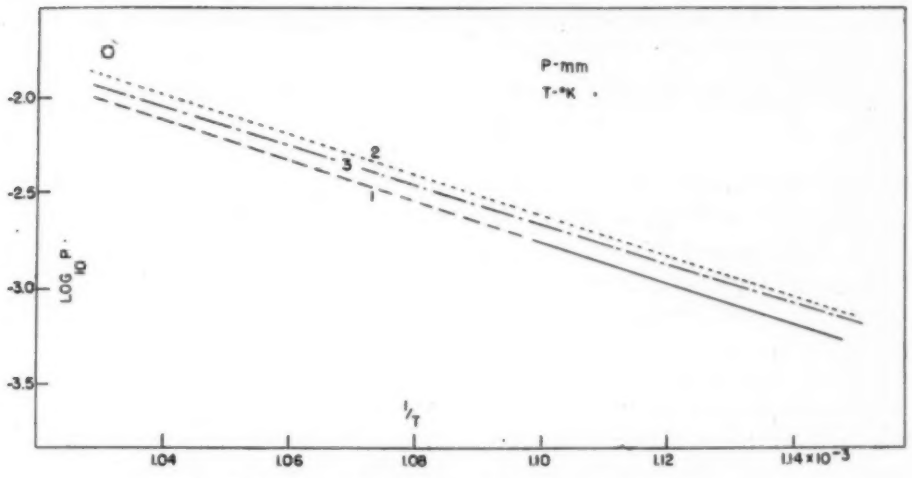

FIG. 2. Comparison of Bi vapor pressure determinations.

passing through the canal becomes 0.7. Hence the vapor pressure near the liquid surface may be greater by as much as 10/7 (provided a depth/diameter ratio equal to 1 is assumed) than the measurements made on the beam which has effused indicate. Another effect of a canal is to cause departure of the effusing particles from the cosine distribution law. This collimation of the vapor-beam by the canal is zero[6] if $\theta = 0$ as it does in the present experiments. Nor is a depth/diameter correction necessary (in the present experiments) for the cavity in the furnace F_M (Fig. 1) was brimful with Bi so that the ratio of depth/diameter is zero and the probability of passage through the canal is unity. Ko in his experiments on the heat of dissociation of Bi gives evidence that Bi vapor is diatomic.[4] The vapor pressure calculated by Eq. (1) must be corrected by multiplying by $1/\sqrt{2}$ if the vapor is diatomic instead of monatomic since the measurement of dN/dt involves the operation of dividing the mass of metal condensed by the *atomic* weight of Bi. Such a correction is not involved in the direct pressure method used in the present experiments as can be seen by examining Eq. (5). The conditions under which the Weber-Kirsch experiments[1] were performed were such that the corrections due to the canal effect and to the diatomic effect cancel each other approximately.

TABLE II. Vapor pressure of Bi in mm-Hg at 969.6°K.

Direct pressure method	Extrapolated values		
	Weber-Kirsch	Ko	I.C.T.
0.0166	0.00966	0.0112	0.0129

[6] R. Fraser, reference 5, p. 17.

Errors in the direct pressure method arise chiefly from vibrations of the quartz spiral, a factor difficult to control, and slight temperature changes in and around the tube. The chief advantages of this method are its directness and rapidity, a pair of readings (with shutter "open" and with shutter "closed") being made in 2–3 minutes as compared with several hours for the previous method.[1] The results of the vapor pressure measurements by this method are of a preliminary nature, the chief purpose of the present investigation was to test the reliability of the method.

The authors express their appreciation to Mr. M. Reddan for the calibration of the microscope scale. The gift by the General Electric Company of the quartz spiral which formed the essential part of the microbalance, and assistance of a Grant-in-Aid from the Sigma Xi Research Fund to the senior author (A.H.W.), are gratefully acknowledged.

Thermodynamic Equilibria of Higher Order

E. F. LYPE
Institute of Gas Technology and Armour Research Foundation, Chicago, Illinois
(Received September 12, 1945)

A NUMBER of observations of the thermodynamic properties of unary systems* has brought about a discussion of the existence of equilibria of higher order in various papers and textbooks between 1933 and 1940. In the following paper, a formulation of the problem of these equilibria is derived from Epstein's suggestion to expand the Taylor series for the thermodynamic potential to terms of higher order. The thermodynamic relations following from this formulation are in agreement with experimental data even in cases where Ehrenfest's equation yields an error of 100 percent. In connection with the equilibrium of the fourth order, the problem of extending the vapor pressure curve beyond the critical point is analyzed, and it is shown that the points of inflexion of various thermodynamic functions in the overcritical region may be regarded as this extension, as was suggested by Eucken.

1. DEFINITION OF THE PHASE EQUILIBRIUM OF HIGHER ORDER

Two phases of the same substance are in equilibrium with each other, if the thermodynamic potential $G=h-Ts$ has the same value in both phases. The equilibrium condition is then

$$G'=G'',$$

where the symbols (′) and (″) indicate the two phases.

The equilibrium curve is the locus of all points for which the above condition is satisfied. For a unary system where G depends only on the variables p and T, this curve is obtained in the following way: it is

$$G'(p, T)=G''(p, T). \qquad (1I)^1$$

For a point $(p+dp,\ T+dT)$ on the equilibrium curve, infinitely close to the former, is

$$G'(p+dp, T+dT)=G''(p+dp, T+dT). \quad (2)$$

In the neighborhood of (p, T), either side of (2) can be expanded in a Taylor series as suggested by Epstein.[2] Therefore

$$G(p+dp, T+dT)=G(p, T)+\frac{1}{1!}\left(\frac{\partial G}{\partial T}dT+\frac{\partial G}{\partial p}dp\right)+\frac{1}{2!}\left(\frac{\partial^2 G}{\partial T^2}dT^2+2\frac{\partial^2 G}{\partial T\partial p}dTdp+\frac{\partial^2 G}{\partial p^2}dp^2\right)$$
$$+\frac{1}{3!}\left(\frac{\partial^3 G}{\partial T^3}dT^3+3\frac{\partial^3 G}{\partial T^2\partial p}dT^2dp+3\frac{\partial^3 G}{\partial T\partial p^2}dTdp^2+\frac{\partial^3 G}{\partial p^3}dp^3\right)$$
$$+\frac{1}{4!}\left(\frac{\partial^4 G}{\partial T^4}dT^4+4\frac{\partial^4 G}{\partial T^3\partial p}dT^3dp+6\frac{\partial^4 G}{\partial T^2\partial p^2}dT^2dp^2+4\frac{\partial^4 G}{\partial T\partial p^3}dTdp^3+\frac{\partial^4 G}{\partial p^4}dp^4\right)+\cdots. \quad (3)$$

This expansion can be discontinued after the first term containing derivatives of G which have a different value in each phase. All subsequent terms can be neglected as infinitely small of higher order.

It follows from the definition of a total differential that the terms in the series (3) represent the total differentials of G. Therefore, (3) can be written

$$G(p+dp, T+dT)=G(p, T)+dG+\frac{1}{2!}d^2G+\frac{1}{3!}d^3G+\frac{1}{4!}d^4G+\cdots.$$

* The term "unäres System" was introduced by W. Schottky in his book *Thermodynamik* (1929) to describe a system which consists of a single substance.

[1] Roman figures refer to the order of the equilibrium in which the respective equation occurs.

[2] P. S. Epstein, *Textbook of Thermodynamics* (1937), pp. 131–132.

This expansion, substituted in (2) yields

$$G'(p,T)+dG'+\frac{d^2G'}{2!}+\frac{d^3G'}{3!}+\frac{d^4G'}{4!}+\cdots$$
$$=G''(p,T)+dG''+\frac{d^2G''}{2!}+\frac{d^3G''}{3!}+\frac{d^4G''}{4!}+\cdots.$$

In view of the equilibrium condition (1I) this reduces to

$$dG'+\frac{d^2G'}{2!}+\frac{d^3G'}{3!}+\frac{d^4G'}{4!}+\cdots$$
$$=dG''+\frac{d^2G''}{2!}+\frac{d^3G''}{3!}+\frac{d^4G''}{4!}+\cdots. \quad (4)$$

In an ordinary phase equilibrium, the first order derivatives of G have different values in both phases. In this case, (4) reduces to

$$dG'=dG''. \quad (5I)$$

This equilibrium is called an equilibrium of the first order. If, however, the nth order derivatives of the thermodynamic potential are the lowest which have different values in both phases, and all derivatives of an order lower than n are equal in both phases, then (4) becomes

$$d^nG'=d^nG''. \quad (5n)$$

Such an equilibrium is called an equilibrium of the nth order.

2. THE EQUILIBRIUM CONDITIONS FOR EQUILIBRIA OF HIGHER ORDER

In order to know where the series (4) can be discontinued, an evaluation of the partial derivatives in (3) is necessary. The differential of G is, according to the second law of thermodynamics,

$$dG=vdp-sdT$$

from which the partial derivatives of the first order are obtained as

$$\left(\frac{\partial G}{\partial T}\right)_p=-s, \quad \left(\frac{\partial G}{\partial p}\right)_T=v. \quad (6I)$$

On account of the relations

$$\left(\frac{\partial s}{\partial T}\right)_p=\frac{c_p}{T}, \quad \left(\frac{\partial s}{\partial p}\right)_T=-\left(\frac{\partial v}{\partial T}\right)_p, \quad \left(\frac{\partial c_p}{\partial p}\right)_T=-T\left(\frac{\partial^2 v}{\partial T^2}\right)_p, \quad (7)$$

the higher order derivatives of G are obtained by continued differentiation as follows:

$$\frac{\partial^2 G}{\partial T^2}=-\frac{c_p}{T}, \quad \frac{\partial^2 G}{\partial T\partial p}=\frac{\partial v}{\partial T}, \quad \frac{\partial^2 G}{\partial p^2}=\frac{\partial v}{\partial p}, \quad (6II)$$

$$\left.\begin{aligned}&\frac{\partial^3 G}{\partial T^3}=\frac{c_p}{T^2}-\frac{1}{T}\frac{\partial c_p}{\partial T}, \quad \frac{\partial^3 G}{\partial T^2\partial p}=\frac{\partial^2 v}{\partial T^2},\\ &\frac{\partial^3 G}{\partial T\partial p^2}=-\frac{\partial^2 s}{\partial p^2}, \quad \frac{\partial^3 G}{\partial p^3}=\frac{\partial^2 v}{\partial p^2},\end{aligned}\right\} \quad (6III)$$

$$\left.\begin{aligned}&\frac{\partial^4 G}{\partial T^4}=-\frac{2c_p}{T^3}+\frac{2}{T^2}\frac{\partial c_p}{\partial T}-\frac{1}{T}\frac{\partial^2 c_p}{\partial T^2},\\ &\frac{\partial^4 G}{\partial T^3\partial p}=\frac{\partial^3 v}{\partial T^3}, \quad \frac{\partial^4 G}{\partial T^2\partial p^2}=-\frac{1}{T}\frac{\partial^2 c_p}{\partial p^2},\\ &\frac{\partial^4 G}{\partial T\partial p^3}=-\frac{\partial^3 s}{\partial p^3}, \quad \frac{\partial^4 G}{\partial p^4}=\frac{\partial^3 v}{\partial p^3},\end{aligned}\right\} \quad (6IV)$$

and so forth.

For an equilibrium of the first order, Eq. (1I) must be satisfied, while (6I) yields the simultaneous conditions

$$s'\neq s'', \quad v'\neq v''. \quad (8I)$$

This means, that there must be a finite change of entropy and volume in the transition from one phase to the other. Consequently, all phase changes of the first order are accompanied by latent heat, and two phases in equilibrium can exist simultaneously.

In the same way, Eqs. (6) yield for the equilibrium of the nth order the following set of conditions which must be satisfied in addition to (1I):

$$s'=s'', \quad v'=v''; \quad (1II)$$

$$c_p'=c_p'', \quad \frac{\partial v'}{\partial T}=\frac{\partial v''}{\partial T}, \quad \frac{\partial v'}{\partial p}=\frac{\partial v''}{\partial p}; \quad (1III)$$

$$\frac{\partial c_p'}{\partial T}=\frac{\partial c_p''}{\partial T}, \quad \frac{\partial^2 v'}{\partial T^2}=\frac{\partial^2 v''}{\partial T^2}, \quad \frac{\partial^2 v'}{\partial p^2}=\frac{\partial^2 v''}{\partial p^2}, \quad \frac{\partial^2 s'}{\partial p^2}=\frac{\partial^2 s''}{\partial p^2}, \quad (1IV)$$

$$\vdots$$

$$\frac{\partial^{n-1}G'}{\partial T^{n-1}}=\frac{\partial^{n-1}G''}{\partial T^{n-1}} \quad \cdots \quad \frac{\partial^{n-1}G'}{\partial p^{n-1}}=\frac{\partial^{n-1}G''}{\partial p^{n-1}}, \quad (1n)$$

while, simultaneously, two or more of the following conditions must be satisfied:

$$\frac{\partial^n G'}{\partial T^n} \neq \frac{\partial^n G''}{\partial T^n} \quad \cdots \quad \frac{\partial^n G'}{\partial p^n} \neq \frac{\partial^n G''}{\partial p^n}. \tag{8n}$$

3. THE EQUILIBRIUM CURVE FOR EQUILIBRIA OF HIGHER ORDER

For an equilibrium of the first order, the equation of the equilibrium curve is obtained by evaluating (5I) according to (3) as

$$\frac{\partial G'}{\partial T}dT+\frac{\partial G'}{\partial p}dp=\frac{\partial G''}{\partial T}dT+\frac{\partial G''}{\partial p}dp$$

or

$$\frac{dp}{dT}=-\frac{\partial G''/\partial T-\partial G'/\partial T}{\partial G''/\partial p-\partial G'/\partial p}.$$

Substituting the partial derivatives from (6I) yields

$$\frac{dp}{dT}=\frac{s''-s'}{v''-v'} \tag{9I}$$

which is the Clausius-Clapeyron equation. All quantities in (9I) refer to the state on the equilibrium curve. When s and v are known as functions of p and T, integration of (9I) gives the equation of the first-order equilibrium curve.

For equilibrium of the second order, taking $n=2$ in Eq. (5n) gives

$$d^2G''=d^2G' \tag{5II}$$

or

$$d^2(G''-G')=0.$$

This can be written

$$d\left(\frac{\partial(G''-G')}{\partial T}dT+\frac{\partial(G''-G')}{\partial p}dp\right)=0.$$

Since, according to the rules of differentiation, for independent variables T and p

$$d^n(dT)=0, \quad d^n(dp)=0, \tag{10}$$

it follows

$$d\left(\frac{\partial(G''-G')}{\partial T}\right)dT+d\left(\frac{\partial(G''-G')}{\partial p}\right)dp=0$$

or

$$\frac{dp}{dT}=-d\left(\frac{\partial(G''-G')}{\partial T}\right)\Big/d\left(\frac{\partial(G''-G')}{\partial p}\right),$$

and, from (6I)

$$\frac{dp}{dT}=\frac{d(s''-s')}{d(v''-v')}.$$

If, on the equilibrium curve, T is considered as the independent variable, this can be written

$$\frac{dp}{dT}=\frac{ds''/dT-ds'/dT}{dv''/dT-dv'/dT}. \tag{9'}$$

The total differential quotients in the numerator can be further transformed. The heat to be supplied during a reversible change of state along the equilibrium curve is

$$dQ=Tds=cdT. \tag{11I}$$

By means of this equation, c is defined as the specific heat for a change of state along the equilibrium curve. If the reversible change of state were carried out first at constant pressure from the initial temperature T to the temperature $T+dT$, and afterwards at constant temperature from the initial pressure p to the pressure $p+dp$, then the first law of thermodynamics gives for the heat to be supplied

$$dQ=dh-vdp,$$

$$=\frac{\partial h}{\partial T}dT+\left(\frac{\partial h}{\partial p}-v\right)dp.$$

But

$$\partial h/\partial T=c_p, \quad \partial h/\partial p=v-T(\partial v/\partial T)_p. \tag{12}$$

Therefore

$$dQ=c_pdT-T(\partial v/\partial T)_pdp. \tag{11II}$$

The heat dQ must be the same for any reversible change of state between the same points, independent of the path. Therefore (11I) and (11II) can be equated, whence

$$c=c_p-T\left(\frac{\partial v}{\partial T}\right)_p\frac{dp}{dT}. \tag{12I}$$

Also, from (11I)

$$ds/dT=c/T. \tag{13}$$

Substitution of (13) into (9') gives finally the equation of the second-order equilibrium curve:

$$\frac{dp}{dT}=\frac{c''-c'}{T(dv''/dT-dv'/dT)}, \tag{9II}$$

where

$$\frac{dv}{dT}=\left(\frac{\partial v}{\partial T}\right)_p+\left(\frac{\partial v}{\partial p}\right)_T\frac{dp}{dT}. \tag{14I}$$

The properties c and dv/dT in (9II) refer to a

change of state in the direction of the equilibrium curve. It follows from (12I) and (14I) that they have different values in both phases. This is caused by the fact that the contact between the surfaces $f'(G, p, T)=0$ and $f''(G, p, T)=0$ which represent the two phases has been treated as occurring in one point only, as suggested by Epstein.[2]

For equilibrium of the nth order, Eq. (5n) requires that

$$d^n(G''-G')=0$$

or

$$d^{n-1}\left(\frac{\partial(G''-G')}{\partial T}dT+\frac{\partial(G''-G')}{\partial p}dp\right)=0.$$

In view of (10), this can be written

$$d^{n-1}\left(\frac{\partial(G''-G')}{\partial T}\right)dT+d^{n-1}\left(\frac{\partial(G''-G')}{\partial p}\right)dp=0,$$

which yields

$$\frac{dp}{dT}=-\frac{\dfrac{d^{n-1}}{dT^{n-1}}\left(\dfrac{\partial(G''-G')}{\partial T}\right)}{\dfrac{d^{n-1}}{dT^{n-1}}\left(\dfrac{\partial(G''-G')}{\partial p}\right)}$$

and, from (6I) and (13),

$$\frac{dp}{dT}=\frac{d^{n-2}}{dT^{n-2}}\left(\frac{c''}{T}-\frac{c'}{T}\right)\Big/\left(\frac{d^{n-1}v''}{dT^{n-1}}-\frac{d^{n-1}v'}{dT^{n-1}}\right). \tag{15}$$

The numerator can be evaluated by means of the mathematical relation

$$\frac{d^n}{dx^n}\left(\frac{y}{x}\right)=\frac{n!}{x}\sum_{r=0}^{n}\left(-\frac{1}{x}\right)^r\frac{y^{(n-r)}}{(n-r)!},$$

where $y^{(n-r)}$ is the differential quotient of y of the order $(n-r)$, and where $y^{(0)}=y$. When the term $r=0$ is taken out from under the summation sign, Eq. (15) can be written

$$\frac{dp}{dT}=\frac{[(c'')^{(n-2)}-(c')^{(n-2)}]+(n-2)!\sum_{r=1}^{n-2}\left(-\dfrac{1}{T}\right)^r\dfrac{(c'')^{(n-2-r)}-(c')^{(n-2-r)}}{(n-2-r)!}}{T\left(\dfrac{d^{n-1}v''}{dT^{n-1}}-\dfrac{d^{n-1}v'}{dT^{n-1}}\right)}. \tag{16}$$

The sum in the numerator is 0 as can be immediately seen from the calculation of the total differential quotients of c. From (12I), using (7), we obtain

$$\frac{dc}{dT}=\frac{\partial c_p}{\partial T}-\left(2T\frac{\partial^2 v}{\partial T^2}+\frac{\partial v}{\partial T}\right)\frac{dp}{dT}+T\frac{\partial^2 s}{\partial p^2}\left(\frac{dp}{dT}\right)^2-T\frac{\partial v}{\partial T}\frac{d^2p}{dT^2}, \tag{12II}$$

$$\frac{d^2c}{dT^2}=\frac{\partial^2 c_p}{\partial T^2}-\left(4\frac{\partial^2 v}{\partial T^2}+3T\frac{\partial^3 v}{\partial T^3}\right)\frac{dp}{dT}+\left(2\frac{\partial^2 s}{\partial p^2}+3\frac{\partial^2 c_p}{\partial p^2}\right)\left(\frac{dp}{dT}\right)^2+T\frac{\partial^3 s}{\partial p^3}\left(\frac{dp}{dT}\right)^3$$
$$-\left(3T\frac{\partial^2 v}{\partial T^2}+2\frac{\partial v}{\partial T}-3T\frac{\partial^2 s}{\partial p^2}\frac{dp}{dT}\right)\frac{d^2p}{dT^2}-T\frac{\partial v}{\partial T}\frac{d^3p}{dT^3}, \tag{12III}$$

and so forth. It is seen that the differential quotient of c of the order n comprises the partial derivatives of c_p up to the order n and the partial derivatives of s and v up to the order $(n+1)$. For equilibrium of the order n, the sum $\sum$ comprises all differential quotients of c up to the order $(n-3)$, i.e., all partial derivatives of c_p up to the order $(n-3)$ and all partial derivatives of s and v up to the order $(n-2)$. Furthermore, Eqs. (1I) to (1n) must be satisfied. This means that all partial derivatives occuring in $\sum$ have the same value for both phases. Therefore,

$$\sum_{r=1}^{n-2}=0$$

and the equilibrium curve for equilibrium of the nth order is given by the equation

$$\frac{dp}{dT}=\frac{\dfrac{d^{n-2}c''}{dT^{n-2}}-\dfrac{d^{n-2}c'}{dT^{n-2}}}{T\left(\dfrac{d^{n-1}v''}{dT^{n-1}}-\dfrac{d^{n-1}v'}{dT^{n-1}}\right)}. \tag{9n}$$

All quantities in (9n) refer to a change of state in the direction of the equilibrium curve.

The differential quotients in the denominator are, with use of (7), obtained from (14I) as

$$\frac{d^2v}{dT^2}=\frac{\partial^2 v}{\partial T^2}-2\frac{\partial^2 s}{\partial p^2}\frac{dp}{dT}+\frac{\partial^2 v}{\partial p^2}\left(\frac{dp}{dT}\right)^2+\frac{\partial v}{\partial p}\frac{d^2p}{dT^2}, \quad (14II)$$

$$\frac{d^3v}{dT^3}=\frac{\partial^3 v}{\partial T^3}-\frac{3}{T}\frac{\partial^2 c_p}{\partial p^2}\frac{dp}{dT}-3\frac{\partial^3 s}{\partial p^3}\left(\frac{dp}{dT}\right)^2+\frac{\partial^2 v}{\partial p^3}\left(\frac{dp}{dT}\right)^3-3\frac{\partial^2 s}{\partial p^2}\frac{d^2p}{dT^2}+\frac{\partial v}{\partial p}\frac{d^3p}{dT^3}+3\frac{\partial^2 v}{\partial p^2}\frac{dp}{dT}\frac{d^2p}{dT^2}, \quad (14III)$$

and so forth. When the differences of the differential quotients in (9n) are calculated, then it follows from the equilibrium conditions (1III) to (1n) that all those terms in (12II), (12III), etc. and (14II), (14III), etc. which contain differential quotients of p of a higher order than the first cancel out.

4. DISCUSSION OF AVAILABLE EXPERIMENTAL RESULTS

a. Equilibrium of the Second Order

Observations of certain substances have shown a sudden change of at least two of the second derivatives of G, while both first derivatives remained constant. This would then indicate the existence of two phases which are with each other in equilibrium of the second order. For such an equilibrium state, Eq. (9II) must hold. If all quantities occurring in (9II) are known from experiments, this equation can be verified. This is possible for the transition between the two modifications of liquid helium and solid methane which have frequently been interpreted as equilibria of the second order.[3-5] In both cases, the transition curve and the thermodynamic properties on this curve are known.

[3] P. Ehrenfest, Leiden Commun. Supp. 75 b (1933).
[4] W. H. Keesom, Leiden Commun. Supp. 80 b (1936).
[5] K. Clusius and A. Perlick, Zeits. f. physik. Chemie **B24**, 313 (1934).

For second-order equilibrium, Eq. (5II) yields[2]

$$\left(\frac{\partial^2 G''}{\partial T^2}-\frac{\partial^2 G'}{\partial T^2}\right)dT^2+2\left(\frac{\partial^2 G''}{\partial T\partial p}-\frac{\partial^2 G'}{\partial T\partial p}\right)dTdp+\left(\frac{\partial^2 G''}{\partial p^2}-\frac{\partial^2 G'}{\partial p^2}\right)dp^2=0.$$

Substituting the derivatives from (6II) gives

$$\left(\frac{c_p''}{T}-\frac{c_p'}{T}\right)dT^2-2\left(\frac{\partial v''}{\partial T}-\frac{\partial v'}{\partial T}\right)dTdp-\left(\frac{\partial v''}{\partial p}-\frac{\partial v'}{\partial p}\right)dp^2=0. \quad (17)$$

This equation can be written in either one of the following two forms:

$$\left(\frac{c_p''}{T}-\frac{c_p'}{T}\right)\left(\frac{dT}{dp}\right)^2-2\left(\frac{\partial v''}{\partial T}-\frac{\partial v'}{\partial T}\right)\frac{dT}{dp}-\left(\frac{\partial v''}{\partial p}-\frac{\partial v'}{\partial p}\right)=0,$$

$$\left(\frac{\partial v''}{\partial p}-\frac{\partial v'}{\partial p}\right)\left(\frac{dp}{dT}\right)^2+2\left(\frac{\partial v''}{\partial T}-\frac{\partial v'}{\partial T}\right)\frac{dp}{dT}-\left(\frac{c_p''}{T}-\frac{c_p'}{T}\right)=0.$$

Solving for dT/dp and dp/dT, respectively, gives

$$\frac{dT}{dp}=\frac{\dfrac{\partial v''}{\partial T}-\dfrac{\partial v'}{\partial T}}{\dfrac{c_p''}{T}-\dfrac{c_p'}{T}}\pm\left[\left[\frac{\dfrac{\partial v''}{\partial T}-\dfrac{\partial v'}{\partial T}}{\dfrac{c_p''}{T}-\dfrac{c_p'}{T}}\right]^2+\frac{\dfrac{\partial v''}{\partial p}-\dfrac{\partial v'}{\partial p}}{\dfrac{c_p''}{T}-\dfrac{c_p'}{T}}\right]^{\frac{1}{2}}, \quad (18a)$$

$$\frac{dp}{dT}=-\frac{\dfrac{\partial v''}{\partial T}-\dfrac{\partial v'}{\partial T}}{\dfrac{\partial v''}{\partial p}-\dfrac{\partial v'}{\partial p}}\pm\left[\left[\frac{\dfrac{\partial v''}{\partial T}-\dfrac{\partial v'}{\partial T}}{\dfrac{\partial v''}{\partial p}-\dfrac{\partial v'}{\partial p}}\right]^2+\frac{\dfrac{c_p''}{T}-\dfrac{c_p'}{T}}{\dfrac{\partial v''}{\partial p}-\dfrac{\partial v'}{\partial p}}\right]^{\frac{1}{2}}. \quad (18b)$$

Equation (18b) is also obtained when (12I) and (14I) are substituted in (9II), and when the resulting equation is solved for dp/dT.

Because of the double sign of the square root in Eqs. (18), there are two possible equilibrium curves for an equilibrium of the second order.

It is compatible with the existence of a second-order equilibrium that one of the three second-

order derivatives of G has identical values in both phases. Thus, according to (6II), any one of the following relations may exist:

$$\partial v''/\partial p=\partial v'/\partial p, \tag{19a}$$

$$c_p''=c_p', \tag{19b}$$

$$\partial v''/\partial T=\partial v'/\partial T. \tag{19c}$$

If Eqs. (19) are introduced alternately in (17), the equilibrium equation becomes, if the trivial solutions $dT\equiv 0$ or $dp\equiv 0$ are excluded,

for case (19a)

$$\left(\frac{c_p''}{T}-\frac{c_p'}{T}\right)dT-2\left(\frac{\partial v''}{\partial T}-\frac{\partial v'}{\partial T}\right)dp=0, \tag{17a}$$

for case (19b)

$$\left(\frac{\partial v''}{\partial p}-\frac{\partial v'}{\partial p}\right)dp+2\left(\frac{\partial v''}{\partial T}-\frac{\partial v'}{\partial T}\right)dT=0, \tag{17b}$$

for case (19c)

$$\left(\frac{c_p''}{T}-\frac{c_p'}{T}\right)dT^2-\left(\frac{\partial v''}{\partial p}-\frac{\partial v'}{\partial p}\right)dp^2=0. \tag{17c}$$

The slope of the equilibrium curves is then, for these three cases,

$$\frac{dp}{dT}=\frac{1}{2}\frac{c_p''-c_p'}{T(\partial v''/\partial T-\partial v'/\partial T)}, \tag{20a}$$

$$\frac{dp}{dT}=-2\frac{\partial v''/\partial T-\partial v'/\partial T}{\partial v''/\partial p-\partial v'/\partial p}, \tag{20b}$$

$$\frac{dp}{dT}=\pm\left(\frac{c_p''/T-c_p'/T}{\partial v''/\partial p-\partial v'/\partial p}\right)^{\frac{1}{2}}. \tag{20c}$$

It is seen from Eqs. (20) that, if conditions (19a) or (19b) hold, only one equilibrium curve will be observed, while two equilibrium curves are possible for case (19c).

There is still the possibility that any one of Eqs. (19) may be satisfied only asymptotically, i.e., that as we proceed on the equilibrium curve the values in the two phases for one of the quantities in (19) approach each other. Then, the slope of the equilibrium curve (18) must asymptotically approach the value given by (20). This can only occur if, in case (19a), the plus sign is used in (18a), and if, in case (19b), the minus sign is used in (18b). For case (19c), either one of the two signs in (18) is valid. Our present knowledge of the equilibrium of the second order is still incomplete. So far, of the three conditions (19), only (19a) has been observed as an asymptotic condition. In this case, only one equilibrium curve will be found with values dT/dp corresponding to those obtained from (18a) for the plus sign. The discriminant of the quadratic form (17) is

$$D=-\left(\frac{c_p''}{T}-\frac{c_p'}{T}\right)\left(\frac{\partial v''}{\partial p}-\frac{\partial v'}{\partial p}\right)-\left(\frac{\partial v''}{\partial T}-\frac{\partial v'}{\partial T}\right)^2.$$

This discriminant will, in general, be different from zero. Epstein[2] has pointed out that the restriction $D\equiv 0$ leads to Ehrenfest's theory of the second-order equilibrium.[3] In this case, the square roots in (18) vanish, and it is

from (18a) $$\left(\frac{c_p''}{T}-\frac{c_p'}{T}\right)dT-\left(\frac{\partial v''}{\partial T}-\frac{\partial v'}{\partial T}\right)dp=0,$$

from (18b) $$\left(\frac{\partial v''}{\partial T}-\frac{\partial v'}{\partial T}\right)dT+\left(\frac{\partial v''}{\partial p}-\frac{\partial v'}{\partial p}\right)dp=0.$$

In view of (7), these equations can be written

$$d(s''-s')=0 \quad \text{and} \quad d(v''-v')=0.$$

These are the conditions which, according to Ehrenfest, should be satisfied on the second-order equilibrium curve. They represent Ehrenfest's formulation of the equilibrium curve of the second order and would make indeterminate the Eq. (9II) which was derived from (5II). The latter is Epstein's formulation of the second-order equilibrium curve on which the present study is based.

Ehrenfest's postulate $D\equiv 0$ implies that the surfaces $f'(G, p, T)=0$ and $f''(G, p, T)=0$ have contact along a finite part of the equilibrium curve. The slope of this curve is, from (18a) with $D\equiv 0$,

$$\frac{dp}{dT}=\frac{c_p''-c_p'}{T(\partial v''/\partial T-\partial v'/\partial T)}, \tag{21}$$

which is twice as large as the value from (20a) for condition (19a). Therefore, for an equilibrium where (19a) is valid, the experiment can decide in favor of one theory or the other.

Equations (18a) and (20a) will now be checked against experimental results.

A comprehensive description of the thermodynamic properties of liquid helium in the region of transition from HeI to HeII is given by

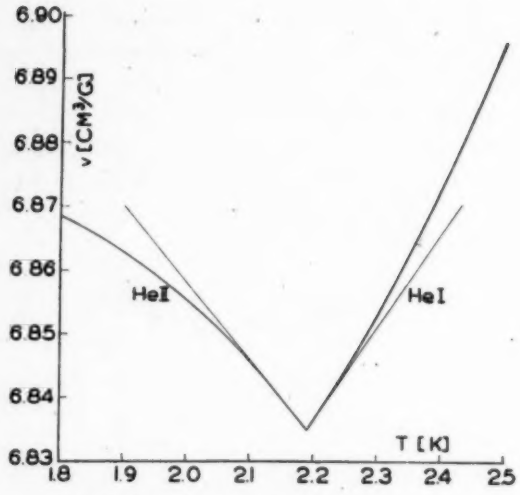

FIG. 1. Specific volume of liquid helium at saturation pressure, according to Kamerlingh Onnes and Boks.

Keesom.[4] It can be seen from Keesom's Fig. 8 that the compressibilities of both phases become equal as the low pressure end of the transition curve is approached. For the lowest pressure, where both HeI and HeII are in equilibrium with saturated vapor, Eq. (19a) is satisfied. The transition curve is then given by (20a). Figure 1 of this paper shows the specific volume for liquid HeI and HeII in equilibrium with saturated vapor, according to experiments by Kamerlingh Onnes and Boks, as computed by Roberts.[6] From this figure, the tangents in the transition point are

$$dv''/dT = -0.1215 \text{ cm}^3/\text{g deg.},$$
$$dv'/dT = 0.1475 \text{ cm}^3/\text{g deg.}$$

Since these quantities refer to a change of state along the vapor pressure curve, it is necessary to calculate the thermal expansion at constant pressure from the formula

$$(\partial v/\partial T)_p = [dv/dT]_{sat} - (\partial v/\partial p)_T [dp/dT]_{sat}. \quad (22)$$

The compressibility which, as already mentioned, is equal for both modifications is found from Keesom's Fig. 8 by a linear extrapolation of $(\partial/\partial p)(1/v')$ against $\log p$ as

$$(\partial v/\partial p)_T = -0.145 \times 10^{-3} \text{ cm}^5/\text{g}^2.$$

The quantity dp/dT is found from empirical equations[7] for the vapor pressure curve as follows:

for HeII $[dp/dT]_{sat} = 130.2$ g/cm² deg.,

for HeI $[dp/dT]_{sat} = 119.5$ g/cm² deg.

Substituting these data in (22) gives

$$(\partial v''/\partial T)_p = -0.1404 \text{ cm}^3/\text{g deg.}$$
$$(\partial v'/\partial T)_p = 0.1302 \text{ cm}^3/\text{g deg.}$$

and

$$\partial v''/\partial T - \partial v'/\partial T = -0.2706 \text{ cm}^3/\text{g deg.}$$

Keesom's Fig. 11 gives, for both modifications in equilibrium with saturated vapor, values of c/R as function of temperature (not c directly). For the transition point is

$$c''/R = 5.84, \quad c'/R = 1.22.$$

These data would have to be converted to c_p according to (121) and by using the above values for $(\partial v/\partial T)_p$ and $[dp/dT]_{sat}$. However, the effect of this conversion is negligible, so that the above values c'' and c' can be taken directly for c_p'' and c_p', respectively. This gives

$$c_p'' = 2.902 \text{ cal./g deg.}, \quad c_p' = 0.606 \text{ cal./g deg.}$$

and

$$c_p'' - c_p' = 2.296 \text{ cal./g deg.} = 9.804 \times 10^4 \text{ cm/deg.}$$

The temperature of the transition point at saturation pressure is

$$T = 2.19° \text{ K.}$$

From (20a) is now obtained

$$\frac{dp}{dT} = -\frac{1}{2}\frac{9.804 \times 10^4}{2.19 \times 0.2706} = -8.27 \times 10^4 \text{ g/cm}^2 \text{ deg.}$$
$$= -82.7 \text{ at./deg.}$$

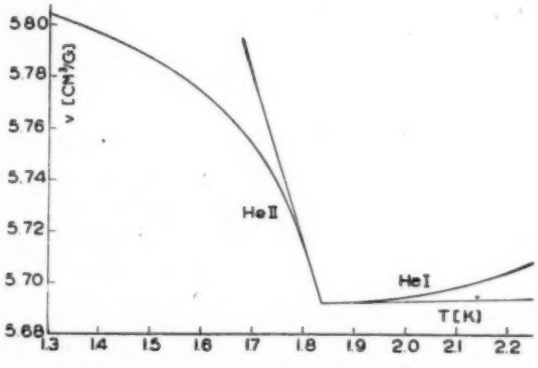

FIG. 2. Specific volume of liquid helium at 25 atmos. pressure, according to Keesom.

[6] J. K. Roberts, *Heat and Thermodynamics* (1940), third edition, p. 328.

[7] Landolt-Börnstein, Phys.-Chem. Tab., Supp. II b, p. 1291.

where 1 at. = 1 kg/cm² = 735.6 mm Hg. The observed value is, according to Keesom,

$$(dp/dT)_{obs} = -83.5 \text{ at./deg.}$$

The discrepancy is only 1 percent. Ehrenfest's Eq. (21) would give dp/dT twice as high as the observed value.

A rough check of the complete formula (18a) can be made for the He transition at 25 atmos. The specific gravity and the compressibility are given by Keesom for this pressure, but the specific heat is given for a pressure described as "about 25 atmos." Therefore, not too good an agreement between the data and Eq. (18a) may be expected.

From Keesom's Fig. 11

$$c_v''/R = 1.98, \quad c_v'/R = 0.84,$$

from which

$$c_v'' = 4.200 \times 10^4 \text{ cm/deg.},$$
$$c_v' = 1.782 \times 10^4 \text{ cm/deg.}$$

For HeI, the difference between c_v' and c_p' is negligible, such that c_v' can be taken for c_p'. For HeII, the difference is considerable, and correct evaluation of c_p'' is necessary. From Keesom's Fig. 8

$$\partial v''/\partial p = -0.3794 \times 10^{-4} \text{ cm}^5/\text{g}^2,$$
$$\partial v'/\partial p = -0.2508 \times 10^{-4} \text{ cm}^5/\text{g}^2,$$
$$\partial v''/\partial p - \partial v'/\partial p = -0.1286 \times 10^{-4} \text{ cm}^5/\text{g}^2.$$

Figure 2 of this paper shows the specific volume according to Keesom's Table I. From this figure, the tangents in the transition point are

$$\partial v''/\partial T = -0.6369 \text{ cm}^3/\text{g deg.},$$
$$\partial v'/\partial T = 0.0048 \text{ cm}^3/\text{g deg.},$$
$$\partial v''/\partial T - \partial v'/\partial T = -0.6417 \text{ cm}^3/\text{g deg.}$$

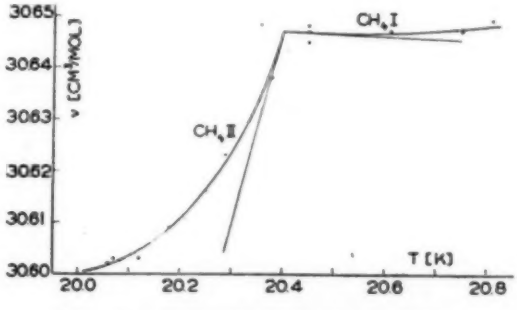

FIG. 3. Specific volume of solid methane, according to Heuse.

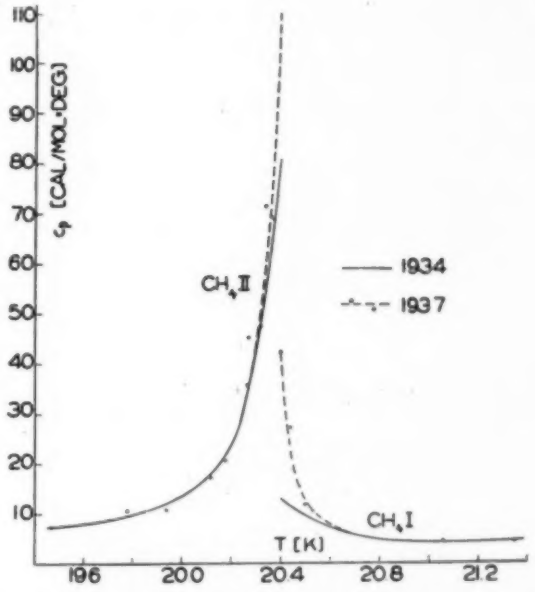

FIG. 4. Specific heat of solid methane. Solid line, according to Clusius and Perlick, 1934. Broken line, according to Frank and Clusius, 1937.

The temperature of transition at 25 atmos. is $T = 1.835°\text{K}$.

For the specific heat at constant pressure follows

$$c_p' = 1.782 \times 10^4 \text{ cm/deg.},$$

$$c_p'' = c_v'' - T\frac{(\partial v''/\partial T)^2}{\partial v''/\partial p}$$

$$= 4.200 \times 10^4 + 1.835\frac{0.6369^2}{0.3794}10^4$$

$$= 6.162 \times 10^4 \text{ cm/deg.},$$

$$c_p'' - c_p' = 4.380 \times 10^4 \text{ cm/deg.}$$

In view of the asymptotic condition (19a), the observed equilibrium curve will correspond to the plus sign in (18a). Using the positive square root in (18a) yields

$$dT/dp = -10^{-4}(0.2688 - (0.07227 - 0.05388)^{\frac{1}{2}})$$
$$= -0.1332 \times 10^{-4} \text{ cm}^2 \text{ deg./g}$$

or

$$dp/dT = -7.50 \times 10^4 \text{ g/cm}^2 \text{ deg.} = -75.0 \text{ at./deg.}$$

The observed value is, according to Keesom,

$$(dp/dT)_{obs} = -63.2 \text{ at./deg.}$$

while Ehrenfest's Eq. (21) would give dp/dT

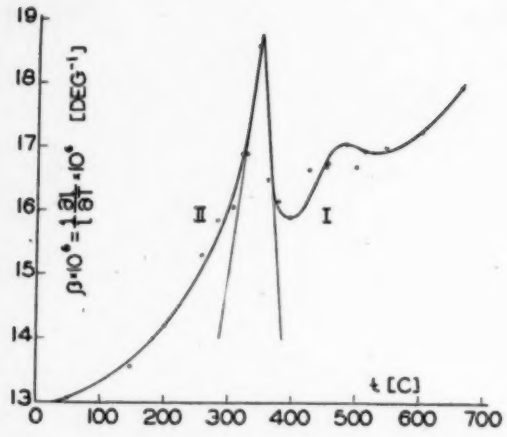

FIG. 5. Coefficient of linear expansion of nickel, according to Eucken and Dannöhl.

$= -37.2$ at./deg. which is an error of 41 percent. The value from (18a) is 19 percent too large, probably because of the fact, that the specific heats are not measured at exactly the same pressure as the other properties.

Clusius and Perlick[8] have described the thermodynamic properties of solid methane in the region of the transition point at atmospheric pressure where the transition temperature is 20.4°K. Observations of the compressibility are not available, but it is reasonable to assume that, in the solid state, the difference in the compressibilities of both modifications is negligible; then, condition (19a) is satisfied, and the equilibrium Eq. (20a) can be applied. Figure 3 shows the molecular volume of both modifications in the neighborhood of this transition point based on the experimental data by Heuse[8] as interpreted by Clusius and Perlick. From this figure, the tangents are

$$(\partial v''/\partial T)_p = 0.376 \text{ cm}^3/\text{mole deg.},$$
$$(\partial v'/\partial T)_p = -0.005 \text{ cm}^3/\text{mole deg.},$$

and

$$\partial v''/\partial T - \partial v'/\partial T = 0.381 \text{ cm}^3/\text{mole deg.} = 0.0238 \text{ cm}^3/\text{g deg.}$$

The molecular heat as given by these authors is represented by the solid curve in Fig. 4. They found c_p' and c_p'' by linear extrapolation from the highest value observed to 20.4°K as

$$c_p'' = 81 \text{ cal./mole deg.}, \quad c_p' = 13 \text{ cal./mole deg.}$$

whence

$$c_p'' - c_p' = 68 \text{ cal./mole deg.} = 18.15 \times 10^4 \text{ cm/deg.}$$

Substituting these data in (20a) yields

$$\frac{dp}{dT} = \frac{1}{2}\frac{18.15 \times 10^4}{20.4 \times 0.0238} = 18.7 \times 10^4 \text{ g/cm}^2 \text{ deg.} = 187 \text{ at./deg.}$$

This is identical with the observed value, as obtained by differentiation from the empirical equation of the transition curve given by Clusius and Perlick. Ehrenfest's Eq. (21) would again give dp/dT twice as large as the observed value.

More recently, Frank and Clusius[9] reported on a new set of experimental data of the c_p's obtained by Perlick. He observed $c_p' = 42.5$ cal./mole deg. In order to restore the agreement between (20a) and these new data, the value of $c_p'' - c_p'$ has to be preserved as 68 cal./mole deg. This would then require to extrapolate c_p'' (which was not observed) to as high a value as 110.5 cal./mole deg. This is done by the broken curve in Fig. 4. It can be seen that this extrapolation is compatible with the observed data. It may be noted, however, that these c_p data give for the entropy change from 20°K to 21°K a value which exceeds slightly the value derived theoretically by Frank and Clusius.

b. Equilibrium of the Third Order

Observations of certain transformations in metals have shown a discontinuity of two of the third derivatives of G, namely the quantities $\partial c_p/\partial T$ and $\partial^2 v/\partial T^2$, while all first and second derivatives of G remained unchanged. This would then indicate the existence of an equilibrium of the third order for these two modifications. One of these transformations is the transition from the ferromagnetic to the paramagnetic state in the Curie point. Another is the transition between two different crystal lattices, as observed for Cobalt at 450°C. That the Curie point represents a point of equilibrium of the third order has first been stated by Clusius and Perlick[5] and Eucken.[10] The equation of the

[8] W. Heuse, Zeits. f. physik. Chemie **A147**, 270 (1930).

[9] A. Frank and K. Clusius, Zeits. f. physik. Chemie **B36**, 291 (1937).

[10] A. Eucken and W. Dannöhl, Zeits. f. Elektrochemie **40**, 814 (1934).

transition curve is obtained from (5n) by taking $n=3$ as

$$\left(\frac{\partial^3 G''}{\partial T^3}-\frac{\partial^3 G'}{\partial T^3}\right)dT^3+3\left(\frac{\partial^3 G''}{\partial T^2\partial p}-\frac{\partial^3 G'}{\partial T^2\partial p}\right)dT^2dp$$
$$+3\left(\frac{\partial^3 G''}{\partial T\partial p^2}-\frac{\partial^3 G'}{\partial T\partial p^2}\right)dTdp^2$$
$$+\left(\frac{\partial^3 G''}{\partial p^3}-\frac{\partial^3 G'}{\partial p^3}\right)dp^3=0.$$

Substituting the derivatives from (6III) gives

$$-\frac{1}{T}\left(\frac{\partial c_p''}{\partial T}-\frac{\partial c_p'}{\partial T}\right)dT^3+3\left(\frac{\partial^2 v''}{\partial T^2}-\frac{\partial^2 v'}{\partial T^2}\right)dT^2dp$$
$$-3\left(\frac{\partial^2 s''}{\partial p^2}-\frac{\partial^2 s'}{\partial p^2}\right)dTdp^2$$
$$+\left(\frac{\partial^2 v''}{\partial p^2}-\frac{\partial^2 v'}{\partial p^2}\right)dp^3=0. \quad (23)$$

Since this is a cubic equation, there can be three transition curves of the third order. For transitions in the solid state, the assumption may be made that the derivatives with respect to pressure are equal for both modifications in equilibrium with each other. Then, the following conditions are satisfied simultaneously:

$$\partial^2 v''/\partial p^2=\partial^2 v'/\partial p^2, \quad \partial^2 s''/\partial p^2=\partial^2 s'/\partial p^2. \quad (24)$$

If (24) is introduced in (23), only one equation for the third-order transition curve is obtained:

$$\frac{dp}{dT}=\frac{1}{3}\frac{\partial c_p''/\partial T-\partial c_p'/\partial T}{T(\partial^2 v''/\partial T^2-\partial^2 v'/\partial T^2)}. \quad (25)$$

This equation can be used to calculate the variation of the transition temperature with pressure from the tangents of observed functions c_p and $\partial v/\partial T$. Reliable data on these properties are available in the neighborhood of the Curie point of nickel to which (25) shall now be applied. Eucken's and Dannöhl's[10] data of the coefficient of linear expansion of Ni,

$$\beta=(1/l)(\partial l/\partial T)$$

are shown in Fig. 5, together with a curve representing the average data and the tangents to this curve in the Curie point. For a regularly crystallizing element, such as Ni, the coefficient of cubic expansion

$$\alpha=(1/v)(\partial v/\partial T)$$

is three times as great: $\alpha=3\beta$. Because of the extremely small variation of v, the quantity $\partial v/\partial T$ can be obtained by multiplying α by an average volume v_0. The values of $\partial v/\partial T$ obtained in this manner with $v_0=0.114$ cm³/g are given in Fig. 6 for a 100-deg. range, together with the same curve and tangents as in Fig. 5.

The specific heat of Ni has been measured by Ahrens.[11] His data for a 99.4 percent pure Ni are likewise given in Fig. 6. For the tangents is now obtained from Fig. 6:

$$\partial^2 v''/\partial T^2=2.51\times10^{-8}\ \text{cm}^3/\text{g deg.}^2,$$
$$\partial^2 v'/\partial T^2=-4.76\times10^{-8}\ \text{cm}^3/\text{g deg.}^2,$$
$$\partial c_p''/\partial T=0.59\times10^{-3}\ \text{cal./g deg.}^2,$$
$$\partial c_p'/\partial T=-5.46\times10^{-3}\ \text{cal./g deg.}^2,$$

which yields

$$\frac{\partial^2 v''}{\partial T^2}-\frac{\partial^2 v'}{\partial T^2}=7.27\times10^{-8}\ \text{cm}^3/\text{g deg.}^2,$$

$$\frac{\partial c_p''}{\partial T}-\frac{\partial c_p'}{\partial T}=6.05\times10^{-3}\ \text{cal./g deg.}^2$$
$$=258\ \text{cm/deg.}^2.$$

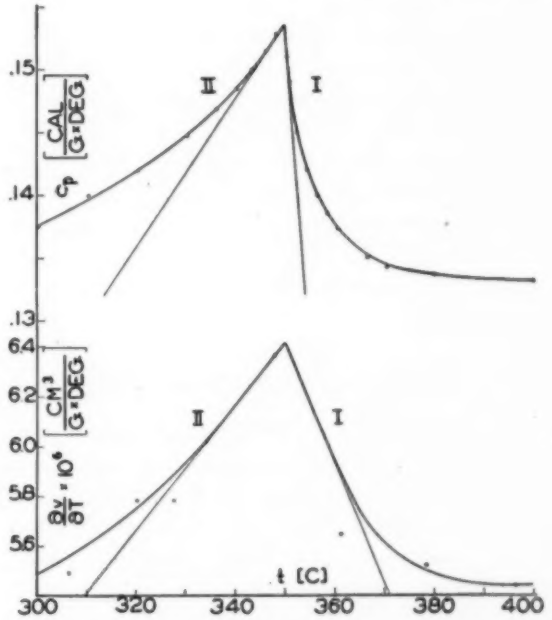

FIG. 6. Specific heat of nickel, according to Ahrens, and thermal expansion of nickel, calculated from the data in Fig. 5.

[11] E. Ahrens, Ann. d. Physik 21, 169 (1934).

The Curie temperature of Ni is $t=350°C$ or $T=623°K$. Substituting these data in (25) gives

$$\frac{dp}{dT}=\frac{1}{3}\cdot\frac{258\times10^8}{623\times7.27}=1.9\times10^6\ \text{g/cm}^2\ \text{deg.}$$
$$=1900\ \text{at./deg.}$$

A pressure of 1900 at. would raise the Curie temperature of Ni by 1 deg. C.

This result is in good agreement with $dp/dT=2000$ at./deg. as obtained by Englert[12] from experiments under two pressures only, but this effect was already of the same order of magnitude as the accuracy of his experiments. It must also be kept in mind that the data of the thermal expansion in Fig. 5 scatter considerably, such that some margin was available in plotting the curve and its tangents. There is, furthermore, extreme disagreement in the experimental data obtained by various authors, ranging from 80 at./deg. to 20,000 at./deg. This discrepancy arises from differences both in the experimental methods and in the interpretation of the data obtained. Others did not observe any effect of pressure on the Curie temperature, not even in experiments[13] which were supposed to show any displacement under 100,000 at./deg. Rutgers' and Wouthuysen's[14] method of calculating equilibria of higher order by substituting a fictitious first-order equilibrium yields, when applied to the Curie point of Ni alloys,[15,16] $dp/dT\approx20{,}000$ at./deg. However, this method is not accurate; for the second-order equilibrium of liquid He in the saturation state, $dp/dT=-136$ is obtained,[14] instead of -83.5. It must be expected that the inaccuracy inherent in this method increases the higher the order of the equilibrium is.

c. Equilibrium of the Fourth Order

The equilibrium of the fourth order is of particular interest as a possible extension of the vapor pressure curve beyond the critical point, though its existence has not yet been observed. If the assumption is made that the vapor pressure curve is not abruptly terminated at the critical point but that an extension of this curve for values p and T greater than the critical values can be defined, then a fundamental requirement of such an extension must be that, at the critical point, the extension and the vapor pressure curve have a common tangent. The tangent of the latter is given by (9I) which yields at the critical point, where condition (11I) is satisfied, the indeterminate form 0/0. The actual value is obtained from de l'Hôpital's rule as

$$\lim_{T\to T_k}\frac{dp}{dT}=\lim_{T\to T_k}\frac{\frac{d}{dT}(s''-s')}{\frac{d}{dT}(v''-v')}=\frac{\frac{c''}{T}-\frac{c'}{T}}{\frac{dv''}{dT}-\frac{dv'}{dT}}$$

in view of (13). If the first lim operation still yields an indeterminate form, this procedure has to be repeated until this is no longer the case. If $n-1$ lim operations are necessary to determine the tangent at the critical point, it is obtained

$$\lim_{T\to T_k}\frac{dp}{dT}=\frac{\frac{d^{n-2}}{dT^{n-2}}\left(\frac{c''}{T}-\frac{c'}{T}\right)}{\frac{d^{n-1}}{dT^{n-1}}(v''-v')}.$$

The evaluation of this equation is given by (16). The sum in the numerator comprises the differences in vapor and liquid phase of the differential quotients of c from the order 0 to the order $n-3$. However, the vanishing of each of these differences is the reason why the preceding lim operations yielded indeterminate forms, and why these operations had to be continued $n-1$ times. Therefore, the entire sum is zero, and the tangent at the critical point is

$$\left[\frac{dp}{dT}\right]_k=\frac{d^{n-2}c''/dT^{n-2}-d^{n-2}c'/dT^{n-2}}{T(d^{n-1}v''/dT^{n-1}-d^{n-1}v'/dT^{n-1})}. \quad (26)$$

It is now seen, that the $(n-1)$st lim of the tangent of the vapor pressure curve is of the same form as the tangent of the equilibrium curve of the nth order, Eq. (9n). This leads to the following conclusion:

If the curve of nth order equilibrium as defined by (9n) extends from the critical point into a region of values p and T greater than the critical values, and if the differential quotients in (9n) can be represented by the same functions

[12] E. Englert, Zeits. f. Physik **97**, 94 (1935).
[13] H. Ebert and A. Kussmann, Physik. Zeits. **39**, 598 (1938).
[14] A. J. Rutgers and S. A. Wouthuysen, Physica **4**, 235, 515 (1937).
[15] A. Michels, *et al.*, Physica **4**, 1007 (1937).
[16] J. C. Slater, Phys. Rev. **58**, 54 (1940).

as the differential quotients in (26), and if these functions are continuous at the critical point, then the curve of nth order equilibrium has at the critical point the same slope as the vapor pressure curve. In this case, the extension of the vapor pressure curve beyond the critical point is represented by a curve of equilibrium of higher order.

A study of d^2p/dT^2 shows that the value of this quantity for the equilibrium curve of higher order is not the same as for the vapor pressure curve at the critical point. Therefore, the curvature has a discontinuity at the critical point, if the liquid-vapor equilibrium is extended beyond the critical point by an equilibrium of higher order.

The thermodynamic properties in the region above the critical point are well known for many vapors. Nowhere has a discontinuity of the second or third derivatives of G been observed. An equilibrium of the second- or third-order can, therefore not be the extension of the vapor pressure curve. The lowest order equilibrium representing such an extension would then be an equilibrium of the fourth order. The equilibrium curve is obtained from (9n) for $n=4$ as

$$\frac{dp}{dT}=\frac{d^2c''/dT^2-d^2c'/dT^2}{T(d^2v''/dT^3-d^2v'/dT^3)}. \tag{27}$$

Substituting (12III) and (14III) with consideration of (1III) and (1IV), and collecting equal derivatives of G, yields

$$\left(\frac{\partial^2 c_p''}{\partial T^2}-\frac{\partial^2 c_p'}{\partial T^2}\right)-4T\left(\frac{\partial^3 v''}{\partial T^3}-\frac{\partial^3 v'}{\partial T^3}\right)\frac{dp}{dT}+6\left(\frac{\partial^2 c_p''}{\partial p^2}-\frac{\partial^2 c_p'}{\partial p^2}\right)\left(\frac{dp}{dT}\right)^2+4T\left(\frac{\partial^3 s''}{\partial p^3}-\frac{\partial^3 s'}{\partial p^3}\right)\left(\frac{dp}{dT}\right)^3-T\left(\frac{\partial^3 v''}{\partial p^3}-\frac{\partial^3 v'}{\partial p^3}\right)\left(\frac{dp}{dT}\right)^4=0. \tag{27I}$$

Any curve which makes (27I) an identity is an equilibrium curve of the fourth order and as such an extension of the vapor pressure curve. As shown by (6IV), the fourth derivatives of G which would have to be different for the two phases in equilibrium correspond to the third derivatives of the directly observed properties h and v. There is little chance that the third derivatives will ever be known with sufficient accuracy to discover whether there are states where two or more of them have discontinuities in exactly such a manner as would satisfy (27I). For this reason, the question whether the equilibrium of the fourth order is an extension of the vapor pressure curve will remain undecided.

There is, however, still another possibility of making (27I) an identity, not along its entire length, but at least in the immediate neighborhood of the critical point. The curves of those states or sets of states which accomplish this will still be extensions of the vapor pressure curve though they may no longer represent an equilibrium of the fourth order.

An experimental investigation of the thermodynamic properties in the region above the critical point shows the following characteristics very distinctly:

(1) the v (p) isothermals have a point of inflexion;
(2) the s (p) isothermals have a point of inflexion;
(3) the v (T) isobares have a point of inflexion;
(4) the h (T) isobares have a point of inflexion.

All these characteristics are also obtained from the van der Waals equation of state. Euken[17] has defined the extension of the vapor pressure curve as the curves by which any or all of the conditions 1 to 4 are satisfied. This can only be so if conditions 1 to 4 make Eq. (27I) an identity, at least near the critical point. This will now be examined.

The four conditions can be expressed as follows:

$$(\partial^2 v/\partial p^2)_T=0, \tag{28I}$$

$$(\partial^2 s/\partial p^2)_T=0; \tag{28II}$$

$$(\partial^2 v/\partial T^2)_p=0, \tag{29I}$$

$$(\partial^2 h/\partial T^2)_p=0. \tag{29II}$$

On account of (7) and (12), Eq. (29) can be written

$$(\partial c_p/\partial p)_T=0, \tag{28III}$$

$$(\partial c_p/\partial T)_p=0. \tag{28IV}$$

Applying (7) to (28II), the four conditions (28) can be interpreted as the minima of $\partial v/\partial p$ and the maxima of c_p. The latter ones are a particularly prominent characteristic for the region

[17] A. Eucken, Physik. Zeits. **35**, 711 (1934).

under discussion.[18] The loci of these extrema, i.e., the curves on which conditions (28) are satisfied can be regarded as transition curves between two different modifications of higher order and are obtained in the same way as (5I) was derived from (1I). On each of these four curves, one of the conditions (28) must hold at an arbitrary point (p, T) as well as at the infinitely close point $(p+dp, T+dT)$. A Taylor expansion discontinued after the second term yields the four equations

$$d(\partial^2 v/\partial p^2)=0, \tag{30I}$$

$$d(\partial^2 s/\partial p^2)=0, \tag{30II}$$

$$d(\partial c_p/\partial p)=0, \tag{30III}$$

$$d(\partial c_p/\partial T)=0, \tag{30IV}$$

where

$$d(\ \ )=\frac{\partial(\ \ )}{\partial T}dT+\frac{\partial(\ \ )}{\partial p}dp.$$

When the differentiations in (30) are carried out it is, with the aid of (7),

$$\frac{\partial^3 v}{\partial p^3}\frac{dp}{dT}=\frac{\partial^3 s}{\partial p^3}, \tag{31I}$$

$$\frac{\partial^3 s}{\partial p^3}\frac{dp}{dT}=-\frac{1}{T}\frac{\partial^2 c_p}{\partial p^2}, \tag{31II}$$

$$\frac{\partial^2 c_p}{\partial p^2}\frac{dp}{dT}=T\frac{\partial^3 v}{\partial T^3}+\frac{\partial^2 v}{\partial T^2}, \tag{31III}$$

$$\left(T\frac{\partial^3 v}{\partial T^3}+\frac{\partial^2 v}{\partial T^2}\right)\frac{dp}{dT}=\frac{\partial^2 c_p}{\partial T^2}. \tag{31IV}$$

Equations (31) represent the curves on which conditions 1 to 4 are satisfied. Obviously, none of them alone could reduce (27I) to an identity, but all four equations combined could do this. Before substituting them in (27I), it must be examined whether the dp/dT is the same quantity in all four equations, i.e., whether the four curves represented by these equations coincide in the p, T plane. For this purpose, the Eqs. (28) may be expressed by Planck's *Characteristic Function*

$$\Phi(p, T)=-G/T=s-(h/T).$$

Differentiation yields

$$d\Phi=(h/T^2)dT-(v/T)dp,$$

whence

$$h=T^2(\partial\Phi/\partial T), \quad v=-T(\partial\Phi/\partial p).$$

From the Eqs. (28) we now obtain, with the aid of (7),

$$\frac{\partial^3\Phi}{\partial p^3}=0, \tag{32I}$$

$$\frac{\partial^2\Phi}{\partial p^2}+T\frac{\partial^3\Phi}{\partial T\partial p^2}=0, \tag{32II}$$

$$2\frac{\partial^2\Phi}{\partial T\partial p}+T\frac{\partial^3\Phi}{\partial T^2\partial p}=0, \tag{32III}$$

$$2\frac{\partial\Phi}{\partial T}+4T\frac{\partial^2\Phi}{\partial T^2}+T^2\frac{\partial^3\Phi}{\partial T^3}=0. \tag{32IV}$$

It is apparent, that none of Eqs. (32) can be derived from any of the others. Therefore, all four conditions (28) are independent, and the points where they hold will not coincide but will be located on four different curves. They all originate in the critical point where all four conditions (28) are satisfied. Since this point is simultaneously a point of the equilibrium curve of the fourth order, the derivatives in (31)will have discontinuities there. If in the immediate neighborhood of the critical point these four curves approach each other, then the (dp/dT)'s in all four Eqs. (31) will be approximately equal. In this region, these four curves will also be infinitely close to the actual fourth-order equilibrium curve (27I) with its discontinuities of the five derivatives. Then, in this particular region, Eqs. (31) may be substituted for both phases in (27I). Substitution of (31I) in (27I) gives

$$\left(\frac{\partial^2 c_p''}{\partial T^2}-\frac{\partial^2 c_p'}{\partial T^2}\right)-4T\left(\frac{\partial^3 v''}{\partial T^3}-\frac{\partial^3 v'}{\partial T^3}\right)\frac{dp}{dT}+6\left(\frac{\partial^2 c_p''}{\partial p^2}-\frac{\partial^2 c_p'}{\partial p^2}\right)\left(\frac{dp}{dT}\right)^2+3T\left(\frac{\partial^3 s''}{\partial p^3}-\frac{\partial^3 s'}{\partial p^3}\right)\left(\frac{dp}{dT}\right)^3=0. \tag{27II}$$

Substitution of (31II) in (27II) gives

$$\left(\frac{\partial^2 c_p''}{\partial T^2}-\frac{\partial^2 c_p'}{\partial T^2}\right)-4T\left(\frac{\partial^3 v''}{\partial T^3}-\frac{\partial^3 v'}{\partial T^3}\right)\frac{dp}{dT}+3\left(\frac{\partial^2 c_p''}{\partial p^2}-\frac{\partial^2 c_p'}{\partial p^2}\right)\left(\frac{dp}{dT}\right)^2=0. \tag{27III}$$

[18] J. H. Keenan and F. G. Keyes, *Thermodynamic Properties of Steam*, Fig. 7.

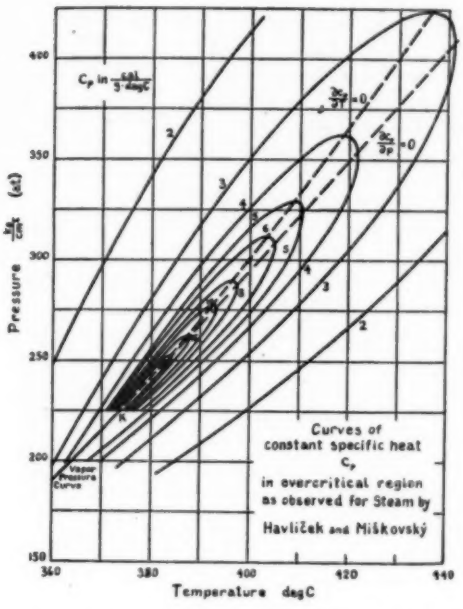

FIG. 7. Curves of constant specific heat of high pressure steam, according to Havliček and Miškovský.

Substitution of (31III) in (27III) gives, in view of (1IV)

$$\left(\frac{\partial^2 c_p''}{\partial T^2}-\frac{\partial^2 c_p'}{\partial T^2}\right)-T\left(\frac{\partial^3 v''}{\partial T^3}-\frac{\partial^3 v'}{\partial T^3}\right)\frac{dp}{dT}=0. \quad (27IV)$$

Substitution of (31IV) in (27IV) gives, in view of (1IV)

$$0=0.$$

Equations (31) reduce (27I) to an identity and, for this reason, the four curves where conditions (28) hold are apparent extensions of the vapor pressure curve.

This is shown in Fig. 7 for the conditions (28III) and (28IV). The specific heat of steam in the overcritical region has been measured with great accuracy by Havliček and Miškovský.[19] Figure 7 is redrawn from these authors' Fig. 17 and shows the curves $c_p=$const. in a p, T diagram. It is seen from the relation

$$\left(\frac{\partial p}{\partial T}\right)_{c_p}=-\frac{(\partial c_p/\partial T)_p}{(\partial c_p/\partial p)_T}$$

that (28III) corresponds to those points where the c_p curves have vertical tangents, while (28IV) corresponds to the points with horizontal tangents. The two curves $\partial c_p/\partial p=0$ and $\partial c_p/\partial T=0$ approach each other in the neighborhood of the critical point K, and both curves are extensions of the vapor pressure curve. There are not sufficient data available to show the same phenomenon for conditions (28I) and (28II).

[19] J. Havliček and L. Miškovský, Helv. phys. acta 9, 161 (1936).

Letters to the Editor

PROMPT publication of brief reports of important discoveries in physics may be secured by addressing them to this department. The closing date for this department is the third of the month. Because of the late closing date for the section no proof can be shown to authors. The Board of Editors does not hold itself responsible for the opinions expressed by the correspondents. Communications should not in general exceed 600 words in length.

A New Type of Electrostatic Generator

P. H. MILLER, JR.
Randal Morgan Laboratory of Physics, University of Pennsylvania, Philadelphia, Pennsylvania
May 6, 1946

AN attractive method of accelerating very high energy particles is the arrangement in cascade, as shown in Fig. 1, of several electrostatic generators whose charging current is provided by the decay of alpha particle emitting radioactive elements. Perhaps the most suitable element is $_{83}Po^{210}$ which emits alpha particles of 5.3-Mev energy while decaying to stable $_{82}Pb^{206}$. When the polonium is surrounded by an isolated metal shield, the emitted alpha particles will continue to reach the shield until it is charged to a potential equal to one-half the maximum kinetic energy of the alpha particles expressed in electron volts.

For a current of 25 μa and 2 Mev per stage, two conditions must be satisfied. If one-half of the emitted alpha particles is collected by the shield about 1 g of Po is required per stage. The second requirement restricts the loss of energy of the alpha particles in the polonium source to about 1 Mev so that the thickness of the active material on the inner sphere should not exceed about 4×10^{-5} cm.

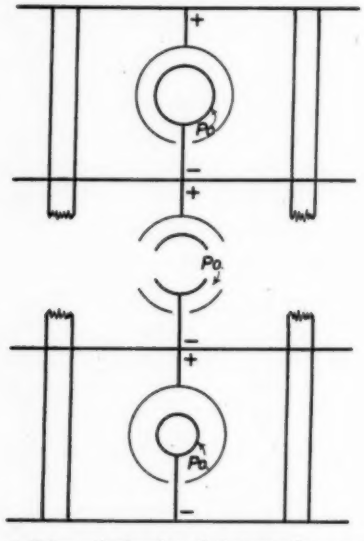

FIG. 1. Schematic drawing of electrostatic generator with several stages in cascade.

Thus the radius of the inner sphere must be bigger than 15 cm.

The cost of commercially available polonium prohibits the construction of such a device. However, it appears possible that polonium can be produced from bismuth in reasonable quantities by the following reaction:[1]

$$_{83}Bi^{209}+n^1\rightarrow{}_{83}Bi^{210}+\gamma$$
$$\sigma=0.023\times10^{-24}\ \text{cm}^{-2}\ \text{(thermal neutrons)}$$
$$_{83}Bi^{210}-(4.975d)\rightarrow{}_{84}Po^{210}+{}_{-1}e^{0}+1.17\ \text{Mev}.$$

It has been estimated[2] that if bismuth is used instead of water to cool a 10^6 kw chain reacting pile, 0.1 g a day can be produced. If a resonance for neutron capture exists, the rate of production will be enhanced.

The number of stages which can be placed in cascade depends on the supply of polonium available and design of the external insulating column.

[1] F. G. Houtermans and I. Bartz, Naturwiss. **30**, 758 (1942).
[2] W. E. Stephens *et al.*, *Nuclear Fission and Atomic Energy*, Section 14.11 (to be published).

Absorption of Slow Neutrons by Cd^{113}

B. J. MOYER, B. PETERS, AND F. H. SCHMIDT
Radiation Laboratory, Department of Physics, University of California, Berkeley, California
April 24, 1946

THE isotopes of cadmium were separated by a mass spectrograph and the absorption of thermal neutrons in Cd samples of different isotopic composition was studied.

Neutrons from a radium-beryllium source surrounded by paraffin were used in the measurements. Inside the paraffin was a glass bulb filled with $CdSO_4$ solutions. Indium foil detectors with and without cadmium shields were held in the center of the bulb.

The solution prepared from a sample of cadmium enriched in isotope 113 gave a cross section for absorption six times larger than a solution of equal concentration containing cadmium of normal isotopic composition. A mass spectrographic analysis of the sample enriched in Cd^{113} is in the process of being carried out.

The absorption in solutions containing cadmium enriched in Cd^{106}, Cd^{108}, Cd^{110}, Cd^{111}, Cd^{112}, Cd^{114} proved to be very small compared to the absorption in normal cadmium. The capture cross section for thermal neutrons in Cd^{116} is known to be small (1.4 barns).[1]

We conclude that the large absorption cross section of cadmium[2] for thermal neutrons is caused by resonance capture in Cd^{113} (whose natural abundance is 12.3 percent) and that none of the other cadmium isotopes make any appreciable contribution.

The above work was carried out under the auspices of the Manhattan District. We are indebted to Professor E. Segrè for valuable advice.

[1] 1.4×10^{-24} cm^2.
[2] H. A. Bethe, Rev. Mod. Phys. **9**, 151 (1937).

A Thermodynamic Criterion for the Fracture of Metals

EDWARD SAIBEL
Carnegie Institute of Technology, Pittsburgh, Pennsylvania
May 20, 1946

THE theoretical evaluation of the tensile stress necessary to bring about the rupture of a metal in a purely brittle manner has been calculated on the basis of interatomic forces[1,2] and on the basis of the energy required to form new surfaces.[3] All of these calculations have led to the values of tensile strength of metals both single crystal and polycrystalline, which are a hundred to a thousand times higher than the observed values. On this account, it has been thought necessary by some investigators, to postulate the existence of a micro-crack structure or distribution of flaws throughout the specimen such that the resulting stress concentrations provide the factor necessary to bring about agreement between calculation and experiment.

TABLE I. (Multiply stresses by 10^6 for lb./sq. in.).

Metal	Fracture stress from (1) and (2)	Theoretical value, Seitz[a]
Fe	2.5	1.7
Cu	1.65	1.26
Al	1.40	0.53
Zn	0.70	0.82
Pb	0.32	0.37
Sn	0.69	0.51

[a] Seitz, *Physics of Metals* (McGraw-Hill Book Company, Inc., New York, 1943).

Another attempt to resolve this seeming discrepancy was made by Fürth[4] who advanced a thermodynamic theory of the tensile strength of metals based on the work of Born relating to the melting of crystals. Fürth compares fracture stresses computed from his equation with the fracture stresses of metals as given in the *Landolt-Börnstein Tables* (1927) and in the *Handbuch der Physik* (1928), extrapolated to absolute zero. The principal objections to Fürth's theory are that his treatment cannot account for variations in fracture strength with alloying elements, heat treatment, cold work, etc.; and that extrapolation of fracture stresses to absolute zero is meaningless.

A theory of fracture proposed by the author, also related to the melting phenomenon, is based on the following assumptions:

1. All of the strain energy is available for the abolition of cohesive strength.
2. The heat of fusion is uniformly partitioned throughout the volume occupied by the substance.
3. The quantity of energy required for the abolition of cohesive strength is that fractional part of the energy of fusion which is associated with the change in volume on passing from the solid to the liquid state.

On the basis of these assumptions, the criterion for fracture may be expressed in the form

$$U = JQ\Delta V/V, \tag{1}$$

where U is the strain energy per unit volume, Q is the latent heat of melting in kg-cal. per mole, V is the volume occupied by a mole of the substance, ΔV is the change in volume of a mole of the substance on passing from the solid to the liquid state, and J is the mechanical equivalent of heat.

The general expression for U is

$$U = \int(\sigma_1 d\delta_1 + \sigma_2 d\delta_2 + \sigma_3 d\delta_3), \tag{2}$$

where σ_1, σ_2, σ_3, and δ_1, δ_2, δ_3, are the principal stresses and strains, respectively. In the case of a purely elastic one-dimensional state of stress, Eq. (2) reduces to

$$U = \sigma^2/2E, \tag{3}$$

where E is the modulus of elasticity.

With data for ΔV from Masing,[5] and that for Q and E from any of the standard tables, the fracture strength of metals in simple tension for the purely brittle case may be calculated. Several examples are shown in Table I. In the case where plastic flow has preceded fracture and little error is involved in neglecting the elastic part of the strain energy, Eq. (2) may be conveniently expressed in the form

$$U = \int \bar{\sigma} d\bar{\delta}, \tag{4}$$

where

$$\bar{\sigma} = \{[(\sigma_1-\sigma_2)^2+(\sigma_2-\sigma_3)^2+(\sigma_3-\sigma_1)^2]/2\}^{\frac{1}{2}},$$

and

$$\bar{\delta} = [(\delta_1^2+\delta_2^2+\delta_3^2)\tfrac{2}{3}]^{\frac{1}{2}}.$$

Under the assumptions that the hydrostatic component of the stress system has no effect on the flow curve and that in the plastic region no changes in volume occur, $\bar{\sigma}$ and $\bar{\delta}$ are invariants. Since in simple tension $\bar{\sigma} = \sigma_1$ and $\bar{\delta} = \delta_1$, the general relationship between $\bar{\sigma}$ and $\bar{\delta}$ may be established from a single tension test. This relationship may be approximated by $\bar{\sigma} = \kappa\bar{\delta}^n$ and U may be evaluated from Eq. (4). This has been done, and in Table II typical comparisons for several metals tested in tension are given.

TABLE II.

Metal	Fracture stress calculated	Observed
SAE 1112 at 70°F	132,000 p.s.i.	121,500 p.s.i.
SAE 1112 at −119°F	139,000	135,000
SAE 2345 Room temp.	406,000	396,500
Pure copper Room temp.	73,000	70,000
Al 24 S-O Room temp.	49,600	48,000
Al 24 S-T Room temp.	101,000	99,600

It is thus seen that the proposed criterion for fracture leads to the theoretical calculations in the case of purely brittle fracture and gives good results in the case where plastic flow precedes fracture. It is doubtful whether purely brittle fractures have been observed in the laboratory even at very low temperatures of testing or at very high rates of strain. Under such conditions plastic flow is probably confined to small regions but sufficient plastic flow in these regions may occur to bring the fracture stresses down to the observed values.

[1] Zwicky, Physik. Zeits., **24**, 1923, 131.
[2] Born and Fürth, Proc. Camb. Phil. Soc. **36**, 1940, 454.
[3] Polyani, Zeits. f. Physik **7**, 1921, 323.
[4] Fürth, Proc. Roy Soc. London **177A**, 1940–41, 217–227.
[5] Masing, *Handbuch der Metallphysik* (Leipzig, 1935), Vol. I, p. 231.

Redundant Zeros in the Discrete Energy Spectra in Heisenberg's Theory of Characteristic Matrix

S. T. MA
Institute for Advanced Study, Princeton, New Jersey
May 29, 1946

AN important recent development in Heisenberg's theory of characteristic matrix is the determination of discrete energy values of closed stationary states.[1] This is made possible by the process of analytic continuation from real values of the momentum variables to imaginary values in the complex plane. Those imaginary values for which the amplitude of the outward scattered wave vanishes correspond to the closed stationary states and the corresponding negative energy values can be identified with the energy values of these states. It has been pointed out by Pauli that this procedure gives correct results for the scattering by a potential hole and the scattering by an attractive Coulomb field. Using this method, the writer has studied the case of an attractive exponential field, which presents a certain new feature.

We consider the spherically symmetrical state in the field

$$V(r)=-V_0e^{-r/a},$$

where V_0 and a are positive constants. Let $u(r)/r$ be the wave function and E the energy of the scattered particle, which is positive. If we write

$$V_0=\frac{\hbar^2}{2m}U_0,\ E=\frac{\hbar^2k^2}{2m},$$

the wave equation takes the form

$$(d^2u/dr^2)+(k^2+U_0e^{-r/a})u=0.$$

The solutions of this equation are

$$u=J\pm 2aki(2a(U_0x)^{\frac{1}{2}})$$

where the J's are Bessel functions and $x=e^{-r/a}$. The condition that the function u should vanish at the origin requires it to be of the form

$$u=c[J-2aki(2a(U_0)^{\frac{1}{2}})J_{2aki}(2a(U_0x)^{\frac{1}{2}}) -J_{2aki}(2a(U_0)^{\frac{1}{2}}J-2aki(2a(U_0x)^{\frac{1}{2}})],$$

where c is a constant. The asymptotic expression for large values of r is

$$u=c[J_{-2aki}(2a(U_0)^{\frac{1}{2}})(a(U_0)^{\frac{1}{2}})^{2aki}e^{-ik\gamma}/\Gamma(2aki+1) -J_{2aki}(2a(U_0)^{\frac{1}{2}})(a(U_0)^{\frac{1}{2}})^{-2aki}e^{ik\gamma}/\Gamma(-2aki+1)].$$

From this asymptotic expression it can be seen that, as usual, there is no closed state when k is real. When k becomes imaginary, however, the above general consideration leads to the following conditions for closed states:

$$J2aki(2a\sqrt{U_0})=0, \quad \text{(i)}$$
$$1/\Gamma(-2aki+1)=0. \quad \text{(ii)}$$

The first condition gives the discrete spectrum obtained by Bethe.[2] The second condition gives

$$-2aki+1=-n \qquad (n=0,\ 1,\ 2,\cdots)$$

or

$$E=-\hbar^2(n+1)^2/8ma^2.$$

These eigenvalues do not correspond to any actual closed states. They may therefore be regarded as redundant zeros.

This special problem is of some interest in connection with the general formulation of the method for determining closed stationary states, as in Heisenberg's new theory there is no longer a wave equation to determine the wave function completely and consequently some other criterion is necessary for discarding such redundant zeros as are given by condition (ii).

[1] Møller, Kgl. Danske Vid. Sels., Math.-Fys. Medd. **23**, No. 1 (1945).
[2] Bethe and Bacher, Rev. Mod. Phys. **8**, 111 (1936).

Physical Interaction of Electrons with Liquid Dielectric Media. The Properties of Metal-Ammonia Solutions

RICHARD A. OGG, JR.
Department of Chemistry, Stanford University, California
May 27, 1946

THE author wishes to outline briefly the primitive theoretical considerations which preceded recent experimental discoveries relating to the properties of metal-ammonia solutions.[1] The basis of the treatment is the model, first proposed by Kraus,[2] of an electrolyte-like character for the solute metal in ammonia solutions, the negative ion constituent being the "solvated" electron. At extremely low concentrations, inter-ionic forces may be neglected. It is proposed that under these conditions individual electrons are "self-trapped" in physical cavities created in the solvent medium. If surface tension effects are neglected, the potential energy is due only to electrical polarization of the medium surrounding the cavity. The dielectric constant D of ammonia is sufficiently large ($\sim$22) so that without serious error the term $1/D$ may be neglected in comparison with unity in the well-known Born expression for the polarization energy. Hence as a first approximation, for a charge Ze symmetrically distributed in a spherical cavity of radius r_0, the potential energy

$$V=-Z^2e^2/2r_0,\ r<r_0;\ V=0,\ r>r_0.$$

The attractive force, tending to shrink the cavity, is opposed by an especially simple quantum-effect repulsion. In essence, the magnitude of the de Broglie wave-length must correspond to the cavity diameter, leading to a zero-point kinetic energy. As a first approximation, the wave function is considered to have a node at the cavity boundary. The problem then reduces to that of a particle in a spherical box.[3] Solution of the Schrödinger equation yields for the lowest s state the kinetic energy $T=\hbar^2/8mr_0^2$. Hence the total energy $W=T+V=(\hbar^2/8mr_0^2)-(e^2/2r_0)$. Setting dW/dr_0 equal to zero, the equilibrium values of W and r_0 are found to be, respectively, $-(me^4/2\hbar^2)$ (i.e., some -0.38 electron volt) and $\hbar^2/2me^2$ (i.e., some 9.9×10^{-8} cm). The corresponding experimental values[1] are approximately -0.8 volt and 7×10^{-8} cm. Consideration of the finite "depth" of the potential well, with resultant penetration of the wave function outside the cavity (requiring a self-consistent field method) should improve the agreement

with experiment. A more accurate treatment should also include the effect of something resembling surface tension of the (probably diffuse) cavity wall.

Extending the simplified particle-in-a-spherical-box treatment to a system of *two* 1*s* electrons trapped in a cavity, application of first-order perturbation theory yields

$$W=\frac{h^2}{4mr_0^2}-\frac{2e^2}{r_0}+\int\frac{e^2}{r_{12}}\psi_0^2 dT.$$

The third term (involving the unperturbed wave functions and the separation r_{12} of the electrons) corresponds to electrostatic repulsion between the electrons, and is evaluated by adaptation of the analogous treatment for the normal helium atom.[4] By numerical methods, its value approximates to $+e^2/r_0$. The corresponding approximate values of r_0 and W would be $h^2/2me^2$ and $-me^4/h^2$. From physical analogy with the helium atom like problem, it appears that higher approximations would yield a value of W numerically *greater* than me^4/h^2. (For example, first order perturbation treatment gives for hydride ion[4] $W=-0.75\ W_H$, while variation methods yield $W=-1.05\ W_H$.) The above theoretical trapping energy for a single electron is $-me^4/2h^2$. That is, the trapped pair should be stable with respect to dissociation into two electrons trapped in separate cavities. This at first sight paradoxical result arises from the greatly increased polarization energy of the pair (*vide* the factor Z^2 in the Born formula) which more than compensates for electrostatic repulsion. It appears highly probable that this energetic stability of the pair would be retained by a more accurate treatment (i.e., one considering the penetration of the wave functions outside the cavity). The Pauli exclusion principle requires the trapped pair to be in a singlet state—i.e., to be diamagnetic.

The hitherto neglected inter-ionic forces become increasingly important with greater solute concentration. In the limit, the electrostatic attractive potential on a cluster of Z electrons at average distance ρ from singly charged positive ions approaches $-AZ(e^2/\rho)$. The Madelung constant A for random configuration should have a value of the order of magnitude of 1.5, and hence this potential can become (for $Z=1$) much larger than the polarization potential $-Z^2e^2/2r_0$. One result is a greatly decreased value of the radius of the electron cavity—the molar volume in concentrated solutions of sodium is about 40 cm³, as compared with some 700 cm³ for highly dilute solutions. Further, the linear dependence on Z gives no appreciable energetic advantage to the pairing of electrons, and their mutual repulsion would render the pairs unstable. This unpairing of electrons in concentrated solutions is indicated by the reappearance of appreciable paramagnetic susceptibility, as contrasted with diamagnetism of the solute at intermediate concentrations.

Extension of the "particle in a box" treatment indicates that the kinetic energy of a trapped electron excited to a p state exceeds the potential energy of the s ground state. By the Franck-Condon principle a continuous absorption spectrum should result, leading to photo-ejection of the electron from the cavity. The infra-red absorption maximum of very dilute metal-ammonia solutions corresponds to transition to the first p state. Current experimental studies reveal a far ultraviolet absorption maximum, corresponding to transition to the second p state. The theory of the continuous absorption spectrum of the trapped pair is developed in like fashion.

The theory as outlined applies in essential detail to any solvent of *high dielectric constant* which is chemically indifferent to free electrons. The known examples would appear to be ammonia, organic amines, and possibly fused alkali metal amides.

[1] Richard A. Ogg, Jr., J. Am. Chem. Soc. **68**, 155 (1946). J. Chem. Phys. **14**, 114, 295 (1946). Phys. Rev. **69**, 243 (1946). Original literature references to earlier experimental work are given in these communications.
[2] C. A. Kraus, *The Properties of Electrically Conducting Systems* (Chemical Catalogue Company, 1922).
[3] For fuller mathematical details, see G. Gamow, *Atomic Nuclei and Radioactivity* (Oxford University Press, New York, 1931), pp. 42–49.
[4] L. Pauling and E. B. Wilson, Jr., *Introduction to Quantum Mechanics* (McGraw-Hill Book Company, Inc., New York, 1935), Appendix V.

Frequency Modulated Cyclotron

J. Reginald Richardson, K. R. MacKenzie, E. J. Lofgren, and Byron T. Wright
Radiation Laboratory, University of California, Berkeley, California
June 3, 1946

THE application of the synchrotron phase stability principle[1,2] to the frequency modulated cyclotron has been investigated experimentally on the 37-inch Berkeley cyclotron. A radial decrease in magnetic field has been used such that it requires a frequency change simulating the change which would be required by the relativistic increase of mass with velocity as the ions are accelerated to high speeds.

The frequency of revolution of an ion of kinetic energy W (units Mc^2) in a magnetic field H is

$$f=\frac{f_e}{1+W}\frac{H}{H_e}$$

where f_e is the frequency the ion would have with very low energy in the field H_e. Thus the change in frequency produced by an increase in W to a large value can be simulated by the proper radial decrease in magnetic field even though ions of a comparatively low energy are used. The purpose of the experiments described here was to simulate the acceleration of deuterons to 200 Mev in the giant 184-inch cyclotron. Here $W=0.107$ so that a total frequency change of 13 percent would leave 2.3 percent for radial decrease of magnetic field in the 184-inch case.

We have succeeded in accelerating a time average deuteron current of 0.2 microampere through a radial fall in magnetic field of 13 percent. This was accomplished by a radio frequency peak potential of 3 kv on the dee which accelerated the deuterons to 7 Mev. Without frequency modulation the maximum energy obtainable is 0.5 Mev with this voltage on the dee (in accord with theory). So far our maximum modulation frequency has been 600 cycles per second which corresponds to an acceleration

time of 500 μs or about 5000 turns. The threshold appears at 5 milliseconds or 5×10^4 turns.

In our experimental arrangement we use a single dee whose diametral edge is perpendicular to the axis of the

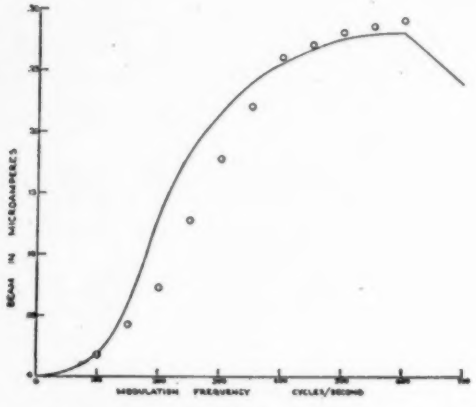

FIG. 1. The beam current collected on a probe at a radius of 17 inches where the field is 11.5 percent smaller than H_c, the field at the center. This current is plotted as a function of the modulator frequency.

resonant line, with the mechanical rotating condenser[3] on the other end of the line. The line resonates with a voltage node near the center moving back and forth as the resonant frequency is changed by the rotating capacitor. A 20 percent change in frequency is produced in this way. The condensor rotor consists of 36 teeth on a circle two feet in diameter. Thus a rotation of 1000 r.p.m. corresponds to 600 cycles per second for the modulating frequency. The grounded grid r-f oscillator required 600 watts of plate power.

Under the usual operating conditions (2800 volts on the dee) the dee and resonant line system float at a potential of about +1500 volts d.c. The output under these conditions is a factor of ten greater than when the dee system is grounded. We believe that this unusual situation is concerned with the ion starting conditions under these low single dee voltages and is not concerned with the frequency modulation characteristics of the instrument.

Figure 1 shows the probe current as a function of the angular velocity of the mechanical condenser expressed in cycles per second of the modulating frequency. Readings on a "protection meter" ionization chamber placed six feet outside the cyclotron indicated strict proportionality between the radiation from the cyclotron and the probe current. The smooth curve shows the theoretical prediction[4] of the yield as a function of modulator frequency. With no modulation and the probe at 2.5-inch radius, 22μa of current was picked up, indicating an efficiency of 1 percent for the f-m system. This is in close agreement with theory, if one takes into account the fact that only about one-sixth of the modulation cycle is used in this experiment.

The results of an investigation of the beam *vs.* radius are shown in Fig. 2. The probe current indicates a very slow fall off with radius, while the onset and rapid increase of ionization chamber reading with radius is consistent with the deuterons being accelerated to about 7 Mev as predicted from the values of magnetic field and radius. The order of magnitude of this energy was verified by excitation of the 12.8-hour radioactivity in copper.

The increase in beam with increasing r.f. voltage on the dee is very marked—a factor of ten in going from 2 to 3 kv. This must be due to an increase in source efficiency since it can easily be shown that the increase in f-m efficiency will only go as the square root of the dee voltage if the shape of the modulation cycle is unchanged. An evacuated rotating condenser is being constructed so that we can raise the voltage to 10 kv on the dee and increase the rate of rotation.

In view of the success of these experiments it has been decided to complete the 184-inch instrument as an f-m cyclotron. From Fig. 2 we can say that appreciable values

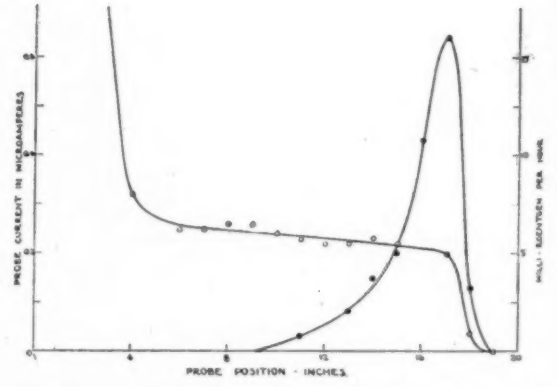

FIG. 2. Beam current as a function of radius. The modulator frequency was 590 cycles per second, the peak r-f dee voltage was 2800 volts, and the dee bias +1500 volts.

for the time average current of 200-Mev deuterons would be expected from the giant cyclotron even with 3 kv on the dee. At ordinary dee voltages of 50 kv, say, the output would be larger both because of the increase in efficiency and the increase in source efficiency. A reasonably conservative expectation would appear to be a time average current of one microampere of 200-Mev deuterons with 50 kv on the dee.

It is clear, also, that the f-m system will have advantages for smaller cyclotrons where it is desired to obtain high energy protons with reasonable dee voltages. Bringing the beam out of the f-m cyclotron is an important problem, but there are several solutions which look feasible and which we intend to try.

We wish to express our thanks to Drs. E. M. McMillan and R. L. Thornton for many helpful suggestions and criticisms and our gratitude to Professor Ernest Lawrence whose inspiration and encouragement made this development possible. This work was done under the auspices of the Manhattan District.

[1] E. M. McMillan, Phys. Rev. **68**, 143 (1945).
[2] V. Veksler, J. Phys. (U.S.S.R.) **9**, 153 (1945).
[3] Fred H. Schmidt (to be published).
[4] Bohm and Foldy (to be published).

Wave Guide Acceleration of Particles

EMMETT L. HUDSPETH
Bartol Research Foundation of the Franklin Institute, Swarthmore, Pennsylvania
May 13, 1946

LINEAR accelerators have been successfully operated to obtain energetic particles, and Hg ions have been accelerated to energies of 1.26 Mev.[1] A major disadvantage in this type of accelerator is the fact that successive electrodes become increasingly longer. This difficulty may be overcome to some extent by using a very high frequency in the accelerator, but a limit is reached when the impressed wave-length becomes comparable to the dimensions of the circuit elements.

The disadvantages mentioned may be overcome by constructing an accelerator from wave guide. The guide could be bent into any suitable geometrical shape, but a relatively simple spiral configuration is shown in Fig. 1. The important point is that the *transverse* field in the guide may be used for the acceleration of particles, and, by proper shaping of the guide, the total ion path may be made quite small. The evacuated system would include the guide and a column of moderate diameter built between the successive spirals of the guide. This type of acceleration should be applicable to either positive ions or to electrons. The problem is relatively simple with electrons, since these particles may be accelerated by very high frequency fields of moderate amplitude; lower frequencies or an initial injection velocity must be used with heavier ions.

Figure 2 shows the maximum potential difference at one megawatt input power which exists between the walls of a wave guide as a function of the width of the guide. This potential difference is inversely proportional to the square-root of the wave-length; values for three different wave-lengths in copper guide at room temperature are shown in Fig. 2. The potential difference becomes arbitrarily large as the width of the guide is diminished to the cut-off point $a_0(=\lambda/2)$, but attenuation also increases rapidly. The value of the attenuation α (if we assume no loss by reflections along the guide) at the various wave-lengths for guides whose width is 1.10 times the cut-off width is given in Table I.

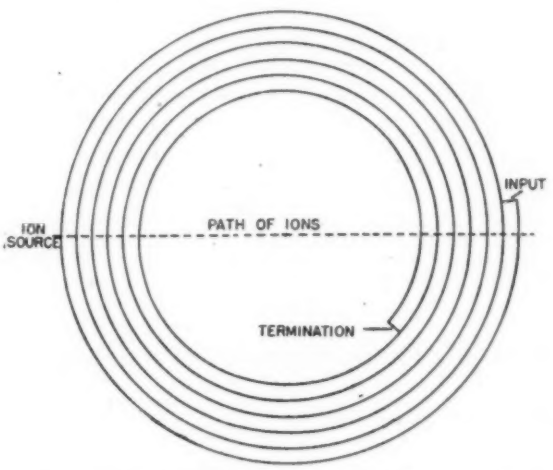

FIG. 1. Schematic diagram of a possible type of wave guide accelerator. If the guide oscillates as a whole, the total length may be as short as will sustain the full input load.

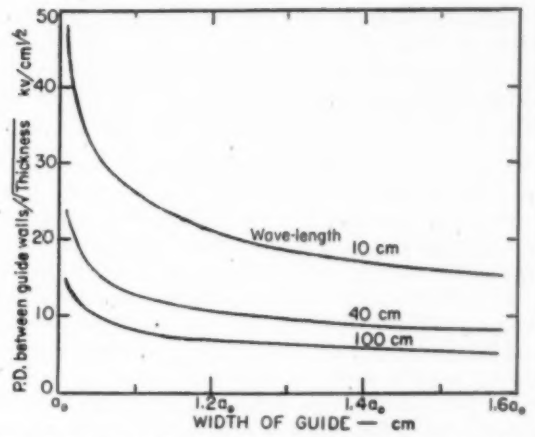

FIG. 2. Potential difference between walls of guide as a function of guide width. The curves were calculated without regard to reflections in the guide. TE_{01} mode; a_0 = critical width of guide; Power = 10^8 watts.

A guide of several meters length could be terminated with a reflector (short circuit), and the whole configuration made to oscillate as a cavity. In such a case, potential differences of perhaps several hundred thousand volts could be realized between the two walls of the guide. Results with single cavity oscillators have already been reported.[2]

TABLE I. Attenuation in wave guide.

λ (cm)	Width of guide (cm)	Thickness of guide (cm)	α (db/meter)
10	5.5	1	0.1075
		2	0.0663
40	22	1	0.0425
		4	0.013
100	55	1	0.0241
		10	0.0030

Proper phasing must be obtained by proper spacing of holes in the guide and by correct separation of the successive turns of the guide. Several units could be operated in tandem to obtain highly energetic particles.

[1] D. H. Sloan and E. O. Lawrence, Phys. Rev. **38**, 2021 (1931).
[2] J. Halpern, E. Everhart, R. A. Rapuano, and J. C. Slater, Phys. Rev. **69**, 688 (A) (1946).

Atmospheric Helium Three and Radiocarbon from Cosmic Radiation

W. F. LIBBY
Institute for Nuclear Studies and Department of Chemistry, University of Chicago
June 1, 1946

A. INTRODUCTION

NUCLEAR physical data indicate that cosmic-ray neutrons produce C^{14} and H^3 from atmospheric nitrogen, the radiocarbon being the principal product. The purpose of this letter is to call attention on this basis

to a possible explanation of the tenfold greater abundance of He^3 (as decay product of H^3) in atmospheric helium as compared to gas well helium, and to suggest that radiocarbon might be found in living matter especially in connection with the concentration of C^{13} for tracer uses.

B. HELIUM THREE

It is well established[1-7] that neutron secondaries are produced in the atmosphere by the cosmic radiation. Less well established is the total number Q, of neutrons produced per cm^2 of the earth's surface per sec. The recent paper of Korff and Hammermesh[7] allows a rough estimate of Q to be made. Integration of their curve for neutron production rate per gram *vs.* depth from the top of the atmosphere gives Q as 0.8 neutrons/cm^2/sec.

The neutrons probably are produced with several Mev energy[8] and collide with air molecules until they are captured. From the known large slow neutron capture cross section for $N^{14}(n, p)C^{14}$ it is quite clear that the main part of Q must result in the formation of C^{14} atoms in the atmosphere. Korff[8] has given this conclusion previously.

Although most neutrons must form C^{14} there is an additional reaction of lower cross section which seems likely and which appears to offer an explanation of the known larger abundance of the mass three helium isotope in atmospheric helium as compared with gas well helium (10^{-7} part *vs.* 10^{-8} part in well He).[9] The reaction is

$$N^{14}+n=C^{12}+H^3+Q_1 \qquad (1)$$

or

$$N^{14}+n=3He^4+H^3+Q_2. \qquad (2)$$

This reaction was found[10] with the neutrons from 16-Mev deuterons on beryllium. This neutron source should have resembled somewhat the initial energies of the cosmic-ray neutrons. Since Q_1 is -4.3 Mev and Q_2 is -11.5 Mev, the production of tritium from N^{14} by neutrons requires energetic neutrons. The cross section obtained by Cornog and Libby was 10^{-26} cm^2 with an accuracy of about a factor of five. This source of tritium is of course a source of He^3 in a geologic sense because the 30-year half-life of tritium is so short (tritium emits a negative beta particle to form He^3). If one assumes that the fraction of the cosmic-ray neutrons forming He^3 in this way is about the ratio of the cross sections 10^{-26} cm^2 for the He^3 process to $1.7\cdot10^{-24}$ cm^2 for the C^{14} process, one expects (1/170) Q He^3 atoms per cm^2 per sec. to be produced. Taking the age of the earth's atmosphere to be approximately 1.5×10^9 years this predicts 1.3×10^{-11} Q cc of He^3 per cc of air, whereas the value reported by Alvarez and Cornog is[9,11a,b] about $10^{-7}\times5.239\times10^{-6}$ or 0.052×10^{-11}. Considering the possibilities of loss by escape from the atmosphere, the likelihood of higher concentrations above 25 kilometers[11a,b], the uncertainty of fivefold in the cross section for the He^3 reaction and our ignorance of the neutron spectrum and dependence of the cross section on energy, the agreement seems to be satisfactory.

C. RADIOCARBON IN NATURE

As stated above, it seems probable that nearly all the neutrons eventually form C^{14} and for purposes of calculation we shall neglect the He^3 and other paths entirely and equate the rate of production of C^{14} to Q. Since the age of the earth is much greater than the life of C^{14} a radioactive equilibrium must exist in which the rate of disintegration of C^{14} is equal to the rate of production, Q. In order to calculate the specific activity of atmospheric carbon due to the C^{14} content produced in this way it is necessary to estimate the amount of carbonaceous matter in the atmosphere and on the earth's surface which will be in exchange equilibrium with the atmospheric carbon. This number we shall call B (units: moles of carbon/cm^2). The specific activity then will be Q/B (disintegrations/sec./mole of C).

The estimation of B is difficult. In order to do so we shall assume that the long half-life of C^{14} ($\gg10^3$ yr)[12a,b,c] will insure that all living matter, dissolved matter in the oceans, and a small amount of solid carbonate rocks will be in equilibrium. Taking the biosphere[13] to contain between 10^{13} and 10^{14} tons of carbon, the atmosphere,[13] 6×10^{11} tons; the ocean carbonate,[14] 3×10^{13} tons; and adding 10^{13} tons for rock carbonate in exchange equilibrium, B calculates to be 1.3 moles/cm^2. The possible error in B certainly is at least of the order of a factor of ten, so we shall expect that the C^{14} specific activity of living matter may lie between $\frac{1}{4}Q$ and $2.5Q$, or be about $\frac{1}{3}$ to 2 disintegrations per sec. per mole of carbon.

This is a low figure corresponding to about 10^{-12} curie per gram. However, such radiation levels are detectable in the case of radium and it seems just possible that it can be accomplished with the techniques used in the study of the natural radioactivities of the ordinary elements. An attempt is intended in these laboratories.

It will be particularly desirable to examine C^{13} concentrates for C^{14} if they are prepared from atmosphere or biosphere carbon compounds, and it is hoped that future C^{13} concentration plants will use plant life carbon, when possible, rather than oil, coal, or limestone material in which the abundance of C^{14} should be very low.

[1] C. G. and D. D. Montgomery, Phys. Rev. **56**, 10 (1939).
[2] S. A. Korff, Rev. Mod. Phys. **11**, 211 (1939).
[3] H. A. Bethe, S. A. Korff, and G. Placzek, Phys. Rev. **57**, 573 (1940).
[4] E. T. Clarke and S. A. Korff, J. Frank. Inst. **232**, 217 (1941).
[5] S. A. Korff and E. T. Clarke, Phys. Rev. **61**, 422 (1942).
[6] S. A. Korff and M. Kupferberg, Phys. Rev. **65**, 253(A) (1944).
[7] S. A. Korff and B. Hammermesh, Phys. Rev. **69**, 155 (1946).
[8] S. A. Korff, *Terrestrial Magnetism and Atmospheric Electricity* (June 1940).
[9] Luis W. Alvarez and Robert Cornog, Phys. Rev. **56**, 613 (1939).
[10] R. Cornog and W. F. Libby, Phys. Rev. **59**, 1046 (1941).
[11a] E. Gluckauf, Proc. Roy. Soc. (London) **185**, 98 (1946).
[b] E. Gluckauf and F. A. Paneth, Proc. Roy. Soc. (London) **185**, 89 (1946).
[12a] Ruben and Kamen, Phys. Rev. **57**, 549 (1940).
[b] Kamen and Ruben, Phys. Rev. **58**, 194 (1940).
[c] Ruben and Kamen, Phys. Rev. **59**, 349 (1941).
[13] W. J. Vernadsky, *Geochemie in Ausgewahlten Kapiteln* (Akademische Verlagsgesellschaft, Leipzig, 1930).
[14] V. M. Goldschmidt, *Geochemische Verteilungsgesetze der Elemente* (Norwegian Academy, Oslo, 1938), Vol. 9.

New Units for the Measurement of Radioactivity

E. U. CONDON AND L. F. CURTISS
National Bureau of Standards, Washington, D. C.
May 18, 1946

IT has become the custom to express the strength of radioactive sources in terms of curies. This is an erroneous use of this unit since by original definition the curie is

that "amount of radon in equilibrium with one gram of radium"[1] as defined by the Radiology Congress in Brussels in 1910. Therefore, the curie can only be used to represent a rate of disintegration in the radium family. It then represents the disintegration rate of radium or its products in equilibrium. Such a use has been indorsed by the International Radium Commission.

The quantity to be specified in designating the strength of radioactive sources in general is the disintegration rate, determined by the decay constant and the number of atoms of the radioactive isotope in the source. This is simply a number and therefore to establish a suitable unit the only requirement is to select a convenient number of disintegrations per second and give it a name. In selecting this number consideration should be given to insure that it can be readily expressed in sub-multiples, and multiples by the usual prefixes, kilo, milli, micro, etc. A number which fits this requirement is 10^6. Since the curie was named in honor of M. and Mme. Curie, the co-discoverers of radium, it is natural to select the name "rutherford" for the new unit. The appropriate abbreviation is "rd" which conflicts with the abbreviation of no other well-accepted physical unit. The micro-rutherford would become one disintegration per second, a convenient number to remember. Furthermore, the rutherford itself is a small unit of the order of magnitude of many sources used in laboratory measurements. It is sufficiently different in size from the curie that no confusion can arise with the curie in connection with measurements of activities in the radium family. Large sources would require the use of positive powers of ten, which would be preferable to the use of a large unit requiring negative powers of ten.

It should be pointed out that the continued use of the curie for all radio-isotopes not only requires a redefinition of the curie. In addition the value of the curie is uncertain to at least 4 percent and values are in current use well outside this limit. The rutherford provides a definite unit. In addition to eliminating the undesirable use of the curie, the proposed unit also eliminates the basic necessity for measuring radio-isotopes in terms of a standard. Any measuring device which will determine the total number of disintegrations per second will provide directly the strength of the source in rutherfords. A counting arrangement for which the solid angle factor is known is an example. Radioactive standards may be used to determine this factor for a given geometrical arrangement, but other methods are also available.

In the measurement of sources of gamma-rays the roentgen has gained increasing use, largely because this unit is independent of the quality (electron volts) of the gamma-radiation. There is need for a unit in which the intensity of gamma-ray sources can be expressed to eliminate the use of the curie for this purpose. An obvious unit derived from the definition of the roentgen is a roentgen-per-hour at one meter. The roentgen-per-hour at one meter can be abbreviated r.h.m., which again is not readily confused with any other common abbreviation. It has been suggested that this abbreviation can be pronounced "rum." It should be noted that a gamma-ray source equal to one r.h.m. will have a gamma-ray strength 1.18 times that of 1 curie of radium. Therefore, the roentgen-per-hour at one meter has the same order of magnitude as the curie in the measurement of gamma-ray sources.

The National Bureau of Standards, at the suggestion of the Committee on Radioactivity of the National Research Council, recommends the general use of these units.

[1] E. Rutherford, "Radioactive Substances and Their Radioactivity," p. 479 (1913). International Radium-Standards Commission Report, "The Radioactive constants as of 1930," Rev. Mod. Phys. 3, 427 (1931).

Erratum: Experimental Test of Beta-Ray Theory for the Positron Emitters Na^{22}, V^{48}, Mn^{52}, Co^{56}

[Phys. Rev. 69, 313 (1946)]

WILFRED M. GOOD, DAVID PEASLEE, AND MARTIN DEUTSCH
Massachusetts Institute of Technology, Cambridge, Massachusetts

THROUGH an oversight, a line was omitted in the manuscript of the above-named paper resulting in a complete reversal of the sense of the last sentence of the abstract. This sentence should read:

> "The type of interaction remains uncertain as does the parity change except that the scalar interaction seems ruled out. The tensor interaction gives consistent results if one assumes parity change in every case except Mn^{52}."

The text of the paper contains the statement in correct form.

Proceedings of the American Physical Society

Minutes of the Meeting of the New York State Section at Hamilton, New York, April 13, 1946

THE Spring Meeting of the New York State Section of the American Physical Society was held at McGregory Hall, Colgate University, on Saturday, April 13, 1946. This meeting was sponsored jointly by the section and the New York State Science Teachers Association. One hundred and twenty-five members and visitors registered at the meeting. The following program of invited papers was presented:

Morning Session

Address of Welcome. Sidney J. French, *Dean of Faculty, Colgate University*

Recent Developments in Color Photography. John A. Tiedeman, *Ansco Corporation*

Nuclear Physics in the Atomic Bomb Development. Robert F. Bacher, *Cornell University*

The Atomic Bomb and International Relations. Charles R. Wilson, *Colgate University*

Afternoon Session

The Physics of Radar. Joseph B. Platt, *University of Rochester*

General Electric Fellowships for Science Teachers

The 1945 Summer Session

1. **Administrative Viewpoint.** V. Rojansky, *Union College*
2. **Teachers' Viewpoint.** Anna M. Pearsall, *Ithaca High School*
3. **Discussion**

Recent Developments in Procuring War Surplus Equipment. C. W. Gartlein, *Cornell University*

In addition to the above program a radar unit was demonstrated through the courtesy of the Signal Corps.

W. R. Fredrickson
Secretary

Proceedings of the American Physical Society

Minutes of the Spring Meeting at Cambridge, April 25–27, 1946

THE 1946 Spring Meeting of the American Physical Society, the 271st of our meetings, was held in the buildings of Harvard University and of the Massachusetts Institute of Technology on Thursday, Friday, and Saturday, April 25–27, 1946. With eleven hundred registrants, this proved to be the greatest meeting we had ever held by ourselves, and second only to the joint convention four months earlier of our Society and the Association of Physics Teachers. Instructed by our advance underestimate of the previous December, we were not taken unawares; and the Local Committee—headed by J. C. Slater and J. H. Van Vleck—had at least a warning of the burden it might be expected to assume. This burden it carried admirably, and its arrangements were adequate in every detail. The Secretary has thanked many a Local Committee in the past, but some of his adjectives ought to have been reserved for the administrators of these postwar meetings, so much more demanding of labor than any that have gone before.

The circumstances of the time conspired to make this the outstanding "radar and microwave meeting" of the Society. Clearance, or declassification as the term is, had recently been granted to much of the work done in the fields so denoted during the war. What was even more important, the clearance had in many cases come so early that it was feasible for an informal committee of physicists familiar with the wartime work to organize a representative programme of invited papers, to solicit suitable contributed papers, and to sift the material apt for our meeting from the even greater amount more appropriate to other societies. Among those who thus helped to build the programme were J. B. Fisk, A. G. Hill, J. B. Kellogg, J. B. Knipp, J. C. Slater, and J. H. Van Vleck.

Three unified groups of invited papers were arranged by the informal committee, their topics

being: Microwave Generation and Transmission, Random Processes and Noise, and Circuits for Precision Measurements. What was planned at first as another such group, devoted to Atmospheric Absorption of Microwaves, was modified into a train of contributed papers led by J. H. Van Vleck's survey "The Atmospheric Absorption of Microwaves." L. A. DuBridge commemorated the M. I. T. Radiation Laboratory in an after-dinner speech under the title "Microwave Radar." A sequence of eleven contributed papers pertained to the subject of Gas-Discharge Transmit-Receive switching tubes, and perhaps a score of the other ten-minute papers (there were of these no fewer than 136 altogether) owed their origin recognizably to radar and microwave investigations.

Other fields of physics were well and abundantly represented. Lise Meitner spoke on many qualities of the fission-process. Nuclear physics, cosmic rays, crystal rectifiers, and shock-waves were the topics of so many ten-minute papers that an almost-complete or a quite-complete half-day session could be devoted to each of these fields; optics and the qualities of the solid state figured prominently. On the Saturday morning the members and guests were refreshed by a most interesting and relatively non-technical programme comprising addresses by J. B. Conant, G. F. Hull, Sr., and K. T. Compton. It is the Secretary's guess that these three and the Meitner address, all four of them held in the Sanders Theatre, were the most numerously attended of all the lectures ever given before the American Physical Society.

The dinner was held on the Thursday evening in the Continental Hotel, and also set a record by being unquestionably the most largely attended of any in our history: 650 members and guests were there. President Condon presided; Vice President DuBridge gave the address which has already been mentioned. The Secretary announced that the Amendments to the Constitution of the Society lately submitted to the Fellows had all been passed. (The tellers of this ballotting, Melba Phillips and M. W. Zemansky, deserve the gratitude of the Society.) The gist of these amendments is that Members are admitted to the franchise on the same terms as Fellows; that in the elections, the name of any Fellow who is nominated to an office by not fewer than one percent of the total number of Members and Fellows together appearing in the latest printed membership list (currently 3751) shall appear on the ballot; and that the functions of the Council in respect to making nominations are transferred to a Nominating Committee composed of seven or nine members, appointed by the Council so that various fields of physics shall be represented.

The Council met on the Friday afternoon and evening, and elected to Fellowship and to Membership the candidates whose names follow hereunder. The Council ratified, on behalf of the Society, the amendments to the Constitution of the American Institute of Physics proposed by its Governing Board.

The Society has lost through death, according to reports reaching the Secretary, the following members: R. E. Hickman (New Zealand), S. J. Simmons (M. I. T.), and W. R. Westhafer (Wooster).

Elected to Membership:

John W. Abrams, John H. Affleck, Leroy R. Alldredge, James R. Ambrose, Raymond K. Appleyard, Erik Backun, Fred L. Bartman, Morris E. Battat, Jane Lucille Berggren, Carl V. Bertsch, Everitt P. Blizard, Harriet May Bredder, Leeroy A. Britton, Vinton A. Brown, Patrick Edward Cavanagh, Harold R. Coish, Henry Milton Crosswhite, Raymond Davis, Jr., John C. Decius, Virginia L. Deno, J. E. Eaton, Herbert P. Eckstein, N. E. Edlefsen, Julian Eisenstein, Milton Q. Ellenby, Joe Oliver Elliot, Raymond J. Emrich, Morris Ettenberg, Jane Faggen, F. J. M. Farley, Francis J. Fennessy, Wilfred J. Ferguson, Jerome L. Flanagan, Paul C. Foote, Richard Foy, Elisabeth J. Fraenkel, Stanley Phillips Frankel, Glenn R. Fryling, Ch'eng-Yi Fu, Raymond L. Garman, Martin A. Garstens, George Abraham Ginsberg, Harold C. Glahe, Lawrence E. Goodman, C. C. Gotlieb, Robert H. Gould, John W. E. Griemsmann, James H. G. Griffiths, Nelson T. Grisamore, Gerard R. Gunther-Mohr, Charles Andrew Hansen, Jr., Gerald Harrison, Hayward W. Henderson, Gerald J. Hine, Claude Wendell Horton, Robert E. Houle, Charlotte R. Houtermans, John Nelson Howard, Clinton D. Janney, Philip Sheldon Jastram, Joseph Kaplan, Leon Katz, Bruria Kaufman, Spurgeon Milton Keeny, Jr., Joseph W. Kennedy, Bernard D. Kern, Donald D. King, Wallace C. Koehler, Richard T. Kropf, Kaiser S. Kunz, Robert Leighton, Edwin S. Lennox, Louis Leprince-Ringuet, Henry Levinstein, Miles A. Libbey, Charles W. Malich, Carl R. Malmstrom, Kenneth C. Mann, Moshinsky B. Marcos, Arleigh H. Markham, Edward G. Martin, Philip K. McGall, Berthus B. McInteer, Jr., Wilkison W. Meeks, Dwight P. Merrill, Siegfried S. Meyers, Ernst Miescher,

Frank L. Moore, Jr., Francis Paul Mooring, George W. Morton, Joseph R. Mottl, Max M. Munk, Henry S. Myers, Per Ohlin, Aadne Ore, Heinz R. Paneth, Thomas D. Phillips, W. M. Pierce, Bruno Pontecorvo, Henry H. Porter, Daniel Q. Posin, Marilyn A. Poth, Robert Byron Quinn, Ora L. Railsback, L. G. Raub, Severin Raynor, Leonard Reiffel, Roland Reisley, Charles N. Rice, Theodore A. Rich, Edmund S. Rittner, D. Roaf, Donald Glenn Rose, Isadore Rudnick, Robert E. Ruskin, Frederick Henry Sanders, John H. Sanders, Norman B. Saunders, John E. Scott, Jr., Leo Seren, David M. Sherwood, Hugh H. Spencer, Lawrence Spruch, John Ellsworth Stecklein, Paul Robert Stein, Ellen Swomley Stewart, John Fredrick Streib, Jr., Paul M. Strickler, Arthur Henry Sully, Mary Anne Summerfield, M. Surdin, Clayton Albert Swenson, Guy C. Tavernier, Gordon K. Teal, Lee Morton Thompson, G. C. Tibbetts, John R. Tolmie, George Vaux, Adolf F. Voigt, Sten Von Friesen, Hugh Gordon Voorhies, Jr., John D. Wallace, Albert Wattenberg, John W. Weigl, David K. Weimer, Benjamin Welber, Aaron Wexler, Locke White, Jr., Hollie C. Williams, John Winckler, Irving Wolff, Barbara A. Wright, Joseph P. Wronski, Kazuo Alan Yamakawa, and Ralph Zirkind.

Elected to Fellowship:

E. Scott Barr, W. H. Bostick, W. M. Cady, Glen D. Camp, B. Chance, Ralph J. Christensen, L. J. Chu, A. M. Clogston, E. A. Coomes, S. M. Dancoff, R. H. Dicke, D. H. Ewing, M. Eastham, J. Halpern, D. R. Hamilton, E. L. Hudspeth, W. H. Jordan, Gilbert W. King, L. B. Linford, A. Longacre, E. M. Lyman, P. H. Miller, Jr., J. Millman, M. D. O'Day, W. M. Preston, F. F. Rieke, E. G. Schneider, Rubby Sherr, C. W. Sherwin, W. H. Souder, G. F. Tape, F. E. Terman, H. C. Torrey, G. E. Valley, Jr., and C. A. Whitmer.

KARL K. DARROW, *Secretary*
American Physical Society
Columbia University
New York, New York

Invited Papers

Microwave Generation and Transmission

Magnetron Generators. J. B. FISK, *Bell Telephone Laboratories.*
The Klystron. DONALD R. HAMILTON, *Radiation Laboratory, M. I. T.*
The Resnatron. J. J. LIVINGOOD, *Collins Radio Corporation.*
Microwave Circuits. A. G. HILL, *Radiation Laboratory, M. I. T.*

Random Processes and Noise

Theory of Random Processes. G. E. UHLENBECK, *University of Michigan.*
Threshold Signals in the Presence of Noise. J. L. LAWSON, *General Electric Company.*
Response of Non-Linear Devices to Signal and Noise. D. O. NORTH, *RCA Laboratories.*
Fourier Series in Random Processes. S. O. RICE, *Bell Telephone Laboratories.*

Circuits for Precision Measurements

Pulse Amplifiers. HENRY WALLMAN, *M. I. T.*
The Amplification of Low Frequency Signals. G. E. VALLEY, *M. I. T.*
Precision Methods for Pulse Time Measurement. BRITTON CHANCE, *M. I. T.*
Techniques of Cathode-Ray Tube Display Circuits. L. J. HAWORTH, *University of Illinois.*

The Atmospheric Absorption of Microwaves. J. H. VAN VLECK, *Harvard University.*
Microwave Radar. L. A. DUBRIDGE, *University of Rochester.*
Attempt to Single Out Some Fission Processes of Uranium by Using the Differences in their Energy Release. LISE MEITNER, *Forskningsinstitutet for Fysik, Stockholm.*
The Interaction of Science and Society. J. B. CONANT, *Harvard University.*
Fifty Years of Physics, a Study in Contrasts. G. F. HULL, SR., *Dartmouth College.*
Scientific Mission to Japan. K. T. COMPTON, *Massachusetts Institute of Technology.*

ABSTRACTS OF CONTRIBUTED PAPERS

A1. Reflection of Sound Signals in the Troposphere. G. W. GILMAN AND F. H. WILLIS, *Bell Telephone Laboratories.*—It is known that many familiar weather phenomena and also the behavior of microwave radio signals depend upon the distribution of temperature, humidity, and momentum in the troposphere. We have attempted to detect the presence of acoustic non-homogeneities in the lower troposphere by using a low-power acoustic "radar." The device has been named the "Sodar." Trains of audio-frequency sound waves were launched vertically upward from the ground, and the echoes were displayed on an oscilloscope and photographed. Periods characterized by strong temperature inversions tended to be accompanied by strong sodar displays, with amplitudes several times as great as those obtained from a standard atmosphere. These periods tended to be coincident with periods of disturbed transmission on a microwave radio path on which the sodar was located. In addition, relatively strong echoes were received when the atmosphere was in a state of considerable turbulence. There was a well-defined fine-weather diurnal characteristic. Limitations in the apparatus as used would prevent the deduction of the vertical distribution of acoustic impedance, even in principle, from the oscilloscope patterns. The experimental evidence leads us to conjecture that the picture of a smooth, quiet, stratiform troposphere, even under conditions of a strong temperature inversion and apparent stability, represents an over simplification of its refractive properties for certain problems in sound and radio wave propagation.

A2. Interaction of Shock Waves. R. J. SEEGER, J. VON NEUMANN, H. POLACHEK, *Bureau of Ordnance, Navy Department. Washington, D. C.*—The interaction of plane shock waves moving with constant velocity has been investigated theoretically for gases and for water-like substances. In the case of one-dimensional interaction for water-like substances there is no peculiar dependence upon the value of the adiabatic exponent γ, as occurs for ideal gases. In the case of oblique collision of two similar shock waves two distinct phenomena are possible: the resulting shock configurations are designated regular and Mach, respectively. A regular, oblique collision may involve pressures higher than those for head-on incidence. A comparison is made between experimental data for stationary configurations and both the simple theory and the simple theory with Prandtl-Meyer modifications. The simple theory appears to be adequate. Mach oblique collision involves three-shock configurations.

A3. Three-Shock Configurations. H. POLACHEK AND R. J. SEEGER, *Bureau of Ordnance, Navy Department, Washington, D. C.*—A common occurrence resulting from shock-wave interactions is a configuration consisting of three confluent shocks, which are invariably accompanied by a plane of density discontinuity. All four planes intersect in a line, and form what is known as a three-shock or Mach configuration. This phenomenon is observable in supersonic wind tunnels, in supersonic jets, in the vicinity of high speed projectiles, etc. In order to obtain a reliable estimate of the physical conditions existing in the neighborhood of the intersecting line, an extensive survey has been made of all theoretically possible intersections of this type. Comparison of the theoretical solutions with experimental results shows good agreement in the case of strong incident shocks. However, in the case of weak shocks a systematic deviation is found to exist between theoretical and observed results. Several modifications of the flow pattern in the neighborhood of the intersecting line are given to illustrate the effects on the disposition of the shock waves.

A4. Normal Reflection of a Shock Wave. R. J. FINKELSTEIN, *Bureau of Ordnance, Navy Department, Washington, D. C.*—Determination of the initial pressure produced by the reflection of a shock wave has been studied as far as this is possible by algebraic means. Knowledge of the complete process of reflection can be obtained, on the other hand, only by solving the non-linear differential equations describing the flow. This has been done for normal reflection by Chandrasekhar, who treated the case of reflection from a rigid surface in air by a numerical method. We also have considered normal reflection from a rigid surface, but we have replaced the numerical method by an analytical one, and have extended the work to reflection in other fluids, including water. It is found that gases and water behave differently. In gases the blow is prolonged and the impulse delivered to the reflector exceeds the value predicted by acoustic theory. In water, on the other hand, the blow is shorter and the impulse is less than one would expect from the acoustic approximation.

A5. Shadowgraph Method of Determining the Strength of a Shock Wave. P. C. KEENAN, *Bureau of Ordnance, Navy Department, Washington, D. C.* (Introduced by R. J. Seeger).—Since the density in the shock wave from an explosion falls off almost linearly in the region immediately behind the shock front, shadowgraphs taken at two screen distances permit determination of the shock parameters: (1) peak density and (2) density gradient. On the basis of International Business Machine computations involving numerical integrations of the equation of the light path and a series approximation developed by Polachek, tables have been prepared to make possible the practical use of this method in the laboratory. The tables apply to shock waves of strengths normally encountered in air or in water. The relative peak density values of (P/P_0) for the air shocks extend from 1.3 to 4.6 and the range of screen distances is from 3 to 50 times the radius of the shock wave. For the underwater shocks the table covers density ratios from 1.04 to 1.35, corresponding to peak pressures ranging from 1000 to 26,000 atmospheres. Copies of the tables will be available in a NavOrd Report of the Bureau of Ordnance.

A6. Numerical Aspects of Quantitative Interferometry. F. JOACHIM WEYL, *Bureau of Ordnance, Navy Department, Washington, D. C.* (Introduced by R. J. Seeger).—The

modern high precision version of the Mach-Zehnder Interferometer exhibits a qualitative sensitivity of such magnitude as to raise the hope that by its use quantitative experimental results in the study of gas dynamics can be obtained which allow a direct check on current theories. A knowledge of the accuracy with which the numerical reduction of an interferogram can be accomplished is therefore of vital interest. The discussion is restricted here to the analysis of axially symmetric flow where the problem presents itself in terms of an integral equation of well-known type whose solution can readily be written down analytically. The currently employed methods of reduction are briefly sketched, especially the one used by the Bureau of Ordnance, which has so far not been published. The error sources are exhibited, and the resulting uncertainties in the final answers are given in terms of the uncertainties in the basic measurements.

A7. Shock Waves in a Tube. WALKER BLEAKNEY, *Palmer Physical Laboratory, Princeton University.*—A tube of uniform cross section is divided into a compression chamber and an expansion chamber by a thin diaphragm. The pressure ratio between the two chambers is adjusted to a pre-assigned value and the diaphragm is burst by puncturing it at the center. If the dimensions are suitably chosen a plane shock having constant pressures on both sides of the discontinuity is propagated along the length of the expansion chamber. This is the simplest possible shock wave and is ideal for studying the properties of such phenomena. The strength of the shock is determined by the initial pressure ratio across the diaphragm and the velocity of propagation is a function of this strength. The measurement of the velocity which can be done with precision allows the shock strength to be computed with considerable accuracy. The shock tube is used to study the behavior of various gauges and in particular to calibrate such devices. By means of optical methods such as shadow and Schlieren photographs, the behavior of shocks on reflection at a boundary have been studied.

A8. Photographic Investigation of the Reflection of Plane Shocks in Air. L. G. SMITH, *Palmer Physical Laboratory, Princeton University.*—Studies by shadow and Schlieren photography of the reflection at a plane rigid wall of plane shocks produced in a tube show that regular reflection occurs for all angles α between incident shock and wall up to an angle slightly greater than the extreme angle α_e beyond which the two-shock theory shows that regular reflection is impossible and that for larger angles α Mach reflection occurs. The angle α at which Mach reflection sets in has been located between the limits α_e where signals from the corner of the wall first affect the entire reflected shock and $\alpha_{s=0}$ an empirically determined value from 1 to 4 degrees larger than α_e. (α_e is larger than α_e by 0.5 degree or less for all shock strengths.) The Mach reflection configuration may be described at any time t after the incident shock struck the corner in terms of two variables x/t and y/t instead of three such as x, y, and t. Thus the triple point moves along a straight line through the corner away from the wall and angles between shocks at the triple point remain unchanged as the configuration grows. Measured values of the angle α' between the reflected shock and the wall in regular reflection agree well with those predicted by the two-shock theory for all but the strongest shocks where slight unexplained discrepancies are observed. In Mach reflection, measured values of the angles agree with those predicted by the three-shock theory only for strong shocks. For weak shocks the measured values show conclusively that the simple three-shock theory is inadequate.

A9. Theory of Reflection of Shock Waves. A. H. TAUB AND L. G. SMITH, *Palmer Physical Laboratory, Princeton University.*—The Schlieren photographs obtained by Smith indicate that the regions bounded by the shocks are not uniform but have variations in density which are to be interpreted as due to variations in pressure. These do not seem to be "angular" in character, that is, they are not independent of the distance from the triple point and a function only of the angle a radial line makes with the incident shock. Because of the fact that the whole phenomenon is a function of x/t and y/t one must expect that pressure variations would be angular around the triple point. The only known pressure variations of this type are the Prandtl-Meyer waves, but such waves are inadequate to account for Smith's results. The experiments of Smith reported in the previous paper conflict with the predictions of the three-shock theory. There are no solutions to the equations describing this system for certain angles of incidence of the flow and certain (weak) shock strengths. However Smith has shown that the Mach configuration exists for just these angles and shock strengths.

A10. Interaction of Shock Waves and Boundary Layers in Supersonic Gas Flow.* JOHN WINCKLER, *Palmer Physical Laboratory, Princeton University* (Introduced by R. Ladenburg).—Recently** it was shown how quantitative values of density, pressure, temperature, velocity, and Mach number in supersonic gas streams could be obtained optically by the use of an interferometer. The Mach number M may be obtained independently by making shadow photographs of the head wave of a narrow probe placed in the stream. Probe and interferometer Mach number values were in good agreement in a homogeneous stream from a Laval nozzle, but in complete disagreement in an inhomogeneous expanding air jet in the region where standing shock waves occur. This discrepancy has been traced to the influence of the standing shocks on the air flowing at low velocity in the boundary layer along the probe. The shock pressure may cause a separation of the stream from the probe, and a configuration of normal and oblique shocks arises as a result at the region of separation. Further experiments made in a strictly one-dimensional stream show an analogous separation of flow when a normal standing shock wave intercepts the boundary layer. The theory of separation is discussed in the light of some earlier work of Prandtl and Stodola.

* This research sponsored by the Navy Department, Bureau of Ordnance.

** R. Ladenburg, C. C. Van Voorhis, and J. Winckler, "Interferometric study of gas flow around various objects in a free supersonic homogenous air-jet"; J. Winckler, C. C. Van Voorhis, and R. Ladenburg, "Optical analysis of the structure of supersonic inhomogeneous air-jets," Bull. Am. Phys. Soc. 21, No. 1 (Jan. 24, 1946).

A11. Influence of Atmospheric Pressure on Water Entry Phenomena. DAVID GILBARG, *Naval Ordnance Laboratory, Washington, D. C.* (Introduced by George H. Shortley).—Systematic high-speed photographic studies are made of the dependence of air-water entry cavities on the relevant physical parameters; in particular on the atmospheric pressure over the water surface. Experiments on the vertical entry of spheres and cylinders ¼″ to 1″ in diameter, with entrance velocities between 15 ft./sec. and 100 ft./sec., and air pressures between 1/60 atmosphere and three atmospheres, show that surface sealing of the cavity is a major factor in controlling cavity formation, and is most responsible for non-scaling of cavity phenomena. Surface sealing is a function chiefly of the atmospheric density and projectile velocity, but for small projectiles, surface tension also has an important effect. The measured drag of the projectiles is independent of cavity size and shape. Jets are found to occur regularly and with great strength at both deep and surface closures of the cavity. The observed presence of jets in finite cavities is predicted by an extension of the Kirchhoff, Helmholtz, Levi-Civita theory of the infinite (two-dimensional) cavity to the case of finite cavities with finite cavitation numbers. This extended theory requires the existence of jets in finite cavities.

A12. Ultrasonic Absorption and Velocity Measurements in Liquids by Means of Pulse Techniques.* JOHN R. PELLAM AND JOHN K. GALT, *Radiation Laboratory, Massachusetts Institute of Technology.*—Radiation Laboratory equipment has been modified for measurements of sound velocity and absorption in liquids at 10–30 mc. Pulses of one micro-second duration are generated by a transducer, which also picks up the resultant echoes returning from a plane reflector. Velocity measurements are made by determining the distance the transducer must be moved to delay the received echoes by a specified increment. Absorption measurements are made by determining the attenuation necessary to keep the receiver signal constant as the transducer is moved. Preliminary results indicate that the attenuation factor can be measured to an accuracy of 5 percent and sound velocity to about 0.05 percent. Measurements of absorption in homologous series of organic liquids will be reported.

* This paper is based on work done for the Office of Scientific Research and Development under Contract OEMar-262.

B1. A High Intensity Velocity Selector for Neutral Atoms. H. LEVINSTEIN AND H. R. CRANE, *University of Michigan.*—A high intensity velocity selector has been constructed and operated in order to investigate the way in which the character of evaporated metal films depends upon the velocity of the atoms during deposition. The selector consists of a duralumin cylinder in which are milled a large number of helical channels. As the cylinder rotates about its axis, atoms having a velocity equal to the pitch of the helices times the angular velocity of rotation will move along the channels without hitting the sides. There are no "overtones," as there are in selectors employing slotted disks, and, for those atoms having the right velocity, the source "sees" the receiver 75 percent of the time. The rotor is enclosed in a vacuum chamber and is driven at 10,000 r.p.m. by means of magnetic pulses from a coil outside the vacuum. The "commutator" for the motor is a photoelectric cell, also outside the vacuum chamber, which sees a black spot on the rotor. Such a motor is self-starting and its speed is limited only by friction in the bearings. A synchronizing signal can be introduced to maintain constant speed. Preliminary results on the metal films deposited will be given.

B2. Control and Recording Circuits for A Magnetic Beta-Ray Spectrograph. W. C. PEACOCK AND R. K. OSBORNE, *Massachusetts Institute of Technology.*—Circuits have been built for the automatic operation of a thin lens magnetic beta-ray spectrograph. Electrons are detected in a Geiger-Muller counter, and the counting rate must be determined for each value of magnetic field strength. Counting rates are determined by recording the time necessary to detect a predetermined number of counts, e.g., 3200. This time interval is stamped on a paper tape. Thereafter the magnetic field is automatically adjusted to a new predetermined value, and the counting rate measurement is repeated. Control of the magnetic field is accomplished by controlling the current in the lens coil. This current is supplied by a d.c. generator (amplidyne) whose field excitation is controlled by means of vacuum tubes. The coil current is monitored by the voltage drop across a small resistor in series with the coil. This voltage is compared with that across a potentiometer and a circuit arranged to control the generator field current to always reduce the voltage difference to zero. This circuit allows control of two important parameters, the probable error of the counting rate measurement, and the size of the momentum interval between successive points.

B3. Beta- and Gamma-Ray Spectra of La^{140}. R. K. OSBORNE AND W. C. PEACOCK, *Massachusetts Institute of Technology.*—The radiations from La^{140} (40 hr.), produced by deuteron bombardment of lanthanum, have been analyzed in a magnetic spectrometer and by the use of $\beta-\gamma$ and $\gamma-\gamma$ coincidence counters. A Fermi plot of the beta-rays from a source 5 mg/cm² thick shows that there are at least three beta-rays of energies 0.90 ± 0.03, 1.40 ± 0.03, and 2.12 ± 0.08 Mev, and intensities 20 percent, 70 percent, and 10 percent, respectively. Some evidence exists for a fourth weak beta-ray of energy 0.40 ± 0.10 Mev. Gamma-rays were studied by observing secondary electrons from a thin gold radiator. Photoelectron lines were observed for gamma-rays of energies 0.333, 0.505, 0.832, 1.61, and 2.52 Mev. These energy values are accurate to about 3 percent. The 1.61 Mev gamma-ray is more intense than the others by roughly a factor of five, and the 0.333 Mev gamma-ray is partially converted. Beta-gamma coincidence measurements with a calibrated gamma-ray counter gave a $\beta-\gamma$ coincidence rate of $(2.88\pm0.12)\times10^{-3}$ per beta-ray. This agrees with the rate expected if the 0.333 and 1.61 Mev gamma-rays are in cascade. Gamma-gamma coincidence measurements gave a $\gamma-\gamma$ coincidence rate of 1.65×10^{-3} per gamma-ray. A tentative disintegration scheme will be given.

B4. Positron Emission, Electron Capture Competition in Zn^{65}. WILFRED M. GOOD AND WENDELL C. PEACOCK, *Massachusetts Institute of Technology.*—Zn^{65}(245 *d*) has been reported to have a 1.14 Mev[1] gamma-ray and positrons of maximum energy 0.4 Mev.[2] Using a calibrated gamma-ray counter, $x-\gamma$ coincidences, and $e^+-\gamma$ coincidences we have found that 54 percent of the electrons are captured in the ground state of Cu^{65} while 46 percent go to the 1.14 Mev excited state. By angular correlation techniques it was found that 2.2 percent of the disintegrations go by positron emission directly to the ground state of Cu^{65}. Comparison will be made with previously studied $_{11}Na^{22}$, $_{23}V^{48}$, $_{25}Mn^{52}$, $_{27}Co^{58}$ [3] and with theory.

[1] Deutsch, Roberts, and Elliott, Phys. Rev. **61**, 389 (1942).
[2] L. A. DuBridge, private communication to Seaborg.
[3] Good, Deutsch, and Peaslee, in publication.

B5. Nuclear Excitation Functions: 14-Mev Deuteron Reactions on Cu, Mg, and Al. E. T. CLARKE AND JOHN W IRVINE, JR., *Massachusetts Institute of Technology.*—Employing previously reported techniques,[1] excitation functions have been obtained for the production of several radioactive isotopes. Bombardment of a stack of 24 copper foils produces curves for the reactions $Cu^{63}(d, p)Cu^{64}$(12.8 hr.), $Cu^{63}(d, 2n)Zn^{63}$(38 min.), $Cu^{65}(d, 2n)Zn^{65}$(250 d.), and $Cu^{65}(d, \alpha)Ni^{62}$(2.5 hr.). The (d, p) reaction cross section begins at about 2 Mev, shows a maximum $\sigma=0.25\times10^{-24}$ cm² at 8.0 Mev, and decreases with further increase in energy. The (d, α) reaction begins at 9.5 Mev and increases with energy. Both $(d, 2n)$ reaction cross sections rise with increase in energy: Zn^{63} exhibits a threshold at 7.0 Mev and reaches a cross section of 0.30×10^{-24} cm² at 14.0 Mev, while Zn^{65} shows a threshold at about 5.5 Mev and rises to $\sigma=0.51\times10^{-24}$ cm² at 14.0 Mev. The two (d, α) reactions in magnesium foils produce similarly shaped excitation functions, both starting at about 2 Mev; Na^{24}(14.8 hr.) reaches a maximum $\sigma=0.095\times10^{-24}$ cm² at 8.7 Mev, while Na^{22}(3.0 y.) reaches a maximum $\sigma=0.15\times10^{-24}$ cm² at 9.5 Mev. Both curves decrease steadily beyond their maxima. Bombardment of aluminum foils produces Na^{24} by an unknown reaction, possibly $(d; p, \alpha)$, beginning at about 10 Mev and reaching a cross section of 0.017×10^{-24} cm² at 14.0 Mev.

[1] E. T. Clarke and John W. Irvine, Jr., Phys. Rev. **66**, 231 (1944).

B6. Nuclear Induction. F. BLOCH, W. W. HANSEN, AND MARTIN PACKARD, *Stanford University, California.*—The nuclear magnetic moments of a substance in a strong magnetic field H_z would be expected to give rise to a small magnetic polarization, provided thermal equilibrium be established, or at least approached. A superimposed oscillating field H_x in the x direction will produce a change in orientation of the polarization with a component perpendicular to the strong field. The latitude of the polarization can be shown to decrease upon adiabatic approach to magnetic resonance, the rotating component having an appreciable value only if the Larmor frequency in the strong field lies very close to the frequency of the oscillating field. The maximum value of its y component is of interest as to its location in frequency, its phase relative to the oscillating field, and its magnitude. The former two yield directly the value and sign of the nuclear gyromagnetic ratio while the latter is related to the quantized spin value j through Langevin's formula for the nuclear magnetic susceptibility. Observation of the voltage induced by the y polarization can therefore be used to obtain these three data and it will also furnish interesting information about relaxation times and the establishment of spin equilibrium.

B7. Nuclear Induction. MARTIN PACKARD, W. W. HANSEN, AND FELIX BLOCH, *Stanford University, California.*—In observing the above effect the horizontal field H_z was varied periodically at 60 c.p.s., the value being $H_0+\Delta H\cos 377t$ with $1650<H_0<2200$ and $\Delta H\sim50$ gauss. The oscillating field H_x of magnitude ~5 gauss and $7.7<\nu<10.7$ mc was produced by a coil with axis horizontal. A second coil, inside the first, and with vertical axis, had voltage induced in it by the rotating moments, and also by the (adjustable) leakage flux from the other coil. The water, which supplied the proton moments used, was contained inside the inner coil in a glass sphere of volume $\sim.5$ cc. The resulting voltage was rectified and amplified, the d.c. due to leakage being removed by the amplifier. The output, whose variations are a measure of the variation of the rotating moment, was applied to the vertical plates of a c-r oscillograph, the horizontal plates being supplied with a voltage proportional to the variations in H_z. Thus the complete magnetic resonance curve is traced cyclically on the oscillograph screen. The curves so plotted showed resonance peaks with the expected aspects and at a constant ratio of the H_z and driving frequency.

B8. Theory of Magnetic Resonance Absorption by Nuclear Moments in Solids. H. C. TORREY, *Radiation Laboratory, Massachusetts Institute of Technology,* AND E. M. PURCELL AND R. V. POUND, *Harvard University.*—If a "diamagnetic" solid containing nuclei of spin I and magnetic moment μ, is placed in a steady magnetic field H, there will be $2I+1$ Zeeman levels separated in energy by $\Delta w=\mu H/I$. Application of a radio-frequency magnetic field perpendicular to H induces transitions between adjacent levels when the frequency is near the resonant value, $\nu=\Delta w/h$. If the population of adjacent levels is unequal, as in thermal equilibrium, there will be a net absorption of energy. At thermal equilibrium the imaginary part of the permeability at resonance is of order $\Delta w/kT$. Although this quantity is small, the effect is easily observable (see the following abstract). Precision measurements of gyromagnetic ratio, (μ/I), are possible for most moderately abundant nuclei. Nuclear spin can be determined[1] by measurement of integrated absorption which is proportional to $I(I+1)$ for constant μ/I. The population of the levels tends to become equalized by transitions induced by the r-f field. This is opposed by transitions induced by spin-lattice coupling tending to restore thermal equilibrium. By balancing these effects through adjustment of the r-f field intensity, the spin-lattice relaxation time may be measured.

[1] We are indebted to Dr. W. W. Hansen for calling our attention to this fact.

B9. Measurement of Magnetic Resonance Absorption by Nuclear Moments in a Solid. R. V. POUND AND E. M. PURCELL, *Harvard University*, AND H. C. TORREY, *Radiation Laboratory, Massachusetts Institute of Technology.*—We have observed resonance absorption at 29.8 mc/sec. by magnetic moments of protons in solid paraffin at room temperature. A capacitatively loaded coaxial line resonator, filled with paraffin, was placed in a large magnet with the steady magnetic field perpendicular to the r-f magnetic field. The resonator formed one arm of an r-f bridge. The unbalance-signal produced by a small change in resonator transmission was amplified, detected and indicated on a meter. Resonance absorption occurred at a field of 7100 gauss, in agreement, within the probable error of our calibrations, with the known gyromagnetic ratio of the proton. The width of the absorption line, at half value, was 10 gauss, perhaps due in part to field inhomogeneities, and the maximum diminution in cavity transmission was 0.4 percent. The integrated line strength is in agreement with the theoretical prediction. The relaxation time was less than one minute, contrary to previous predictions of several hours. A more uniform and controllable field, more flexible circuit and detection of an a.c. component in the resonator output, coherent with modulation of the steady field would allow the method to be applied for a wide range of gyromagnetic ratios and nuclear concentrations.

B10. Spontaneous Emission Probabilities at Radio Frequencies. E. M. PURCELL, *Harvard University.*—For nuclear magnetic moment transitions at radio frequencies the probability of spontaneous emission, computed from

$$A_\nu = (8\pi\nu^2/c^3)h\nu(8\pi^2\mu^2/3h^2) \text{ sec.}^{-1},$$

is so small that this process is not effective in bringing a spin system into thermal equilibrium with its surroundings. At 300°K, for $\nu = 10^7$ sec.$^{-1}$, $\mu = 1$ nuclear magneton, the corresponding relaxation time would be 5×10^{21} seconds! However, for a system coupled to a resonant electrical circuit, the factor $8\pi\nu^2/c^3$ no longer gives correctly the number of radiation oscillators per unit volume, in unit frequency range, there being now *one* oscillator in the frequency range ν/Q associated with the circuit. The spontaneous emission probability is thereby increased, and the relaxation time reduced, by a factor $f = 3Q\lambda^3/4\pi^2V$, where V is the volume of the resonator. If a is a dimension characteristic of the circuit so that $V\sim a^3$, and if δ is the skin-depth at frequency ν, $f\sim\lambda^3/a^2\delta$. For a non-resonant circuit $f\sim\lambda^3/a^3$, and for $a<\delta$ it can be shown that $f\sim\lambda^3/a\delta^2$. If small metallic particles, of diameter 10^{-3} cm are mixed with a nuclear-magnetic medium at room temperature, spontaneous emission should establish thermal equilibrium in a time of the order of minutes, for $\nu = 10^7$ sec.$^{-1}$.

B11. Fast Neutron Collision Cross Sections of C and H. WILLIAM SLEATOR, JR., *University of Michigan.*—Collision cross sections of C and H for D-Li neutrons have been measured at several neutron energies. The intensity of the neutron beam in each energy interval was determined with a detector consisting of a thin layer of paraffin, placed in the beam, and a coincidence ionization chamber[1] arranged to count recoil protons from the paraffin. Protons due to neutrons with energies outside the desired interval were eliminated with absorbers or included in the background count. The scatterers, blocks of graphite, and paraffin 15-cm square, were placed at the hole in the water wall, 274 cm from the cyclotron target and 154 cm from the detector (sensitive area 8 cm in diameter). The observed cross sections σ for five energies are given in Table I. In each run the uncertainty in σ due to statistical fluctuations was below 10 percent. Runs on different days and with scatterers of different thickness agreed within this range.

TABLE I.

Energy (Mev) Center of interval	Limits of interval	$\sigma\times10^{24}$ (cm^2) $n-C$	$n-p$
15	13.4–16.5	1.23	0.61
16.6	15.3–17.8	1.29	0.66
18	16.8–19.1	1.13	0.55
19.5	18.3–20.6	1.32	0.52
21	19.7–22.3	1.17	0.41

[1] Howard Tatel, Phys. Rev. **61**, 450 (1942).

B12. Polarization of Neutrons by Resonance Scattering in Helium. JULIAN SCHWINGER, *Harvard University.*—Neutron scattering in helium exhibits an anomaly for neutron energies in the vicinity of 1 Mev, which has been attributed to a P resonance associated with the formation of the unstable He^5 nucleus. The energy dependence of the cross section for back-scattering is accounted for qualitatively on the assumption of a splitting of the two P levels associated with $J = 1/2$ and $3/2$, with an energy separation comparable with the width of each level, $|E_{1/2}-E_{3/2}| \sim\Gamma\sim0.4$ Mev. In consequence of the large energy difference between the levels, a neutron scattered by He in the resonance region is effectively subjected to a strong spin-orbit interation, which manifests itself in a polarization of neutrons scattered through a definite angle. The polarization effects are quite large; neutrons scattered through 90° in the center of mass system are practically completely polarized at energies corresponding roughly to the positions of the two levels, the direction of polarization being reversed at the two resonances. The polarization effect can be exhibited by a second scattering process, the resultant intensity being asymmetrical relative to the direction of the first scattered neutron. For neutrons scattered twice through 90° in the center of gravity system, the intensity ratio can be as great as ten. An essential factor contributing to this large ratio is that the energy loss on the first collision is comparable with the doublet separation, whence large polarization effects can occur at both collisions. The polarization effect offers the possibility of producing strongly polarized beams of thermal neutrons by slowing down polarized neutrons in a non-depolarizing medium. The investigation of depolarization in various substances is also of interest.

C1. Noise in Radar Crystal Detectors.[1] L. I. SCHIFF, *University of Pennsylvania.*—The minimum noise produced by a radar crystal detector has been calculated with the assumption that the thickness of the blocking layer is small compared to the electron mean free path. For d.c. bias voltage V, current I, and dynamic resistance $R=dV/dI$, the ratio of noise temperature to actual temperature is $(eIR/2kT)\coth(eV/2kT)$. This is equal to unity for $V=0$, as it must be, but can be less than unity for finite V. The mechanism considered is the shot effect of electrons crossing the blocking layer; this gives a frequency-independent noise spectrum. Superposed on this, there is often a large amount of "excess noise" which increases at low frequencies;[2] this is not understood at present.

[1] This work was done in whole under Contract No. OEMsr-388 with The Trustees of the University of Pennsylvania under the auspices of the Office of Scientific Research and Development, which assumes no responsibility for the accuracy of the statements contained herein. Original report issued March 10, 1943.
[2] P. H. Miller, Jr., "Noise Spectrum of Crystal Mixers," 1946 IRE Winter Technical Meeting.

C2. High Frequency Rectification Efficiency of Radar Crystal Detectors.[1] A. W. LAWSON, B. GOODMAN, AND L. I. SCHIFF, *University of Pennsylvania.*—The rectification efficiency of a radar crystal detector is expected to decrease with increasing frequency because of the shunting effect of the capacity of the blocking layer. The observed decrease is not as great as that predicted by a theory which assumes that the capacity is constant. If however a finite time is required to ionize the semi-conductor donator levels in the blocking layer, the capacity of the contact will depend on the frequency. For oscillation periods of the order of or smaller than the ionization time, the charging current and hence the capacity will be smaller than their low frequency values. This ionization time has been calculated by considering the interaction between the electrons and the Debye waves of the crystal lattice. The transition probability of an electron from a bound donator state to the continuum is found to be 10^9 to 10^{10} sec.$^{-1}$ for a typical silicon rectifier. This is of the right order of magnitude to explain the frequency dependence of the rectification efficiency in the microwave region.

[1] This work was done in whole under Contract No. OEMsr-388 with The Trustees of the University of Pennsylvania under the auspices of the Office of Scientific Research and Development, which assumes no responsibility for the accuracy of the statements contained herein. Original report issued July 7, 1943.

C3. Rectification Series. WALTER H. BRATTAIN, *Bell Telephone Laboratories, Inc.*—It is known that point contacts between metals and certain crystals rectify. Considering only the sign of rectification, one classifies all such crystals into two types, P and N. For the P type the direction of easy flow occurs when the crystal is positive, and for the N type when the crystal is negative. Taking one of these crystals and making a point out of it, one finds that the contacts between it and the other crystals rectify and that using this crystal point as a reference a new division depending on sign of rectification will be obtained. If this process is continued on a given group of crystals it has been found that the group can be arranged in a rectification series such that any crystal in the series will rectify one way with those above it and the other way with those below it. Crystals of silicon, SiC, ZnO, and PbS, one or more of each, have been arranged in such a series. Different crystals of any given element or compound will, in general, be found in different places in the series, sometimes far apart.

C4. D.C. Characteristics of Ge and Si Crystal Rectifiers.* H. J. YEARIAN, *Purdue University.*—Current theories of crystal rectification predict currents in the low resistance (forward) direction which rise exponentially with the voltage across the contact for $V \gg e/kT$, and which approach a saturation current in the high resistance direction. In i *vs.* V plots for the forward direction should have a slope $\alpha=e/kT=40$ volt^{-1} at 300°K. Characteristics of Ge and Si rectifiers usually have an exponential behavior, but α is always less than e/kT, frequently between $\frac{1}{3}$ and $\frac{1}{2}$ of this value. The current in the back direction has a saturation component but also an ohmic component, and a rapidly increasing "tail" at higher voltages. More elaborate theories which include the effects of image forces in lowering the barrier, and of penetration of the barrier, give logarithmic slopes less than e/kT and a "tail" in the back direction. However, such corrections cannot explain the values of α most frequently found without eliminating at the same time the conditions necessary for rectification.

* This work was part of a research program carried out under Contract No. OEMsr-362 between Purdue University Research Foundation and the Office of Scientific Research and Development. Based on NDRC reports, December 3, 1942 and August 14, 1943.

C5. Theory of Crystal Rectifiers.* R. G. SACHS, *Purdue University.***—The observed d.c. current-voltage characteristics for point contacts between metal and semiconductor, Ge and Si, cannot be explained by the diffusion of electrons through a blocking layer at the contact. The ordinary diode theory predicts a characteristic with too steep a slope in the forward direction. Consideration of tunnel effect and the effect of positive space charge does not produce agreement. The multi-contact theory, introduced to explain the observed characteristics, assumes that: (1) The contact potential ϕ varies continuously over the surface of contact. (2) The total current is the sum of the partial currents flowing through regions of varying ϕ. (3) The area of a region with a contact potential ϕ may be a function of ϕ. (4) The number of spots having contact potential between ϕ and $\phi+d\phi$ is a function of ϕ. A Gaussian distribution of ϕ values is assumed. Correction is made for the effect of the image force. Characteristics calculated under these assumptions approximately agree with the observed characteristics.

* This work was part of a research program carried out under Contract No. OEMsr-362 between Purdue University Research Foundation and the Office of Scientific Research and Development. Based on NDRC report on June 15, 1943.
** At present, Metallurgical Laboratory, University of Chicago.

C6. Semi-Quantitative Explanation of D.C. Characteristics of Crystal Rectifiers.* V. A. JOHNSON, R. N. SMITH, AND H. J. YEARIAN, *Purdue University.*—The multi-contact theory is employed to explain the observed d.c. current-voltage characteristics for contacts between metal

and semi-conductor (Ge and Si). The area of each spot having contact potential ϕ and the number of spots having contact potential between ϕ and $\phi+d\phi$, are assumed to be exponential functions of ϕ. The parameters of these functions may be determined from measured values of the limiting current in the back direction, the back resistance, and the intercept at zero applied voltage of the forward current. Current limitation is introduced so that the current density does not exceed the maximum current density carried by N electrons per cm³ (known from Hall effect) moving with thermal velocity. The proper slopes are obtained for the forward current. The variation of characteristic with temperature change can be explained by assuming a corresponding change in distribution of ϕ values. A graphical method of applying the multi-contact theory has been developed such that any characteristic may be rapidly synthesized.

* This work was part of a research program carried out under Contract No. OEMsr-362 between Purdue University Research Foundation and the Office of Scientific Research and Development. Based on NDRC report August 14, 1943.

C7. Small Deviations from Diode Behavior in Crystal Rectification.* K. F. HERZFELD, *Catholic University of America.*—The blocking layer in a crystal rectifier, may be treated according to diode theory if the mean free paths of the electrons is very large compared to the dimensions of the blocking layer so that no collisions occur. The diffusion theory assumes a mean free path very small compared to the thickness of the blocking layer. To get a better insight into the behavior of the electrons it has been assumed that the mean free path is large, but not infinitely large compared with the thickness of the blocking layer, so that some collisions occur, but multiple scattering can be neglected. It is assumed that "collision" means absorption and reevaporation. Simple formulae derived from these assumptions give less dependence of the current on voltage then in pure diode theory, but the effect is very small.

* This work was part of a research program carried out under Contract No. OEMsr-362 between Purdue University Research Foundation and the Office of Scientific Research and Development. Based on NDRC report, May 5, 1944.

C8. Contact Capacity of Crystal Rectifiers.* R. N. SMITH, *Purdue University.*—The capacity across the rectifying point contact formed at a metal semi-conductor interface, has been measured by an indirect method for germanium and silicon mixer crystals. The decrease in efficiency of rectification as the frequency is increased to very high (microwave) frequencies is used to calcu ate the capacity. Two assumptions are made. (1) Crystal rectifiers may be represented by a non-linear contact resistance in parallel with the contact capacity, both in series with a fixed "spreading" resistance. (2) The resistance elements of the rectifier model are independent of frequency. The contact capacity was measured as a function of d.c. bias voltage between + and − one volt bias. For silicon units, the capacity increased slowly at first, as the bias was increased in the forward (low resistance) direction, increasing more rapidly as the voltage across the contact approached the contact potential of the metal-semiconductor. This behavior is in qualitative agreement with that predicted for a rectifying contact of the "natural barrier" type. For germanium units, however, the increase in capacity with forward bias voltage, was much greater. The discrepancy is great enough to necessitate modification of the simple model and/or the theory of rectification for germanium.

* This work was part of a research program carried out under Contract No. OEMsr-362 between Purdue University Research Foundation and the Office of Scientific Research and Development. Based on report given at NDRC Crystal Meeting, on October 1, 1945.

C9. High Voltage and Photo-Sensitive Characteristics in Germanium.* S. BENZER, *Purdue University.*—Some germanium crystal rectifiers are able to withstand high inverse voltages (as high as several hundred volts) without damage, while large currents are passed in the low resistance direction. The back direction characteristic is double-valued; a voltage peak occurs followed by a negative resistance region. The effects upon the characteristic of temperature, frequency, composition of the germanium sample and the metal electrode at the point contact, treatment of the surface and the contact, and illumination will be described. Other unusual characteristics with pronounced sensitivity to illumination and temperature have also been observed in germanium crystals: (1) a saturated $i-V$ characteristic where the saturation current varies with illumination and temperature and (2) a triple-valued characteristic exhibiting a voltage peak followed by a negative resistance region which becomes positive again at higher currents. In the latter type, illumination or increased temperature eradicates (reversibly) the voltage peak and negative resistance, leaving a single-valued curve. These photo-effects are observable with light in the visible and near infra-red, the maximum sensitivity occurring at about 1.3μ.

* This work was part of a research program carried out under Contract No. OEMsr-362 between Purdue University Research Foundation and the Office of Scientific Research and Development. Based on NDRC Reports: November 1, 1944; December 26, 1944; and October 31, 1945.

C10. Effect of Various Atmospheres on Germanium Crystal Rectifiers.* R. M. WHALEY AND K. LARK-HOROVITZ, *Purdue University.*—Quantitative measurements of voltage-current characteristics have been made for point contacts on various germanium samples prepared in a high vacuum ($\sim 3\times 10^{-6}$ mm Hg), tested in a vacuum, and after admission of gases at various pressures. Samples fall into three classes. (a) Relatively high purity germanium which provided poor rectification in a vacuum and was unchanged by admission of gas. (b) One sample which showed reversible changes upon admission of air. (c) Samples of relatively high conductivity, due to impurity content, which provided good rectification in vacuo and showed irreversible increases in back resistance by factors of 10 to 1000 upon admitting air. Similar changes, usually to lesser extent, followed admission of nitrogen. Observed changes can be accounted for using the multi-contact theory by assuming the removal of very small areas of low positive contact potentials, either by covering them with insulating layers or by converting them to regions of

higher positive contact potential. On highly conducting samples, irreversible increases in back resistance were most pronounced at low voltages, but increases did extend to the voltage peak. The peak voltage sometimes was increased by admission of air, usually by factors less than two.

* This work was part of a research program carried out under Contract No. OEMsr-362 between Purdue University Research Foundation and the Office of Scientific Research and Development. Based on paper given on November 19, 1943, at OSRD Crystal Group meeting in New York City.

C11. Image Force and Tunnel Effect in Crystal Rectifiers.* E. D. COURANT, *Cornell University.*—According to elementary theory, the current i through a rectifying junction between a metal and a semi-conductor should vary with the applied voltage U according to

$$i=i_0\left[\exp\left(-\frac{V_c-U}{kT}\right)-\exp\left(-\frac{V_c}{kT}\right)\right], \qquad (1)$$

where V_c is the contact potential, and V_c-U the height of the potential barrier. Experimentally it is found that i increases with U less rapidly than indicated by (1), for positive U, and $|i|$ increases with increasing negative U instead of tending to a constant value, as indicated by (1). Both these effects may be explained by assuming that the height of the potential barrier is reduced by the image force and that some electrons tunnel through the barrier near its top. As a result of these two effects the potential barrier is in effect reduced to $\theta(V_c-U)$, where $\theta<1$, and (1) must be multiplied by

$$\exp\left[-(1-\theta)\frac{V_c-U}{kT}\right].$$

Graphs of θ as a function of U are shown and compared with experimental measurements.

* Work done in 1943 under Contract OEMsr-429 between Cornell University and OSRD, which assumes no responsibility for statements contained herein.

C12. Some Thoughts about Gravitation of Celestial Bodies and Photophoretic Forces. FELIX EHRENHAFT, *New York.*—The law of conservation of momentum in electrodynamics, is in contradiction with the experimental facts. The ponderomotive forces exerted by radiation on matter cause helical paths in longitudinal and transversal photophoresis.* A connecting link between celestial bodies is radiation including magnetic current. The movements in the atom cannot directly be observed, however the atom model was originally taken from observable movements in the solar system. It will be attempted to correlate the directly observable photophoretic paths of testbodies moving with six degrees of freedom in the field of solar radiation** with the paths of celestial bodies, for instance, the planets in the sun's radiational field. If these movements around the sun are regarded as transversal photophoresis, Newton's attractive force as negative longitudinal photophoresis, the excess of the earth's electric charge could be calculated being negative, the earth moving clockwise when looking from the magnetic north (geographic south) to south in accord with Ampère's rule. Because of the ponderomotive actions of solar radiation the usual thermally measured solar constant seemingly represents only part of the energy as indicated by the behavior of test bodies in solar radiation. The author does not claim to explain herewith all gravitational actions but any unified field theory should reckon with these phenomena.

* F. Ehrenhaft, Ann. d. Physik **56**, 81 (1918); Comptes rendus **190**, 263 (1930); Ann. de physique **13**, 151 (1940); J. Frank. Inst. **230**, 381 (1940); **233**, 235 (1942); Science **101**, 676 (1945).
** F. Ehrenhaft, Bull. Am. Phys. Soc., Metropolitan Meeting **19** (Nov. 9, 1945); St. Louis Meeting, E 7 (Dec. 1, 1945); New York Meeting, A 10 and T 1 (Jan. 24, 1946).

C13. World Peace Established on Natural Law and Order Instead of Legislation. H. G. WEHE, *Summit, New Jersey.*—The proposition is offered that world peace depends upon law and order; that the alternative to law and order is chaos; that with chaos there can be neither security nor peace. There are two kinds of law and order. There is the natural law and order built into the universe by the Creator and revealed by careful observation, analysis, and synthesis of ideas and controlled reproducible experiment both objective and subjective. This law and order has five classifications: (a) the Creator's relationship with man, (b) man's relationship with his fellow men, (c) man's relationship with other forms of life in all parts of the universe, (d) man's relationship to energy including matter, and (e) matter and energy interrelationships. Because of ignorance of natural law and order—man's scientific knowledge of the universe is very recent historically—man has permitted lawyer-politicians to set up various forms of government which attempt by edicts and legislation to establish a man-made law and order often in direct violation of natural law and order. Would not peace—harmony with natural law and order—be better attained if lawyer-politicians in government were replaced with scientists skilled in discovering and administering natural law and order?

F1. Diffraction Pattern of a Circular Aperture at Short Distances. C. L. ANDREWS, *General Electric Research Laboratory.*—The diffraction pattern of a circular aperture was studied at distances from zero to five wave-lengths from a circular aperture. Microwaves of 12.8 cm wavelength were employed. The aperture was an iris diaphragm that could be varied between one and six wave-lengths in diameter. The beam was incident normally upon the plane of the aperture from a 4-ft. parabolic reflector 24 ft. away. The sharpest diffraction patterns were in the plane of the aperture. Measurements were made of the intensity of radiation in the electric and magnetic planes through the axis. The individual plots were made of intensities along the diameter and along lines parallel to the diameter at steps of quarter-wave-lengths from the diameter. Measurements were also made of the intensities at fixed points along the axis as the diameter of the iris was varied from one to six wave-lengths. It was seen that Fresnel zone theory could be employed as a rule of thumb even in the illogical case of predicting the intensity at the center of the aperture. Checks were made against Kirchhoff's theorem.

F2. An Interferometric Method for the Determination of the Resolving Power of Spectroscopes. K. W. MEISSNER, *Physics Department, Purdue University.*—If a Perot-Fabry interferometer is crossed with a stigmatic spectroscope in the usual manner and continuous light is employed, a "channeled spectrum" is obtained, provided that the slit of the spectroscope is very narrow. The channeled spectrum consists of parabolic fringes which are convex towards longer wave-lengths. The distance between consecutive fringes decreases with incereasing separation of the interferometer plates and when a certain separation has been reached the fringes cannot be resolved anymore. By determining this critical separation of the interferometer plates, one is able to find the resolving power of the spectroscope. If the resolving power of the interferometer is much greater than that of the spectroscope, a condition which is always fulfilled, the resolving power of the spectroscope is given by $R=2t_c/\lambda$, where t_c is the critical separation and λ the wave-length of the observed region. The method can also be employed for astigmatic spectroscopes if only the central part of the slit is used.

F3. The Light of the Night Sky in the Ultraviolet Range. GEORGES DEJARDIN AND JEAN DUFAY, *Université de Lyon.*—From study of the data obtained by other observers (Elvey, Swings, and Linke; Barbier) and by ourselves, we have set up a wave-length table of emission-maxima in the ultraviolet part of the spectrum of the night sky, comprising only such maxima as we consider to be certainly present. Also we have made a critical study of the identifications hitherto proposed for these maxima, testing the identifications by comparing the number of coincidences (between observed and conjectured maxima) with the number to be expected at random. The Vegard-Kaplan bands are certainly present, but are few and weak in the ultraviolet. Apart from these, our study indicates that the most probable systems are: (a) the Herzberg bands (v' uncertain) and the Schumann-Runge bands ($v'=0$ and $v'=1$) of O_2 and (b) the Lyman bands ($v'=0$ and $v'=1$) of N_2. The Herzberg band system, little known as yet, seems to account for some of the strongest and most characteristic features. Bands of OH and CH are doubtful but possible, and there may also be bands not yet observed in the laboratory. In the ultraviolet as elsewhere, the spectrum of the night sky appears as a "weak-excitation" spectrum: the transitions to the normal state (of O_2 and N_2) are the most reliably identified of all.

F4. The Normal Coordinates of a Mono-Substituted Benzene Molecule. N. GINSBURG AND J. L. GAMMEL, *The University of Texas, Austin, Texas.*—By means of group theoretical methods the kinetic energy of the molecule is written down in terms of symmetry coordinates. The potential energy is expanded in terms of nine potential constants of the type used by Wilson[1] for benzene. Since the frequencies appearing most strongly in the observed spectra of molecules of this type are the eleven totally symmetric frequencies, the secular determinant for these is expanded in order to obtain the mass dependency of the frequencies.

[1] E. B. Wilson, Phys. Rev. **45**, 706 (1934).

F5. Ultraviolet Lamps and Ozone. ARTHUR W. EWELL, *Worcester Polytechnic Institute.*[1]—Bactericidal radiation (2537A) from a bactericidal lamp must often be supplemented, at completely shaded surfaces and stagnant air pockets, by a few tenths of one part per million of ozone, produced from the oxygen of the air by a few percent of 1850A radiation, also emitted by the lamp. The important factor is the ozone concentration—determined by the rates of ozone production and decomposition. The former is roughly proportional to the surrounding volume of air (up to a few cubic feet), and the amount of 1850 radiation, which depends upon the transmission of the glass of the lamp, is independent of the temperature (20° to 60°C) and is somewhat reduced by high humidity. The decomposition increases with rise in temperature and/or humidity, the presence of oxydizable or catalytic surfaces, and intense 2537 radiation. Approximately the same bactericidal effect upon surface infection is achieved by equal quantities of energy whether in absorption of 2537 radiation or in formation heat of required equivalent ozone. With air borne infection the bactericidal killing by ozone is nil at low humidity and very great at high humidity.

[1] Consultant, Westinghouse Electric Corporation.

F6. The Photoelectric Mechanism of the Thallous Sulfide Photo-Conductive Cell. A. VON HIPPEL, F. G. CHESLEY, H. S. DENMARK, P. B. ULIN AND E. S. RITTNER, *Laboratory for Insulation Research, Massachusetts Institute of Technology.*—This research was undertaken because the importance of the thallous sulfide cell for war communication systems required a better understanding of the properties and limitations of this photo-element. A quantitative study of the oxidation reaction, correlated step by step with x-ray and electron-diffraction photographs, established that the photo-sensitization is produced by oxygen, entering the structure in solid solution. Thermoelectric measurements showed that pure Tl_2S is an "excess" semi-conductor changing to a "defect" conductor on oxidation. Determination of the cell characteristics as a function of voltage, temperature, light intensity, wavelength, modulating frequency, and composition as well as an examination of the photo-response to light flashes of very short duration led to the formulation of a theory in quantitative agreement with all facts observed. The underlying physical picture is that light is absorbed in the Tl_2S proper and in the presence of oxygen, positive "holes" and negative oxygen ions are formed. The "holes" and ions recombine at a rate proportional to the product of their concentrations. During their lifetime, the negative ions act as space charge compensators for the defect conduction and allow correspondingly higher currents to flow. This space charge compensating action, which is similar to the role played by positive ions in gas discharges, seems to be one essential mechanism of producing secondary photo-effects.

F7. Some Properties of Infra-Red Sensitive Phosphors. R. T. ELLICKSON, *Polytechnic Institute of Brooklyn.*—There have been developed recently* by Urbach, Ward, Fonda

and others, a group of phosphors that show a large increase in phosphorescence when irradiated by infra-red. Some properties of alkaline earth sulfide and selenide phosphors activated with two rare earths will be described. They show the effect to a marked degree. The shape of the brightness *vs.* time curves under constant infra-red stimulation indicates that the process is bi-molecular. Measurements of the amount of light stored in the phosphor indicate that under optimum conditions the number of quanta emitted by a fully excited phosphor is about 6×10^{17} per cubic cm. For these samples, the concentration of activators was 2×10^{17} Sm. and 16×10^{17} Ce ions per cubic cm.

* See the group of papers at the March, 1946 meeting of the Optical Society of America.

F8. The Velocity of Propagation of the Transmitted Photo-Effect in Silicon Crystals. F. C. BROWN, *Radiation Laboratory, Massachusetts Institute of Technology.*—The photo-conductivity effect, previously reported as transmitted in selenium crystals, is likewise transmitted in crystals of silicon. The relative magnitude of the transmitted effect is measured over a distance of 2 cm and is a function of the velocity, the coefficient of recapture (α), and the distance travelled. It is expressed by the equation,

$$1/N-1/N_0=\alpha(e^{\alpha}-1)/V.$$

The velocity is measured directly for a distance of travel from 0.4 cm to 1 cm. This was carried out with a special oscilloscope and a light beam interrupted by a rotating disk. Within the above range the velocity is 400 meters/sec., with a probable error of about 5 percent. Thus far it has not seemed possible to check the velocity for a longer distance in order to satisfy the equation above. The set up made possible the use of an electronic method for determining the effective distance of travel.

F9. A New Bridge Photo-Cell Employing a Photo-Conductive Effect in Silicon. Some Properties of High Purity Silicon. G. K. TEAL, J. R. FISHER, AND A. W. TREPTOW, *Bell Telephone Laboratories, Inc.*—A pure photo-conductive effect was found in pyrolytically deposited and vaporized silicon films. An apparatus is described for making bridge type photo-cells by reaction of silicon tetrachloride and hydrogen gases at ceramic or quartz surfaces at high temperatures. The maximum photo-sensitivity occurs at 8400–8600A with considerable response in the visible region of the spectrum. The sensitivity of the cell appears about equivalent to that of the selenium bridge and its stability and speed of response are far better. For pyrolytic films on porcelain there are three distinct regions in the conductivity as a function of temperature. At low temperatures the electronic conductivity is given by the expression $\sigma=Af(T)\ \exp\ -(E/2kT)$. At temperatures between 227°C and a higher temperature of 400–500°C, $\sigma=A\ \exp\ -(E/2kT)$, where E lies between 0.3 and 0.8 ev; and at high temperatures, $\sigma=A\ \exp\ -(E/2kT)$, where $E=1.12$ ev. The value 1.12 ev represents the separation of the conducting and non-conducting bands in silicon. The long wave limit of the optical absorption of silicon was found to lie at approximately 10,500A (1.18 ev). The data lead to the conclusion that the same electron bands are concerned in the photoelectric, optical, and thermal processes and that the low values of specific conductances found (1.8×10^{-5} ohm^{-1} cm^{-1}) are caused by the high purity of the silicon rather than by its polycrystalline structure.

F10. Corpuscular vs. Undulatory Excitation of Phosphors. H. W. LEVERENZ, *RCA Laboratories, Princeton, New Jersey.*—Phosphors may be broadly classified, according to phosphorescence, as: (1) initially-exponential-decay (ϵ^{-t}), exhibited when oxygen or fluorine are dominant in the crystal anions and (2) power-law-decay (t^{-n}), exhibited when sulphur or selenium are dominant. Excitation of a phosphor to a given peak luminescence by ultraviolet affords a slower latter-stage decay than is obtained after cathode-ray (CR) excitation. This differential effect on phosphorescence is much greater for t^{-n}-decay phosphors. Normal CR excitation of efficient phosphors results in an expenditure of about 40 ev of CR energy per emitted quantum ($\approx$2 ev), whereas ultraviolet excitation quanta are about 5 ev with quantum efficiency near unity. The tenfold lower energy efficiency during CR excitation heats the phosphor more, thereby accelerating at least the latter stages of decay. Phosphorescence may be augmented at the expense of fluorescence by cascading suitable cathodo-luminescent and photo-luminescent materials. The much larger differential effect on phosphorescence of t^{-n}-decay phosphors is attributed to the greater thermal sensitivity of their presumably interstitially-located activator centers as contrasted with the less perturbable activator centers in normal lattice sites of ϵ^{-t}-decay phosphors. The differential effect is related to the approximately 100-fold greater activator content and the toleration of 100-fold greater impurity content in ϵ^{-t}-decay phosphors.

F11. A Small Scale Hydrogen Liquefier. HENRY A. FAIRBANK, *Yale University.*—A simple inexpensive Hampson-type hydrogen liquefier, which combines many of the advantages of other small scale liquefiers,[1] has been built at Yale. The apparatus can be constructed from inexpensive and readily obtainable materials in any moderately equipped machine shop and occupies only a few feet of wall space in a laboratory room. No equipment which is unavailable in the majority of laboratories is required. Commercial compressed cylinder hydrogen is used, obviating the necessity of expensive compressors and bulky gasometers and considerably simplifying the purification system. A single charcoal trap immersed in liquid air or nitrogen removes the impurities from the hydrogen gas. The liquefier proper consists of a heat interchanger, a precooler using liquid air or nitrogen under reduced pressure as a refrigerant, a regenerative heat interchanger, a needle-type Joule-Thomson valve, and finally a can to contain the portion of the gas liquefied after expansion through the Joule-Thomson valve. The unliquefied gas passes back through the interchangers and is allowed to

escape out the window. The liquid can be syphoned out to any external specimen flask through a double-walled Dewar-type metal syphon. Other details of design, operation, and efficiency are discussed.

[1] C. Starr, Rev. Sci. Inst. 12, 193 (1941).

G1. The Dependence of the Diffusion Coefficient on Concentration. B. SERIN, *University of Pennsylvania.*—It is assumed that the activation energy for the diffusion of foreign atoms in a solid lattice depends on the surrounding number of nearest neighbor foreign atoms. For equal *a priori* probabilities for the formation of different foreign atom configurations in the lattice, the diffusion coefficient D is

$$D=\delta^2\sum_{a_i=0}^{a} q_{ai}\left\{\frac{a!(a_i+1)}{(a-a_i)!a_i!}\left[1-\frac{(a+1)}{(a_i+1)}f\right]f^{a_i}(1-f)^{a-a_i-1}\right\}.$$

q_{ai} is the probability that a foreign atom with a_i other foreign atoms as nearest neighbors will make a jump in the lattice, a is the total number of nearest neighbors, δ is the interatomic spacing and f is the fractional atomic concentration of foreign atoms. The statistical terms in the bracket in the above expression change very rapidly with f. While the detailed dependence of D on concentration is determined by the relative magnitudes of the q_{ai}, it would seem that this dependence is conditioned in large part by the statistical terms.

G2. The Effect of Grain Structure on the Electrical Conductivity of Semiconductors. B. GOODMAN, *University of Pennsylvania.*—Only the effect due to the discontinuities introduced into the periodic lattice potential is considered, although there are probably other phenomena occurring at the grain boundaries which also hinder the flow of electrons. The boundary layers can be considered as local regions at very high "temperatures" with the atoms displaced up to half the interatomic distance. A simplified calculation shows that the mean free path relating to the grain size is approximately equal to the linear dimension of the grain, as might be expected. The added resistivity may sometimes be comparable with that part of the room temperature resistance of silicon and germanium semiconductors due to lattice vibrations. However, it is probably always small compared to the total resistivity which is caused mostly by the scattering from charged impurity ions. These ions result from the excitation of electrons to the otherwise empty conduction band or from the capture of electrons by acceptor impurities in the lattice.

G3. The Plastic Deformation of Zinc as a Function of Strain Rate. SOLOMON LASOF,* *University of Pennsylvania.*—The influence of strain rate on the plastic behavior of single crystals of high purity zinc deformed by compression at constant strain rates of relative magnitude $1.08\times10^7:81:9:1$ has been investigated. The highest strain rate studied corresponds to an impact velocity of 690 cm sec.$^{-1}$. Room temperature stress-strain, or load-compression, curves were obtained for single crystal specimens of various orientations and for polycrystal specimens having a grain size of about 2 mm. All specimens were right circular cylinders 9.5 mm long and 4.75 mm in diameter. The direction of compression was along the cylinder axes. For favorably oriented single crystals, varying the speed of deformation was found to have little or no effect for the three relatively low strain rates studied. Definite evidence for a speed effect was found for the high strain rate. Polycrystals and unfavorably oriented single crystals showed no speed effect for relatively small deformations; but a marked speed effect was observed for larger deformations throughout the range of strain rates studied.

* Now at RCA Laboratories, Princeton, New Jersey.

G4. Recrystallization of Quartz as a Result of Flexure. D. D'EUSTACHIO, *Bliley Manufacturing Corporation, Erie, Pennsylvania.*—The manner in which quartz wafers change from single crystals to "poly-crystalline" material when they are thinner than 25 microns, has been described.[1] Further studies show that the material thus formed is composed of a number of comparatively poor crystals. The area of these crystals varies from a few tenths of a square millimeter to several square millimeters. The photograph of such a crystal, obtained with a Bragg spectrograph using filtered copper radiation, is a network of broad, curved lines. The character of a radiograph of the same areas taken after the quartz is "cold-worked" by flexing the thin plate a few times is entirely different. It is now composed of several short, sharp, straight lines. As the crystal is rotated through several degrees the pattern changes continuously, though retaining the same character. The evidence appears to point to recrystallization of quartz on mild cold-working.

[1] D. D'Eustachio and S. B. Brody, Paper presented at the New York meeting of the American Physical Society, January, 1946.

G5. Oscillographic Study of the Dielectric Properties of Barium Titanate. A. DE BRETTEVILLE, JR.,* *Laboratory for Insulation Research, Massachusetts Institute of Technology.*—Dielectric measurements on barium titanate and solid solutions of barium and strontium titanates indicated that these materials were a new class of ferroelectric compounds exhibiting saturation of the dielectric flux density with increase of field strength.[1] The dielectric properties of such non-linear circuit elements can best be studied throughout the changing and discharging cycle by the oscillograph method of Sawyer and Tower.[2] Barium titanate was investigated by this method over a temperature range from -175°C to $+135$°C at field strength of 59, 134, 234, 580, and 4800 volts per cm. Peaks in the dielectric constant were observed near -70°C, $+10$°C, and 120°C. As the field strength was increased, the two lower peaks increased in magnitude and all peaks shifted to slightly lower temperatures. The loop area which is proportional to the loss per cycle also exhibits irregularities at these three temperatures.

* Present address: Squier Signal Laboratory, Fort Monmouth, New Jersey.

[1] "High dielectric constant ceramics," Laboratory for Insulation Research, Report VII (August 1944), N.D.R.C. 14-300.

[2] C. B. Sawyer and C. H. Tower, Phys. Rev. 35, 269 (1930).

G6. Temperature Coefficients of Interfacial Polarization in Dielectrics. R. F. FIELD, *General Radio Company.*—Gross and Denard[1] have shown by means of current-time curves that a permanent charge may be stored in a capacitor made of carnauba wax by charging it at an elevated temperature and then cooling to a lower temperature. On discharge only that charge is recovered which could be stored at the lower temperature. The remainder is "frozen" in. Graphical analysis of the discharge current curves by the method of Cole and Cole[2] shows that temperature coefficients of all three polarization parameters, change in dielectric constant, relaxation time and storage coefficient are positive. This is in distinction to corresponding negative values for most dipole polarizations. Similar experiments with capacitors made of oil-filled paper, glass steatite, and mica show a positive temperature coefficient of change in dielectric constant and a "frozen" charge when the capacitor is cooled. It seems reasonable to expect similar behavior for other materials.

[1] B. Gross and L. F. Denard, Phys. Rev. **67**, 253 (1945).
[2] K. S. Cole and R. H. Cole, J. Chem. Phys. **10**, 98 (1942).

G7. Thermodynamics of Relaxation Processes. G. E. KIMBALL, *Columbia University.*—Relaxation processes can be divided into two classes: simple and complex. A simple relaxation process is defined as one which can be described in terms of a single variable in addition to the temperature and the external stresses on the relaxing material. For a simple relaxation process a thermodynamic variable X can be introduced which has the property that an infinitely rapid reversible process can be characterized by the condition $dX=0$. For any process in which there is equilibrium between the material and its environment, the energy change can be expressed in the form

$$dE=TdS-\Sigma\sigma d\epsilon+YdX,$$

where σ and ϵ represent the external stresses and the corresponding displacements, and Y is the thermodynamic variable conjugate to X. For slow reversible processes $Y=0$. From this fundamental equation many thermodynamic relationships for slow and rapid processes can be derived.

G8. On the Statistical Mechanics of Systems Involving Molecular Flow. GEORGE JAFFÉ, *Louisiana State University, Baton Rouge, Louisiana.*—If the method of statistical mechanics is to be extended so as to include phenomena like heat conduction or viscosity, the distribution function must be made anisotropic. This can be done, in analogy to Boltzmann's gas kinetic treatment, by multiplying the distribution function for the canonical ensemble by a series progressing by powers of all moments. The distribution function so obtained must be subjected to Gibbs' principle of "conservation of density-in-phase" which thereby takes the place of Boltzmann's integro-differential equation. Thus a system of differential equations for the coefficients of the distribution function is obtained. The treatment of the stationary case leads to satisfactory results under isothermal conditions but fails to determine the heat current in case of a temperature gradient. It, therefore, becomes necessary to solve the time-dependent equations. This can be done, for a linear time-dependent external potential, by a method of successive approximations, and leads to the determination of the heat current and the temperature gradient. Their ratio still depends, in a significant way, on the time rate of change but yields, under suitable restrictions, the time-independent coefficient of heat conduction.

G9. The Stationary Solution of the Fokker-Planck Equation for a Reflecting Boundary. T. H. BERLIN, *University of Michigan.*—The Fokker-Planck Eq. (1) in one dimension describes the diffusion, in x, of heavy particles, subject to an external force $F(x)$, in a medium of temperature T and friction coefficient η.

$$\frac{\partial}{\partial v}\left\{\frac{\eta kT}{m^2}\frac{\partial f}{\partial v}+\frac{\eta}{m}vf\right\}=\frac{\partial f}{\partial t}+v\frac{\partial f}{\partial x}+\frac{F(x)}{m}\frac{\partial f}{\partial v}. \qquad (1)$$

Wang and Uhlenbeck[1] conjectured that if a reflecting boundary is required, at $x=0$, the appropriate boundary condition at $x=0$ is $f(0, v, t)=f(0, -v, t)$. It will be shown that in the stationary case the Maxwell-Boltzmann solution is *uniquely* determined by the suggested boundary condition. The proof covers an arbitrary force $F(x)$ and requires weak conditions, in a physical sense, on the distribution function $f(x, v)$. The essence of the proof lies in showing that the diffusion current in velocity space due to collisions between heavy particles and particles of the medium is zero. Similarly, it can be shown that the boundary condition $f(0, v)=0$ for $v>0$ (conjectured for an absorbing wall) leads to a stationary solution identically zero.

[1] M. C. Wang and G. E. Uhlenbeck, Rev. Mod. Phys. **17**, 323 (1945).

G10. Preliminary Studies on the Design of a Microwave Linear Accelerator.* J. HALPERN, E. EVERHART, R. A. RAPUANO, AND J. C. SLATER, *Radiation Laboratory, Massachusetts Institute of Technology.*—We have began the study of several problems connected with the application of microwaves to the acceleration of electrons, namely, the problem of feeding energy from a pulsed magnetron into a high Q cavity; the locking of several magnetrons in phase; and the coupling of many cavities together so that they are excited in a single desired mode. The output of a tunable magnetron operating at 2800 megacycles, with a peak power output of approximately one megawatt and pulsed at two microseconds, was divided between a cavity and resistive load such that 70 percent of the power was fed into the cavity. The magnetron locked to the frequency of the cavity, and from measurements of power into the cavity and its shunt resistance, the peak voltage (across 5 cm of gap) was estimated to be in the neighborhood of two million volts. Preliminary results will be given on phasing of magnetrons and methods of coupling cavities.

* This paper is based on work done for the Office of Scientific Research and Development under contract OEMsr-262.

G11. Phase Stability of Synchrotron Orbits. N. H. FRANK, *Massachusetts Institute of Technology.*—Calculations have been made investigating the phase stability of synchrotron orbits, extending the analysis of Veksler[1] to the case of variation of magnetic field with radius. The first-order theory, using number of revolutions as independent variable, indicates phase stability for small oscillations about the stable phase. Studies are continuing for large amplitudes of oscillation and the bunching process in the betatron-synchrotron transition.

[1] Vaksler, J. Phys. U.S.S.R. **9**, 153 (1945).

H1. System for High Speed Counting of Nuclear Particles. H. L. SCHULTZ, *Yale University.*—The system, designed for high resolution counting of charged particles, is composed of the four following units. (1) Ionization chamber with high collecting field. (2) Pre-amplifier (attached to the ionization chamber) making use of a stable negative capacitance created by positive feedback in a wide band, low phase shift amplifier. This makes possible an input circuit of wide band width for moderately high input resistance. The output connects to a terminated 75-ohm transmission line. (3) Main wide band amplifier with calibrated attenuator for pulse height measurements. (4) Frequency meter with a biased diode circuit to establish an accurately known counting level. This instrument indicates frequency directly from 0 to greater than several hundred kc/sec. and can be used for either random or uniform spaced pulses. Measurements have shown that electrical pulses, corresponding to alpha-rays in the chamber, of the order of 10^{-6} sec. duration are realized with no special sharpening devices used. The system has been used to record fast protons and deuterons at rates exceeding 10^4 per minute with small error. This type of system has also been designed with time of flight experiments in mind.

H2. Use of a Proportional Counter for Meson Detection. E. C. POLLARD, *Yale University.*—Experiments using a small proportional counter operating at about 20 cm pressure of argon show that oscilloscope deflections proportional to ionization are readily obtainable. The operation of the counter is simplified and made faster by using an input circuit as devised by H. L. Schultz. Estimates of the ionization produced by RaE beta-particles by comparison with Po alpha-particles can be made within a factor of two with certainty and probably much better with adequate collimation. The counter operates satisfactorily in a magnetic field of several thousand gauss. It is proposed to combine such a counter with two Geiger counters arranged in a definite circular arc to operate in triple coincidence. By correct setting of the detection level of the proportional counter and a magnetic field applied across the counter the coincidences can be made to be operative for protons, electrons, or mesons.

H3. Improved Decade Counting Circuit.* VICTOR H. REGENER, *University of New Mexico.*—Ten triodes are used for triggering a ring-of-ten consisting of ten pentodes type 6AK6 through ten states of electrical equilibrium. If twin-triodes type 6J6 are used as triggering tubes, two pairs of input terminals can be provided for clockwise and counter-clockwise feeding (adding and subtracting), respectively. This is applicable to differential counting-rate measurements on two sources. While this circuit uses twenty tubes per ring-of-ten it has a high degree of stability and there are only ten resistors and no condensers. As was the case with previously described circuits, several of these rings can be connected in cascade. With the addition of five resistors to a ring, the number of counted events can be indicated on the screen of a small cathode-ray tube. The resolving time of this circuit (the smallest time interval between two events to be counted separately) is two microseconds.

* Work was done at the University of Chicago.

H4. Organic Vapors for Self-Quenched G-M Counters. E. DERMATEOSIAN AND H. FRIEDMAN, *Naval Research Laboratory.*—A study was made of the characteristics of self-quenched G-M counters filled with mixtures of argon and 28 different organic vapors comprised mainly of aliphatic halides and alcohols. Threshold voltage, length and slope of plateau, sparking voltage, and sensitive volume were observed for each vapor. Methylene bromide, propylene bromide, propylene chloride, nitromethane, and nitroethane produced counters with good characteristics. Marked differences in behavior from that normally observed with alcohol quenched tubes were obtained with methylene bromide vapor. Useful "plateaux" extended over 2000 volts with slopes of 3 percent per 100 volts. Life tests of 10^9 counts produced little change in tube characteristics. No effects of the cathode composition or treatment on the performance of the methylene bromide-argon counters could be detected. The photo-sensitivity of a copper cathode tube was greatly suppressed for wavelengths as low as the ultraviolet transmission limit of fused quartz. These properties may be explained by the experimental observation that the sensitivity of the counter decreased very rapidly with distance from the wire, limiting the sensitive volume of the counter to a small region around the wire.

H5. Influence of Multiple Scattering on Curvature Measurements. H. A. BETHE, *Cornell University and Consultant at General Electric Research Laboratory.*—It has often been attempted to determine the mass of a particle from the measurement, in a cloud chamber, of its curvature in a magnetic field and its residual range. Great caution is necessary in evaluating such experiments because of the multiple scattering of the particles by the gas atoms in the chamber. Evaluation shows that the curvature measurement is only significant if the velocity of the particle is greater than a certain critical value, i.e., that only tracks of relatively *small* curvature are significant. In the measurements made recently on the GE betatron, argon was used as the cloud-chamber gas and the magnetic field was 1000 gauss. In this case the critical velocity is about 0.1 the velocity of light. Curvature measurements on tracks ending in the chamber are therefore in general not significant. To reduce the multiple scattering a gas of small atomic number should be used, either hydrogen or helium.

Higher magnetic fields are also desirable. The most promising method is to use a thin plate across the cloud chamber and to measure the curvature on both sides of the plate. With hydrogen, this permits the determination of the meson mass to about 10 percent.

H6. Fluctuations in Measurements of Ionization per Centimeter of Path in Proportional Counters. W. F. G. SWANN, *Bartol Research Foundation of the Franklin Institute, Swarthmore, Pennsylvania.*—In experiments of Swann and Weisz cited in this programme, it became desirable to compare the ionization produced by an individual mesotron in traveling equal path lengths in two similar proportional counters. Wide differences were found in such pairs of observations, the path length being about 20 cm at a pressure of 40 cm (Hg) in argon. A proposed explanation is as follows: The mesotron ejects secondaries along its path, and these in turn emit tertiaries, and so on. The fraction of the secondaries emitted with energies between Q and $Q+dQ$ is, on the average, AdQ/Q^2, where A is a constant, and the lower and upper limits are customarily taken as 10 volts and 10^8 volts, respectively. From this it results, for example, that half of the total ionization is produced by secondaries of energy greater than 30,000 volts. In a tube of normal dimensions, the situation is modified by the limited active range of the secondaries; nevertheless, these events of high energy are so rare in a mesotron path length of about 20 cm that fluctuations are enough to account for large differences between the total ionization recorded for a single mesotron ray in passing successively through equal lengths in two similar proportional counters.

H7. The Ionization Spectrum of Cosmic-Ray Electrons and Mesotrons. PAUL B. WEISZ AND W. F. G. SWANN, *Bartol Research Foundation of the Franklin Institute, Swarthmore, Pennsylvania.*—With a proportional counter arrangement a spectrum of specific ionization values was obtained for about 800 cosmic-ray particles with and without lead shield. Without lead two major peaks were obtained. With 11.5 cm lead the second (higher ionization) peak virtually disappeared. Assigning the first peak to mesotrons, the second to electrons, and averaging the ionization values for each peak, one finds that the average ionization of mesotrons is only about 68 percent of that of the electron component. Both peaks show some "spread" in ionization values, the mesotron peak being particularly broad. Taking the energy distribution from cloud-chamber data, and calculating the resulting ionization spectrum from the normal Bethe-Bloch ionization formula one finds a much smaller difference in average ionization between mesotrons and electrons, and a spread in values not sufficient to account for the experimental spread. However, specific ionization formulae yield average energy-losses, while these experiments have to be analyzed in the light of the statistical distribution of energy-losses as applied to a finite sample of "trials" (primary ionization events), each measurement representing a sample in this sense. Comparing mesotron-electron ionizations, mesotron spin and magnetic moment may not be negligible should there be mesotrons of small rest masses.

H8. Production of Mesons by Electrons. HERMAN FESHBACH, *Physics Department, Massachusetts Institute of Technology.*—The production of "pseudoscalar" mesons originating in the meson field associated with the nucleus has been calculated using the Weiszäcker-Williams method of impact parameters. In the Lorentz system in which the electron is at rest, the nucleus may be replaced by mesons according to a formula given by Heitler and Peng. These mesons are then scattered by the electron. The results for this collision have been calculated by Corben and Schwinger. Using the criterion that the electron, in the system in which the nucleus is at rest, must at least lose an energy equal to the meson mass, it is possible to compute the cross section for the process. Calculation of the production of other meson types by this method is in progress.

H9. Non-Electrical Scattering of Charged Mesotrons. GERHART GROETZINGER AND LLOYD SMITH, *Ohio State University.*—Counter experiments were performed to obtain further data on the "wide angle" scattering of mesotrons. A vertical telescope with 13 cm of lead between its two counters was placed above a 4.5-cm lead block and a second telescope with 15 cm of lead between the counters was pointed at the lead block from below at an angle of 25°. In addition, the lowest counter was surrounded by at least 12 cm of lead to reduce the effect of showers. To determine the number of mesotrons scattered by the 4.5-cm block into the lower telescope, fourfold coincidences were recorded with and without the scattering block in position and the difference compared with the number of mesotrons traversing the upper telescope. Out of 190,000 incident mesotrons, 30 ± 14 were scattered into the lower telescope. Calculations of single and multiple Coulomb scattering in the various lead blocks show that a negligible portion of the 30 counts may be attributed to electrical scattering. It follows that the differential cross section for the non-electrical scattering of mesotrons of energies greater than 6×10^8 ev is of the order of 1×10^{-28} cm^2 per unit solid angle for the angular range 15°–35°.

H10. Determination of the Average β-Ray Energy in Artificial Radioactivity and Its Use in Radiation Dosimetry. L. D. MARINELLI, R. F. BRINCKERHOFF, *Memorial Hospital, New York,* AND E. H. QUIMBY, *College of Physicians and Surgeons, Columbia University.*—In many biological and medical studies where radioactive isotopes are used it is important to estimate rather closely the radiation dose delivered to living tissues by β-radiation. It has been shown[1] for β-ray isotopes that the dose is proportional to the average kinetic energy $\bar{E}$ of the β spectrum. $\bar{E}$, however, is infrequently stated in the literature. Values of $\bar{E}$ obtained from several β-ray spectra by direct graphical computation will be given. In addition it will be shown that once the energy limit, E_{max}, of a spectrum is known (and in the case of complex spectra the relative proportions are given), $\bar{E}$ can be calculated satisfactorily (±6 percent) from the Fermi β-ray distribution function.

[1] L. D. Marinelli, Am. J. Roentgen. Rad. Therapy **47**, 210 (1942).

H11. A Convenient Dosage Unit for Radioactive Isotopes Internally Administered. G. FAILLA, *College of Physicians and Surgeons, New York.*—When irradiation equilibrium exists at a point in a mass of tissue, the rate of energy absorption is $3.7\times10^{10}qV$ ev/sec./gram, q being the concentration of isotope in the tissue in curies per gram and V the average energy per disintegration in ev. By incorporating the isotope in the "walls" of an ionization chamber, suitably constructed, it is possible to determine this quantity without knowing q and V. Since this quantity forms the basis of all biological dosage, it is convenient to express it in *roentgen-curies*. One roentgen-curie then represents the amount of any radioactive isotope that emits energy at the rate of 5.35×10^{13} ev/sec. (this being the amount of energy released by one roentgen in one gram of air). Since q and V (especially V) are difficult to measure accurately, the practical advantages of the scheme are obvious. For a given isotope, measurements of this type need be made only once. Thereafter ordinary methods suffice.

H12. A Radium Source Ion Gauge. G. L. MELLEN, *National Research Corporation* (Introduced by R. L. McCreary).—An ion gauge using a radioactive source is described. Constructional details are given and a brief coverage is made of the d.c. amplifier circuits associated with the gauge. Designed to measure pressures between one micron and ten millimeters, the gauge is not harmed by exposure to any pressure. Ionization is produced by the alpha-particles from a small "source" plaque containing approximately 200 micrograms of radium. The active deposit is a gold-radium alloy bonded to a silver backing and is only a few microns in thickness so that it is a highly efficient alpha-emitter. Since ionization is the mode of pressure measurement, the gauge response is a linear function of pressure throughout its operating range. Extension of the range allows for calibration at any higher pressures. By suitable choice of gauge constants, a measuring device may be made for any pressure interval. Of rugged mechanical construction, this gauge has found immediate use in the high vacuum field.

J1. A Pulsed Mass Spectrometer with Time Dispersion. W. E. STEPHENS, *University of Pennsylvania.*—Advances in electronics seem to make practical a type of mass spectrometer in which microsecond pulses of ions are selected every millisecond from an ordinary low voltage ion source. In travelling down the vacuum tube, ions of different M/e have different velocities and consequently separate into groups spread out in space. If the ions are collected in a fixed Faraday cage and the current amplified, then pulses of current corresponding to different ion M/e will be dispersed in time. If the amplified current pulses are put on the vertical plates of an oscillograph whose sweep is synchronized with the pulses, then an M/e spectrum of the ions will be exhibited. This type of mass spectrometer should offer many advantages over present types. The response time should be limited only by the repetition rate (milliseconds). The indication would be continuous and visual and easily photographed. Magnets and stabilization equipment would be eliminated. Resolution would not be limited by smallness of slits or alignment. Such a mass spectrometer should be well suited for gas composition control, rapid analysis, and portable use. A mass spectrometer of this type is being constructed.

J2. The Ionization Potential of CH_2. A. LANGER AND J. A. HIPPLE, *Westinghouse Research Laboratories, East Pittsburgh, Pennsylvania.*—The free radical, CH_2, was produced in the ionization region of a mass spectrometer by the thermal decomposition of diazomethane. The arrangement was similar to that used previously[1] in the measurements of the ionization potentials of CH_3 and C_2H_5 from the decomposition of $Pb(CH_3)_4$ and $Pb(C_2H_5)_4$. Only preliminary measurements of the ionization potential of CH_2 are available since events have intervened which temporarily prevent the completion of the experiment. This preliminary value is $I(CH_2)=11.9\pm0.2$ volts. From the process in methane

$$CH_4+e\rightarrow CH_2^++H_2+2e$$

it is predicted that $I(CH_2)\leqq12.0$ volts.[2] The agreement of this value with that measured directly indicates the formation of CH_2^+ in methane occurs with little excitation or kinetic energy of the fragments.

[1] J. A. Hipple and D. P. Stevenson, Phys. Rev. **63**, 121 (1943).
[2] L. G. Smith, Phys. Rev. **51**, 263 (1937).

J3. Scattering and Absorption of High Voltage X-Rays in Steel. HERMAN FESHBACH AND JOHN A. HORNBECK,* *Physics Department, Massachusetts Institute of Technology.*—The passage of a parallel x-ray beam through steel has been investigated theoretically and experimentally. The x-rays were produced by electrons striking a thick gold target. The electron energy varied from one to two Mev. Using steel thicknesses up to twelve inches, intensity measurements were made of the total radiation immediately below the steel and of the "direct radiation" coming directly from the x-ray source. The difference between these is scattered radiation. The absorption coefficient of the total radiation approached a value independent of steel thickness. This, it can be shown, equals the absorption coefficient of the maximum energy x-ray present in the beam. The Klein-Nishina formula was verified. It was found that the ratio of scattered to direct radiation was proportional to steel thickness. The theory begins by resolving the incident beam into "equilibrium" energy distributions; distributions whose absorption coefficients are independent of steel thickness. An integral equation for these distributions was derived and solved approximately. Using the experimental data for the total radiation it was possible to compute the scattered radiation. The agreement with measured values was good. The effects of filtration and the angular distribution of the scattered radiation could then be calculated.

* Now at the Bell Telephone Laboratories, Inc., Murray Hill, New Jersey.

J4. Measurement of Betatron Radiation with G-M Counter. C. O. MUEHLHAUSE AND H. FRIEDMAN, *U. S. Naval Research Laboratory.*—The pulses of x-rays from a betatron are of shorter duration than the deadtime of

self-quenched Geiger-Mueller counters. As the intensity increases from zero to a maximum the counting rate varies from zero to the pulse frequency of 180 per second. The counting rate is given by:

$$N = M(1 - \exp[-N_0\bar{E}])^{\alpha},$$

where M is the betatron pulse rate, N_0 the number of quanta irradiating the counter, $\bar{E}$ the efficiency, and α the number of counters in coincidence arrangement. In monitoring radiographic exposures at the film position the efficiency of the counter should be reduced by a factor of 100 from the optimum obtainable for the betatron wavelengths. Further reduction in response can be accomplished by coincidence counting.

J5. The Insulation of High Voltages in Vacuum. JOHN G. TRUMP, *Massachusetts Institute of Technology.*—Studies from 50 to 700 kv constant potential further demonstrate the inadequacy of the field emission theory to account generally for high voltage breakdown in vacuum. Experiments are described which investigate the 'total voltage' mechanisms proposed by Van de Graaff, including positive ion emission by electron impact (A), electron emission by positive ion impact (B), and photoelectric emission. In the d.c. case these processes contribute to a steady interchange of charged particles between cathode and anode which increases with voltage until breakdown ensues. At the higher breakdown voltages the cathode gradient has diminished far below the value for field emission. Photoelectric emission may be an important contributing mechanism as the product of the particle coefficients (A) and (B) is still well below unity at voltage values close to breakdown. Measurements of electron emission by electrons with energies up to 300 kv for tungsten, steel, aluminum, and graphite are also reported. The properties of vacuum insulation for high constant potentials are discussed, as well as some preliminary results on the insulation in vacuum of high microwave voltages.

J6. A Compact High Voltage Electrostatic Generator Using Sulphur Hexafluoride Insulation. W. W. BUECHNER, R. J. VAN DE GRAAFF, A. SPERDUTO, E. A. BURRILL, L. R. MCINTOSH, AND R. C. URQUHART, *Massachusetts Institute of Technology.*—An electrostatic generator enclosed in a pressure tank 3.5 feet in diameter and 13 feet long will be described. When operated with sulphur hexafluoride[1-3] at a pressure of 200 pounds per square inch as the insulating medium, a potential of 5.6 million volts was produced. An account will be given of observations of the insulating properties at high voltages of air, nitrogen, sulphur hexafluoride, freon, and certain mixtures. Some problems associated with the charging belt, the resistors for controlling the potential distribution along the column, and other aspects of the generator will be discussed.

[1] We are greatly indebted to Professor W. C. Schumb, Director of the M.I.T. Research Laboratory of Inorganic Chemistry, for his recent research on sulphur hexafluoride and for the development of the method for producing the large amounts of the gas supplied for our use.
[2] W. C. Schumb and E. L. Gamble, J. Am. Chem. Soc. **52**, 4302 (1930).
[3] E. E. Charlton and F. S. Cooper, Gen. Elec. Rev. **40**, 438 (1937).

J7. Preparation and Physical Properties of Sulfur Hexafluoride. WALTER C. SCHUMB, *Massachusetts Institute of Technology.*—For the preparation of sulfur hexafluoride, referred to in the preceding abstract, sulfur was burned in fluorine at atmospheric pressure and the mixture of gases thus obtained, containing, besides a preponderance of the hexafluoride, other lower fluorides of sulfur, as well as some air and hydrogen fluoride, was purified by a process carried out largely in metal apparatus. This process included thermal decomposition of an unstable lower fluoride, thorough washing with water and with sodium hydroxide solution, drying with solid absorbents, and condensation as solid in Pyrex traps, from which the purified hexafluoride was transferred to steel storage cylinders by vaporization and recondensation as liquid under a total pressure at room temperature of about 350 pounds per square inch. Sulfur hexafluoride is remarkably stable and inert chemically, comparable even to nitrogen in these respects. Some of the physical properties to be discussed include melting point, sublimation temperature, critical temperature, density (as gas, solid, or liquid), vapor pressure (as solid or liquid), and heat of fusion.

J8. A Method of Determining Focal Spot Size in High Voltage Radiography. ANTHONY SPERDUTO, *Massachusetts Institute of Technology.*—The accurate determination of focal spot size in high voltage radiography presents certain difficulties not encountered at lower voltages. The more penetrating nature of the radiation prevents the use, particularly in the range of very small spots, of the conventional pinhole camera technique used at low voltage. The apparatus developed to meet this need includes two lead blocks bolted together in such a way as to from between them an accurately defined vertical slit .002 inch wide. This assembly is placed under the target and made to move back and forth along a line perpendicular to the plane of the vertical slit. A stationary film is placed horizontally beneath the moving blocks. The width of the darkened line on the film will then afford an approximate measure of the spot size in one dimension. By turning the apparatus 90° about a vertical axis, the width and position of the spot in the other dimension can be observed. A method will be described for determining the necessary correction to obtain the exact spot size. With 2 Mev x-rays, focal spots as small as .006 inch in diameter were measured, and their location on the target accurately determined.

J9. Dissociation Energies of Surface Films of Various Oxides as Determined by Emission Measurements of Oxide Coated Cathodes. HAROLD JACOBS, *Sylvania Electric Products Inc., Kew Gardens, New York.*—A mechanism of falling emission in vacuum tubes is discussed. It is demonstrated that when an electron achieves a critical kinetic energy in moving from the cathode to the anode, and if the anode is an oxide, the electrons will cause a dissociation of the oxide. The liberated oxygen will return to the cathode and falling emission will result. The critical energy of the electron starting the dissociation is found to be equivalent to the heats of formation of the oxides bombarded in the

case of five different oxides. Using this equivalence principle, the heats of formulation of two compounds are found which have not been recorded in the literature, Ta_2O_4 and ZrO. In addition, the contact potential between barium oxide cathodes and seven various oxides are determined and the work function of the seven oxides computed.

J10. The Poisoning of Oxide Cathodes by Gold. JEROME ROTHSTEIN, *Evans Signal Laboratory, Belmar, New Jersey.*—A cylindrical indirectly heated (BaSrCa) oxide cathode, central third coated, was divided into equal halves by 5-mil slots extending over most of the length of the Ni base metal. A concentric Ta anode, split, permitted measurement of current from each half of the cathode. One half of the cathode, after exposure to Au evaporated from a Pd-Au wire (80 percent Au), turned gray when cold, the other half remaining white. Emission decreased with time first for the exposed and then for both halves, after which both were uniformly very light gray. Reactivation would occur suddenly whenever the plates ran bright yellow for about a second, after which the emission decayed, decay rate increasing with increasing cathode temperature. Conclusions are that Au readily migrates (diffuses) over (BaSrCa)O and Ni, that Au inhibits emission, and that suitable thermal gradients can alter Au concentration and restore emission. It seems likely that Au exerts its maximum inhibiting effect when present at the outer surface of the oxide.

J11. Secondary Emission of Thermionic Oxide Cathodes. J. B. JOHNSON, *Bell Telephone Laboratories, Inc.*—Secondary emission from thermionic oxide layers has been studied by the use of short pulses of primary electron bombardment, in the micro-second range. The number of secondaries emitted per primary, δ, resembles in general that of insulators rather than that of metals. It reaches unity at about 30 ev primary energy, and a maximum of 4 to 10 in the region of 1200–1500 volts. The cold oxide has the higher δ, but acts as an insulator and quickly acquires a surface charge that limits the escape of secondaries. As the temperature is raised δ decreases from about 8 and remains nearly constant in the neighborhood of 5 between 500° and 850°C. The high temperature value is fairly reproducible but that for the lower temperature is more variable, being apparently sensitive to matter evaporated from the source of primary electrons. The exponential rise of δ with temperature which has been reported[1] is found not to be caused by a true secondary emission but by a temporary increase in thermionic activity resulting from the bombardment.[2]

[1] Morgulis and Nagorsky, J. Tech. Phys. U.S.S.R. **5**, 848 (1938).
[2] J. B. Johnson, Phys. Rev. **66**, 352 (1944).

J12. Velocity of the Anode Spark produced in $CuSO_4$ Solutions by Application of an Impulsive Potential. HUGH F. HENRY, *University of Georgia.*—If a high potential is applied impulsively across two electrodes immersed in a conducting solution, a spark will appear at one, or both, of the electrodes and proceed across the interelectrode space.[1,2] A 0.5-mf condenser was charged to 20 kv potential which was applied to pointed copper electrodes in the solution. The anode spark velocity was determined from measurements of the lengths of the streamers produced when the potential was applied for a predetermined time interval. Gap spaces of 10 to 50 mm and $CuSO_4$ solution concentrations of 1 to 5 g/liter were investigated. In no case was a spark shorter than about 5 mm observed when time interval differences of 0.5 microsecond were used. Beyond that distance, the spark velocity was independent of the interelectrode space for concentrations less than 2.5 g/liter, but at higher concentrations, a velocity dependence was found for gaps longer than 30 mm. For a concentration of 2.5 g/liter, the velocity was 450 m/sec., varying to 600 m/sec. for a 1 g/liter concentration and 1400 m/sec. for a 5 g/liter concentration.

[1] L. B. Snoddy and J. W. Beams, Phys. Rev. **55**, 879 (1939).
[2] Hugh F. Henry, Phys. Rev. **57**, 939 (1940).

J13. High Velocity Vapor Jets in Sparks at Mercury Electrodes. J. R. HAYNES, *Bell Telephone Laboratories, Inc.*—Photographs show that when sparks of microsecond duration are made to pass in hydrogen gas to a mercury surface, a jet of high velocity vapor is ejected from the mercury regardless of polarity. Measurements of the velocity of these jets were made through the use of a photo-multiplier cell. It was found that the jet from a mercury cathode has an initial velocity of 1.9×10^5 cm/sec. and that from the anode is 1.5×10^5 cm/sec. These velocities are found independent of current or gas pressure, but decrease linearly with distance from the electrodes. Through Stark effect broadening of the hydrogen β line the ionization is shown to be of the order of 30 percent. These jet velocities may be accounted for on the assumption that the momentum of the anode jet is acquired by positive ions in the anode drop, and that of the cathode jet by both negative and positive ions in the cathode drop. A close relationship exists between these jets and those found by Tanberg in the vacuum arc.

K2. Absorption in Oxygen at One-Half cm. ROBERT BERINGER,* *Radiation Laboratory, Massachusetts Institute of Technology.*—The absorption of ½ cm electromagnetic waves in gaseous O_2 and several O_2–N_2 mixtures has been measured as a function of wave-length and pressure. Microwave radio techniques were used and will be described. The theory of Van Vleck predicts a band of resonant absorption lines in the region of ½ cm wavelengths. Although these lines are not resolved at atmospheric pressure, the collision-width of the individual lines can be deduced from a comparison with the observations. At atmospheric pressure a collision-width (half-width at half-intensity) in the range .02 to .05 cm^{-1} brings the theoretical and observed absorption coefficients into good agreement, both as regards absolute value and variation with wave-length. Furthermore, the agreement is excellent at .54 cm where the theoretical absorption coefficient is quite insensitive to the collision-width. The observed pressure dependence of the absorption coefficients is also in good agreement with the theory, and it is found empirically that the absorption per O_2 molecule is a function of

the total gas pressure alone. The sensitivity of the apparatus was not great enough to measure the absorption at low pressures where the lines are resolved.

* Present address, Sloane Physics Laboratory, Yale University, New Haven, Connecticut.

K3. A Radiometer for Measuring Thermal Radiation at Microwave Frequencies.[1] R. H. DICKE,[2] *Radiation Laboratory, Massachusetts Institute of Technology.*—In addition to the usual power sensitivity, a microwave radiometer may be given a temperature sensitivity rating. The temperature sensitivity of a radiometer is defined as the minimum change in the temperature of a black body which can be detected. The minimum detectable power of the radiometer to be described is 10^{-16} watts. Its measured temperature sensitivity is $\frac{1}{2}$°C. The radiometer operated in the region of 1 cm, but the same techniques are applicable at longer wave-lengths. The radiometer consists of a superheterodyne receiver with a wide band intermediate frequency amplifier followed by a second detector and narrow band 30 c/sec. amplifier. The input circuit to the receiver contains a motor-driven eccentrically-mounted modulating wheel which dips 30 times a second into a slot in the wave guide feeding the receiver. When the wheel is out of the wave guide, the radiation intercepted by the antenna is able to get into the receiver. Thus the output from the second detector of the receiver varies by an amount indicative of the difference in the radiation received from the modulator wheel and that received from the antenna. This modulation frequency is then detected by comparison methods.

[1] This paper is based on work done for the Office of Scientific Research and Development under Contract OEMsr-262.
[2] Now with Princeton University.

K4. The Absorption of 1-cm Electromagnetic Waves by Atmospheric Water Vapor.[1] R. L. KYHL, R. H. DICKE,* AND ROBERT BERINGER,** *Radiation Laboratory, Massachusetts Institute of Technology.*—The isolated weak absorption line of water vapor at a wave-length of 1.3 cm has been measured recently by several others, namely J. A. Saxton, J. M. B. Kellogg, and J. W. Miller and R. S. Bender. The present authors have determined the atmospheric absorption indirectly by measuring the thermal radiation from the atmosphere, using the microwave radiometer of R. H. Dicke. With the addition of the humidity and temperature obtained from meteorological soundings it is possible to determine the absorption of the entire atmosphere, and to separate the contribution due to water vapor. Measurements were made at wave-lengths of 1.00 cm, 1.25 cm, and 1.50 cm. The observed atmospheric attenuations due to water vapor at these wave-lengths are, respectively, 0.011, 0.026, and 0.014 db/km/(g H_2O/m^3). From these results it was deduced that the absorption line is centered at a wave-length of 1.34 cm and has a width of 0.11 cm^{-1}. These results are, within the rather broad limits of error, in fair agreement with those of other observers. This absorption was predicted theoretically by Van Vleck, in an unpublished report, using results of infra-red measurements. The observed line width and position are in agreement with the theory but the absolute absorption observed is greater than predicted.

* Now with Princeton University.
** Now at Yale University.
[1] This paper is based on work done for the Office of Scientific Research and Development under Contract OEMsr-262.

K5. Absorption of Microwaves by Water Vapor.* STANLEY H. AUTLER, GORDON E. BECKER, AND J. M. B. KELLOGG, *Columbia Radiation Laboratory, Columbia University.*—A determination of the location and shape of the water vapor absorption line situated in the cm wave-length region has been made by a new method. Radiation is fed into a cubical copper cavity 8½ ft. on an edge. Strings of thermocouples with alternate junctions coated with a "lossy" material are placed at random in the cavity. The e.m.f. of these couples is proportional to the Q of the cavity and its contents (see following abstract), and a measurement of the change in e.m.f. with humidity yields a value for the losses in the water vapor provided the Q of the cavity is known. This quantity may be determined from additional measurements taken with an aperture opened in the side of the cavity. The wave-length range between 0.7 cm and 1.69 cm has been explored. The peak of the absorption curve is at $\lambda = 1.33$ cm and the attenuation there is 0.044 db per nautical mile for 1 g of water vapor per cubic meter.

* This paper is based on work done for the OSRD under Contract OEMsr-485.

K6. Theory of a Microwave Spectroscope.* WILLIS E. LAMB, JR., *Columbia Radiation Laboratory, Columbia University.*—The measurement of the absorption of centimeter radiation in water vapor described by Autler, Becker, and Kellogg (preceding abstract) is based on the assumption that the thermocouple readings are proportional to the Q of the cavity and its contents. The conditions for this are investigated theoretically and seem to be well satisfied in this experimental case. An expression for the Q of a hole in the wall of the cavity is derived for use in the measurements of Q's on an absolute scale.

* This paper is based on work done for the OSRD under Contract OEMsr-485.

K7. Absorption of Microwaves by Gases II. JOHN E. WALTER and W. D. HERSHBERGER, *RCA Laboratories, Princeton, New Jersey.*—The absorption coefficients and dielectric constants of sixteen gases have been measured at the two wave-lengths $\lambda = 1.24$ cm and $\lambda = 3.18$ cm. The gases are H_2S, SO_2, COS, $(CH_3)_2O$, C_2H_4O, NH_3, six halogenated methanes, and three amines. Certain improvements in waveguide technique are described; these improvements permit detection of absorption coefficients as small as 0.2×10^{-4} cm^{-1} and measurement of larger coefficients with an accuracy of ±5 percent. The measured dielectric constants at these wave-lengths are essentially equal to the static values. A quantitative interpretation of the absorption coefficients in terms of the known structure and spectra of the individual molecules is given. The theory indicates that all heavy non-planar molecules which possess a permanent dipole moment should show appreciable absorption in the microwave region.

K8. Thermal and Acoustic Effects Attending Absorption of Microwaves by Gases. W. D. HERSHBERGER, *RCA Laboratories, Princeton, New Jersey.*—The conversion of microwave energy into thermal and acoustic energy by the use of any of the gases which absorb microwaves is described. Thermal conversion may be shown by confining an absorbing gas in a cavity resonator which communicates with a manometer, then impressing a microwave field on the gas and noting the temperature rise. In this device, a rise of 0.5 degree per watt of average microwave power is observed. The response is rapid enough to follow line voltage fluctuations and is governed by the thermal capacity of the enclosed gas. Sound, both audible and supersonic, is generated in an absorbing gas liberated in a modulated microwave field, or confined in a rubber container held in a field, with the character of the sound determined by the modulation. A gas-filled resonator capable of detecting 10 milliwatts of microwave power is described which consists of a cavity which resonates electrically to the microwave frequency and acoustically to the modulating frequency. A piezo crystal coupled to one end of this absorbing column is employed and the device functions as a square-law detector.

K9. Interpretation of Cosmic Noise—Radio Waves from Extraterrestrial Sources. CHARLES HARD TOWNES, *Bell Telephone Laboratories, Inc., Murray Hill, New Jersey.*—Interstellar ionized gas is proposed as a source of radio waves observed from the milky way.[1] This gas appears nearly opaque for wave-lengths longer than a few meters, and quite transparent for wave-lengths shorter than a few centimeters as shown by the theoretical formula below. With some simplifying assumptions, the apparent temperature of the milky way at frequency ν is

$$Ta = T\left[1-\exp\left(-8\times10^{-6}\frac{n^2S}{\nu^2}\right)\right],$$

where T = temperature of interstellar gas, S = distance from observer to the milky way boundary in the direction of observation, and n = density of positive ions. Reber's measurements at $\nu = 160\times10^6$ and Southworth's failure to find radiation at $\nu = 3\times10^9$ agree well with this expression using accepted values of T, n, and S although Jansky's measurements at $\nu = 18\times10^6$ give temperatures several times greater than would be expected. Some of the sun's excess radio radiation appears to be explained as similar emission from its corona.

[1] Jansky, Proc. I. R. E. **25**, 1517 (1937). Reber, Astrophys. J. **100**, 279 (1944). Southworth, J. Frank. Inst. **239**, 285 (1945).

K10. The Frequency Dependence of Radar Echoes from the Surface of the Sea. HERBERT GOLDSTEIN,* *Radiation Laboratory, Massachusetts Institute of Technology.*—Under certain conditions microwave radar reflections are obtained from the surface of the sea. It has been variously suggested that the scatterers responsible for this "sea echo" are small spray droplets, or large surfaces of the sea waves. Irrespective of the actual mechanism involved the echo intensity can be specified by a scattering cross section per unit area of the sea surface, denoted by σ. The frequency dependence of σ affords a crucial experiment for distinguishing between the proposed mechanisms. The scattering from small spray droplets would follow the Rayleigh $1/\lambda^4$ law, while the echo from surfaces of dimensions large compared to λ should be sensibly independent of wavelength. Simultaneous absolute measurements of σ have been made at wave-lengths of 9.2, 3.2, and 1.25 cm, for several sea states, using three specially designed radar systems. The observed frequency dependence varied considerably with the state of the sea, but spray drops small enough to obey Rayleigh's law are definitely excluded as the scatterers involved. On the other hand, it is difficult to account for the changes of the cross section with polarization, and the frequency dependence of these changes, solely on the basis of scattering from large sea surfaces.

* Now at Jefferson Physical Laboratory, Harvard University.

L1. Fast Sweep Synchroscope. D. F. WINTER, *Radiation Laboratory, Massachusetts Institute of Technology, Cambridge, Massachusetts** (Introduced by A. G. Hill).—This paper describes the development of a sealed tube cathode-ray oscillograph (synchroscope) used to measure time intervals of 10^{-9} second to ±10 percent. The cathode-ray tube for this instrument was designed in collaboration with the Du Mont Company, and several tubes have been built by them. Such basic problems are discussed as: (1) Effect of electron transit time under the deflecting plates of the cathode-ray tube and its effect on frequency response, (2) coaxial signal input to the deflecting plates, (3) generation of linear sweeps with speeds up to 100 inches/microsecond, (4) photographic recording of single trace writing speeds up to 300 inches/microsecond, (5) sweep speed and writing speed calibration, (6) pulse intensification of the cathode-ray tube, and (7) reduction of time jitter between the transient to be studied and the sweep to 10^{-9} second. Circuits and formulas for producing linear sweeps of any speed are given. Pictures showing simultaneous plate current and r-f build-up in a 3000 mc/sec. pulsed magnetron on a single pulse are presented.

* This paper is based on work done for the Office of Scientific Research and Development under Contract OEMsr-262.

L2. Minimal Noise Amplifiers. E. J. SCHREMP, *Radiation Laboratory, Massachusetts Institute of Technology.*—Various restricted methods of devising minimal noise amplifiers have been published, utilizing controlled variations of passive impedances attached to the low level amplifier tubes. The present unified method, employing a simple principle valid at all frequencies, consists of two successive steps: (1) for each independent *internodal* tube noise generator, apply the constraint that the ratio vanish between its output response and that of the signal source; and (2) introduce small variations from the resulting constraints, to secure a compromise in gain, bandwidth, stability, and noise figure. For a triode at low frequencies there is one such constraint. When the input and output terminals of the stage are electrodes of the triode itself, there result nine basic minimal noise amplifier types, of which three are familiar; namely, the grounded-cathode, grounded-grid, and grounded-plate. Successively wider

amplifier classes occur when the terminals are not electrodes, and when the stage includes one or more triodes. For a triode at high frequencies or a pentode[1] at low frequencies there are two independent constraints. The method applies similarly here and in general, at any frequency, when the stage considered includes tubes having one or more grids.

[1] Cf. abstract No. L3.

L3. Equivalent Noise Representation of Multi-Grid Amplifier Tubes. R. Q. TWISS[1] AND E. J. SCHREMP, *Radiation Laboratory, Massachusetts Institute of Technology.*—North and others have given equivalent circuits for the noise generated by multi-grid amplifier tubes, valid at low frequencies when all collector electrodes but one are grounded. These results are here extended to the general case where there are arbitrary impedances in all the electrode leads, by statistical and Fourier transform methods. A simpler, less rigorous derivation is also given.

For a pentode with cathode k, screen s, and anode a, the sources of noise are here represented by three statistically independent constant current generators, located, respectively, between cathode-screen (i_{ks}), screen-anode (i_{sa}), and anode-cathode (i_{ak}). Their mean square values for the frequency interval $d\nu$ are given by

$$\langle i_{ks}^2\rangle_{Av}d\nu = 2eI_s\Gamma^2 d\nu, \tag{1a}$$

$$\langle i_{sa}^2\rangle_{Av}d\nu = 2e[I_sI_a/(I_s+I_a)](1-\Gamma^2)d\nu, \tag{1b}$$

$$\langle i_{ak}^2\rangle_{Av}d\nu = 2eI_a\Gamma^2 d\nu, \tag{1c}$$

where I_s and I_a are the screen and anode direct currents, Γ^2 is the space-charge reduction factor, and e is the electronic charge. The results for the general multi-grid tube are simple extensions of Eqs. (1).

[1] Permanent address: T.R.E., Great Malvern, Worcestershire, England.

L4. The Cylindrical Antenna: Comparison of Theories and Experiment. RONOLD KING AND DAVID MIDDLETON, *Cruft Laboratory, Harvard University.*—The hypotheses and approximations underlying the integral equation of Hallén

$$\int_{-h}^{h}\frac{I_z'}{R_1}\exp(-j\beta R_1)dz' = -j\frac{4\pi}{So}[C_1\cos\beta z + C_2\sin\beta|z|]$$

are outlined and discussed. The several approximate solutions of the equation including those by Hallén,[1] Gray,[2] and King and Middleton[3] are compared with each other and with experimental results.

[1] E. Hallén, Nova Acta, Roy. Soc. Sci. (Upsala) **11**, 1 (1938).
[2] M. C. Gray, J. App. Phys. **15**, 61 (1944).
[3] R. King and D. Middleton, Quart. Appl. Math. **3**, 302 (1946); J. App. Phys. **17** (April, 1946).

L5. Antenna Impedance Measurement. D. D. KING, *Cruft Laboratory, Harvard University.*—The determination of antenna impedance is considered with reference to cylindrical dipoles. Practical approximations to the theoretical models of dipoles are examined. The elimination and compensation of errors in the associated transmission-line apparatus are discussed together with an innovation in microwave measuring-line design. Curves of recent experimental data give an indication of the present status of measuring technique.

[1] D. D. King, J. App. Phys. **16**, 8 (1945); D. D. King, Thesis, Harvard University, 1946.

L6. Electrical Breakdown in Air at Microwave Frequencies. D. Q. POSIN, *Radiation Laboratory Massachusetts Institute of Technology.**—Experiments were conducted on electrical breakdown at microwave frequencies, using air gaps, from 6 to 100 mils, in wave guide. The range in pressures used was 1 cm Hg to 2 atmospheres. The Paschen Law was found to be approximately valid in this range, as in d.c.,[1] though dependent upon the length of time that the microwave field is applied. The dependence of the breakdown field on the time-width of the applied microwave voltage pulse indicates that when breakdown occurs in a finite time the sparking condition of Holstein[2] that rate of ionization is greater than rate of diffusion must be amplified to include the width of the voltage pulse. The breakdown field was found to depend also on the frequency with which voltage pulses are applied to the gap, giving indication of the nature of the electron loss mechanism between pulses. The sparking field was found dependent on the initial ionization, when intense, as in d.c.[3]

* This paper is based on work done for the Office of Scientific Research and Development under Contract OEMsr-262.
[1] D. Q. Posin, Phys. Rev. **50**, 650 (1936).
[2] T. Holstein, Phys. Rev. **69**, 50A (1946).
[3] Varney, White, Loeb, and Posin, Phys. Rev. **48**, 818 (1935); H. J. White, Phys. Rev. **49**, 507 (1936).

L7. Complex Conductivity of Electrical Discharge in Gas at Microwave Frequencies. MELVIN A. HERLIN AND SANBORN C. BROWN, *Massachusetts Institute of Technology.*—An electrodeless discharge produced at microwave frequencies in a resonant cavity has been studied. The cavity used is cylindrical and oscillates in the $TM_{0,1}$ mode in which the electric field is parallel to the axis and maximum along the axis. The discharge takes place in a cylindrical glass tube coaxial with the cavity. The tube diameter is limited to the region of nearly uniform field near the axis of the cavity. The cavity and discharge are excited with a tunable continuous wave 3000-megacycle magnetron. The input admittance of the cavity is measured as a function of power by standing wave technique. The complex conductivity of the discharge is determined as a function of power from the measured and computed constants of the cavity. The complex conductivity as a function of power gives the voltage and current characteristic of the discharge. Voltage and complex current characteristics have been studied as a function of cavity dimensions, tube dimensions, and pressure.

L8. Characteristics of the Pre-Corona Discharge and Its Use as a Reference Potential in Voltage Stabilizers. SANBORN C. BROWN, *Massachusetts Institute of Technology.*—The sensitivity of the current to changes in voltage in the pre-corona region of electrical discharges in gases is very high. The current-voltage characteristics of the pre-corona discharge maintained by radiation from radioactive disintegration has been studied extensively. Data will be

presented showing the characteristics of this type of discharge between coaxial cylinder electrodes as a function of geometry, gas, radiation source strength, and pressure. Under typical conditions, at 2000 volts the current increases from 10^{-3} amp to 10^{-6} amp for a seven-volt change in potential. The use of this nearly constant voltage pre-corona discharge as a reference potential for simple high impedance electronic voltage stabilizers is discussed. Stabilizers of this type have been tested in routine use for controlling high voltage sources for Geiger-Müller counters. They have proved as reliable and satisfactory as the usual type of electronic stabilizers with much greater circuit simplicity.

L9. The Scattering of Electromagnetic Radiation by a Thin Circular Ring in a Circular Wave Guide. PAULA FEUER AND EDWARD S. AKELEY, *Purdue University*.—The field in a circular wave guide when a TE_{11} wave is scattered by an infinitely thin, perfectly conducting, narrow circular ring is obtained to a certain degree of approximation. Let (r, θ) be polar coordinates in the plane of the ring. The current density in the ring will vary as $C \cos\theta$. The field produced in the guide by this current is determined, and the remaining terms of the scattered field are obtained by requiring that the total tangential electric field vanish on the infinitely conducting walls of the guide. The constant C is evaluated by requiring the tangential electric field, E_θ, to vanish on the ring. The ratio of the scattered field to the incident field at a great distance from the obstacle is computed and also the position and shape of the resonance maximum. At resonance, all the incident radiation is scattered, which means that the intensity far from the ring on the side away from the source, is zero. The position of the maximum is given by the relation $ka = 1 - \delta$ where a is the radius of the ring and δ a positive quantity that approaches zero as the width of the ring decreases.

L10. A Theory of the Narrow Resonant Slit in a Wave Guide Partition. EDWARD S. AKELEY, *Purdue University*.—Boundary conditions at the slit can be satisfied by assuming such a distribution of surface magnetic current density j in the slit that the total field on the slit is zero. The following assumptions are made: (1) only the TE_{10} mode can be propagated, its transverse magnetic field being parallel to the slit and (2) the slit is so narrow that the electric vector potential F at a point on the slit is mainly due to j in immediate neighborhood of the point j and F are determined together by a method of successive approximations by making use of the relation $d^2F/dx^2 + k^2F = (a)\mu H \sin \pi x/g$ and the expression of F as an integral of j over the slit and its infinite system of images in the conducting planes. The ratio r of the amplitude of the transmitted radiation at infinity to the incident amplitude is determined. Resonance occurs at $k = \pi/2L$ for infinitely narrow slit and $r = 1$ at resonance. These results are independent of the position of slit in partition. Formulas are given for the determination of the shape of the resonance maximum and shift of same from $k = \pi/2L$.

L11. Pulse Transformer Ratings Based on Energy Considerations, and Methods of Design Based on Thermodynamical Considerations. W. H. BOSTICK, *Radiation Laboratory, Massachusetts Institute of Technology*.—A simple, yet generally applicable, equivalent circuit for most pulse transformers consists of a shunt inductance L_P (representing the core), a series leakage inductance L_L, and an effective distributed capacitance C_D across the load. The sum of the energy α stored in the core and the energy β stored in the coil may be minimized to give the conditions for maximum transfer of pulse energy to a load of impedance Z. These conditions are: (1) $(L_L/C_D)^{\frac{1}{2}} = Z$, (2) the optimum pulse length $\delta_{opt} = (2L_PC_D)^{\frac{1}{2}}$, and (3) at $\delta = \delta_{opt}$, $(\alpha+\beta) \equiv (\alpha+\beta)_{opt}$ = a minimum. Condition (3) may be achieved with (1) and (2) as constraining conditions by designing a transformer which, at the end of the pulse, is in the lowest possible energy state. The lowest possible energy state may be achieved by choosing equal energy densities, volumes, and perimeters for core and coil. Such a design procedure yields approximate analytical expressions to be used in the calculation of the optimum flux density of the core, optimum core volume, the optimum number of turns, and the value of $(\alpha+\beta)_{opt}$.

L12. A Circle Diagram for Resonant Microwave Systems. WILLIAM ALTAR, *Westinghouse Research Laboratories*.—A new circle diagram is presented for systems having an isolated single resonant mode, in addition to frequency insensitive structures of arbitrary complexities and ending in an outgoing wave guide or other transmission line. The diagram is obtained from standing wave measurements in the outgoing line performed at three or more frequencies near resonance. The diagram permits the mapping, in the complex plane of load impedances or reflection coefficients, of such contour lines as loaded resonator Q, frequency pulling, and the circuit efficiency when the resonator is electronically excited. The proof of these relations rests on field theory and establishes in effect the validity of general circuit methods in the realm of microwave applications.

L13. Robot Dynamics—Theory of Non-Linear Automatic Control Systems. MELVIN AVRAMY, *Columbia University*.—The theory of *robots* or reproducing power-amplifying systems is considered. After a general orientation the study in the first part is confined to *simple robots*, the theory of which is equivalent to that of non-linear springs with inertia and friction. The alacrity and fidelity of control are well exhibited by studying the behavior of a robot under constant tracking. Among the results obtained are: Criteria for oscillation or overdamping of non-linear robots (these are generalizations of the usual criteria for linear systems). Generally valid results on the asymptotic approach to the steady state, and the steady state itself. Through these, the asymptotic behavior of any faithful robot may be studied in terms of the two limiting cases of proportional and on-off robots which are analyzed in detail. Special emphasis is placed on the specification of conditions for *optimum performance*, i.e., minimum deviation or maximum fidelity after any given time. Charts are given with curves from which the parameter values

for optimum performance may be read off. Approximation methods for studying the entire history of non-linear robots are developed.

X1. Low Pressure Gas Discharges in Microwave TR Tubes. LOUIS D. SMULLIN, *Radiation Laboratory, Cambridge, Massachusetts and Federal Telecommunications Laboratory, New York.*—A TR tube is essentially a rapidly acting switch in a radar duplexing circuit. It breaks down in less than 10^{-9} sec. after the beginning of the transmitter pulse. The energy (about 0.5 erg) going to the receiver during this interval is the spike energy. The power going to the receiver after the discharge has formed is the arc leakage power. Both quantities are sensitive to the gas and pressure in which the discharge takes place. Measurement techniques and typical data for 10- and 3-cm TR tubes will be presented. Possible applications of these techniques to further gas studies will be indicated.

X2. Design of Copper Disk Seal TR Tubes. J. W. CLARK, A. E. ANDERSEN, AND A. L. SAMUEL, *Bell Telephone Laboratories.*—The copper disk seal method of construction for microwave vacuum tubes, in which a part of the resonant cavity is outside the vacuum envelop and so is available to the circuit designer for adjustment will be described. Such tubes are well suited for use in physical experiments as they are not restricted to use in particular frequency bands. Design principles of copper disk seal TR tubes will be discussed with reference to optimization of cavity Q and to compensation against undesirable thermal effects. Specific tube designs for use in the vicinity of 1000, 3000, and 10,000 mc will be shown.

X3. The Integral Cavity TR Switch. D. ALPERT AND S. KRASIK, *Westinghouse Research Laboratories.*—An integral cavity TR switch is one in which the resonant circuit used with the discharge gap is included within the vacuum enclosure. This design permits close manufacturing tolerances and a performance otherwise difficult to obtain at frequencies of 10,000 megacycles per second and higher. The design problems of such a switch include electrical tuning, electrical coupling, mechanical mounting, and vacuum sealing. Some of these problems have been solved in the 1B24 TR switch by the introduction of novel techniques.

X4. Gas Discharge Switches for Controlling Low Power Microwave Signals. T'ING-SUI KE* and LOUIS D. SMULLIN,** *Radiation Laboratory, Massachusetts Institute of Technology.*—In a TR tube, the keep-alive electrode is placed comparatively deep inside the lower cone to prevent excessive "keep-alive interaction." The keep-alive was placed nearer to the r-f gap so that electrons furnished from the keep-alive discharge cause an attenuation of the incoming signals. This provides an electronic switch for controlling microwave signals which are not powerful enough to breakdown the gap. Attenuation was found to be proportional to the current. Nitrogen was found to be most suitable as the gas-filling. In a modified 1B24 filled with 12-mm nitrogen, 44-db attenuation was obtained when the keep-alive current was 0.4 ma. No detectable microwave noise was introduced. The ionized gas appears to have a large microwave conductance and a comparatively small susceptance.

* Now at Institute for the Study of Metals, University of Chicago.
** Now at Federal Telecommunications Laboratory, New York.

X5. Recovery Time Measurements on TR Tubes. C. F. CRANDELL,* A. L. SAMUEL, AND J. W. CLARK, *Bell Telephone Laboratories.*—A method used for measuring the recovery time of TR tubes will be described. The principal problem is the accurate measurement of time intervals of the order of 5 to 10 microseconds. Data will be presented showing the relation between loss through the TR cavity and time for several different gases, and showing temperature effects. The variation of recovery time with operation of the tube will be discussed.

* Now at Southwestern Bell Telephone Company, Dallas, Texas.

X6. Phenomenological Theory of the TR Switch Spike. T. HOLSTEIN, *Westinghouse Research Laboratories.*—The essential feature of the initiation of a TR switch spike is the mutual interaction between the ionization in the gas and the electromagnetic field of the cavity. The time variation of the gap voltage is affected by the incident high power pulse, the cavity geometry, and the electron density at the gap; under certain conditions these effects may be described by the equation

$$\frac{2Q_L}{\omega}\dot{V} = (2R_T P_M)^{\frac{1}{2}}\phi(t) - rV.$$

Here, V is the amplitude of the gap voltage, Q_L the loaded Q, $\phi(t)$ the time variation of the incident field amplitude normalized so that $\phi(t)$ is unity when the pulse power has reached its peak, P_M, R_T the transmission shunt resistance and r a quantity proportional to the electron conductivity of the gap. Assuming the phenomenological equation $d \log r/dt = \theta V$, with θ a constant depending upon the gap spacing and the gas, we are able to solve for V for arbitrary $\phi(t)$. Explicit solutions have been obtained for $\phi \sim e^{t/\tau}$.

X7. Conductivity of Electrons in a Gas at Microwave Frequencies. HENRY MARGENAU, *Radiation Laboratory, Cambridge, Massachusetts, and Yale University, New Haven, Connecticut.*—The conductivity of electrons in gases is well understood in two limiting cases: that of low frequencies and high pressures (Langevin's formula), and of high frequencies and low pressures (free electron formula). To provide a satisfactory treatment for intermediate conditions, the distribution-in-energy of electrons in a high frequency field is here derived by kinetic-theory methods. Using the distribution law the complex conductivity is calculated as function of electron density, gas pressure and frequency of the field. From the conductivity, the dielectric constant of the medium, its extinction coefficient, etc., are deduced. Application of these results to the experiments of Montgomery, McMillan, Dearnley, and Pearsall (paper No. X8) clarifies understanding of the fundamental processes taking place in TR-tube recovery.

X8. Cross Sections for Capture of Electrons from TR-tube Recovery Measurements. C. G. MONTGOMERY, F. L. MCMILLAN, I. H. DEARNLEY, AND C. S. PEARSALL, *Radiation Laboratory, Cambridge, Massachusetts.*—To accelerate the disappearance of free electrons from a TR tube after a discharge has taken place it is customary to employ a gas which attaches the electrons to form negative ions. Because of their large masses, negative ions do not absorb energy at microwave frequencies. Observations of the attenuation of a microwave signal as a function of the time after the cessation of a discharge can be used to calculate the capture cross section by means of the theory of H. Margenau (paper No. X7). Within about a microsecond, electrons that have a high energy during the discharge period come into thermal equilibrium with the gas molecules because of elastic collisions. The capture cross sections are thus determined for the thermal energy range. Measurements with water vapor give a value of 10^{-4} per collision. In oxygen, capture takes place to form both O^- and O_2^-. In argon it seems necessary to postulate the formation of A_2^-. Many organic vapors capture electrons readily, but the ions formed are not easily identified.

X9. An Equivalent Circuit for the Microwave TR Tube. A. L. SAMUEL, *Bell Telephone Laboratories.*—A lumped circuit equivalent for a TR cavity will be presented. All the important properties of the TR (except recovery time) can be predicted from this circuit. The point of view here presented is particularly useful in system design, where the opposing considerations of low level and high level performance must be reconciled. Application of the theory to broadband TR and ATR tubes will be given.

X10. The Band-Pass TR Switch. Part I: The Switching Action, MILAN D. FISKE, *Research Laboratory, General Electric Company, Schenectady, New York.*—The band-pass TR switch consists of a number of resonant breakdown gaps uniformly spaced within a wave-guide section which is closed at either end by a resonant window and filled with low pressure gas. During the transmission pulse of the radar set a glow discharge is established across each gap and across the entrant window by the strong electric fields existing during the pulse. The loading of the window and gaps by the conductance of the discharges provides the switching action. Rapid breakdown is assured by a small steady discharge (the "keep-alive") maintained near at least one gap. When the TR is filled with argon at a pressure of 10 mm of mercury, the first gap breaks down within 5×10^{-9} second after initiation of the pulse, limiting leakage of the incident r-f energy through the tube to less than 0.1 erg. Leakage is independent of line powers ranging from 1 watt to more than 30-kw peak. Post-pulse deionization in pure argon requires more than 100 μsec. When a pressure of 0.5 mm of water vapor is added to the argon, the ion density decays to that maintained by the keep-alive in less than 3 μsec.

X11. The Band-Pass TR Switch. Part II: Linear Electrical Characteristics, WALLACE C. CALDWELL, *Radiation Laboratory, Massachusetts Institute of Technology, now at Cornell University.*—Considerable effort has been directed toward the extension of the transmission band of the TR Switch using the scheme proposed by M. D. Fiske.[1] It is possible to combine several resonant circuits in wave guide in such a way that the insertion loss due to reflection is less than 0.5 db over a 12 percent wave-length range. The absorption loss can be made as low as 0.5 db. The elemental resonant structures are described and their equivalent circuit can be regarded as shunt inductance and capacitance across the transmission line. Insertion loss as a function of wave-length are presented for one, two, three, and four resonant elements spaced along the line at equal intervals of a quarter guide wave-length.

[1] Milan D. Fiske, "A Broad-Band T-R Switch," General Electric Report (October 1943).

X12. Microwave Duplexing Circuits. H. K. FARR, *Radiation Laboratory, Cambridge, Massachusetts, and General Electric Company, Pittsfield, Massachusetts.*—The "duplex" radar system which uses the same antenna for transmitting and receiving ordinarily employs automatic electronic switches to connect the antenna alternately to transmitter and receiver. Two separate switches are frequently used although one may suffice if the transmitting oscillator satisfies certain conditions when quiescent. The techniques are discussed for connecting these switches to the radar components by wave-guide or coaxial transmission lines, and the properties of the wave-guide junctions used are described. Methods of achieving good efficiency over a range of wave-lengths are considered, especially with regard to the most serious problem, the loss of received signal. Several examples are presented of circuits for 1.25, 3, and 10 centimeter wave-lengths.

Y1. Improvements in the Stability of the FP-54 Electrometer Tube. J. M. LAFFERTY AND K. H. KINGDON, *General Electric Company.*—It was found that a considerable portion of the instability in the FP-54 is due to variations in emission from the thoriated tungsten filament. Operation of the filament at a current which neither activates nor deactivates it was found to be a good criterion for adjusting the circuits employing these tubes. Large fluctuations were observed in emission immediately after activation of the filament. Greater stability was obtained by increasing the activation time from 8 to 40 minutes. Filament end shields improved the stability, showing that some rapid fluctuations in emission occur at the poorly activated end portions of the filaments. Long-time drifts were not improved by end shields. Tubes with oxide-coated filaments gave greater sensitivity and less grid current than tubes with thoriated tungsten filaments. These tubes, however, had a tendency to drift. A split type of FP-54 was constructed with a common filament and space-charge grid, but with twin control grids and plates. Both oxide-coated and thoriated tungsten filaments were used. Operation of these tubes in a bridge type circuit eliminated long-time drift and decreased the amplitude of rapid fluctuations by a factor of ten.

Y2. Influence of Space-Charge on the Bunching of Electron Beams. L. BRILLOUIN, *Cruft Laboratory, Harvard University.*—A rigorous computation of electron trajectories within plane structures may be made, with the inclusion of space-charge effects, by use of the Llewellyn method of integration. These computations can be used for a discussion of conditions leading to intercrossing trajectories, i.e., bunching. The discussion has been carried out for a conventional plane diode, for a diode wherein electrons are injected with a given initial velocity, for a velocity-modulated beam, for a plane magnetron and for a plane magnetron with velocity modulation. In many cases it can be proved that trajectories intercross not once but twice, thus disentangling themselves after a while. This occurs only for weak bunching and disappears for strong bunching.

Y3. The Maximum Efficiency of Reflex Oscillators. E. G. LINDER AND R. L. SPROULL, *RCA Laboratories, Princeton, New Jersey.*—The theory of velocity-modulation reflex oscillators is developed and extended. The maximum efficiency with optimum electron bunching and optimum loading is shown to be

$$\eta_0 = 0.17 M^2 R_c i_1 / V_0,$$

where M is the gap efficiency, R_c is the unloaded shunt resistance, i_1 is the beam current, and V_0 is the beam voltage. Possible methods of increasing efficiency are investigated, including the use of multiple transits. The relationship between efficiency, range of electronic frequency modulation, and load resistance is discussed.

Y4. Theory of the Diode. JULIAN K. KNIPP, *Radiation Laboratory, Massachusetts Institute of Technology.*—A theory is developed for the r-f behavior of a region bounded by parallel plane grids into which electrons are injected at the first grid and none or some are reflected. The small amplitude approximation is made and variations parallel to the grids are neglected. However, the distribution in velocity of the electrons is taken fully into account and effects of space charge are included. The r-f phenomena are completely described in terms of the total r-f current (as determined by the load), the injected r-f electronic current distribution (as determined by the preceding regions), and certain impedance and transfer coefficients which are explicit functions of a resolving kernel. The resolving kernel is the solution of a Fredholm integral equation the kernel of which is calculated from the d.c. component of the injected current distribution and phase factors containing products of the r-f frequency and times of passage of electrons to planes within the region, calculated in the absence of the r-f field.

Y5. Principles of Operation of the Resnatron. F. W. BOGGS, *Westinghouse Research Laboratories.*—During the war there was developed at Westinghouse a tube for ultra-high frequency generation which, although it has many features in common with the Class C oscillator, differs from it sufficiently to warrant special consideration. This tube, which has proved to be the most powerful source of ultra-high frequencies yet constructed, is characterized by the fact that it operates with a substantial transit time, by the unusual design of its grid, and by the use of resonant cavities in the vacuum envelope. It can be shown by means of trajectory plots that a gain in efficiency can be achieved by placing a high voltage screen between the anode and the grid; and it can be further shown that better efficiencies will be obtained when the voltage of the screen is close to that on the anode. The tracing of electron trajectories through the grid shows that its action is to focus the electron beam away from the grid and the screen; and that the effective grid-cathode spacing is very small. At the same time the massive construction of the grid makes it much easier to cool.

Y6. Modulation and Tuning of Cavity Oscillators by Electron Beams.* DAVID S. SAXON,** *Radiation Laboratory, Massachusetts Institute of Technology, Cambridge, Massachusetts.*—The frequency of cavity oscillators such as the magnetron can be shifted by sending a beam of electrons through the cavity or through an auxiliary cavity which is tightly coupled to the oscillator.[1] Calculations of the frequency shift produced in this way have been carried out for simple rectangular geometries.[1,2] The theory has now been generalized so that it applies when the electron beam is sent parallel to the axis of a cylindrical cavity of arbitrary cross section which is operating in any of its H (or TE) modes. The detailed nature of the cross section enters only through a proportionality constant—the ratio of electric energy stored in the volume of the system occupied by the beam to that stored in the entire system. Since this ratio is less than unity, upper limits to the tuning can be established and the design features can be discussed from a general point of view.

* This paper is based on work done for the OSRD under contract OEMsr-262 with the Massachusetts Institute of Technology.

** Now at Philips Laboratories, Inc., Irvington, New York.

[1] L. P. Smith and C. Shulman, RCA Technical Report PTR-22C (2/14/45).

[2] A. Banos, Jr. and D. S. Saxon, Radiation Laboratory Report 748 (5/26/45).

Y7. Energy Build-Up in Magnetrons. L. P. HUNTER, *Westinghouse Research Laboratories.*—An analysis of the operation of resonant cavity magnetrons is made without regard to the mechanism of conversion of the d.c. input power into the r-f output power. The magnetron is represented by its equivalent circuit and is assumed to be essentially in equilibrium at every point of its energy build-up curve. The last assumption is shown to be reasonable on the basis of measured starting times. From the data of load impedance charts and the rise of the r-f pulse, the relation between power generated and vane voltage is deduced. By considering the division of the energy between that stored in the resonant system, and that dissipated in the load, the law of build-up is derived. The dependence of starting time on load is calculated and agrees with experiment when the extra energy stored in the connecting line is taken into account. The starting time is affected slightly by the initial noise level and becomes infinite below a minimum Q. For high Q values the starting time can be varied only by changing the energy stored in the line, which may enable one to design a line for "mode" suppression.

Y8. "Crown of Thorns" Tuning of Magnetrons.* SIMON SONKIN, *Columbia Radiation Laboratory, Columbia University.*—A mechanically tunable vane type magnetron is described. The tuning mechanism consists of a set of pins or rods ("crown of thorns") mounted so that they can be introduced into the cavities of the magnetron anode without touching the walls. Curves of the variations of wave-length and power output as a function of pin penetration are given for a magnetron in the centimeter wave-length range. Tuning of the order of 10 percent was obtained and found to be quite linear. Causes and elimination of variations in power output with wave-length are discussed.

* This paper is based on work done for the OSRD under Contract OEMsr-485.

Y9. Development of the Rising Sun Magnetron Anode Structure,* SIDNEY MILLMAN AND ARNOLD NORDSIECK, *Columbia Radiation Laboratory, Columbia University.*—Modern magnetron anode structures for generating centimeter waves are very tiny and must have a very large number of segments. Because of the many segments the problem of keeping the operating "plus-minus" mode sufficiently separated in frequency from other resonant modes of the structure is a severe one. The small size makes it difficult and costly to secure mode separation by "strapping," i.e., inserting metallic connectors between alternate segments. Some time ago, the authors engaged in a program to improve the operation of unstrapped magnetrons oscillating in a mode other than the plus-minus mode by introducing regular asymmetries in the anode structure. This led to a scheme for solving the mode separation problem for the plus-minus mode by making the resonator cavities alternately large and small, with the ratio of the resonant wave-lengths of large and small cavities in the range of about 1.5 to 2.5. The mode spectrum of such an oscillating system is described. The advantages and limitations of magnetrons possessing this anode structure are discussed. Very successful magnetron oscillators of this design have been built in the wave-length regions of one and three centimeters.

* This paper is based on work done for the OSRD under Contract OEMsr-485.

Y10. Theory of the Rising Sun Magnetron Anode.* NORMAN KROLL AND WILLIS E. LAMB, JR., *Columbia Radiation Laboratory, Columbia University.*—An electromagnetic field theory for the rising sun type magnetron anode block has been developed, from which the wave-length spectrum and the electromagnetic fields can be computed. The method is analogous to that developed by Clogston for the symmetric anode. The anode block is divided into regions of simple geometry, namely the cathode-anode space and the side resonators. In each of these regions it is possible to find a solution of Maxwell's equations for any specified boundary values of E_T, the tangential electric field. At a junction between regions of different geometry the behavior of E_T must be such that a frequency exists for which the resultant magnetic fields are continuous. E_T is partially guessed, resonance being determined by the condition that the average value of the magnetic field over the various junctions be continuous. The computed spectrum is a sufficiently good representation of the observed spectrum to be of great use in magnetron design. The method has been generalized to discuss anodes having different symmetry from the rising sun.

* This paper is based on work done for the OSRD under Contract OEMsr-485.

Y11. One Centimeter Rising Sun Magnetrons with 26 and 38 Cavities.* A. V. HOLLENBERG, S. MILLMAN, AND N. KROLL, *Columbia Radiation Laboratory, Columbia University.*—The advantages of large numbers of cavities for very short wave-length magnetrons are discussed. Difficulties of realizing operation in the plus-minus mode without disturbance from other modes are shown in a discussion of the rising sun mode spectrum. The solution of these difficulties by closing the ends of the anode is described. Pulsed operation of 26 and 38 cavity closed end magnetrons in the one to two centimeter wave-length range is described.

* This paper is based on work done for the OSRD under Contract OEMsr-485.

Y12. Space-Charge Frequency Dependence of a Magnetron Cavity.* M. PHILLIPS AND W. E. LAMB, JR., *Columbia Radiation Laboratory, Columbia University.*—The effect on the resonant frequencies of a magnetron cavity produced by the presence of a thin layer of charge surrounding the cathode is investigated. The corresponding experimental procedure is the "cold impedance testing" of a magnetron with a hot cathode in the presence of a magnetic field and a low d.c. cathode-anode voltage. A small amplitude theory is used, based on the single stream steady state. The correction to the frequency of the empty cavity due to a thin cloud of charge surrounding the cathode is given by a resonance type formula about the "cyclotron frequency," $eB/2\pi m$. The validity of the theory is limited to low level oscillations, but the comparison of theory with experimental results seems to support the existence of the single stream steady state for non-operating magnetrons.

* This paper is based on work done for the OSRD under Contract OEMsr-485.

Y13. A High Power Rising Sun Magnetron.* ARTHUR ASHKIN, *Columbia Radiation Laboratory, Columbia University.*—One of the advantages of the rising sun magnetron design is that the mode separation is independent of the anode length. This permits one to build a magnetron in which the anode is very much longer than that of the conventional strapped magnetrons. Advantage has been taken of this fact in the design of a high power 3-cm region magnetron for pulsed operation at 35 kv and 6500 gauss. Tubes have been constructed which give peak powers of 1 megawatt at an output efficiency of about 45 percent. At lower power levels efficiencies in excess of 55 percent have been observed. The circuit efficiency in these magnetrons is about 75 percent.

* This paper is based on work done for the OSRD under Contract OEMsr-485.

SP1. Enhanced Thermionic Emission from Oxide Cathodes. J. B. JOHNSON, *Bell Telephone Laboratories.*[1]—When an oxide-coated cathode in the temperature range of thermionic emission is bombarded by short pulses of electrons, current of three kinds is emitted: (1) The original thermionic current, (2) The relatively constant secondary current, and (3) A current which rises at a decreasing rate during the pulse and persists with decreasing amplitude after the end of the pulse. As seen on an oscilloscope, the emission of the third kind induced by a pulse a few microseconds in length can be observed to persist for many microseconds. It may be larger or smaller than the original thermionic current, depending on the bombarding current and voltage, on the length of pulse and on the state of the cathode. The enhanced emission follows roughly Richardson's law with the same value of b as the original emission. Its origin cannot be that of the Malter effect for the resistivity of the hot oxide is too low to support a surface charge. Similarly, rise of surface temperature owing to the bombardment is far too small to account for the increase in emission. One must conclude that the bombardment temporarily increases the thermionic activity of the oxide-coated cathode.

[1] To be presented after session J if time permits.

SP2. Radioautography With P^{32} and Sr^{89}. DANIEL Q. POSIN,* *University of Montana.*[1]—Studies were conducted on the nature and intensity of the self-rays or radioautographs produced by radiophosphorus and radiostrontium when pictures are made by rats born radioactive, eggs laid radioactive; and bacteria *E. coli* rendered radioactive by growth in a synthetic medium in which the disodium phosphate is radioactive. Approximate figures are given for radiation density and time of exposure to the negatives for producing satisfactory self-rays.

* Now at Radiation Laboratory, Massachusetts Institute of Technology.
[1] To be presented after session H if time permits.

SP3. Electron Orbits in the Synchrotron. DAVID S. SAXON* AND JULIAN SCHWINGER, *Radiation Laboratory, Massachusetts Institute of Technology and Harvard University.*[1]—Equations for the electron orbital motion in synchrotrons have been derived by a method which avoids the inaccuracies of previous treatments.[2,3] The localized accelerating field is replaced by an equivalent rotating electric field in the mathematical analysis. This situation could be physically realized in a microwave synchrotron. For small deviations from the equilibrium orbit, a fourth-order differential equation for the motion of the electron phase relative to that of the electric field is obtained which includes the effect of the changing magnetic field and of radiation losses. This equation enables one to discuss the phase motion in the various regions of operation of a device which, as has been suggested, is operated initially as a betatron. The new features are the transient effects accompanying the switching on of the electric field and of the failure of the betatron flux condition preceding operation as a synchrotron. A discussion of the characteristics of the various regimes will be given.

* Now at Philips Laboratories, Inc., Irvington, New York.
[1] To be presented after session B if time permits.
[2] V. Veksler, J. Phys. USSR 9, 153 (1945).
[3] E. M. McMillan, Phys. Rev. 68, 143 (1945).

T1. Astrophysical Phenomena and the Magnetic Current. FELIX EHRENHAFT, *New York City.*—The constant magnetic current as visualized by Hertz and experimentally demonstrated by the author permits the performance of model experiments of astronomical phenomena in the darkfield of the microscope. Ultimately no more can be done in science than to correlate phenomena and to trace them back to a common cause. The author asks whether the following is acceptable to astronomers. The photographs of spiral nebulae resemble photographs of helical photophoretic movements in the field of radiation. Phenomena similiar to the separation of Schmidt's nebula* (see also Bredichin), apparently can be explained as separation by light-positive and light-negative photophoretic movements. The formation of circulating rings in gases and liquids occurring around magnets, analogous to Saturn's rings, seem due to electric action of magnetic currents. Could not the simultaneously direct and retrograde movement of Jupiters and Saturns moons be explained in this way? Sunspots are sources of magnetic discharges, from them a magnetic current is flowing. The electric vortices in them are due to electric action of magnetic currents. A model experiment was performed demonstrating the reversibility or occasional non-reversibility of these electric vortices associated with changes of magnetic polarity. This is in accord with new results showing reciprocal effects between changes of magnetic fields and electric charges and in accord with phenomena in the sunspots.

* Physik. Zeits. 20, 93 (1919).

T2. The Measurement of Ultra-Short Time Differences. S. H. NEDDERMEYER, *Los Alamos, New Mexico.*—A device has been constructed[1] which utilizes the superposition of electromagnetic pulses to determine the time interval between the pulses.[2] The present arrangement consists of a coaxial line bent into a closed loop, and a detector coupled to any desired point on one section. Pulses are introduced at the center of the opposite section by discharging a short length of line through a matching network so that equal pulses are sent simultaneously in opposite directions. A simple two-stage detector discriminates the superposition region nicely so that when output is plotted against position, the center is located to about ± 0.5 cm. This implies that time differences can be measured to an accuracy of about $\pm 3 \times 10^{-11}$ sec. That the instrument behaves properly has been verified by noting: (a) disappearance of the superposition region when one side of the line is cut and terminated, and (b) shifting of the superposition locus when a lag is introduced on either side by inserting dielectric.

[1] Dubbed a "chronotron."
[2] Same principle has been used in a different way by M. Newman, Phys. Rev. 52, 652 (1937). It occurred to the writer independently as the electromagnetic version of the Dautriche method of comparing detonation rates in explosives.

Proceedings of the American Physical Society

MINUTES OF THE MEETING OF THE OHIO SECTION AT COLUMBUS, OHIO, MAY 4, 1946

THE Ohio Section of the American Physical Society met at Columbus on May 4, 1946 conjointly with Section F (Physics) of the Ohio Academy of Sciences. W. E. Singer was elected chairman of the Section, R. S. Shankland was elected vice chairman, Leon E. Smith was re-elected secretary. The programme follows.

The Application of the Curved Crystal Spectrograph to the Chemical Analysis of Alloys. JACK BALL AND F. C. BLAKE, *The Ohio State University.*—It was found by using a beam of x-rays from a molybdenum target that fluorescent radiation from various elements could be quite readily registered by the curved crystal spectrograph. The L-series for tungsten and lead, as well as the K-series for copper and zinc, were obtained. By using a series of bronzes of different compositions the K lines for copper and zinc were obtained even down to as low a percentage of 3 percent for zinc. This method could be applied to solid sections, metallic coatings, etc. without damage to the materials.

The Curved Crystal Spectrograph Applied to Determine the Complete Spectrum of All Orders Obtained, and the Evaluation of Same with Varying Technique. JACK BALL AND F. C. BLAKE, *The Ohio State University.*—This is a continuation of the report presented at the St. Louis Meeting of the American Physical Society. The Bragg angle for several orders of faces 100 and 110 were measured with the curved crystal method and compared with those obtained by the powder method. The effect of the useful width of the crystal was investigated. Results were obtained with both 15- and 8-inch cameras and with molybdenum, copper, and iron radiations. These values are also compared with Berquist's values and with his evaluation of the index of refraction.

On the Proper Indexing of the Faces Obtained in the Powder Method of X-Ray Analysis for α-Quartz. F. C. BLAKE, *The Ohio State University.*—Continuing the analysis reported at the St. Louis Meeting of the American Physical Society, a critical study of α-quartz has been made using Fe, Cu, and Mo K-α doublet x-rays with cameras of different radii. A study has been made of the several corrections found to be important, such as film shrinkage, absorption, proper extrapolation to large values of the Bragg angle. Allowance is made for the correction for index of refraction, and its variation with wave-length is shown.

An Instrument for Measurement of the Magnetic Properties of Samples of Small Cross-Sectional Area. EUGENE C. CRITTENDEN, JR., CHARLES S. SMITH, JR., AND LEONARD O. OLSEN, *Case School of Applied Science, Cleveland, Ohio.*—Conventional methods for measuring magnetic properties encounter difficulties for samples of small cross-sectional area because only a small part of the flux threading a pick-up coil is the flux through the sample. An instrument has been constructed employing two identical opposed pick-up coils in two identical magnetizing coils. This allows the flux through the pick-up coils outside the sample to be effectively balanced out. The signal from the two opposed pick-up coils is integrated, amplified, and applied to the vertical deflecting plate of a cathode-ray oscillograph. The signal from a non-inductive resistance in series with the magnetizing coils provides the horizontal deflection for the cathode-ray oscillograph, so that the hysteresis loop of the sample is displayed on a fluorescent screen. The instrument is well suited for measurement of the magnetic properties of samples having cross-sectional areas of the order of magnitude of 10^{-6} cm^2.

Symmetrical R-C Parallel-T Networks: Output Voltage Phase as a Function of Frequency and of Load Resistance. C. E. HOWE, *Oberlin College.*

A Vacuum Tube Spark Timer. M. W. SCHWINN, *Oberlin College.*

Thermal Emissivities of Certain Glasses and Plastics. ROBERT H. NOBLE, *The Ohio State University.*

Studies on X-Rays Scattered at Small Angles as Applied to Carbon Black Used in the Rubber Industry. W. D. DAVIDSON, *The B. F. Goodrich Company, Akron.*

Hollow Cathode for Spectrographic Analysis. J. RAND MCNALLY, GEORGE R. HARRISON, AND EUGENE H. ROWE, paper given by Mr. Rowe of *The B. F. Goodrich Company, Akron.*

Meeting

A Problem for the Physicists of Ohio. MR. J. H. DILLON, *Assistant Director of Chemical and Physical Research Laboratories, Firestone Company, Akron.*

Invited Papers

Atomic Energy Research Program for the Immediate Future. DR. M. L. POOL, *The Ohio State University.*

Current Developments in National Policy Affecting Scientific Research. (1) Science Foundation Legislation; (2) Domestic Control of Atomic Energy; (3) World Control of Atomic Energy. MR. J. HAROLD RUSH, *Federation of American Scientists, Washington, D. C.*

LEON E. SMITH, *Secretary*
Denison University, Granville, Ohio

Author Index to Volume 69

References with (A) are to abstracts of papers presented at meetings of the American Physical Society. References with (L) are to Letters to the Editor, and those with (T) designate title only.

Adams, Norman I., Jr. (see Page, Leigh)—492, 494

Aebersold, Paul C. and Gladys A. Anslow. Fast neutron energy absorption in gases, walls and tissue—1

Ageno, Mario. Albedo of thermal neutrons—241(L)

Aicher, J. O. (see Kenty, Carl)—36(L)

Akeley, E. S. On the design of a cavity of a linear electron accelerator—255(A)

—— Study of stationary electromagnetic modes for region between parallel perfectly conducting planes and application to electron accelerator—50(A)

Akeley, Edward S. Theory of the narrow resonant slit in a wave guide partition—697(A)

—— (see Feuer, Paula)—697(A)

Alpert, D. and S. Krasik. Integral cavity TR switch X 698(A)

Altar, William. Circle diagram for resonant microwave systems—697(A)

Andersen, A. E. (see Clark, J. W.)—698(A)

Anderson, Scott. Mechanism of natural oxidation of aluminum, iron, and copper—52(A)

Andrews, C. L. Diffraction pattern of a circular aperture at short distances—684(A)

Anslow, Gladys A. (see Aebersold, Paul C.)—1

Anthony, R. L. (see Dart, S. L.)—52(A)

—— (see Mrowca, B. A.)—51(A)

Ashkin, Arthur. High power rising sun magnetron—701(A)

Autler, Stanley H., Gordon E. Becker, and J. M. B. Kellogg. Absorption of microwaves by water vapor—694(A)

Avramy, Melvin. Robot dynamics—theory of non-linear automatic control systems—697(A)

Bachelet, M. (see Tsien, San-Tsiang)—39(L)

Bacher, R. F., C. P. Baker, and B. D. McDaniel. Experiments with a slow neutron velocity spectrometer II—443

Bacher, Robert F. Nuclear physics in the atomic bomb development—674(T)

Baker, C. P. (see Bacher, R. F.)—443

Ball, Jack and F. C. Blake. Application of the curved crystal spectrograph to the chemical analysis of alloys—703(A)

—— **and F. C. Blake.** Curved crystal spectrograph applied to determine the complete spectrum of all orders obtained, and the evaluation of same with varying technique—703(A)

Band, William. Diamagnetism and superconductivity—241(L)

—— Occurrence of superconductivity in a collective electron assembly—41(L)

—— Superconductivity and magnetic energy between currents—241(L)

Barnett, S. J. Rotating ring sine-wave generator especially suitable for measurement of magnetic intensities and their variations—133(A)

—— Rotating magnetic-rod generator suitable for the measurement of small magnetic intensities and their variation, and their variations, and for other purposes—135(A)

Barton, Vola P. and George A. Lindsay. X-ray K absorption edge of silicon—48(A)

Beams, J. W. Balancing sedimentation by electrophoresis in high centrifugal fields—546(A)

—— **and J. L. Young, III.** Production of high centrifugal fields—537(L)

Beck, Guido. Remarks on the fine structure of "positronium"—532(L)

Becker, Gordon E. (see Autler, Stanley H.)—694(A)

Becker, R. and G. Leibfried. On the method of second quantization—34(L)

Bennett, W. E., C. E. Mandeville, and H. T. Richards. Yield function and angular distribution of the D+D neutrons—418

Benzer, S. High voltage and photo-sensitive characteristics in germanium—683(A)

Berger, F. B. (see Manley, J. H.)—254(A)

Bergmann, Peter G. Propagation of radiation in a medium with random inhomogeneities—255(A)

Beringer, Robert. Absorption in oxygen at one-half cm—693(A)

—— (see Kyhl, R. L.)—694(A)

Berlin, T. H. Stationary solution of the Fokker-Planck equation for a reflecting boundary—688(A)

—— (see Dennison, D. M.)—542(L)

Berry, Clifford E. Computor for solving linear simultaneous equations—135(A)

Bethe, H. A. Influence of multiple scattering on curvature measurements—689(A)

Birks, L. S. and H. Friedman. Thickness measurements of this coatings by x-ray absorption—49(A)

Blake, F. C. On the proper indexing of the crystal faces of α-quartz by the power method and the calculation of their structure factors for both right-handed and left-handed α-quartz—49(A)

—— On the proper indexing of the faces obtained in the powder method of x-ray analysis for α-quartz—703(A)

—— (see Ball, Jack)—703(A)

—— (see Farnham, John W.)—48(A)

Blatt, John M. On the heavy-electron pair theory in the limit of strong coupling—285

Bleakney, Walker. Shock waves in a tube—678(A)

Bless, A. A. (see Fuller, Wallace F.)—545(A)

Blewett, John P. Radiation losses in the induction electron accelerator—87

Bloch, F., W. W. Hansen, and Martin Packard. Nuclear induction—127(L), 680(A)

Bloch, Felix (see Packard, Martin)—680(A)

Bloch, Ingram. Production of mesotrons in the stratosphere—575

Boggs, F. W. Principles of operation of the resnatron—700(A)
Bohm, David (see Lewis, Harold)—129(L)
Boissières, G. (see Tsien, San-Tsiang)—39(L)
Bostick, W. H. Pulse transformer ratings based on energy considerations, and methods of design based on thermodynamical considerations—697(A)
Brattain, Walter H. Rectification series—682(A)
Braun, Milton L. Plasticity *versus* elasticity in stretched rubber as indicated by creep interference with the Joule effect—545(A)
Breit, G. Schematic treatment of nuclear resonances—472
Brillouin, L. Influence of space-charge on the bunching of electron beams—700(A)
Brinckerhoff, R. F. (see Marinelli, L. D.)—690(A)
Brody, S. B. (see D'Eustachio, D.)—256(A)
Brown, F. C. Velocity of propagation of the transmitted photo-effect in silicon crystals—686(A)
Brown, Sanborn C. Characteristics of the pre-corona discharge and its use as a reference potential in voltage stabilizers—696(A)
—— (see Herlin, Melvin A.)—696(A)
Broxon, James W. Recurrences of small bursts of cosmic-rays—46(A)
Buechner, W. W. (see Van de Graff, R. J.)—47(A), 452
—— **R. J. Van de Graaff, A. Sperduto, E. A. Burrill, L. R. McIntosh, and R. C. Urquhart.** Compact high voltage electrostatic generator using sulphur hexafluoride insulation—692(A)
Burbank, C. J. Acoustic reflection from triplanes, spheres, and disks—136(A)
Burrill, E. A. (see Buechner, W. W.)—692(A)

Caldirola, B. Relativistic correction in calculating the magnetic moment of the deuteron—608
Caldwell, Wallace C. Band-pass TR switch. Part II: Linear electrical characteristics—699(A)
Camp, Glen D. Impedance representation of tangential boundary conditions—501
—— Impedance representation of tangential boundary surface forces—135(A)
—— Variational method for linear dissipative anisotropic elastic systems—134(A), 502
Chance, Britton. Precision methods for pulse time measurement—676(T)
Chang, W. Y. Study of the alpha-particles from Po with a cyclotron-magnet alpha-ray spectrograph—60
—— Low energy alpha-ray spectra and mechanism of alpha-decay—254(A)
Chesley, F. G. (see Hippel, A. von)—685(A)
Christian, Schuyler. Integration of $\sin xdx/x$—546(A)
Ch'u, Sheng-Lin (see Oster, Francis)—531(L)
Clark, J. W. (see Crandell, C. F.)—698(A)
—— **A. E. Andersen, and A. L. Samuel.** Design of copper disk seal TR tubes—698(A)
Clarke, E. T. and John W. Irvine, Jr. Nuclear excitation functions: 14-Mev deuteron reactions on Cu, Mg, and Al—680(A)
Coggeshall, Norman D. and Eleanor L. Saier. Infra-red absorption of methane as influenced by foreign gases—257(A)
Coheur, Francine P. and Pierre M. Coheur. On the intensity distribution among the rotational lines of AlO—240(L)
Coheur, Pierre M. (see Coheur, Francine P.)—240(L)
Coltman, J. W. (see Ebbighausen, E. G.)—48(A)
—— **and M. Goldhaber.** Capture cross sections for slow neutrons—411
Compton, K. T. Scientific mission to Japan—676(T)
Conant, J. B. Interaction of science and society—676(T)
Condon, E. U. (see Hipple, J. A.)—257(A), 347
—— **and L. F. Curtiss.** New units for the measurement of radioactivity—672(L)
Conwell, E. and V. F. Weisskoff. Theory of impurity scattering in semiconductors—258(A)
Cooper, D. Absorptive effects relating to fine structure in the angular distribution of cosmic-ray intensity—546(A)
Cooper, John N. X-ray energy level widths of tungsten—48(A)
Corben, H. C. Classical theory of electromagnetism and gravitation. I. Special theory—225
Courant, E. D. Image force and tunnel effect in crystal rectifiers—684(A)
Crandell, C. F., A. L. Samuel, and J. W. Clark. Recovery time measurements of TR tubes—698(A)
Crane, H. R. Racetrack: a proposed modification of the synchrotron—542(L)
—— (see Levinstein, H.)—679(A)
Crawley, Clyde B. (see Pardue, L. A.)—545(A)
Crittenden, Eugene C., Jr., Charles S. Smith, and Leonard O. Olsen. Instrument for measurement of the magnetic properties of samples of small cross-sectional area—703(A)
Curtiss, L. F. (see Condon, E. U.)—672(L)

Dart, S. L., R. L. Anthony, and P. E. Wack. Fast stress-strain machine—52(A)
Daunt, J. D. and K. Mendelssohn. Transfer phenomena and indeterminacy—126(L)
Davidson, W. D. Studies on x-rays scattered at small angles as applied to carbon black used in the rubber industry—703(T)
Dearnley, I. H. (see Montgomery, C. G.)—699(A)
deBethune, A. J. and R. D. Present. On the flow of binary gas mixtures through a long capillary when the mean free path is comparable to the capillary diameter—259(A)
De Bretteville, A., Jr. Oscillographic study of the dielectric properties of barium titanate—687(A)
Dejardin, Georges and Jean Dufay. Light of the night sky in the ultraviolet range—685(A)
Denmark, H. S. (see Hippel, A. von)—685(A)
Dennison, D. M. (see Hadley, L. N.)—258(A)
—— **and T. H. Berlin.** Stability of orbits in the racetrack—542(L)
DerMateosian, E. and H. Friedman. Organic vapors for self-quenched G-M counters—689(A)

D'Eustachio, D. Rapidly acting vacuum valve—251(A)
—— Recrystallization of quartz as a result of flexure—687(A)
—— **and S. B. Brody.** Breaking up of single crystals of quartz—256(A)
—— **and S. Greenwald.** Thermal recrystallization of quartz—532(L)
Deutsch, Martin (see Good, Wilfred M.)—313, 673(L)
—— (see Peacock, Wendell C.)—306
Dicke, R. H. Radiometer for measuring thermal radiation at microwave frequencies—694(A)
—— (see Kyhl, R. L.)—694(A)
Dickey, F. P. (see Lagemann, R. T.)—545(A)
Dillon, J. H. Problem for the physicists of Ohio—703(T)
DuBridge, L. A. Microwave radar—676(T)
Dufay, Jean (see Dejardin, Georges)—685(A)
Dunning, J. R. (see Wu, C. S.)—236(L)
Dželepow, B., M. Kopjova, and E. Vorobjov. β-ray spectrum of K^{40}—538(L)

Ebbighausen, E. G. and J. W. Coltman. Fluorescent yield of calcium tungstate excited by x-rays—48(A)
Edwards, J. E. (see Farnham, John W.)—48(A)
—— (see Pool, M. L.)—49(A)
—— **and M. L. Pool.** Characteristic x-rays excited by beta-particles—549
—— **and M. L. Pool.** Characteristic x-rays excited by beta-particles—49(A)
—— **and M. L. Pool.** Radioactive Te from Sb bombardment—140
—— **and M. L. Pool.** Radioactive isotopes of Mo and Ma—253(A)
Ehrenhaft, Felix. Astrophysical phenomena and the magnetic current—702(A)
—— Helical movements of matter in the beam of light and the magnetic current—52(A)
—— Further observations on the helical movement of matter in sunlight—251(A)
—— Constant magnetic current and Heinrich Hertz—260(A)
—— Some thoughts about gravitation of celestial bodies and photophoretic forces—684(A)
Eisenstein, A. An x-ray method for measuring the thickness of thin crystalline films—252(A)
Ekstein, H. Forced vibration of piezoelectric crystals—257(A)
Ellickson, R. T. Some properties of infra-red sensitive phosphors—685(A)
—— **and W. L. Parker.** Effect of absorption on decay of infra-red sensitive phosphors—534(L)
Elsasser, Walter M. Induction effects in terrestrial magnetism. Part I. Theory—106
Estermann, I., S. N. Foner, and O. Stern. Mean free paths of cesium atoms in helium, nitrogen, and cesium vapor—256(A)
Everhart, E. (see Halpern, J.)—688(A)
Ewell, Arthur W. Ultraviolet lamps and ozone—685(A)
Eyring, Henry (see Williams, Ferd E.)—257(A)

Failla, G. Convenient dosage unit for radioactive isotopes internally administered—691(A)
Fairbank, Henry A. Small scale hydrogen liquefier—686(A)
Fankucken, I. Orientation of single crystals by the use of two simultaneous Bragg reflections—256(A)
Farnham, John W., J. E. Edwards, and F. C. Blake. Curved crystal spectrograph applied to determine the complete spectrum of all orders obtained when the camera is rotated about a proper pivot—48(A)
Farr, H. K. Microwave duplexing circuits—699(A)
Ferrell, Oliver Perry. Meteoric impact ionization observed on radar oscilloscopes—32(L)
Feshbach, H. (see Van de Graff, R. J.)—452, 47(A)
Feshbach, Herman. Production of mesons by electrons—690(A)
—— (see Hornbeck, John A.)—691(A)
Feuer, Paula and Edward S. Akeley. Scattering of electromagnetic radiation by a thin circular ring in a circular wave guide—697(A)
Field, R. F. Temperature coefficients of interfacial polarization in dielectrics—688(A)
Finkelstein, R. J. Normal reflection of a shock wave—677(A)
Fisher, J. R. (see Teal, G. K.)—686(A)
Fisher, Leon H. Some aspects of Meek's sparking equation—530(L)
Fisk, J. B. Magnetron generators—676(T)
Fiske, Milan D. Band-pass TR switch. Part I: The switching action—699(A)
Foley, H. M. Pressure broadening of spectral lines—616
—— Self-broadening in the 14μ band of HCN—628
Foner, S. N. (see Estermann, I.)—256(A)
Fowler, W. A. Matrix elements for positron decay—134(A)
Fox, R. E. (see Hipple, J. A.)—347, 257(A)
Frank, N. H. Phase stability of synchrotron orbits—689(A)
French, Sidney J. Address of welcome—674(T)
Friedman, H. (see Birks, L. S.)—49(A)
—— (see DerMateosian, E.)—689(A)
—— (see Muehlhause, C. O.)—46(A), 691(A)
Frondel, Clifford. Elastic deficiency and color of natural smoky quartz—543(L)
Fuller, Wallace F. and A. A. Bless. Geiger counter as an x-ray dosimeter—545(A)
Furry, W. H. and R. Clark Jones. Isotopes separation by thermal diffusion: Cylindrical case—459

Galt, John K. (see Pellam, John R.)—679(A)
Gamertsfelder, G. R. and M. Goldhaber. Reproducible neutron standard—368(L)
Gammel, J. L. (see Ginsburg, N.)—685(A)
Gartlein, C. W. Recent developments in procuring war surplus equipment—674(T)
George, D. E. (see Wells, J. W.)—540(L)
Gilbarg, David. Influence of atmospheric pressure on water entry phenomena—679(A)
Gillette, F. N. (see Haworth, L. J.)—254(A)
—— (see Manley, J. H.)—254(A)
Gilman, G. W. and F. H. Willis. Reflection of sound signals in the troposphere—677(A)
Ginsburg, N. and J. L. Gammel. Normal coordinates of a mono-substituted benzene molecule—685(A)

Goertzel, G. and I. S. Lowen. Angular correlation of successive γ-rays—533(L)
Goldhaber, M. (see Coltman, J. W.)—411
—— (see Gamertsfelder, G. R.)—368(L)
—— (see Yalow, A. A.)—47(A), 253(A)
—— **and A. A. Yalow.** Resonance scattering of group electrons—47(A)
Goldstein, Herbert. Frequency dependence of radar echoes from the surface of the sea—695(A)
Good, Wilfred M. and Wendell C. Peacock. Positron emission, electron capture competition in Zn^{65}—680(A)
—— **David Peaslee, and Martin Deutsch.** Experimental test of beta-ray theory for the positron emitters Na^{22}, V^{48}, Mn^{52}, Co^{58}—313; Erratum—673(L)
Good, William E. Inversion spectrum of ammonia—539(L)
Goodman, B. Effect of grain structure on the electrical conductivity of semiconductors—687(A)
—— (see Lawson, A. W.)—682(A)
Gordy, Walter. New method of determining electronegativity from other atomic properties—604
—— Relation between characteristic bond constants and electronegativities of the bonded atoms—130(L)
Grahame, David C. Resonance scattering of fast neutrons —369(L)
Gray, R. B. X-ray measurement of the thickness of silver plating—49(A)
Greanias, E. C. (see Kaiser, H. F.)—536(L)
Green, J. B. and J. T. Lynn. Zeeman effect in the spectrum of chlorine I—165
Greenwald, S. (see D'Eustachio, D.)—532(L)
Grinten, W. van der (see Swartz, C. E.)—252(A)
Groetzinger, G. K. (see Kurbatov, J. D.)—253(A)
Groetzinger, Gerhart and Lloyd Smith. Non-electrical scattering of charged mesotrons—690(A)
Guth, Eugene. Nuclear processes by polarization scattering of deuterons—47(A)

Hackman, E. E. Preliminary investigation of spark discharges along shock waves—130(L)
Hadley, L. N. and D. M. Dennison. Method of preparing absorbing surfaces for the infra-red—258(A)
Haggenmacher, J. E. Heat of vaporization of helium II below 1.5°K—242(L)
Halpern, J., E. Everhart, R. A. Rapuano, and J. C. Slater. Preliminary studies on the design of a microwave linear accelerator—688(A)
Hamermesh, B. (see Korff, S. A.)—155, 252(A)
Hamermesh, M. and Julian Schwinger. Scattering of slow neutrons by ortho- and paradeuterium—145
Hamill, W. H. (see Mrowca, B. A.)—51(A)
Hamilton, Donald R. Klystron—676(T)
Hamtil, Charles N. Effect of transverse pressure on the steady-state electrical conductivity of rocksalt—50(A)
Hansen, W. W. (see Bloch, F.)—127(L), 680(A)
—— (see Packard, Martin)—680(A)
Harrison, George R. (see McNally, J. Rand)—703(T)
Havens, W. W., Jr. (see Wu, C. S.)—236(L)
Haworth, L. J. Techniques of cathode-ray tube display circuits—676(T)
—— (see Manley, J. H.)—405
—— **and F. N. Gillette.** Slow neutron velocity spectrometer—254(A)
Haynes, J. R. High velocity vapor jets in sparks at mercury electrodes—693(A)
Hazen, W. E. (see Nassar, Salwa)—298
Hector, L. Grant and Donald L. Woernley. Dielectric constants of eight gases—101
Heller, Wilfried. New and rapid method for constructing quarter-wave plates, half-wave plates, half shades and ellipticity compensators—53(A)
—— Simple apparatus for demonstrating fluorescence, light scattering, and its polarization and depolarization—53(A)
Henry, Hugh F. Velocity of the anode spark produced in $CuSO_4$ solutions by application of an impulsive potential—693(A)
Herlin, Melvin A. and Sanborn C. Brown. Complex conductivity of electrical discharge in gas at microwave frequencies—696(A)
Hershberger, W. D. Thermal and acoustic effects attending absorption of microwaves by gases—695(A)
—— (see Walter, John E.)—694(A)
Herzberg, G. On the electronics structure of the nitrogen molecule—362
Herzfeld, K. F. Small deviations from diode behavior in crystal rectification—683(A)
Hicks, Bruce L. Diabatic flow of a compressible fluid—135(A)
—— Diabetic, rotational flow in two dimensions—250(A)
Hill, A. G. Microwave circuits—676(T)
Hill, E. L. Note on the relativistic problem of uniform rotation—488
Hippel, A. von, F. G. Chesley, H. S. Denmark, P. B. Ulin, and E. S. Rittner. Photoelectric mechanism of the thallous sulfide photo-conductive cell—685(A)
Hipple, J. A. (see Langer, A.)—691(A)
—— **R. E. Fox, and E. U. Condon.** Metastable ions formed by electron impact in hydrocarbon gases—347
—— **R. E. Fox, and E. U. Condon.** Study of metastable ions with the mass spectrometer—257(A)
Hirsh, Frederick R., Jr. Auger transitions—32(L)
Hollenberg, A. V., S. Millman, and N. Kroll. One centimeter rising sun magnetrons with 26 and 38 cavities—701(A)
Holstein, T. Initiation of high frequency gas discharges—50(A)
—— Phenomenological theory of the TR switch spike—698(A)
Honig, Richard E. Deuteron bombardments of organic compounds—257(A)
Hornbeck, John A. and Herman Feshbach. Scattering and absorption of high voltage x-rays in steel—691(A)
Howe, C. E. Symmetrical R-C parallel-T networks: output voltage phase as a function of frequency and of load resistance—703(T)
Hudspeth, Emmett L. Wave-guide acceleration of particles —671(L)
Hughes, Donald J. Cloud-chamber photographs of heavy particles at high altitudes—371

Hull, G. F. Fifty years of physics, a study in contrasts—676(T)
Hunter, L. P. Energy build-up in magnetrons—700(A)
—— (see Marshall, Fitz-Hugh)—48(A)

Irvine, Jr., John W. (see Clarke, E. T.)—680(A)

Jabloński, Alexander. Errata: General theory of pressure broadening of spectral lines—31
Jacobs, Harold. Dissociation energies of surface films of various oxides as determined by emission measurements of oxide coated cathodes—692(A)
Jacobsmeyer, Vincent P. Investigation of the surface photoelectric effect of metallic films under the influence of strong electrostatic fields—50(A)
Jaffé, George. On the statistical mechanics of systems involving molecular flow—688(A)
Jauch, J. M. On the inelastic photo-dissociation of the deuteron—275
—— On the inelastic photo-effect of the deuteron—252(A)
Jehle, Herbert. Statistical hypotheses in stellar dynamics—254(A)
—— Transformation theory of hydrodynamical equations—260(A)
Jnanananda, Swami. Beta-radiations of uranium X_1—570
Johnson, J. B. Enhanced thermionic emission from oxide cathodes—702(A)
—— Secondary emission of thermionic oxide cathodes—693(A)
Johnson, V. A. (see Lark-Horovitz, K.)—258(A)
—— **and K. Lark-Horovitz.** Theory of thermoelectric power in germanium—259(A)
—— **R. N. Smith and H. J. Yearian.** Semi-quantitative explanation of d.c. characteristics of crystal rectifiers—682(A)
Jones, R. Clark (see Furry, W. H.)—459

Kaiser, H. F. and E. C. Greanias. Synchro-betatron, electron accelerator guide fields—536(L)
Kaplan, Joseph. Forbidden line source—133(A)
Ke, T'ing-Sui and Louis D. Smullin. Gas discharge switches for controlling low power microwave signals—698(A)
Keenan, P. C. Shadowgraph method of determining the strength of a shock wave—677(A)
Kellogg, J. M. B. (see Autler, Stanley H.)—694(A)
Kennedy, Joseph W. (see Seaborg, G. T.)—366(L), 367(L)
—— **and Arthur C. Wahl.** Search for spontaneous fission in 94-239—367(L)
Kenty, Carl, J. O. Aicher, E. B. Noel, A. Poritsky, and V. Paolino. New band system in the green excited in a mixture of xenon and oxygen and the energy of dissociation of CO—36(L)
Kikuchi, Chihiro. Theory of the low mass neutral mesotron—125(L)
Kimball, G. E. Thermodynamics of relaxation processes—688(A)
King, Allen L. Maximum rate of multiplication of unicellular organisms—256(A)
King, D. D. Antenna impedance measurement—696(A)
King, Ronold and David Middleton. Cylindrical antenna: comparison of theories and experiment—696(A)
Kingdon, K. H. (see Lafferty, J. M.)—699(A)
Kingshill, Konrad L. and Lloyd G. Lewis. Structure of cosmic-ray air showers—159
Kittel, Charles. Theory of long period magnetic relaxation—640
Knipp, Julian K. Theory of the diode—700(A)
Knowles, H. L. Static direction finder—546(A)
Koch, Jørgen. Device producing ion beams homogeneous as to mass and energy—238(L)
Koenig, H. P. Absorption of slow mesotrons in lead, iron, aluminum, and water—253(A)
Koenig, H. Paul. Absorption of slow mesotrons in lead, iron, aluminum, and water—590
Koller, R. Fundamental properties of the vacuum switch—134(A)
Kopjova, M. (see Dželepow, B.)—538(L)
Korff, S. A. and B. Hamermesh. Energy distribution and number of cosmic-ray neutrons in the free atmosphere—155, 252(A)
Krasik, S. (see Alpert, D.)—698(A)
Kroll, N. (see Hollenberg, A. V.)—701(A)
Kroll, Norman and Willis E. Lamb, Jr. Theory of the rising sun magnetron anode—701(A)
Kurbatov, J. D. and G. K. Groetzinger. Correction of G-M counter data II—253(A)
Kyhl, R. L., R. H. Dicke, and Robert Beringer. Absorption of 1-cm electromagnetic waves by atmospheric water vapor—694(A)

Ladenburg, R., C. C. Van Voorhis, and J. Winckler. Interferometric study of gas flow around various objects in a free supersonic homogeneous air-jet—251(A)
—— (see Winckler, J.)—251(A)
Lafferty, J. M. and K. H. Kingdon. Improvements in the stability of the FP-54 electrometer tube—699(A)
Lagemann, R. T., A. H. Nielsen, and F. P. Dickey. New measurements on the infra-red spectrum of $C^{12}O^{16}$ and $C^{13}O^{16}$—545(A)
Lamb, W. E., Jr. (see Phillips, M.)—701(A)
Lamb, Willis E., Jr. Theory of a microwave spectroscope—694(A)
—— (see Kroll, Norman)—701(A)
Langer, A. and J. A. Hipple. Ionization potential of CH_2—691(A)
Lapp, R. E. Origin of large cosmic-ray bursts—321
—— Transition effect for large cosmic-ray bursts in iron—253(A)
Lark-Horovitz, K. (see Johnson, V. A.)—259(A)
—— (see Whaley, R. M.)—683(A)
—— **and V. A. Johnson.** Theory of resistivity in germanium alloys—258(A)
—— **A. E. Middleton, E. P. Miller, and I. Walerstein.** Electrical properties of germanium alloys. I. Electrical conductivity and hall effect—258(A)
—— **A. E. Middleton, E. P. Miller, W. W. Scanlon, and I. Walerstein.** Electrical properties of germanium alloys. II. Thermoelectric power—259(A)

Lasof, Solomon. Plastic deformation of zinc as a function of strain rate—687(A)
Lassen, N. O. On the variation along range of the $H\rho$-distribution and the charge of the fission fragments of the light group—137
Lattes, C. and G. Wataghin. On the abundance of nuclei in the universe—237(L)
Lawson, A. W., B. Goodman, and L. I. Schiff. High frequency rectification efficiency of radar crystal detectors—682(A)
Lawson, J. L. Threshold signals in the presence of noise—676(T)
Leibfried, G. (see Becker, R.)—34(L)
Leonard, R. W. Critical examination of sound velocity measurements—136(A)
—— Method for the precision measurement of the velocity of sound in air—136(A)
Leverenz, H. W. Corpuscular *vs.* undulatory excitation of phosphors—686(A)
Levinstein, H. and H. R. Crane. High intensity velocity selector for neutral atoms—679(A)
Lewis, Harold and David Bohm. Low energy β-spectrum of Cu^{64}—129(L)
Lewis, Lloyd G. (see Kingshill, Konrad L.)—159
Lewis, Margaret N. (see Stephens, William E.)—43(L)
Libby, W. F. Atmospheric helium three and radiocarbon from cosmic radiation—671(L)
Liebowitz, Benjamin. Calculus of finite precision—A correction—131(L)
Linder, E. G. and R. L. Sproull. Maximum efficiency of reflex oscillators—700(A)
Lindsay, George A. (see Barton, Vola P.)—48(A)
Little, R. N., R. W. Long, and C. E. Mandeville. Scattering of neutrons by magnesium—414
Livingood, J. J. Resnatron—676(T)
Lofgren, E. J. (see Richardson, J. Reginald)—669(L)
London, F. On an inequality of quantum hydrodynamics—254(A)
Long, R. W. (see Little, R. N.)—414
Lopes, J. Leite. High energy neutron-proton scattering and the meson theory of nuclear forces with strong coupling—252(A)
Lovell, William Vail. An electromagnet for non-magnetic substances—251(A)
Lowen, I. S. (see Goertzel, G.)—533(L)
Lü, Lieh-Yang (see Oster, Francis)—531(L)
Lucht, C. M., M. Mann, and R. Smoluchowski. X-ray microradiographic study of strains in crystals—256(A)
Luebke, E. A. (see Manley, J. H.)—405
Lynn, J. T. (see Green, J. B.)—165
Lype, E. F. Thermodynamic equilibria of higher order—652

Ma, S. T. Redundant zeros in the discrete energy spectra in Heisenberg's theory of characteristic matrix—668(L)
MacKenzie, K. R. (see Richardson, J. Reginald)—669(L)
Mandeville, C. E. (see Bennett, W. E.)—418
—— (see Little, R. N.)—414
Manley, J. H., F. B. Berger, and F. N. Gillette. Experiments with a slow neutron velocity spectrometer—254(A)
—— **L. J. Haworth and E. A. Luebke.** Velocity dependence of the absorption of boron for slow neutrons—405
Mann, Alfred K. (see Ney, Edward P.)—239(L)
Mann, M. (see Lucht, C. M.)—256(A)
Margenau, H. Conduction and dispersion of ionized gases at high frequencies—508
Margenau, Henry. Conductivity of electrons in a gas at microwave frequencies—698(A)
Marinelli, L. D., R. F. Brinckerhoff, and E. H. Quimby. Determination of the average β-ray energy in artificial radioactivity and its use in radiation dosimetry—690(A)
Marshall, Fitz-Hugh and L. P. Hunter. Photomultiplier x-rays detector—48(A)
Marx, Erich. Influence of polarized light on the falling-off effect of the limiting potential of Einstein's photoelectric law—523
Masket, A. Victor. Forced vibrations of a whirling wire—52(A)
Mason, W. P. Elastic, piezoelectric, and dielectric constants of potassium dihydrogen phosphate and ammonium dihydrogen phosphate—173
Mayer, Ernest. Extinction of gaseous discharges—51(A)
McDaniel, B. D. (see Bacher, R. F.)—443
McIntosh, L. R. (see Buechner, W. W.)—692(A)
McMillan, Edwin M. Origin of the synchrotron—534(L)
—— (see Seaborg, G. T.)—366(L)
McMillan, F. L. (see Montgomery, C. G.)—699(A)
McMillen, J. Howard. Elastic waves in bars—250(A)
McNally, J. Rand, George R. Harrison, and Eugene H. Rowe. Hollow cathode for spectrographic analysis—703(T)
McQueen, John H. (see Ney, Edward P.)—41(L)
Mehta, G. K. (see Tawde, N. R.)—245(L)
Meissner, K. W. Interferometric method for the determination of the resolving power of spectroscopes—685(A)
Meitner, Lise. Attempt to single out some fission processes of uranium by using the differences in their energy release—676(T)
Mellen, G. L. Radium source ion gauge—691(A)
Mendelssohn, K. (see Daunt, J. D.)—126(L)
Merchant, M. Eugene. Studies in friction I. "Solid" *versus* "polar" boundary films—250(A)
Meyerhof, W. E. (see Stephens, W. E.)—42(L), 244(L)
Middleton, A. E. (see Lark-Horovitz, K.)—258(A), 259(A)
Middleton, David (see King, Ronold)—696(A)
Miller, E. P. (see Lark-Horovitz, K.)—258(A), 259(A)
Miller, P. H., Jr. New type of electrostatic generator—666(L)
Millman, S. (see Hollenberg, A. V.)—701(A)
Millman, Sidney and Arnold Nordsieck. Development of the rising sun magnetron anode structure—701(A)
Montgomery, C. G., F. L. McMillan, I. H. Dearnley, and C. S. Pearsall. Cross sections for capture of electrons from TR tube recovery measurements—699(A)
Montgomery, D. J. Relativistic interaction of electrons on Podolsky's generalized electrodynamics—117
Morris, T. F. Two-body problem in Einstein's and Birkhoff's theories—541(L)

Moyer, B. J., B. Peters and F. H. Schmidt. Absorption of slow neutrons by Cd^{113}—666(L)
Mrowca, B. A., R. L. Anthony, and W. H. Hamill. Specific heats of hevea—51(A)
Mrozowski, S. Forbidden lines of Bismuth BiI—169
Muehlhause, C. O. and H. Friedman. Geiger-Muller counter technique for high counting rates—46(A)
—— **and H. Friedman.** Measurement of betatron radiation with G-M counter—691(A)

Nassar, Salwa and W. E. Hazen. Cascade showers and mesotron-produced secondaries in lead—298
Neddermeyer, S. H. Measurement of ultra-short time differences—702(A)
Neher, H. V. Some electrical characteristics of reflex tubes —134(A)
Neumann, J. von (see Seeger, R. J.)—677(A)
Ney, Edward P. and Alfred K. Mann. Mass measurement with a single field mass spectrometer—239(L)
—— **and John H. McQueen.** Mass-spectrographic study of the isotopes of silicone—41(L)
Nielsen, A. H. (see Lagemann, R. T.)—545(A)
Nierenberg, W. A. Separation of gas-mixtures flowing through porous media—259(A)
Noble, Robert H. Thermal emissivities of certain glasses and plastics—703(T)
Noel, E. B. (see Kenty, Carl)—36(L)
Nordsieck, Arnold (see Millman, Sidney)—701(A)
North, D. O. Response of non-linear devices to signal and noise—676(T)

Ogg, Jr., Richard A. Bose-Einstein condensation of trapped electron pairs. Phase separation and superconductivity of metal-ammonia solutions—243(L); Erratum—544(L)
—— Physical interaction of electrons with liquid dielectric media. Properties of metal-ammonia solutions—668(L)
Olsen, Leonard O. (see Crittenden, Eugene C., Jr.)—703(A)
O'Neal, R. D. and G. Scharff-Goldhaber. Determination of absolute neutron intensities—368(L)
Opatowski, I. On the deviation of the biological effects of radiations from the Bunsen-Roscoe law—54(A)
—— On a statistical approach to biological effects of radiations—51(A)
Osborne, R. K. (see Peacock, W. C.)—679(A)
—— **and W. C. Peacock.** Beta- and gamma-ray spectra of La^{140}—679(A)
Oster, Francis, Sheng-Lin Ch'u, and Lieh-Yang Lü. East-west asymmetry of cosmic radiation at a geomagnetic latitude of 28°31′ and an estimation of the difference of the exponents of the absorption law for the polar and the equatorial regions—531(L)

Packard, Martin (see Bloch, F.)—127(L), 680(A)
—— **W. W. Hansen, and Felix Bloch.** Nuclear induction—680(A)
Page, Leigh. Magnetic antenna—645
—— **and Norman I. Adams, Jr.** Space charge in cylindrical magnetron—494
—— **and Norman I. Adams, Jr.** Space charge in plane magnetron—492
Paolino, V. (see Kenty, Carl)—36(L)
Pardue, L. A. and Clyde B. Crawley. Kentucky electrostatic generator—545(A)
Parker, W. L. (see Ellickson, R. T.)—534(L)
Patterson, A. L. Ambiguities in x-ray and electron diffraction analysis—256(A)
Peacock, W. C. (see Osborne, R. K.)—679(A)
—— **and R. K. Osborne.** Control and recording circuits for a magnetic beta-ray spectrograph—679(A)
Peacock, Wendell C. (see Good, Wilfred M.)—680(A)
—— **and Martin Deutsch.** Disintegration schemes of radioactive substances IX. Mn^{52} and V^{48}—306
Pearsall, Anna M. General Electric fellowships for science teachers. 1945 summer session. 2. Teachers' viewpoint—674(T)
Pearsall, C. S. (see Montgomery, C. G.)—699(A)
Peaslee, David (see Good, Wilfred M.)—313, 673(L)
Pellam, John R. and John K. Galt. Ultrasonic absorption and velocity measurements in liquids by means of pulse techniques—679(A)
Pepinsky, R. Multi-element x-ray tube for diffraction studies—546(A)
Peters, B. (see Moyer, B. J.)—666(L)
Phillips, M. and W. E. Lamb, Jr. Space-charge frequency dependence of a magnetron cavity—701(A)
Placzek, C. On the theory of the slowing down of neutrons in heavy substances—423
Plantenberg, Sister Gonzaga (see Weber, A. H.)—649
Plantenberg, M. Gonzaga (see Weber, A. H.)—51(A)
Platt, Joseph B. Physics of radar—674(T)
—— Structure in the x-ray K absorption edge of metallic potassium—337
Podolsky, Boris. Relativistic transformation of current and charge densities—255(A)
Polachek, H. (see Seeger, R. J.)—677(A)
—— **and R. J. Seeger.** Three-shock configurations—677(A)
Pollard, E. C. Use of a proportional counter for meson detection—689(A)
Pollard, W. G. (see Present, R. D.)—53(A)
Pollock, H. C. Combination of betatron and synchrotron for electron acceleration—125(L)
Pool, M. L. Atomic energy research program for the immediate future—703(T)
—— (see Edwards, J. E.)—49(A), 140, 253(A), 549
—— **and J. E. Edwards.** X-rays from radioactive Te—49(A)
Poritsky, A. (see Kenty, Carl)—36(L)
Posin, D. Q. Electrical breakdown in air at microwave frequencies—696(A)
Posin, D. Q. Lowering of electrical breakdown field strength at microwave frequencies due to externally-applied magnetic field—541(L)
Posin, Daniel Q. Radioautography with $P^{32}Sr^{89}$—702(A)
Post, Richard F. Proposed high energy particle accelerator —the cavitron—126(L)
Pound, R. V. (see Purcell, E. M.)—37(L)
—— (see Torrey, H. C.)—680(A)
—— **E. M. Purcell, and H. C. Torrey.** Measurement of magnetic resonance absorption by nuclear moments in a solid—681(A)

Powell, Wilson M. Cloud-chamber analysis of cosmic rays at 14,120 feet—385
Present, R. D. (see DeBethune, A. J.)—259(A)
—— **and W. G. Pollard.** On the self-diffusion of a pure gas through a long capillary when the mean free path is comparable to the capillary diameter—53(A)
Preston, M. A. Radii of the nuclei of natural α-emitters—535(L)
Purcell, E. M. Spontaneous emission probabilities at radio frequencies—681(A)
—— (see Pound, R. V.)—681(A)
—— (see Torrey, H. C.)—680(A)
—— **H. C. Torrey, and R. V. Pound.** Resonance absorption by nuclear magnetic moments in a solid—37(L)

Quimby, E. H. (see Marinelli, L. D.)—690(A)

Rainwater, L. J. (see Wu, C. S.)—236(L)
Rapuano, R. A. (see Halpern, J.)—688(A)
Rathgeber, Henri D. Influence of intercrystalline forces on beta-ray absorption—239(L)
Regener, Victor H. Decade counting circuits—46(A)
—— Improved decade counting circuit—689(A)
Reid, Allen F. Synthesis by nuclear recoil—530(L)
Rice, S. O. Fourier series in random processes—676(T)
Richards, H. T. (see Bennett, W. E.)—418
Richardson, J. Reginald, K. R. MacKenzie, E. J. Lofgren, and Bryon T. Wright. Frequency modulated cyclotron—669(L)
Richardson, John M. and William Shockley. Solution of the equation for the propagation of waves of finite amplitude in one dimension—250(A)
Rittner, E. S. (see Hippel, A. von)—685(A)
Roe, Glenn M. Normal modes in the theory of wave guides—255(A)
Rogers, F. T., Jr. On the theory of the electrostatic beta-particle energy-spectrograph. IV—537(L)
Rojansky, V. General Electric fellowships for science teachers. 1945 summer session. 1. Administrative viewpoint—674(T)
Rothstein, Jerome. Poisoning of oxide cathodes by gold—693(A)
Rowe, Eugene H. (see McNally, J. Rand)—703(T)
Rubin, S. Excitation energy of excited Li^7—134(A)
Rush, J. Harold. Current developments in national policy affecting scientific research. (1) Science foundation legislation; (2) Domestic control of atomic energy; (3) World control of atomic energy—703(T)

Sachs, R. G. Some properties of very intense shock waves—514
—— Theory of crystal rectifiers—682(A)
Sachs, Robert G. Magnetic moments of light nuclei—514
Saibel, Edward. Thermodynamic criterion for the fracture of metals—667(L)
Saier, Eleanor L. (see Coggeshall, Norman D.)—257(A)
Samuel, A. L. Equivalent circuit for the microwave TR tube—699(A)
—— (see Crandell, C. F.)—698(A)
—— (see Clark, J. W.)—698(A)
Saxon, David S. Modulation and tuning of cavity oscillators by electron beams—700(A)
—— **and Julian Schwinger.** Electron orbits in the synchrotron—702(A)
Scanlon, W. W. (see Lark-Horovitz, K.)—259(A)
Scanlon, Wayne. Quantitative method for the spectroscopic analysis of potassium-sodium solution—52(A)
Scharff-Goldhaber, G. (see O'Neal, R. D.)—368(L)
Schiff, L. I. Noise in radar crystal detectors—682(A)
—— (see Lawson, A. W.)—682(A)
Schmidt, F. H. (see Moyer, B. J).—666(L)
Schönberg, Mario. Classical theory of the point electron—211
Schremp, E. J. Generalization of Nyquist's thermal noise theorem—255(A)
—— Minimal noise amplifiers—695(A)
—— Theorem on equivalent representations of an arbitrary linear network—259(A)
—— (see Twiss, R. Q.)—696(A)
Schultz, H. L. System for high speed counting of nuclear particles—689(A)
Schumb, Walter C. Preparation and physical properties of sulfur hexafluoride—692(A)
Schwinger, Julian. Polarization of neutrons by resonance scattering in helium—681(A)
—— (see Hamermesh, M.)—145
—— (see Saxon, David S.)—702(A)
Schwinn, M. W. Vacuum tube spark timer—703(T)
Seaborg, G. T., E. M. McMillan, J. W. Kennedy, and A. C. Wahl. Radioactive element 94 from deuterons on uranium—366(L)
—— **A. C. Wahl, and J. W. Kennedy.** Radioactive element 94 from deuterons on uranium—367(L)
Seeger, R. J. (see Polachek, H.)—677(A)
—— **J. von Neumann, and H. Polachek.** Interaction of shock waves—677(A)
Serin, B. Dependence of the diffusion coefficient on concentration—687(A)
—— Heat treatment of semi-conductors and contact rectification—357
—— (see Stephens, W. E.)—42(L), 244(L)
Sherr, R. (see Sommers, Jr., H. S.)—21
Shockley, William (see Richardson, John M.)—250(A)
Shrader, E. F. Partial separation of the isotopes of chlorine by thermal diffusion—439
Shutt, R. P. Concerning the anomalous scattering of mesotrons—128(L)
—— Some experimental results concerning mesotrons—261
Simon, Ralph. Performance of a hot wire Clusius and Dickel column—596
Slater, J. C. (see Halpern, J.)—688(A)
Sleator, William, Jr. Fast neutron collision cross sections of C and H—681(A)
Smith, Charles G. Cathode dark space and negative glow of a mercury arc—96
—— (see Crittenden, Eugene C., Jr.)—703(A)
Smith, L. G. Photographic investigation of the reflection of plane shocks in air—678(A)
—— (see Taub, A. H.)—678(A)

Smith, Lloyd (see Groetzinger, Gerhart)—690(A)
Smith, Lloyd P. Quantum effects in the interaction of electrons with high frequency fields and the transition to classical theory—195
Smith, R. N. Contact capacity of crystal rectifiers—683(A)
—— (see Johnson, V. A.)—682(A)
Smoluchowski, R. (see Lucht, C. M.)—256(A)
Smullin, Louis D. Low pressure gas discharges in microwave TR tubes—698(A)
—— (see Ke, T'ing-Sui)—698(A)
Snowdon, S. C. Multivibrator theory—134(A)
Sommers, H. S., Jr. and R. Sherr. Activity of N^{16} and He^{6}—21
Sonkin, Simon. Crown of thorns tuning of magnetrons—701(A)
Sperduto, A. (see Buechner, W. W.)—692(A)
Sperduto, Anthony. Method of determining focal spot size in high voltage radiography—692(A)
Sproull, R. L. (see Linder, E. G.)—700(A)
Stephens, W. E. Pulsed mass spectrometer with time dispersion—691(A)
—— **and Margaret N. Lewis.** Autoradiographic detection of aluminum—43(L)
—— **B. Serin, and W. E. Meyerhof.** Method for measuring effective contact e.m.f. between a metal and a semiconductor—42(L); Erratum—244(L)
Stern, O. (see Estermann, I.)—256(A)
Stewart, Ellen Swomley. Dispersion of the velocity and anomalous absorption of sound in hydrogen—632
Stewart, G. W. Heat conduction effects with liquid crystals and suspended particles—51(A)
—— Theory of the Herschel-Quincke tube—53(A)
Stuhlman, Otto, Jr. Modulus of elasticity and column action as applied to the structure of the giant reed (*Arundo donax*)—547(A)
Sun, Kuan-Han. Mass of the neutron—240(L)
Swann, W. F. G. Fluctuations in measurements of ionization per centimeter of path in proportional counters—690(A)
—— (see Weisz, Paul B.)—690(A)
Swanson, D. C. Ceramic dielectrics—546(A)
Swartz, C. E. and W. van der Grinten. Motion of electrolytes in magnetic field—252(A)

Tamburino, Sara. Particular type of cosmic-ray stars observed with photographic plate—35(L)
Taub, A. H. and L. G. Smith. Theory of reflection of shock waves—678(A)
Tawde, N. R. and G. K. Mehta. Spectrum of high frequency discharge in air in relation to active nitrogen—245(L)
Teal, G. K., J. R. Fisher, and A. W. Treptow. New bridge photo-cell employing a photo-conductive effect in silicon. Some properties of high purity silicon—686(A)
Tiedeman, John A. Recent developments in color photography—674(T)
Torrey, H. C., E. M. Purcell, and R. V. Pound. Theory of magnetic resonance absorption by nuclear moments in solids—680(A)
—— (see Pound, R. V.)—681(A)
—— (see Purcell, E. M.)—37(L)
Townes, Charles Hard. Interpretation of cosmic noise—radio waves from extraterrestrial sources—695(A)
Treptow, A. W. (see Teal, G. K.)—686(A)
Trump, John G. Insulation of high voltages in vacuum—692(A)
Tsien, San-Tsiang. γ-rays of radium D—38(L)
—— **M. Bachelet, and G. Bouissiéres.** Fine structure of the α-rays from protoactinium—39(L)
Turner, Louis A. Atomic energy from U^{238}—366(L)
Twiss, R. Q. and E. J. Schremp. Equivalent noise representation of multi-grid amplifier tubes—696(A)

Uhlenbeck, G. E. Theory of random processes—676(T)
Ulin, P. B. (see Hippel, A. von)—685(A)
Urquhart, R. C. (see Buechner, W. W.)—692(A)

Valente, Frank A. and Herbert Ivan Zagor. Fast neutron resonance with nitrogen—55
Valley, G. E. Amplification of low frequency signals—676(T)
Van de Graaff, R. J. (see Buechner, W. W.)—692(A)
—— **W. W. Buechner, and H. Feshbach.** Experiments on the elastic single scattering of electrons by nuclei—452, 47(A)
Van Vleck, J. H. Atmospheric absorption of microwaves—676(T)
Van Voorhis, C. C. (see Ladenburg, R.)—251(A)
—— (see Winckler, J.)—251(A)
Veksler, V. Concerning some new methods of acceleration of relativistic particles—244(L)
Vorobjov, E. (see Dželepow, B.)—538(L)

Wack, Paul E. Phase transitions at low temperatures in natural and synthetic rubber—52(A)
—— (see Dart, S. L.)—52(A)
Wahl, A. C. (see Seaborg, G. T.)—366(L), 367(L)
—— (see Kennedy, Joseph W.)—367(L)
Walerstein, I. (see Lark-Horovitz, K.)—258(A), 259(A)
Wallman, Henry. Pulse amplifiers—676(T)
Walter, John E. and W. D. Hershberger. Absorption of microwaves by gases II—694(A)
Wang, Theodore J. On increasing the effectiveness of a betatron—42(L)
Warburton, F. W. Reciprocal electric force—40(L)
—— Note on accelerational-velocital magnetic forces—49(A)
Warren, Dana T. Analysis of cosmic-ray fine structure. Part I. Earlier Missouri observations—78
—— Analysis of cosmic-ray fine structure. Part II. Mexico City observations—382
Wataghin, Gleb. On the nuclear photo-effect—33(L)
—— (see Lattes, C.)—237(L)
Watts, J. M. (see Wells, H. W.)—540(L)
Weber, A. H. and M. Gonzaga Plantenberg. Rapid and direct measurement of vapor pressure of liquid metals—51(A)
—— **and M. Gonzaga Plantenberg.** Rapid and direct measurement of vapor pressure of liquid metals—649
Wehe, H. G. World peace established on natural law and order instead of legislation—684(A)

Weisskoff, V. F. (see Conwell, E.)—258(A)
Weisz, Paul B. and W. F. G. Swann. Ionization spectrum of cosmic-ray electrons and mesotrons—690(A)
Welles, Sherrerd B. Partial separation of the oxygen isotopes by thermal diffusion and the deuteron bombardment of O^{17}—586
Wells, H. W., J. M. Watts, and D. E. George. Detection of rapidly moving ionospheric clouds—540(L)
Weyl, F. Joachim. Numerical aspects of quantitative interferometry—677(A)
Whaley, R. M. and K. Lark-Horovitz. Effect of various atmospheres on germanium crystal rectifiers—683(A)
Wiedenbeck, Marcellus L. Lifetimes of metastable states—47(A)
—— Neutron yields from the photo- and electro-disintegration of beryllium—235(L)
—— Note on the lifetime of metastable states—567
Williams, Dudley and Philip Yuster. Isotopic constitution of tellurium, silicon, tungsten, molybdenum, and bromine—556
Williams, Ferd E. and Henry Eyring. Mechanism of the luminescence of solids—257(A)
Willis, F. H. Measured values of ultrasonic absorption and velocity in liquid mixtures—250(A)
—— (see Gilman, G. W.)—677(A)
Wilson, Charles R. Atomic bomb and international relations—674(T)
Wilson, H. A. Spherical shell nuclear model—538(L)
Winckler, J. (see Ladenburg, R.)—251(A)
—— **C. C. Van Voorhis, and R. Ladenburg.** Optical analysis of the structure of supersonic inhomogeneous air-jets—251(A)
Winckler, John. Interaction of shock waves and boundary layers in supersonic gas flow—678(A)
Winter, D. F. Fast sweep synchroscope—695(A)
Woernley, Donald L. (see Hector, L. Grant)—101
Woodyard, J. R. Comparison of the high frequency accelerator and betatron as a source of high energy electrons—50(A)
Wright, Byron T. (see Richardson, J. Reginald)—669(L)
Wu, C. S., L. J. Rainwater, W. W. Havens, Jr., and J. R. Dunning. Neutron scattering in ortho- and parahydrogen and the range of nuclear forces—236(L)

Yalow, A. A. (see Goldhaber, M.)—47(A)
—— **and M. Goldhaber.** Wide and sharp neutron groups—47(A)
—— **R. S. Yalow, and M. Goldhaber.** Upper limit of the number of low energy neutrons from a Ra-α-Be source—253(A)
Yalow, R. S. (see Yalow, A. A.)—253(A)
Yearian, H. J. D.c. characteristics of Ge and Si crystal rectifiers—682(A)
—— (see Johnson, V. A.)—682(A)
Young, J. L., III (see Beams, J. W.)—537(L)
Yuster, Philip (see Williams, Dudley)—556

Zagor, Herbert Ivan (see Valente, Frank A.)—55
Zener, Clarence. Theoretical criterion for the initiation of slip bands—128(L)

Analytic Subject Index to Volume 69

References with (A) are to abstracts of papers presented at meetings of the American Physical Society. References with (L) are to Letters to the Editor.

Absorption
- Of microwaves by gases, W. D. Hershberger—695(A); II, J. E. Walter and W. D. Hershberger—694(A)
- Of microwaves by water vapor, S. H. Autler, G. E. Becker, and J. M. B. Kellogg—694(A)
- In oxygen of one-half cm waves, R. Beringer—693(A)
- Of 1-cm electromagnetic waves by water vapor, R. L. Kyhl, R. H. Dicke, and R. Beringer—694(A)

Acoustics
- Dispersion and anomalous absorption of sound in hydrogen, E. S. Stewart—632
- Reflection of signals in the troposphere, G. W. Gilman and F. H. Willis—677(A)
- Reflection from triplanes, spheres, and disks, C. J. Burbank—136(A)
- Sound velocity measurements, R. W. Leonard—136(A)
- Theory of Herschel-Quincke tube, G. W. Stewart—53(A)
- Ultrasonic absorption and velocity measurements in liquids, F. H. Willis—250(A); J. R. Pellam and J. K. Galt—679(A)
- Velocity of sound at high pressures, R. G. Sachs—514

Aerodynamics (see also **Hydrodynamics**)
- Gas flow in free supersonic homogenous air-jet, R. Ladenburg, C. C. Van Voorhis, and J. Winckler—251(A)
- Optical analysis of supersonic inhomogeneous air-jets, J. Winckler, C. C. Van Voorhis, and R. Ladenburg—251(A)

Astrophysics
- Astrophysical phenomena and magnetic current, F. Ehrenhaft—702(A)
- Light of night sky in ultraviolet, G. Dejardin and J. Dufay—685(A)
- Nuclear photo-effect, G. Wataghin—33(L)
- Radio waves from extraterrestrial sources, C. H. Townes—695(A)
- Statistical hypotheses in stellar dynamics, H. Jehle—254(A)
- Transformation theory of hydrodynamical equations, H. Jehle—260(A)

Biophysics
- Artificial radioactivity and radiation dosimetry, L. D. Marinelli, R. F. Brinckerhoff, and E. H. Quimby—690(A)
- Bunsen-Roscoe law, deviations, I. Opatowski—54(A)
- Effects of radiations, statistical approach, I. Opatowski—51(A)
- Geiger counter as x-ray dosimeter, W. F. Fuller and A. A. Bless—545(A)
- Multiplication of unicellular organisms, A. L. King—256(A)
- Neutron absorption in tissue, P. C. Aebersold and G. A. Anslow—1
- Radioactive isotopes internally administered, dosage, G. Failla—691(A)
- Radioautography with P^{32} and Sr^{89}, D. Q. Posin—702(A)
- Synthesis by nuclear recoil, A. F. Reid—530(L)
- Ultraviolet lamps and ozone, A. W. Ewell—685(A)

Broadening of spectral lines
- General theory, errata, A. Jabloński—31
- Of HCN, H. M. Foley—628
- Pressure broadening, theory, H. M. Foley—616

Chemical reactions
- Deuteron bombardments of organic compounds, R. E. Honig—257(A)
- Natural oxidation of Al, Fe, and Cu, S. Anderson—52(A)
- Properties of sulfur hexafluoride, W. C. Schumb—692(A)
- Synthesis by nuclear recoil, A. F. Reid—530(L)

Cosmic radiation
- Absorption of slow mesotrons in Pb, Fe, Al, and H_2O, H. P. Koenig—253(A); 590
- Absorptive effects relating to fine structure, D. Cooper—546(A)
- Analysis of fine structure, D. T. Warren—78; 382
- C^{14} and He^3 produced by neutrons, W. F. Libby—671(L)
- Cloud-chamber photographs of heavy particles at 15,000 feet, D. J. Hughes—371
- Cosmic-ray stars observed with photographic plate, S. Tamburino—35(L)
- East-west asymmetry, F. Oster, Sheng-Lin Ch'u, and Lieh-Yang Lü—531(L)
- Heavy particles in cloud chambers at 14,000 feet, W. M. Powell—385
- Ionization spectrum of electrons and mesotrons, P. B. Weisz and W. F. G. Swann—690(A)
- Large cosmic-ray bursts, origin of, R. E. Lapp—321
- Neutrons in the atmosphere, S. A. Korff and B. Hamermesh—155; 252(A)
- Non-electrical scattering of charged mesotrons, G. Groetzinger and L. Smith—690(A)
- Production of mesotrons, I. Bloch—575
- Recurrences of small bursts, J. W. Broxon—46(A)
- Showers and mesotron-produced secondaries in Pb, S. Nassar and W. E. Hazen—298
- Structures of air showers, K. L. Kingshill and L. G. Lewis—159
- Transition effect for cosmic-ray bursts in Fe, R. E. Lapp—253(A)

Crystal structure
- Indexing of crystal faces of α-quartz, F. C. Blake—49(A), 703(A)

Crystalline state
- Bose-Einstein condensation of trapped electron pairs, R. A. Ogg, Jr.—243(L); 544(L)

Crystalline state (*continued*)
Breaking up of single thin crystals of quartz, D. D'Eustachio and S. B. Brody—256(A)
Criterion for initiation of slip bands, C. Zener —128(L)
Long period magnetic relaxation, C. Kittel—640
Properties of high purity silicon, G. K. Teal, J. R. Fisher, and A. W. Treptow—686(A)
Plastic deformation of Zn, S. Lasof—687(A)
Recrystallization of quartz, flexure, D. D'Eustachio—687(A)
Thermal recrystallization of quartz, D. D'Eustachio and S. Greenwald—532(L)

Dielectric constants (see **Dielectrics and dielectric properties**)
Dielectrics and dielectric properties
Of barium titanate, oscillographic study, A. de Bretteville, Jr.—687(A)
Ceramic dielectrics, D. C. Swanson—546(A)
Electrons in liquid dielectric media, R. A. Ogg, Jr.—668(L)
Of He, Ne, A, H_2, O_2, N_2, CO_2, and air, L. G. Hector and D. L. Woernley—101
Of potassium dihydrogen phosphate and ammonium dihydrogen phosphate, W. P. Mason—173
Temperature coefficients of interfacial polarization, R. F. Field—688(A)
Diffraction of electrons (see **Electron diffraction**)
Diffusion (see also **Thermal diffusion**)
Dependence of coefficient on concentration, B. Serin—687(A)
Flow of binary gas mixtures through a capillary, A. J. DeBethune and R. D. Present—259(A)
Separation of gas-mixtures; flow through porous media, W. A. Nierenberg—259(A)
Through a long capillary, R. D. Present and W. G. Pollard—53(A)
Discharge of electricity in gases
Cathode dark space and negative glow, Hg arc, C. G. Smith—96
Complex conductivity at microwave frequencies, M. A. Herlin and S. C. Brown—696(A)
Conduction of ionized gases at high frequencies, H. Margenau—508; 698(A)
Cross sections for capture of electrons, C. G. Montgomery, F. L. McMillan, I. H. Dearnley, and C. S. Pearsall—699(A)
Electrical breakdown at microwave frequencies, D. Q. Posin—696(A); 541(L)
Extinction of gaseous discharges, E. Mayer—51(A)
High frequency gas discharges, T. Holstein—50(A)
Meek's sparking equation, L. H. Fisher—530(L)
Vapor jets in sparks at Hg electrodes, J. R. Haynes—693(A)
Discharge of electricity in high vacua (see also **Thermionic emission; High voltage tubes and machines**)
Insulation of high voltages in vacuum, J. G. Trump—692(A)
Space charge in cylindrical magnetron, L. Page and N. I. Adams, Jr.—494
Space charge in plane magnetron, L. Page and N. I. Adams, Jr.—492
Disintegration and excitation of nucleus (see also **Radioactivity**)
Angular correlation of successive γ-rays, G. Goertzel and I. S. Lowen—533(L)
Deuteron bombardment of O^{17}, S. B. Welles—586
Excitation energy of excited Li^7, S. Rubin—134(A)
Excitation functions, deuteron reactions on Cu, Mg, and Al, E. T. Clarke and J. W. Irvine, Jr.—680(A)
Fast neutron resonance with nitrogen, F. A. Valente and H. I. Zagor—55
Inelastic photo-dissociation of the deuteron, J. M. Jauch —252(A); 275
Matrix elements for positron decay, W. A. Fowler—134(A)
Neutron yields from photo- and electro-disintegration of Be, M. L. Wiedenbeck—235(L)
Nuclear photo-effect, G. Wataghin—33(L)
Nuclear processes by polarization, E. Guth—47(A)
Dissociation
Energies of surface films of oxides; Ta_2, O_4, and ZrO, H. Jacobs—692(A)
Dissociation, heat of (see also **Molecular structure and constants**)
Dissociation of CO, C. Kenty, J. O. Aicher, E. B. Noel, A. Poritsky, and V. Paolino—36(L)
Dynamics
Forced vibrations of a whirling wire, A. V. Masket—52(A)

Elasticity (see also **Wave motion**)
Of colored quartz, C. Frondel—543(L)
Constants of potassium dihydrogen phosphate and ammonium dihydrogen phosphate, W. P. Mason—173
Elastic waves in bars, J. H. McMillen—250(A)
Elasticity and column action, giant reed (*Arundo Donax*), O. Stuhlman, Jr.—547(A)
Forced vibrations of piezoelectric crystals, H. Ekstein—257(A)
Linear dissipative anisotropic elastic systems; solutions for, G. D. Camp—134(A); 502
Plasticity *versus* elasticity in stretched rubber, M. L. Braun—545(A)
Propagation of waves of finite amplitude, J. M. Richardson and W. Shockley—250(A)
Reflection of a shock wave, R. J. Finkelstein—677(A)
Reflection of shock waves, theory, A. H. Taub and L. G. Smith—678(A)
Shock waves and boundary layers in supersonic gas flow, J. Winckler—678(A)
Shock waves in gases, R. G. Sachs—514
Shock waves in a tube, W. Bleakney—678(A)
Spark discharges along shock waves, E. E. Hackman—130(L)
Strains in crystals, C. M. Lucht, M. Mann, and R. Smoluchowski—256(A)
Tangential boundary conditions, impedance representation, G. D. Camp—501
Thermodynamic criterion for fracture, E. Saibel—667(L)

Elasticity (*continued*)
Three-shock configurations, H. Polachek and R. J. Seeger—677(A)
Electrical circuits
Cavity of a linear electron accelerator, E. S. Akeley—255(A)
Equivalent circuit for microwave TR tube, A. L. Samuel—699(A)
Equivalent representations of an arbitrary linear network, E. J. Schremp—259(A)
Interaction of shock waves, R. J. Seeger, J. v. Neumann, and H. Polachek—677(A)
Minimal noise amplifiers, E. J. Schremp—695(A)
Modulation and tuning of cavity oscillators, D. S. Saxon—700(A)
Multivibrator theory, S. C. Snowdon—134(A)
Noise in radar crystal detectors, L. I. Schiff—682(A)
Noise representation of multi-grid amplifier tubes, R. Q. Twiss and E. J. Schremp—696(A)
Normal modes in wave guides, G. M. Roe—255(A)
Nyquist's thermal noise theorem, E. J. Schremp—255(A)
Pre-corona discharge, reference potential in voltage stabilizers, S. C. Brown—696(A)
Pulse transformer, W. H. Bostick—696(A)
Rectification efficiency of radar crystal detectors, A. W. Lawson, B. Goodman, and L. I. Schiff—682(A)
Electrical conductivity and resistance
Contact capacity of rectifiers, R. N. Smith—683(A)
Contact e.m.f. between a metal and a semi-conductor, W. E. Stephens, B. Serin, and W. E. Meyerhof—42(L)
Diamagnetism and superconductivity, W. Band—241(L)
Diode behavior in crystal rectification, K. F. Herzfeld—683(A)
Effect of gases on Ge rectifiers, R. M. Whaley and K. Lark-Horovitz—683(A)
Of germanium alloys, K. Lark-Horovitz, A. E. Middleton, E. P. Miller, and I. Walerstein—258(A)
Ge and Si crystal rectifiers, H. J. Yearian—682(A)
Grain structure and electrical conductivity, B. Goodman—687(A)
High voltage characteristics of Ge rectifiers, S. Benzer—683(A)
Image force and tunnel effect in rectifiers, E. D. Courant—684(A)
Noise in radar crystal detectors, L. I. Schiff—682(A)
Rectification efficiency of radar crystal detectors, A. W. Lawson, B. Goodman, and L. I. Schiff—682(A)
Rectification series, W. H. Brattain—682(A)
Semi-conductors and contact rectification, B. Serin—357
Semi-quantitative explanation of crystal rectifiers, V. A. Johnson, R. N. Smith, and H. J. Yearian—682(A)
Spark produced in $CuSO_4$ solutions, H. F. Henry—693(A)
Superconductivity in an electron assembly, W. Band—41(L)
Superconductivity and magnetic energy, W. Band—241(L)
Superconductivity of metal-ammonia solutions, R. A. Ogg, Jr.—243(L); 544(L)
Thallous sulfide photo-conductive cell, A. v. Hippel, F. G. Chesley, H. S. Denmark, P. B. Ulin, and E. S. Rittner—685(A)
Theory of crystal rectifiers, R. G. Sachs—682(A)
Theory of impurity scattering in semiconductors, E. Conwell and V. F. Weisskopf—258(A)
Theory of resistivity in germanium alloys, K. Lark-Horovitz and V. A. Johnson—258(A)
Transfer phenomena and indeterminacy, superconductivity, J. G. Daunt and K. Mendelssohn—126(L)
Transverse pressure, conductivity of rocksalt, C. N. Hamtil—50(A)
Velocity of propagation of photo-effect, F. C. Brown—686(A)
Electromagnetic theory
Accelerational-velocital magnetic forces, F. W. Warburton—49(A)
Antenna impedance measurement, D. D. King—696(A)
Classical theory of point electron, M. Schönberg—211
Cylindrical antenna, R. King and D. Middleton—696(A)
Diffraction pattern of a circular aperture, C. L. Andrews—684(A)
Electromagnetism and gravitation, H. C. Corben—225
Interaction of electrons with fields, quantum effects, L. P. Smith—195
Movements of matter in a beam of light, F. Ehrenhaft—52(A); 251(A)
Narrow resonant slit in a wave guide partition, E. S. Akeley—697(A)
Photophoretic forces, F. Ehrenhaft—684(A)
Radar echoes from surface of the sea, H. Goldstein—695(A)
Radiation in a medium with random inhomogeneities, P. G. Bergmann—255(A)
Reciprocal electric force, F. W. Warburton—40(L)
Relativistic interaction of electrons, D. J. Montgomery—117
Scattering of radiation by a thin circular ring, P. Feuer and E. S. Akeley—697(A)
Space-charge frequency dependence of magnetron cavity, M. Phillips and W. E. Lamb, Jr.—701(A)
Electron diffraction
Ambiguities in diffraction analysis, A. L. Patterson—256(A)
Electronic tubes (see also **Methods and instruments**)
Characteristics of reflex tubes, H. V. Neher—134(A)
Conduction of ionized gases at high frequencies, H. Margenau—508; 698(A)
Copper disk seal TR tubes, J. W. Clark, A. E. Andersen, and A. L. Samuel—698(A)
Cross sections for capture of electrons in TR tubes, C. G. Montgomery, F. L. McMillan, I. H. Dearnley, and C. S. Pearsall—699(A)
Efficiency of reflex oscillators, E. G. Linder and R. L. Sproull—700(A)
Electron orbits in the synchrotron, D. S. Saxon and J. Schwinger—702(A)
Energy build-up in magnetrons, L. P. Hunter—700(A)
Equivalent circuit for microwave TR tube, A. L. Samuel—699(A)

Electronic tubes (*continued*)
Gas discharge switches for low power microwave signals, T'ing-Sui Ke and L. D. Smullin—698(A)
Gas discharges in microwave TR tubes, L. D. Smullin—698(A)
High power 'rising sun' magnetron, A. Ashkin—701(A)
Integral cavity TR switch, D. Alpert and S. Krasik—698(A)
Linear electrical characteristics of band-pass TR switch, W. C. Caldwell—699(A)
Magnetron anode structure, S. Millman and A. Nordsieck—701(A)
Modulation and tuning of cavity oscillators, D. S. Saxon—700(A)
Principles of the resnatron, F. W. Boggs—700(A)
Recovery time of TR tubes, C. F. Crandell, A. L. Samuel, and J. W. Clark—698(A)
'Rising sun' magnetron anode, theory of, N. Kroll and W. E. Lamb, Jr.—701(A)
Space-charge and bunching of electron beams, L. Brillouin—700(A)
Space charge in cylindrical magnetron, L. Page and N. I. Adams, Jr.—494
Space-charge frequency dependence of magnetron cavity, M. Phillips and W. E. Lamb, Jr.—701(A)
Space charge in plane magnetron, L. Page and N. I. Adams, Jr.—492
Stability of FP-54 electrometer tube, J. M. Lafferty and K. H. Kingdon—699(A)
Switching action of band-pass TR switch, M. D. Fiske—699(A)
Theory of the diode, J. K. Knipp—700(A)
Theory of TR switch spike, T. Holstein—698(A)
Tuning of magnetrons, S. Sonkin—701(A)
One centimeter magnetrons with numerous cavities, A. V. Hollenberg, S. Millman, and N. Kroll—701(A)

Electrons (see also **Positron**)
Classical theory of point electron, M. Schönberg—211

Electrophoresis
Balancing sedimentation by electrophoresis in high centrifugal fields, J. W. Beams—546(A)

Errata
Bose-Einstein condensation of trapped electron pairs. Phase separation and superconductivity of metal-ammonia solutions, R. A. Ogg, Jr.—544(L)
Calculus of finite precision—A correction, B. Liebowitz—131(L)
Experimental test of beta-ray theory for the positron emitters Na^{22}, V^{48}, Mn^{52}, Co^{56}, W. M. Good, David Peaslee, and Martin Deutsch—673(L)
General theory of pressure broadening of spectral lines, A. Jabloński—31
A method for measuring effective contact e.m.f. between a metal and a semi-conductor, W. E. Stephens, B. Serin, and W. E. Meyerhof—244(L)

Evaporation
Of helium II below 1.5°K, J. E. Haggenmacher—242(L)

Field currents
Insulation of high voltages in vacuum, J. G. Trump—692(A)

Fission of nucleus
Atomic energy from U^{238}, L. A. Turner—366(L)
$H\rho$-distribution and charge of the fission fragments, N. O. Lassen—137
In 94–239, J. W. Kennedy and A. C. Wahl—367(L)

Fluorescence
Fluorescent yield of calcium tungstate, E. G. Ebbighausen and J. W. Coltman—48(A)

Friction
"Solid" *versus* "polar" boundary films, M. E. Merchant—250(A)

Gamma-rays (see **Radioactivity**)

Hall effect
Of germanium alloys, K. Lark-Horovitz, A. E. Middleton, E. P. Miller, and I. Walerstein—258(A)

Heat conduction (see **Thermal conductivity**)

Heat of vaporization
Of helium II below 1.5°K, J. E. Haggenmacher—242(L)

High voltage tubes and machines (see also **Methods and instruments**)
Acceleration of relativistic particles, new method, V. Veksler—244(L); E. M. McMillan—534(L)
Combination of betatron and synchrotron, H. C. Pollock—125(L)
High energy particle accelerator—the cavitron, R. F. Post—126(L)
Radiation losses in the induction accelerator, J. P. Blewett—87
Wave-guide accelerator, E. L. Hudspeth—671(L)

Hydrodynamics
Air-water entry cavities, D. Gilbarg—679(A)
Diabatic flow of a compressible fluid, B. L. Hicks—135(A)
Diabatic, rotational flow in two dimensions, B. L. Hicks—250(A)
Impedance representation of tangential boundary surface forces, G. D. Camp—135(A)
Inequality of quantum hydrodynamics, F. London—254(A)
Transformation theory of hydrodynamical equations, H. Jehle—260(A)

Instruments (see **Methods and instruments**)

Ionization by collision (see **Ionization potentials**)

Ionization potentials
Of CH_2, A. Langer and J. A. Hipple—691(A)
Metastable ions in hydrocarbon gases, J. A. Hipple, R. E. Fox, and E. U. Condon—257(A); 347

Ionosphere
Meteoric ionization observed on radar oscilloscopes, O. P. Ferrell—32(L)
Rapidly moving ionospheric clouds, H. W. Wells, J. M. Watts, and D. E. George—540(L)

Isotopes
Abundance of nuclei in the universe, C. Lattes and G. Wataghin—237(L)
Mass measurement with a single field mass spectrometer, E. P. Ney and A. K. Mann—239(L)
Separation of A isotopes by thermal diffusion, R. Simon—596

Isotopes (*continued*)
Separation of isotopes of Cl, E. F. Shrader—439
Separation of O isotopes by thermal diffusion, S. B. Welles—586
Of Si, E. P. Ney and J. H. McQueen—41(L)
Of Te, Si, W, Mo, and Br, D. Williams and P. Yuster—556

Kinetic theory
Flow of binary gas mixtures through a capillary, A. J. DeBethune and R. D. Present—259(A)
Fokker-Planck equation for a reflecting boundary, T. H. Berlin—688(A)

Liquids (see also **Hydrodynamics**)
Boundary films, friction, M. E. Merchant—250(A)
Luminescence
Mechanism of luminescence, F. E. Williams and H. Eyring—257(A)

Magnetic properties
Diamagnetism and superconductivity, W. Band—241(L)
Long period magnetic relaxation, C. Kittel—640
Magnetic current, F. Ehrenhaft—260(A)
Magnetic moments of light nuclei, R. G. Sachs—611
Motion of electrolytes in magnetic field, C. E. Swartz and W. Van der Grinten—252(A)
Of small samples, E. C. Crittenden, Jr., C. S. Smith, Jr. and L. O. Olsen—703(A)
Mechanics (see **Dynamics**)
Mechanics, quantum—general
Calculus of finite precision—A correction, B. Liebowitz—131(L)
Discrete energy spectra in Heisenberg's theory, S. T. Ma—668(L)
Inequality of quantum hydrodynamics, F. London—254(A)
Interaction of electrons with fields, L. P. Smith—195
Second quantization, R. Becker and G. Leibfried—34(L)
Theory of point electron, M. Schönberg—211
Mechanics, statistical
Of systems involving molecular flow, G. Jaffé—688(A)
Mesotrons
Absorption in Pb, Fe, Al, and H_2O, H. P. Koenig—253(A); 590
Anomalous scattering, R. P. Shutt—128(L); 261
Low mass neutral mesotron, theory of, Chihiro Kikuchi—125(L)
Non-electrical scattering, G. Groetzinger and L. Smith—690(A)
Production by electrons, H. Feshbach—690(A)
Production in stratosphere, I. Bloch—575
Microwaves (see **Electromagnetic theory; Electronic tubes**)
Methods and instruments
Absorbing surfaces for the infra-red, L. N. Hadley and D. M. Dennison—258(A)
Acceleration of relativistic particles, V. Veksler—244(L); E. M. McMillan—534(L)
Alpha-ray spectrograph, W. Y. Chang—60
Antenna impedance measurement, D. D. King—696(A)
Balancing sedimentation by electrophoresis in high centrifugal fields, J. W. Beams—546(A)
Bridge photo-cell, G. K. Teal, J. R. Fisher, and A. W. Treptow—686(A)
Cavity of a linear electron accelerator, E. S. Akeley—255(A)
Chemical analysis of alloys, J. Ball and F. C. Blake—703(A)
Circle diagram for resonant microwave systems, W. Altar—697(A)
Combination of betatron and synchrotron, H. C. Pollock—125(L)
Computer for solving linear simultaneous equations, C. E. Berry—135(A)
Contact e.m.f. between a metal and a semi-conductor, W. E. Stephens, B. Serin, and W. E. Meyerhof—42(L)
Copper disk seal TR tubes, J. W. Clark, A. E. Andersen, and A. L. Samuel—698(A)
Counting of nuclear particles, H. L. Schultz—689(A)
Curved crystal spectrograph, J. W. Farnham, J. E. Edwards, and F. C. Blake—48(A); J. Ball and F. C. Blake—703(A)
Decade counting circuits, V. H. Regener—46(A); 689(A)
Detection of Al in Si, W. E. Stephens and M. N. Lewis—43(L)
Effectiveness of betatron, T. J. Wang—42(L)
Electromagnet for non-magnetic substances, W. V. Lovell—251(A)
Electron accelerator, stationary electromagnetic modes, E. S. Akeley—50(A)
Electrostatic generator at Kentucky, L. A. Pardue and C. B. Crawley—545(A)
Electrostatic generator using sulphur hexafluoride insulation, W. W. Buechner, R. J. Van de Graaff, A. Sperduto, E. A. Burrill, L. R. McIntosh, and R. C. Urquhart—692(A)
Fast sweep synchroscope, D. F. Winter—695(A)
Fluorescence, light scattering, and its polarization and depolarization, demonstration, W. Heller—53(A)
Focal spot size in high voltage radiography, A. Sperduto—692(A)
Focusing of electrostatic analyzer, F. T. Rogers, Jr.—537(L)
Frequency modulated cyclotron, J. R. Richardson, K. R. MacKenzie, E. J. Lofgren, and B. T. Wright—669(L)
Geiger counter as x-ray dosimeter, W. F. Fuller and A. A. Bless—545(A)
G-M counter data, correction of, J. D. Kurbatov and G. K. Groetzinger—253(A)
G-M counter technique, C. O. Muehlhause and H. Friedman—46(A)
Generator suitable for measurement of small magnetic intensities, S. J. Barnett—135(A)
Guide fields in the synchro-betatron, H. F. Kaiser and E. C. Greanias—536(L)
High centrifugal fields, J. W. Beams and J. L. Young, III—537(L)
High energy particle accelerator—the cavitron, R. F. Post—126(L)

Methods and instruments (*continued*)
High frequency accelerator and betatron, comparison, J. R. Woodyard—50(A)
Hydrogen liquefier, H. A. Fairbank—686(A)
Integral cavity TR switch, D. Alpert and S. Krasik—698(A)
Integration of $\sin^2 x\,dx/x$, S. M. Christian—546(A)
Ion beams homogeneous as to mass and energy, J. Koch—238(L)
Ion gauge with radium source, G. L. Mellen—691(A)
Ionization in proportional counters, fluctuations, W. F. G. Swann—690(A)
Magnetic antenna, L. Page—645
Magnetic beta-ray spectrograph, recording circuits, W. C. Peacock and R. K. Osborne—679(A)
Magnetic properties of small samples, E. C. Crittenden, Jr., C. S. Smith, Jr., and L. O. Olsen—703(A)
Mass measurement with a single field mass spectrometer, E. P. Ney and A. K. Mann—239(L)
Microwave duplexing circuits, H. K. Farr—699(A)
Microwave linear accelerator, J. Halpern, E. Everhart, R. A. Rapuano, and J. C. Slater—688(A)
Microwave spectroscope, theory of, W. E. Lamb, Jr.—694(A)
Minimal noise amplifiers, E. J. Schremp—695(A)
Multi-element x-ray tube, R. Pepinsky—546(A)
Multivibrator theory, S. C. Snowdon—134(A)
New type electrostatic generator, P. H. Miller, Jr.—666(L)
Non-linear automatic control systems, M. Avramy—697(A)
Nuclear magnetic moments, measurement of, F. Bloch, W. W. Hansen, and M. Packard—127(L); 680(A); M. Packard, W. W. Hansen, and F. Bloch—680(A)
Optical analysis of supersonic inhomogeneous air-jets, J. Winckler, C. C. Van Voorhis, and R. Ladenburg—251(A)
Orientation of single crystals, Bragg reflections, I. Fankuchen—256(A)
Phase stability of synchrotron orbits, N. H. Frank—689(A)
Photographic investigations of reflection of plane shocks, L. G. Smith—678(A)
Photomultiplier x-ray detector, F. H. Marshall and L. P. Hunter—48(A)
Pre-corona discharge, reference potential in voltage stabilizers, S. C. Brown—696(A)
Proportional counter for meson detection, E. C. Pollard—689(A)
Pulse transformer design, W. H. Bostick—697(A)
Pulsed mass spectrometer, W. E. Stephens—691(A)
Quantitative interferometry, gas dynamics, F. J. Weyl—677(A)
Quarter-wave plates, half-wave plates, half shades and ellipticity compensators, W. Heller—53(A)
"Racetrack" accelerator for electrons, H. R. Crane—542(L)
"Racetrack" accelerator, stability of orbits, D. M. Dennison and T. H. Berlin—542(L)
Radiation losses in the induction accelerator, J. P. Blewett—87
Radioautography with P^{32} and Sr^{89}, D. Q. Posin—702(A)
Radiometer for microwave frequencies, R. H. Dicke—694(A)
Resolving power of spectroscopes, interferometric method, K. W. Meissner—685(A)
Separation of gas-mixtures, W. A. Nierenberg—259(A)
Sine-wave generator, S. J. Barnett—133(A)
Slow neutron velocity spectrometer, L. J. Haworth and F. N. Gillette—254(A)
Sound velocity, precision measurement, R. W. Leonard—136(A)
Spectroscopic analysis of K-Na solution, W. Scanlon—52(A)
Static direction finder, H. L. Knowles—546(A)
Strains in crystals, x-ray microradiographic study, C. M. Lucht, M. Mann, and R. Smoluchowski—256(A)
Strength of a shock wave, P. C. Keenan—677(A)
Stress-strain machine, S. L. Dart, R. L. Anthony, and P. E. Wack—52(A)
Sulfur hexafluoride, preparation of, W. C. Schumb—692(A)
Synchrotron, origin of, E. M. McMillan—534(L)
Thallous sulfide photo-conductive cell, A. v. Hippel, F. G. Chesley, H. S. Denmark, P. B. Ulin, and E. S. Rittner—685(A)
Thermal diffusion column, R. Simon—596
Thermal diffusion, cylindrical case, W. H. Furry and R. C. Jones—459
Thickness measurements of coatings by x-ray absorption, L. S. Birks and H. Friedman—49(A); R. B. Gray—49(A)
Thickness of thin crystalline films, x-ray method, A. Eisenstein—252(A)
Ultra-short time measurement, S. H. Neddermeyer—705(A)
Ultrasonic absorption and velocity measurements in liquids, pulse techniques, J. R. Pellam, and J. K. Galt—679(A)
Ultraviolet lamps and ozone, A. W. Ewell—685(A)
Vacuum switch, R. Koller—134(A)
Vacuum valve, rapidly acting, D. D'Eustachio—251(A)
Vapor pressure of liquid metals, A. H. Weber and G. Plantenberg—51(A); 649
Vapors for self-quenched G-M counters, E. DerMateosian and H. Friedman—689(A)
Velocity selector for neutral atoms; vacuum rotor, H. Levinstein and H. R. Crane—679(A)
Wave-guide accelerator, E. L. Hudspeth—671(L)
Molecular structure and constants (see also **Spectra, molecular**, etc.)
Bond constants and electronegativities of the bonded atoms, W. Gordy—130(L)
Electronegativity; other atomic properties, W. Gordy—604
Electronic structure of N_2, G. Herzberg—362
Normal coordinates of benzene, N. Ginsburg and J. L. Gammel—685(A)

Neutrons
Absorption by boron-velocity dependence, J. H. Manley, L. J. Haworth, and E. A. Luebke—405
Absorption by Cd^{113}, B. J. Moyer, B. Peters, and F. H. Schmidt—666(L)
Absorption in gases, walls, and tissue, P. C. Aebersold and G. A. Anslow—1
Absorption of neutrons, velocity spectrometer, R. F. Bacher, C. P. Baker, and B. D. McDaniel—443
Albedo of thermal neutrons, M. Ageno—241(L)
Capture cross sections, J. W. Coltman and M. Goldhaber—411
Collision cross sections of C and H, W. Sleator, Jr.—681(A)
Cosmic-ray neutrons in the atmosphere, S. A. Korff and B. Hamermesh—155; 252(A)
Determination of absolute intensities, R. D. O'Neal and G. Scharff-Goldhaber—368(L)
Low energy neutrons from a Ra-α-Be, upper limit, A. A. Yalow, R. S. Yalow, and M. Goldhaber—253(A)
Mass of neutron, Kuan-Han Sun—240(L)
Neutron groups, A. A. Yalow and M. Goldhaber—47(A)
Polarization by resonance scattering, J. Schwinger—681(A)
Reproducible neutron standards, G. R. Gamertsfelder and M. Goldhaber—368(L)
Resonance scattering of group neutrons, M. Goldhaber and A. A. Yalow—47(A)
Scattering by Mg, R. N. Little, R. W. Long, and C. E. Mandeville—414
Scattering in ortho- and parahydrogen, range of nuclear forces, C. S. Wu, L. J. Rainwater, W. W. Havens, Jr., and J. R. Dunning—236(L)
Slow neutron velocity spectrometer, L. J. Haworth and F. N. Gillette—254(A)
Slow neutron velocity spectrometer, experimental results, J. H. Manley, F. B. Berger, and F. N. Gillette—254(A)
Slowing down in heavy substances; theory, G. Placzek—423
Spin of neutron, M. Hamermesh and J. Schwinger—145
Yield function of D+D neutrons, W. E. Bennett, C. E. Mandeville, and H. T. Richards—418
Yields from photo- and electro-disintegration of Be M. L. Wiedenbeck—235(L)

Nuclear moments and spin
Absorption by nuclear magnetic moments, E. M. Purcell, H. C. Torrey, and R. V. Pound—37(L)
Magnetic moments of light nuclei, R. G. Sachs—611
Magnetic resonance absorption, nuclear moments, experimental, R. V. Pound, E. M. Purcell, and H. C. Torrey—681(A)
Magnetic resonance absorption, nuclear moments, theory, H. C. Torrey, E. M. Purcell, and R. V. Pound—680(A)
Nuclear induction, F. Bloch, W. W. Hansen, and M. Packard—127(L); 680(A); M. Packard, W. W. Hansen, and F. Bloch—680(A)
Relativistic correction, P. Caldirola—608
Spontaneous emission probabilities, relaxation time, E. M. Purcell—681(A)

Nuclear structure (see also **Disintegration and excitation of nucleus**)
Excited states of nucleus, J. M. Jauch—252(A); 275
Heavy-electron pair theory, J. M. Blatt—285
Lifetime of metastable states, M. L. Wiedenbeck—567
Neutron-proton scattering, meson theory of nuclear forces, J. L. Lopes—252(A)
Nuclear resonances, schematic treatment, G. Breit—472
Spherical shell nuclear model, H. A. Wilson—538(L)

Optical instruments (see **Methods and instruments**)

Philosophy of physics
Natural law and order, H. G. Wehe—684(A)

Phosphorescence
Corpuscular *vs.* undulatory excitation, H. W. Leverenz—686(A)
Decay of infra-red sensitive phosphors, R. T. Ellickson and W. L. Parker—534(L)
Infra-red sensitive phosphors, R. T. Ellickson—685(A)

Photo-conductivity
Photo-sensitive characteristics of Ge rectifier, S. Benzer—683(A)
Thallous sulfide photo-conductive cell, A. v. Hippel, F. G. Chesley, H. S. Denmark, P. B. Ulin, and E. S. Rittner—685(A)
Velocity of propagation of photo-effect, F. C. Brown—686(A)

Photoelectric effect and properties; cells
Falling-off effect of limiting potential, E. Marx—523
Influence of strong electrostatic fields, V. P. Jacobsmeyer—50(A)

Piezoelectric effect
Constants of potassium dihydrogen phosphate and ammonium dihydrogen phosphate, W. P. Mason—173
Forced vibrations of piezoelectric crystals, H. Ekstein—257(A)

Polymerization; Properties of polymers
Phase transitions at low temperatures in rubber, P. E. Wack—52(A)
Plasticity *versus* elasticity in stretched rubber, M. L. Braun—545(A)
Use of polymers in quarter-wave plates, half-wave plates, half shades and ellipticity compensators, W. Heller—53(A)

Positrons
Fine structure of positronium, G. Beck—532(L)

Proceedings of the American Physical Society
St. Louis, Missouri, Meeting November 30–December 1, 1945—44
University of California, Los Angeles, California, Meeting January 12, 1946—133
New York, Annual Meeting January 24–26, 1946—246
Southeastern Section, Atlanta, Georgia, Meeting April 12–13, 1946—545
New York State Section, Hamilton, New York, Meeting April 13, 1946—674
Cambridge, Massachusetts, Meeting April 25–27, 1946—674

Proceedings of the American Physical Society (*continued*)
Ohio Section, Columbus, Ohio, Meeting May 4, 1946—703

Quantum mechanics (see **Mechanics, quantum**)

Radar (see **Electromagnetic theory; Electronic tubes;** and **Electrical circuits**)
Radio (see also **Ionosphere; Electromagnetic theory; Electronic tubes;** and **Electrical circuits**)
Radioactivity (see also **Disintegration of nucleus**)
Alpha-ray spectra of Po, W. Y. Chang—254(A)
Alpha-particles from Po, W. Y. Chang—60
Artificial radioactivity and radiation dosimetry, β-ray energy, L. D. Marinelli, R. F. Brinckerhoff, and E. H. Quimby—690(A)
Beta-radiations of uranium X_1, S. Jnanananda—570
Beta-ray theory for positron emitters, test of, W. M. Good, D. Peaslee, and M. Deutsch—313; Erratum—673(L)
β-spectrum of Cu^{64}, H. Lewis and D. Bohm—129(L)
C^{14} and He^3 from atmospheric N, W. F. Libby—671(L)
Disintegration of substances IX. Mn^{52} and V^{48}, W. C. Peacock and M. Deutsch—306
Fine structure of α-rays from protoactinium, Tsien San-Tsiang, M. Bachelet, and G. Bouissières—39(L)
γ-rays of radium D, Tsien San-Tsiang—38(L)
Intercrystalline forces and beta-ray absorption, H. D. Rathgeber—239(L)
Lifetimes of metastable states, M. L. Wiedenbeck—47(A)
Of Mo and Ma, J. E. Edwards and M. L. Pool—253(A)
Of N^{16} and He^6, H. S. Sommers, Jr. and R. Sherr—21
Nuclear radii of α-emitters, M. A. Preston—535(L)
Positron emission, electron capture competition in Zn^{65}, W. M. Good and W. C. Peacock—680(A)
Of K^{40}, B. Dželepow, M. Kopjova, and E. Vorobjov—536(L)
Radioactive element 94, G. T. Seaborg, E. M. McMillan, J. W. Kennedy, and A. C. Wahl—366(L); G. T. Seaborg, A. C. Wahl, and J. W. Kennedy—367(L)
Radioactive isotopes in compounds, A. F. Reid—530(L)
Radioactive isotopes, dosage, G. Failla—691(A)
Spectra of La^{140}, R. K. Osborne and W. C. Peacock—679(A)
Of Te, J. E. Edwards and M. L. Pool—49(A); 140
Units of strength of sources, E. U. Condon, L. F. Curtiss—672(L)
Rectifiers (see **Electrical conductivity and resistance**)
Relativity
Electromagnetism and gravitation, H. C. Corben—225
Interaction of electrons, D. J. Montgomery—117
Magnetic moment of deuteron, relativistic correction, P. Caldirola—608
Transformation of current and charge densities, B. Podolsky—255(A)
Two-body problem, T. F. Morris—541(L)
Uniform rotation, E. L. Hill—488

Scattering of atoms and molecules
Mean free paths of Cs atoms in He, N_2, and Cs vapor, I. Estermann, S. N. Foner, and O. Stern—256(A)

Scattering of electrons, neutrons, and ions (see also **Electron diffraction**)
Albedo of thermal neutrons, M. Ageno—241(L)
Anomalous scattering of mesotrons, R. P. Shutt—128(L); 261
Elastic single scattering of electrons, R. J. Van de Graaff, W. W. Buechner, and H. Feshbach—47(A)
Multiple scattering and curvature measurements, H. A. Bethe—689(A)
Neutron collision cross sections of C and H, W. Sleator, Jr.—681(A)
Neutron-proton scattering and the meson theory, J. L. Lopes—252(A)
Of neutrons by Mg, R. N. Little, R. W. Long, and C. E. Mandeville—414
Polarization of neutrons by scattering, J. Schwinger—681(A)
Resonance scattering of fast neutrons, D. C. Grahame—369(L)
Resonance scattering, M. Goldhaber and A. A. Yalow—47(A)
Single scattering of electrons, R. J. Van de Graaff, W. W. Buechner, and H. Feshbach—452
Spin dependence of neutron-proton interaction, M. Hamermesh and J. Schwinger—145
Semi-conductors (see **Electrical conductivity and resistance**)
Solid state (see **Crystalline state**)
Sound (see **Acoustics**)
Specific heat
Of hevea, GR-S and GR-I polymers, B. A. Mrowca, R. L. Anthony, and W. H. Hamill—51(A)
Spectra, absorption
Of NH_3, W. E. Good—539(L)
Infra-red absorption of methane, foreign gases, N. D. Coggeshall and E. L. Saier—257(A)
Spectra, atomic
Forbidden lines of BiI, S. Mrozowski—169
Spectra, general
Forbidden lines, source of, J. Kaplan—133(A)
High frequency discharge in air, active nitrogen, N. R. Tawde and G. K. Mehta—245(L)
Light of night sky in ultraviolet, G. Dejardin and J. Dufay—685(A)
Pressure broadening, theory, H. M. Foley—628
Spectra, molecular (see also **Molecular structure and constants**)
Electronic structure of N_2, G. Herzberg—362
Infra-red spectrum of $C^{13}O^{16}$ and $C^{13}O^{18}$, R. T. Lagemann, A. H. Nielsen, and F. P. Dickey—545(A)
Intensity distribution, rotational lines of AlO, F. P. Coheur and P. M. Coheur—240(L)
Self broadening of HCN, H. M. Foley—628
Superconductivity (see **Electrical conductivity and resistance**)

Terrestrial magnetism
Induction effects, theory, W. M. Elsasser—106
Thermal conductivity
Effects with liquid crystals and suspended particles, G. W. Stewart—51(A)

Thermal diffusion
Isotope separation, cylindrical case, W. H. Furry and R. C. Jones—459
Performance of a diffusion column, R. Simon—596
Separation of isotopes of Cl, E. F. Shrader—439
Separation of isotopes of O, S. B. Welles—586
Thermionic emission; Emitting surfaces
Enhanced thermionic emission, J. B. Johnson—702(A)
Poisoning of oxide cathodes by Au, J. Rothstein—693(A)
Secondary emission of oxide cathodes, J. B. Johnson—693(A)
Thermodynamics
Equilibria of higher order, E. F. Lype—652
Of relaxation processes, G. E. Kimball—688(A)
Thermoelectric effects
In germanium alloys, K. Lark-Horovitz, A. E. Middleton, E. P. Miller, W. W. Scanlon, and I. Walerstein—259(A)
In germanium, theory of, V. A. Johnson and K. Lark-Horovitz—259(A)

Vacuum tubes (see **Electronic tubes**)
Vapor pressure
Direct measurement for liquid metals, A. H. Weber and G. Plantenberg—51(A); 649

Wave guide (see **Electromagnetic theory**; and **Electrical circuits**)
Wave mechanics (see **Mechanics, quantum,** etc.)
Wave motion
Elastic waves in bars, J. H. McMillen—250(A)
Interaction of shock waves, R. J. Seeger, J. v. Neumann, and H. Polachek—677(A)
Propagation of waves of finite amplitude, J. M. Richardson and W. Shockley—250(A)
Reflection of a shock wave, R. J. Finkelstein—677(A)
Reflection of shock waves, theory, A. H. Taub and L. G. Smith—678(A)
Shock waves and boundary layers in supersonic gas flow, J. Winckler—678(A)
Shock waves in a tube, W. Bleakney—678(A)
Strength of a shock wave, P. C. Keenan—677(A)
Three-shock configurations, H. Polachek and R. J. Seeger—677(A)

X-rays, absorption
K absorption edge of Si, V. P. Barton and G. A. Lindsay—48(A)
X-rays, absorption
Structure in *K* edge of potassium, J. B. Platt—337
X-rays, diffraction, scattering, reflection, refraction, and polarization
Absorption in steel, J. A. Hornbeck and H. Feshbach—691(A)
Ambiguities diffraction analysis, A. L. Patterson—256(A)
X-rays, emission (see also **X-rays, spectra and spectroscopy,** etc.)
Auger transitions, F. R. Hirsh, Jr.—32(L)
Betatron radiation, C. O. Muehlhause and H. Friedman—691(A)
Characteristic x-rays excited by beta-particles, J. E. Edwards and M. L. Pool—49(A); 549
From radioactive Te, M. L. Pool and J. E. Edwards—49(A)
X-rays, spectra and spectroscopy, wave-length measurements (see also **X-rays, emission**)
Energy level widths of W, J. N. Cooper—48(A)
X-rays, tubes, apparatus
Fluorescent yield of calcium tungstate, E. G. Ebbighausen and J. W. Coltman—48(A)
Focal spot size in high voltage radiography, A. Sperduto—692(A)
Indexing of crystal faces of α-quartz, F. C. Blake—49(A)
Multi-element x-ray tube, R. Pepinsky—546(A)
Photomultiplier x-ray detector, F. H. Marshall and L. P. Hunter—48(A)

Zeeman effect
Of Cl I, J. B. Green and J. T. Lynn—165

Physics Lib.

THE PHYSICAL REVIEW

VOLUME 69 *Second Series* NUMBERS 11 AND 12

JUNE 1 AND 15, 1946

Published for the

AMERICAN PHYSICAL SOCIETY

by the

AMERICAN INSTITUTE OF PHYSICS
Incorporated

LANCASTER, PA., AND NEW YORK, N. Y.

THE PHYSICAL REVIEW

A journal of experimental and theoretical physics established by E. L. Nichols in 1893

Published by the American Institute of Physics for the

AMERICAN PHYSICAL SOCIETY

Officers

President

R. U. Cosmos
National Bureau of Standards
Washington, D. C.

Vice-President

L. A. DuBridge
University of Rochester
Rochester, New York

Secretary

E. T. Darrow
Bell Telephone Laboratories
Office:
Columbia University
New York 27, New York

Treasurer

G. B. Pegram
Columbia University
New York 27, New York

Local Secretary
for the Pacific Coast

R. T. Birge
University of California
Berkeley, California

Editor

John T. Tate
University of Minnesota
Minneapolis, Minnesota

BOARD OF EDITORS

John T. Tate, *Editor* J. W. Buchta, *Assistant Editor*

Associate Editors

J. W. Beams	J. B. Fisk	E. J. Konopinski
V. Rojansky	W. Pauli	H. H. Nielsen
F. Seitz	L. I. Schiff	R. C. Pollard

Manuscripts for publication should be submitted to John T. Tate, University of Minnesota, Minneapolis, Minnesota.

Proof and all correspondence concerning papers in the process of publication should be addressed to the Publications Manager, American Institute of Physics, 57 East 55 Street, New York 22, New York.

Subscription Price

United States and Canada $15.00
Elsewhere $16.50

Back Numbers

Complete set: Series 2,[1] Vol. 1, 1913–Vol. 68, 1945—$495.00
Yearly rate: $16.50
Single copies: $1.50 each, prior to July, 1929;
$0.75 each, July, 1929–December, 1941.
Current issues: $1.50 each.

Subscriptions and orders for back numbers should be addressed to Prince and Lemon Streets, Lancaster, Pennsylvania, or to the American Institute of Physics, 57 East 55 Street, New York 22, New York.

Changes of address in the case of members of the American Physical Society should be addressed to the Treasurer; in the case of other subscribers to the Business Manager, American Institute of Physics.

[1] For Series 1 inquire of Physics Department, Cornell University, Ithaca, New York.

The Physical Review is published monthly at Prince and Lemon Streets, Lancaster, Pennsylvania.

Entered as second-class matter January 27, 1933, at the Post Office at Lancaster, Pennsylvania, under the Act of March 3, 1879.

Acceptance for mailing at special rate of postage provided for in paragraph 4, section 538, P. L. & R., authorized January 23, 1933.

THE AMERICAN INSTITUTE OF PHYSICS

INCORPORATED

57 East 55 Street New York 22, N.Y.

MEMBER SOCIETIES:

American Physical Society
KARL K. DARROW, *Secretary*, Columbia University, New York 27, New York.

Optical Society of America
ARTHUR C. HARDY, *Secretary*, Massachusetts Institute of Technology, Cambridge 39, Massachusetts.

Acoustical Society of America
WALLACE WATERFALL, *Secretary*, 350 Fifth Avenue, 64th floor, New York 1, New York.

Society of Rheology
R. B. DOW, *Secretary*, Bureau of Ordnance, Navy Department, Washington 25, D. C.

American Association of Physics Teachers
C. J. OVERBECK, *Secretary*, Northwestern University, Evanston, Illinois.

ASSOCIATED SOCIETIES:

American Society for X-Ray and Electron Diffraction

Electron Microscope Society of America

Physical Society of Pittsburgh

Physics Club of Chicago

Physics Club of Philadelphia

ASSOCIATES:

Over seventy-five leading industrial enterprises and other institutions which contribute to the support of the Institute.

JOURNALS:

The Physical Review
Reviews of Modern Physics
JOHN T. TATE, *Editor*—J. W. BUCHTA, *Assistant Editor*

Journal of the Optical Society of America
GEORGE R. HARRISON, *Editor*

The Journal of the Acoustical Society of America
FLOYD A. FIRESTONE, *Editor*

American Journal of Physics
DUANE ROLLER, *Editor*—JOSEPH D. ELDER, *Assistant Editor*

The Review of Scientific Instruments
GAYLORD P. HARNWELL, *Editor*

The Journal of Chemical Physics
JOSEPH E. MAYER, *Editor*

Journal of Applied Physics
ELMER HUTCHISSON, *Editor*

OFFICERS

PAUL E. KLOPSTEG, *Chairman*
Northwestern University

WALLACE WATERFALL, *Secretary*
The Celotex Corporation

GEORGE B. PEGRAM, *Treasurer*
Columbia University

JOHN T. TATE,
Adviser on Publications
University of Minnesota

GOVERNING BOARD

R. B. DOW
L. A. DUBRIDGE
W. F. FAIR, JR.
FLOYD A. FIRESTONE
HARVEY FLETCHER
R. C. GIBBS
K. S. GIBSON
PAUL E. KLOPSTEG
W. H. MARKWOOD, JR.
GEORGE B. PEGRAM
A. H. PFUND
JOHN T. TATE
L. W. TAYLOR
WALLACE WATERFALL
A. G. WORTHING

ADMINISTRATIVE STAFF

HENRY A. BARTON, *Director*

MARGARET S. GRIFFIN,
Publications Manager

THEODORE VORBURGER,
Business Manager

THE American Institute of Physics was founded in 1931 as a federation of leading societies in the field of Physics. It combines into one operating agency those functions on behalf of physics which can best be done by the Societies jointly. Its purpose is the advancement and diffusion of physics and its applications to human welfare. To this end it publishes for itself or the Societies the eight journals listed on this page; promotes unity and effectiveness of effort among all who are interested in physics; renders numerous direct services to physicists and to the public; and cooperates with government agencies, national associations, educational institutions, technical industries and others in such manner as to realize the opportunities and fulfill the responsibilities of physics as an important and constructive human activity.

CONTENTS

PHYSICAL REVIEW — SECOND SERIES, VOL. 69, NOS. 11 AND 12 — JUNE 1 AND 15, 1946

Artificial K-Rays Excited by Beta-Particles . . . . . J. S. EDWARDS AND M. L. FOGG 549

Crystal Constitution of Tellurium, Silicon, Tungsten, Molybdenum, and Bismuth . . . . . DUDLEY WILLIAMS AND PHILIP YOUTZ 556

Note on the Lifetime of Metastable States . . . . . MARSHALL L. WIEDENBECK 567

Wave Functions of Uranium X_2 . . . . . SWAMI JNANANANDA 570

Production of Mesotrons in the Stratosphere? . . . . . ISIDOR BLOCH 576

Partial Separation of the Oxygen Isotopes by Thermal Diffusion and the Deuteron Bombardment of O^{17} . . . . . SHERFRED B. WELLES 586

Absorption of Slow Mesotrons in Lead, Iron, Aluminum, and Water . . . . . H. PAUL KOEHNE 590

Characteristics of a Hot Wire Cracker and Diesel Columns . . . . . RALPH SIEGEL 596

Method of Determining Electronegativity from Other Atomic Properties . WALTER GORDY 604

Diamagnetic Correction in Calculating the Magnetic Moment of the Deuteron . P. CALDIROLA 608

Magnetic Moments of Light Nuclei . . . . . R. G. SACHS 611

Pressure Broadening of Spectral Lines . . . . . H. M. FOLEY 616

Line Broadening in the 14μ Band of HCN . . . . . H. M. FOLEY 636

Dispersion of the Velocity and Anomalous Absorption of Sound in Hydrogen . . . . . ELLIS SWORLEY STEWART 632

Theory of Long Period Magnetic Relaxation . . . . . CHARLES KITTEL 640

Loop Antenna . . . . . LEIGH PAGE 645

Method of Direct Measurement of Vapor Pressure of Liquid Metals . . . . . A. H. WARNER AND SERAFIN GONZAGA PLANTENBERG 649

Thermodynamic Equilibria of Higher Order . . . . . E. F. LITER 652

Letters to the Editor:

New Type of Electrostatic Generator . . . . . P. H. MILLER, JR. 666

Absorption of Slow Neutrons by Cl^{35} . . . . . R. J. MOORE, B. PONTECORVO, AND F. H. SCHMIDT 666

Thermodynamic Criterion for the Fracture of Metals . . . . . EDWARD SAIBEL 667

Independent Terms in the Discrete Energy Spectra in Heisenberg's Theory of Characteristic Matrix . . . . . S. T. MA 668

Physical Interaction of Mercury with Liquid Dielectric Media. The Properties of Metal-Ammonia Solutions . . . . . RICHARD A. GOO, JR. 669

Spontaneously Modulated Cyclotron . . . . . J. REGINALD RICHARDSON, K. R. MACKENZIE, E. J. LOFGREN, AND ROBERT T. WRIGHT 669

Phase Guide Acceleration of Particles . . . . . ERNEST L. BUDDEMEIER 671

Atmospheric Helium Three and Radiocarbon from Cosmic Radiation . . . . . W. F. LIBBY 671

New Units for the Measurement of Radioactivity . . . . . E. U. CONDON AND L. F. CURTISS 672

Neutrons: Experimental Test of Beta-Ray Theory for the Positron Emitting Rb^{84}, Y^{91}, Mn^{52}, Co^{58} . . . . . WILFRED M. GOOD, DAVID PRESSLER, AND MARTIN DEUTSCH 675

Proceedings of the American Physical Society:

Minutes of the Meeting of the New York State Section at Hamilton, New York, April 13, 1946 . . . 674

Meeting at Cambridge, Massachusetts, April 25-27, 1946: Minutes and Abstracts 674

Minutes of the Meeting of the Ohio Section at Columbus, Ohio, May 4, 1946 703

Author Index to Volume 69 704

Analytic Subject Index to Volumes 714

Volume Table of Contents iii

LANCASTER PRESS, INC., LANCASTER, PA.